Analysis of the effect of a singular triangular vane vortex generator on the boundary layer properties of an incompressible turbulent flow over a flat plate in CFD

C.W.H. Beumer

Thesis for the bachelor: Advanced Technology
University of Twente
Faculty of Science and Technology (TNW)
Supervisor: Dr. H. Ozdemir

July 24th, 2024

Abstract

Vortex generators are a form of flow separation control that improves the aerodynamic performance of aerodynamic objects. This form of flow separation control is still being used/researched for modern-day problems, for example, to improve wind turbines. This study investigates the change in boundary layer properties of a CFD simulated turbulent flow on a flat plate, due to the vortex created by a singular triangular vane vortex generator. In addition, the velocity and turbulent shear stress profiles from the CFD results are compared to the experimental results of Y.Bay. From the results, it is concluded that the boundary layer properties are affected by the vortex created by the VG such that flow separation is delayed. The shapes of the velocity and turbulent shear profiles from the CFD results were often similar in shape but not in magnitude compared to the experimental results.

Keywords— vortex generator, boundary layer, CFD, turbulent flow, incompressible

Nomenclature

β	Incidence angle
δ	Boundary layer thickness
δ^*	Displacement thickness
μ	laminar viscosity
μ_t	eddy viscosity
Ω	Vorticity
ω	Specific dissipation ratio
ρ	Density
τ	Shear stress
τ_t	Turbulent Shear stress
τ_w	Wall Shear stress
θ	Momentum thickness
CFD	Computational Fluid Dynamics
H	Shape Factor
h_{vg}	height of the VG
k	Turbulent kinetic energy
l	Turbulence length scale
NSD	Numerical solutions design
T	Temperature
U, V, W	Vector components of the velocity field
u	Velocity
U_∞	Free-stream velocity
VG	Vortex generator
x_{vg}	x-coordinate of the trailing edge of the VG

Contents

1 Introduction

1.1 Vortex Generator Introduction

VG's are applied to improve the aerodynamic performance of an object (aircraft, turbine blades, automotive). This improvement is done through flow-separation control. Aerodynamic objects often have the problem of where the flow separates from the object. This is because, in the boundary layer of the object, the pressure gradient will go from favorable to adverse going downstream the length of the object. When the pressure gradient is adverse, the air flowing, close to the surface of the object, will decelerate as shown in figure 1. If this adverse pressure gradient is big enough and/or the airflow is under this adverse pressure gradient for a long time, the deceleration of the airflow will be enough to reverse the direction of the airflow. At the point where this happens, the flow separates from the object which creates a low-pressure region behind the separation point called wake. This wake is often not desired, for example, aircraft wings can experience an increase in pressure drag due to the wake, which decreases the aerodynamic performance of the aircraft or can even cause an aerodynamic stall when the angle of attack is increased sufficiently.

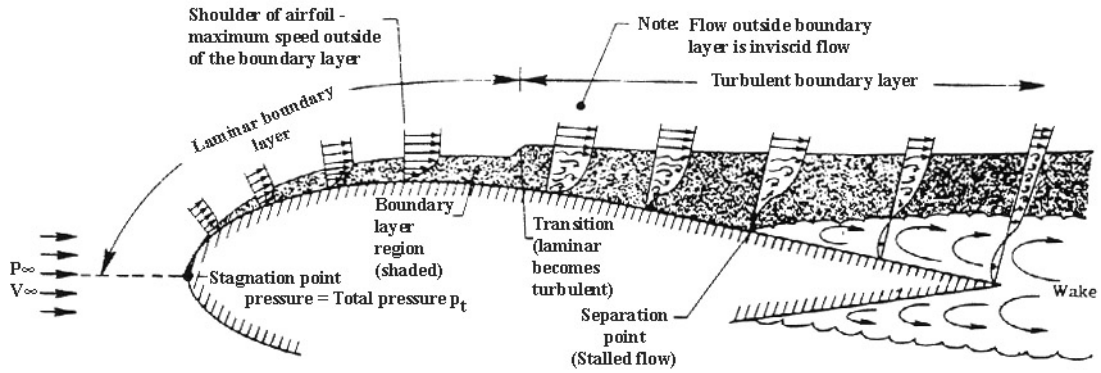

Figure 1: Boundary Layer evolution over an airfoil [1]

To counter this, VG's are applied. VG's delay the separation point of the flow, by re-energizing the boundary layer with air coming outside of the boundary layer. This transitions the boundary layer from laminar to turbulent much quicker, which is beneficial because a turbulent boundary layer has a steeper velocity gradient [2], which is illustrated in figure 1. Because the airflow close to the wall has a higher velocity, due to the steeper velocity gradient, it takes longer for the deceleration to reverse the direction of the airflow, thus delaying the separation point.

VG's can be applied to numerous modern issues, which is why it is/still being researched thoroughly. For example, to extract wind energy using turbine blades, it is desired that the turbine blades increase in size to gain more electricity. This is because the turbine blades can extract more energy from the wind when its surface area is bigger. However, increasing the surface area comes with a drawback. Erosion can occur on the turbine blades due to the raindrops colliding with the turbine blades. To limit erosion, the speed of the tips of the turbine blade is limited [3]. Assuming a constant tip-speed ratio, the rotational velocity of the rotor needs to decrease when the turbine blade increases in size [4]. The decrease in rotational velocity means that the turbine blades must deflect more wind for the same amount of power, meaning that the turbine blades' aerodynamic performance needs to be increased. The effect of VG's on thick turbine blades has been researched experimentally by Zhang et al [5] and they found that installing VG's on the thick wind turbine airfoils: CAS-W2-350, CAS-W2-400, and CAS-W1-450, increased the aerodynamic performance of those airfoils.

Applying VG's can also increase the post-stall performance of an aerodynamic object. For example, placing a VG near the leading edge of an airfoil increases the stall angle of attack, which delays the stall, and post-stall performance. Choudhry et al [6] researched this effect of VG's on the dynamic stall behavior of the NACA 0021 airfoil and concluded that the use of VG's improves the post-stall performance and reduces the created drag caused by the dynamic stall vortex.

1.2 Mathematical model

The optimization of aerodynamic components for an object, on which VG's are applied, happens within the initial design phase of said object. For this optimization, NSD tools, such as XFOIL [7], are used instead of CFD simulations. This is because the NSD tools are often cheaper and are faster with computing results. The only drawback of these NSD tools is that they can not compute the effect of VG's on the airflow, as the NSD tools compute results that are in 2D. VG's however are 3D prisms, so trying to add a VG to a 2D geometry within an NSD tool does not give correct results. So currently in the optimization of applying VG's, CFD simulations are required. But because it is known that VG's re-energize the boundary layer by transitioning the boundary layer from laminar to turbulent, the effect of a VG on the boundary layer in 2D can be approached with the plane mixing layer theory [8]. With this approach, a mathematical model can be created which can be inserted into an NSD, so that the NSD can compute the 2D results which includes the 3D effect of an VG. However, to determine this mathematical model, the exact mathematical relations between the VG parameters and the affected boundary layer parameters need to be determined, which still has not been achieved yet.

1.3 Objectives

The main objective of this paper is to analyze the effects of a singular triangular vane VG on the boundary layer properties of an incompressible turbulent flow, that is simulated to flow over a flat plate using CFD. This will be done by comparing the: δ, δ^*, θ, H values between the cases where there is a VG on the flat plate and when there is not. In addition, the velocity and turbulent shear stress profiles from the CFD results are compared to experimental data found by Y.Bay [9] to see if the CFD results are in line with real cases.

2 Theory

2.1 Vortex creation

A streamwise vortex is created by a VG through pressure difference. When the airflow strikes the frontal surface of a VG, the pressure at the frontal surface will be bigger than at the back of the VG. Because the airflow tends to flow from high pressure to low pressure, the airflow "curls" around the VG to reach the low-pressure region behind the VG. This is the creation of the vortex that develops behind the VG. This vortex will increase the Ω within the airflow.Ω can be calculated by taking the curl of the velocity of the airflow:

$$\Omega = (\frac{\partial W}{\partial y} - \frac{\partial V}{\partial z})\hat{i} + (\frac{\partial U}{\partial z} - \frac{\partial W}{\partial x})\hat{j} + (\frac{\partial Y}{\partial x} - \frac{\partial U}{\partial y})\hat{k} \tag{1}$$

The lateral path of the vortex is dependent on the β angle, this is also shown in the study of F.Gamiz [10]. F.Gamiz also concluded that the peak Ω decreases downstream of the flow. A sketch of the expected vortex created by a VG with a positive β angle is shown in figure 2

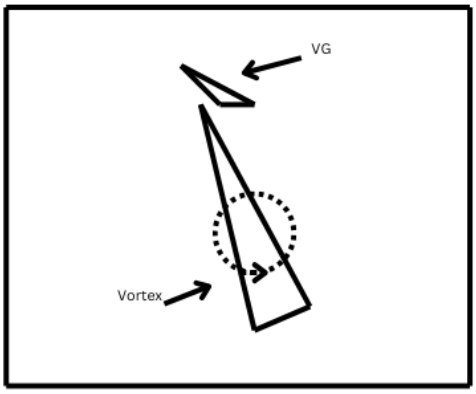

Figure 2: Sketch of the vortex created by single vane VG with positive (β) angle

2.2 Shear Stress

Within the boundary layer, the velocity of the fluid is lower than U_∞. This is because the "wall" of the surface is not moving, so the fluid slows down due to the viscosity. The closer the fluid is to the "wall", the slower the fluid gets due to the no-slip condition that states that the velocity at the wall is zero [11]. Within the boundary layer, layers of fluid generate shear stresses between each other due to these velocity differences. The total shear stress for a turbulent boundary layer can be stated as follows:

$$\tau = \tau_w + \tau_t \tag{2}$$

Where in the wall shear stress can written as [2]:

$$\tau_w = \mu \frac{du}{dy} \tag{3}$$

When the wall shear stress equals zero at the wall, then that would mean that the velocity gradient is zero and flow separation has occurred.

The turbulent shear stress can be written as $-\rho < u_i' u_j' >$, which is known as the Reynolds stress [12]. This form of the Reynolds stress can be rewritten for turbulence models according to the Boussinesq hypothesis:

$$-\rho < u_i' u_j' > = \mu_t (\frac{\partial u_i}{\partial x_j} + \frac{\partial u_j}{\partial x_i}) \tag{4}$$

Where μ_t is calculated by the CFD program depending on which turbulence model is used.

The composition of the shear stresses in the turbulent boundary layer goes as follows: closer to the wall, the wall shear stress in the turbulent boundary layer is larger than the turbulent shear stress. And farther away from the wall the opposite can be said. At the boundary layer's edge, both shear stresses should equal zero as seen in figure 3. [13].

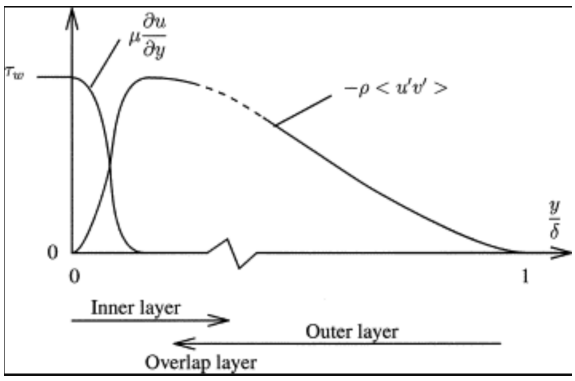

Figure 3: Shear stress profiles for a turbulent boundary layer [13]

2.3 Boundary Layer Thickness

δ is the distance between the fluid and the wall where the fluid's velocity reached 99% of U_∞ [2]. For laminar boundary layer flow it is easier to spot where in the velocity profile the fluid's velocity equals 99% of the U_∞, but for turbulent boundary layer flow it is more complicated due to the unsteadiness of the flow.

This is why δ for turbulent boundary layer flows is determined using different methods, for example looking at when τ within the boundary layer equals zero.

2.4 Displacement Thickness

The physical interpretation of δ^* is the distance in the wall's normal direction, that the streamlines of the fluid need to be displaced due to the formation of the boundary layer [2]. It can be calculated using the following equation [2]:

$$\delta^* = \int_0^\delta (1 - \frac{U}{U_\infty})dz \tag{5}$$

2.5 Momentum Thickness

θ is the distance from δ such that the momentum corresponding to U_∞ for the corresponding θ is equal to the momentum deficit within the boundary layer [2]. It can be determined with the following equation:

$$\theta = \int_0^\delta \frac{U}{U_\infty}(1 - \frac{U}{U_\infty})dz \tag{6}$$

When θ gets bigger it means that there is more momentum within the boundary layer, because θ is in relation to the momentum deficit within the boundary layer.

2.6 Shape Factor

H for boundary layer flow is a measurement to determine the nature of the flow [2]. This is calculated with:

$$H = \frac{\delta^*}{\theta} \tag{7}$$

The physical interpretation is that a higher H means that more mass flow is being displaced than momentum is being transferred. This means that for lower H values, the velocity gradient close to the wall is steeper than for higher H values as more momentum is being transferred to the boundary layer.

2.7 Turbulence model variables

For modeling turbulent flow in CFD programs, it is important to specify the turbulence model variables at the inlet of the mesh grid. The turbulence model variables are dependent on which turbulence model is used. For external flows, the $k-\omega$ SST turbulence model is often used, as it is considered to be in good agreement with simulating turbulence compared to real cases [14]. The $k-\omega$ SST turbulence model has k and ω as turbulence variables. These variables can be determined by the following equations [15]:

$$k = \frac{3}{2}(UI)^2 \tag{8}$$

$$\omega = \frac{\sqrt{k}}{l} \tag{9}$$

l for wall-bounded inlet flows can be set as 0.22 times the δ [16] of the inlet velocity profile.

3 Methodology

3.1 Simulation setup and meshes

3.1.1 CFD program

The CFD program that was used during this project is SU2. "SU2 is an open-source collection of software tools written in C++ and Python for the analysis of partial differential equations (PDEs) and PDE-constrained optimization problems on unstructured meshes with state-of-the-art numerical methods." [17]. For this project, the incompressible RANS solver of SU2 is used as the RANS solver solves for the Reynolds stresses which are needed for the turbulence modeling of the flow for this project. The incompressible solver has been chosen because the flow is incompressible due to M_∞ being below 0.3 for this project [2].

3.1.2 Configuration files

The configuration file used for the no VG case is taken from the SU2 tutorial: "Incompressible turbulent flat plate" github [18]. As explained above, the solver is set to the incompressible RANS solver. Additional changes made to that configuration file are that the turbulence model is set to SST, the option that specifies a velocity inlet profile is set to "ON" (inlet profiles are explained in section 3.1.4), ρ is set to 1.204 kg/m^3 and μ is set to 1.825e-05 $(N * s)/m^2$.

The same configuration file is used for the case when there is a VG but with more changes to it. Because the mesh of the no VG case is 2D and the mesh of the case with VG is 3D, more markers need to have boundary conditions specified [19] in the configuration file for the case where there is a VG. For the 3D mesh, there are 7 markers: inlet, outlet, left, right, top, bottom, and vg. The "Inlet" boundary condition is assigned to the inlet marker, the "Outlet" boundary condition is assigned to the top, left, right, and outlet markers. The "Outlet" boundary condition is set to be as a pressure outlet with the pressure set to 0. Finally, the constant heatflux (no slip) wall marker option with heatflux=0 is assigned to the bottom and vg markers. One of the used configuration files for the case with VG can be seen in Appendix A.

3.1.3 Mesh files

The 545x385 mesh file from the SU2 tutorial: "Incompressible turbulent flat plate" github is used as mesh for the case when there is no VG [18]. This 2D mesh has 208896 elements and 209825 points. The length of the mesh is 2.33 meters and the height is 1 meter.

For the case when there is a VG, a mesh file is given by the EFD research group of the University of Twente. As explained in section 3.1.2, the 3D mesh file has 7 markers which can be seen visualized in figure 4. The 3D mesh file has 2283336 elements and 2341094 points. The length of the mesh is 1.3 meters, the width of the mesh is 0.8 meters and the height is 0.5 meters. The trailing edge of the VG is located at [0.2403,0.00562,-0.25] meters. The height of the VG is 0.05 m. The β angle of the VG is 12°.

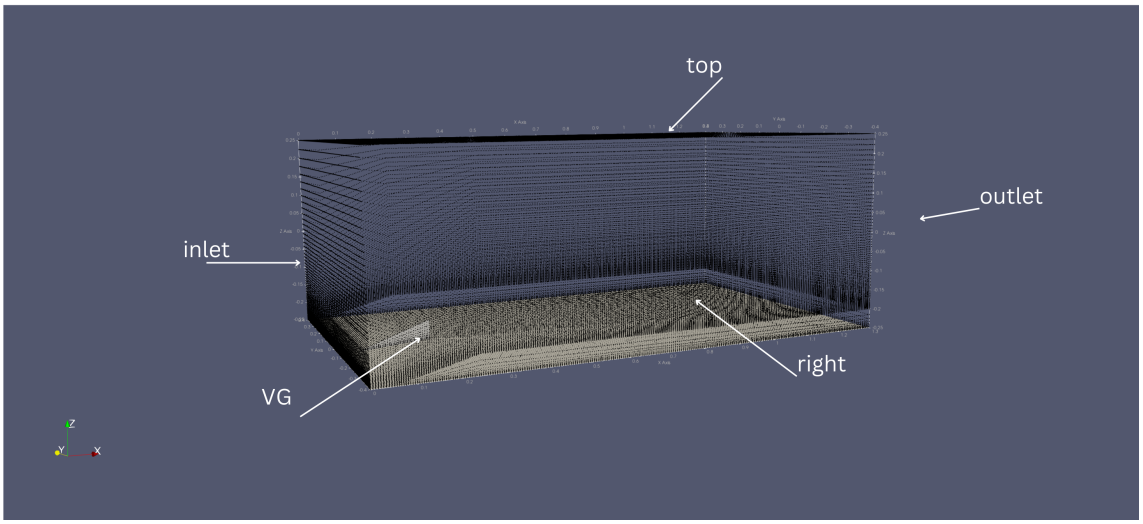

Figure 4: Mesh domain for the VG on flat plate case (the "left" marker grid is the grid opposite to the "right" marker grid and the "bottom" marker is underneath the "vg" marker

3.1.4 Inlet profiles

The inlet profile file for the SU2 specified velocity inlet profile using the SST turbulence model, consists of the following data: The coordinates of the inlet grid points of the corresponding mesh, T, the velocity magnitude, the normal vector components of the flow, k and ω. The T for all points of the mesh is set to 0K as T does not matter since the density of the flow does not change due to it being incompressible. The normal vector components are set so that the flow, flows in parallel to the x direction. k and ω are calculated using equations 8 and 9 using the data acquired from the experimental measurements. For the velocity magnitude, k, and ω, experimental data has been interpolated/extrapolated for each inlet grid mesh point using MATLAB's pchip command [20]. For interpolation, linear interpolation has been used so that the data curves are not smoothed out, as that would take away the turbulence fluctuations of the turbulent flow. For extrapolation, the maximum value for each corresponding data variable has been assigned to the inlet grid mesh points that were applicable for extrapolation.

The experimental data measured by Y.Bay [9], had 3 different types of inlet profiles. This means that for each mesh there are 3 inlet profiles. The 3 cases of inlet profiles are: the inflow is not tripped ("free"), the inflow is tripped by an 8mm zigzag tape ("8mm"), and the inflow is tripped by a 12mm zigzag tape("12mm). For each experimental inflow case, 3 measurements are taken. For the inlet profiles made for the CFD configuration, the mean of these experimental measurements has been taken for all variables that are interpolated/extrapolated. The resultant data arrays from taking the mean are used for the interpolation/extrapolation. A zoomed-in velocity profile acquired from using interpolation/extrapolation can be seen in figure 5. The mean velocity profiles and interpolated/extrapolated velocity profiles are shown in Appendix A.

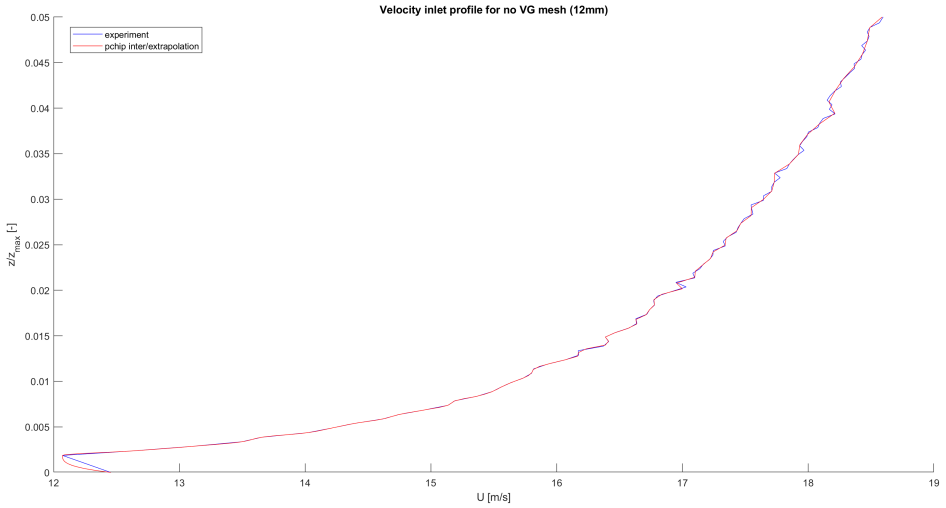

Figure 5: Interpolated inlet velocity profile for the 12mm trip inlet (Zoomed in)

3.2 Post processing

3.2.1 Airflow data extraction/visualization

Paraview [21] was used during this project to extract and visualize the airflow data generated by SU2. Within Paraview the gradients and curl of the velocity are calculated through a "pythoncalculator" filter. To visualize the vortex created by the VG, a threshold filter is applied in which the x-component of Ω needs to be 50 or higher.

3.2.2 Experimental Domain

The experimental results from Y.Bay [9] are analyzed using a different domain from the 3D mesh grid used in this project. The experimental domain has a length of 0.3 meters, a width of 0.16 meters, and a height of 0.15 meters. The coordinates of the trailing edge of the VG for the experimental domain are [-154.5,-154.5,23.53] mm. The h_{vg} is the same as the 3D mesh domain which is 0.05m and the β angle of the VG is 12°. Because the coordinates of the trailing edge of the VG of the computational domain are different compared to the experimental domain, a coordinate transformation needs to be used to make sure that the computational domains are in line with the experimental domain:

Computational coordinates	Transformations
$x_{computational}$	$(X_{experimental}/1000) + 0,3948$
$y_{computational}$	$0,02914 - (Z_{experimental}/1000)$
$z_{computational}$	$(Y_{experimental}/1000) - 0,0955$

Table 1: Coordinate transformation

For the 2D mesh, the x-coordinate transformation is chosen for the x-coordinates. For the y-coordinates, the following equation is used: $y_{computational} = arc_{length}(Y_{experimental})$. The results in Chapter 4 will be shown in the experimental coordinates.

3.2.3 Boundary Layer Properties

For all boundary layer properties, the equations shown in Chapter 2 are used. To determine δ three methods are used.

1: Vorticity
The first method is by applying a threshold for Ω. The boundary layer is reached when the Ω magnitude reaches a certain threshold that is in relation to the maximum Ω magnitude. For this project, it is chosen that δ is observed at the first point after the maximum Ω magnitude is reached when the following threshold holds:

$$\Omega < 0.001 * \Omega_{max} \tag{10}$$

2: Turbulent shear stress The second method is also by applying a threshold, but now for τ_t. As explained in Chapter 2, τ_t should equal/be close to 0 at the boundary layer edge. For this project, it is chosen that δ is observed at the last point where the following threshold holds:

$$\tau_t > 0.005 * \tau_{t_{max}} \tag{11}$$

The xy-component of τ_t is used for the case without VG and the xz-component of τ_t is used for the case with VG. This is calculated using equation 4.

3: Mean of both methods The third method is taking the mean between the δ observed from Ω and τ_t. The conclusions from the results will be drawn from this method.

4 Results

4.1 Vortexes

For the results, 3 different experimental z-coordinates are analyzed. These 3 coordinates are: z=-40mm, z=0mm, and z=40mm. These z-coordinates are chosen because the influence of the vortexes for each of these coordinates looks different when going downstream of the flat plate, from looking at figures 6,7,8. For each figure, 3 red lines are drawn which show the z=-40mm, z=0mm, and z=40mm lines from the top down in this order. Looking at the vortex after x=0.25 m, it can be seen that for z=-40mm the vortex reaches the z-coordinate further downstream compared to the other coordinates. For z=0mm, there is no vortex influence for a small distance, but after that distance, the z=0mm coordinate is constantly within the presence of the vortex. For z=40mm it can be seen that in the beginning it is within the presence of the vortex, but further downstream there is no influence of the vortex to the z=40mm coordinate. It also seems like the vortex created for the "12mm" inlet case is smaller compared to the vortexes of the other inlet cases.

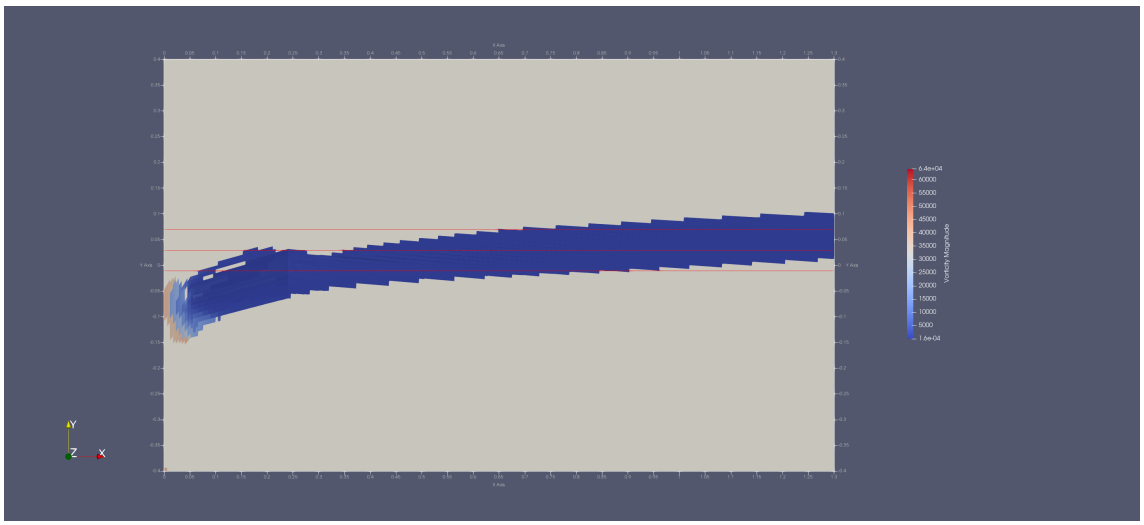

Figure 6: Vortex created by VG visualized for the "free" inlet case (axis coordinates are in computational coordinates)

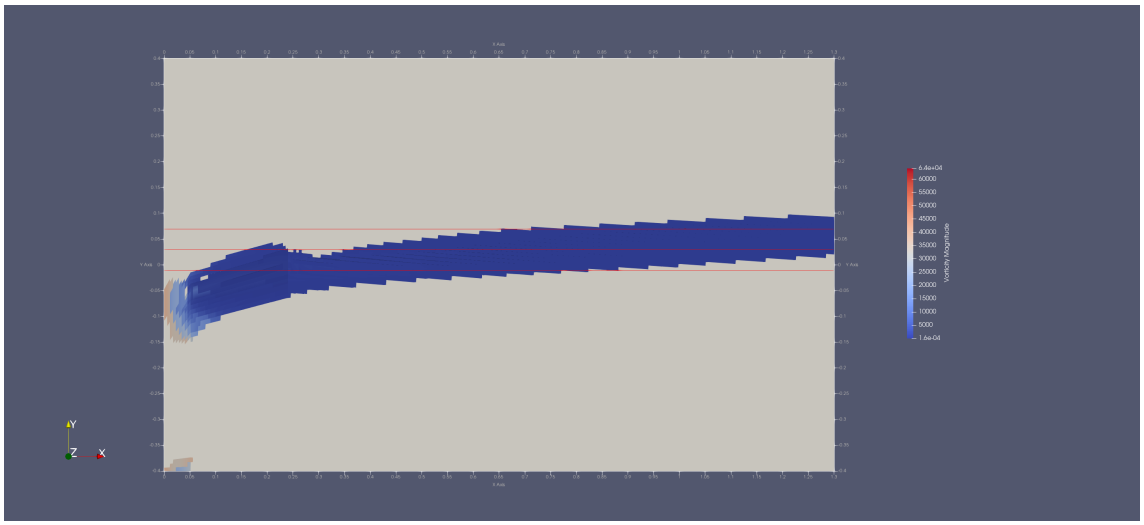

Figure 7: Vortex created by VG visualized for the "8mm" inlet case (axis coordinates are in computational coordinates)

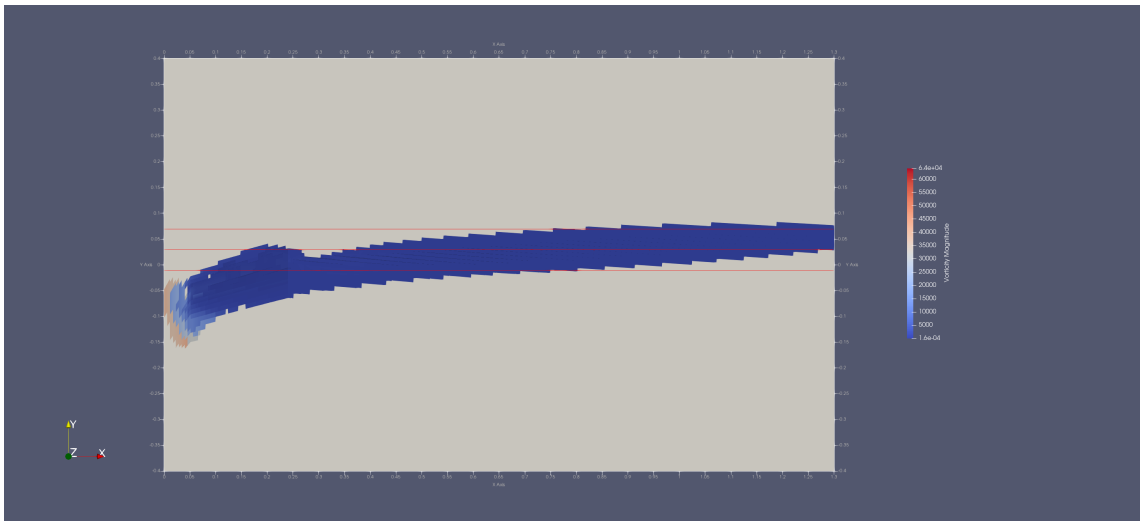

Figure 8: Vortex created by VG visualized for the "12mm" inlet case (axis coordinates are in computational coordinates)

4.2 Velocity profiles

4.2.1 z=-40mm

From figures 9,10 and 11 it can be seen that the velocity profiles do not differ that much between the noVG and VG case upstream of the flat plate. The velocity profiles for z=-40mm in Appendix B show that further downstream, the velocity profiles for the case with VG have an increased velocity gradient close to the wall, "curve" back a bit, and then stabilize back to U_∞. The change in the velocity profiles is around the same x-coordinates as where the vortex starts to influence the z=-40mm coordinate.

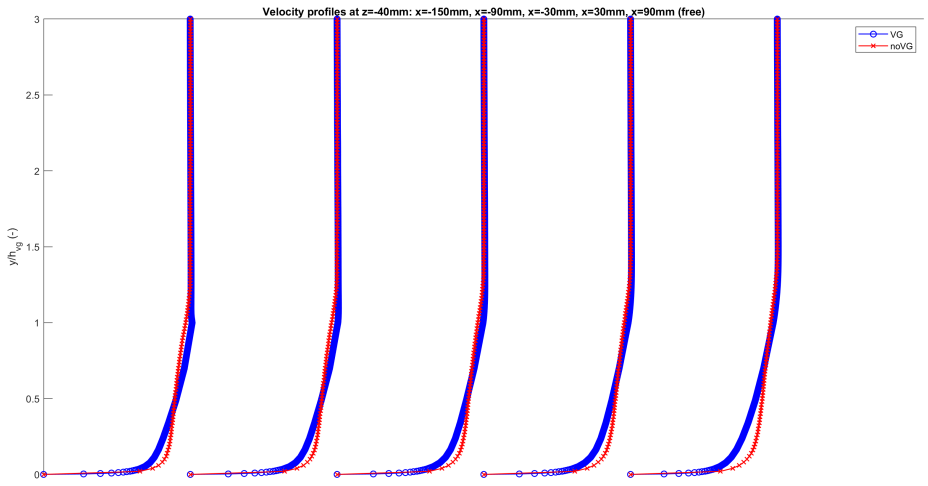

Figure 9: Velocity profiles comparison between the VG and noVG case for the experimental setup's domain at z=-40mm ("free" inlet)

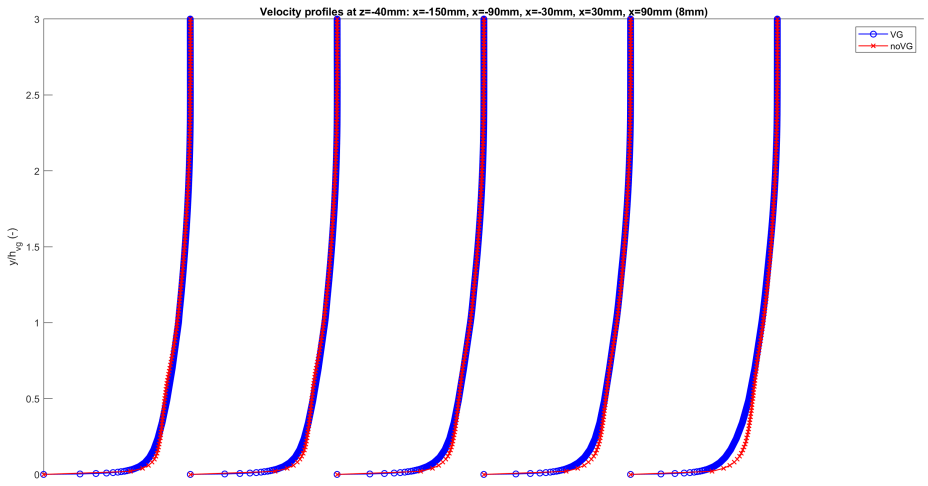

Figure 10: Velocity profiles comparison between the VG and noVG case for the experimental setup's domain at z=-40mm ("8mm" inlet)

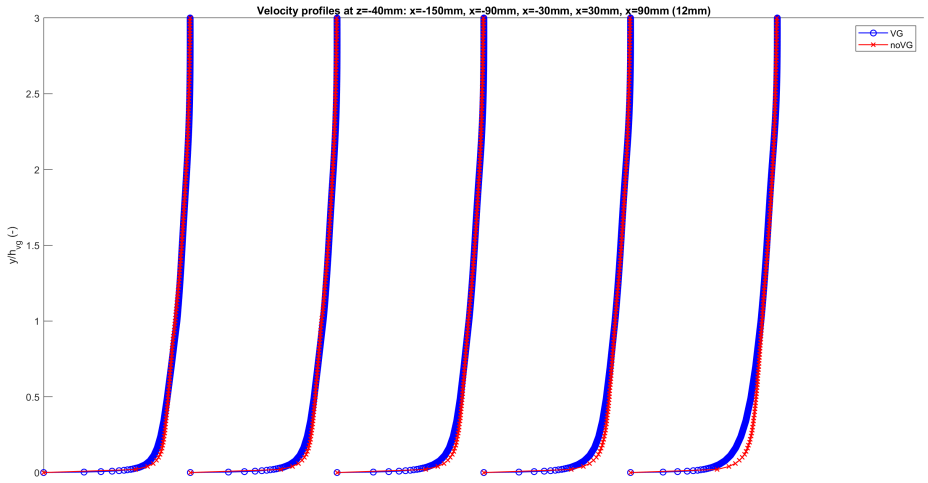

Figure 11: Velocity profiles comparison between the VG and noVG case for the experimental setup's domain at z=-40mm ("12mm" inlet)

4.2.2 z=0mm

From figures 12,13 and 14 it can be seen that the velocity profiles are getting an increase of the velocity gradient closer to the wall much earlier than for the z=-40mm coordinate. This is as expected as the z=0mm is within the presence of the vortex much earlier. In Appendix B for z=0mm, it can be seen for all inlet cases that the velocity gradient becomes steeper after the z=0mm coordinate is in the presence of the vortex for the VG case compared to the noVG case.

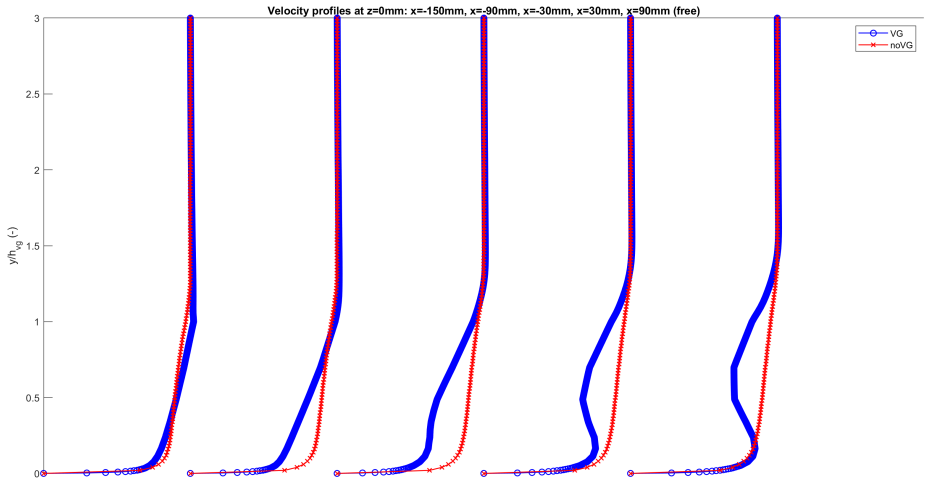

Figure 12: Velocity profiles comparison between the VG and noVG case for the experimental setup's domain at z=0mm ("free" inlet)

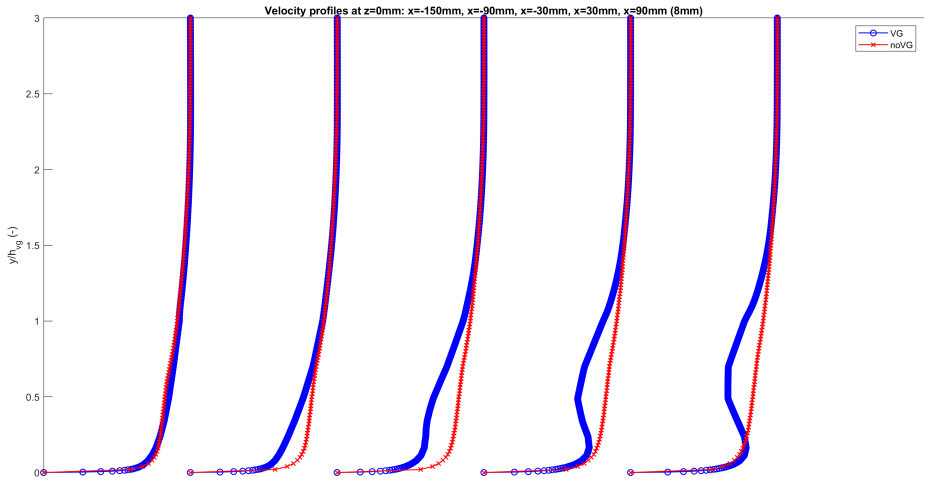

Figure 13: Velocity profiles comparison between the VG and noVG case for the experimental setup's domain at z=0mm ("8mm" inlet)

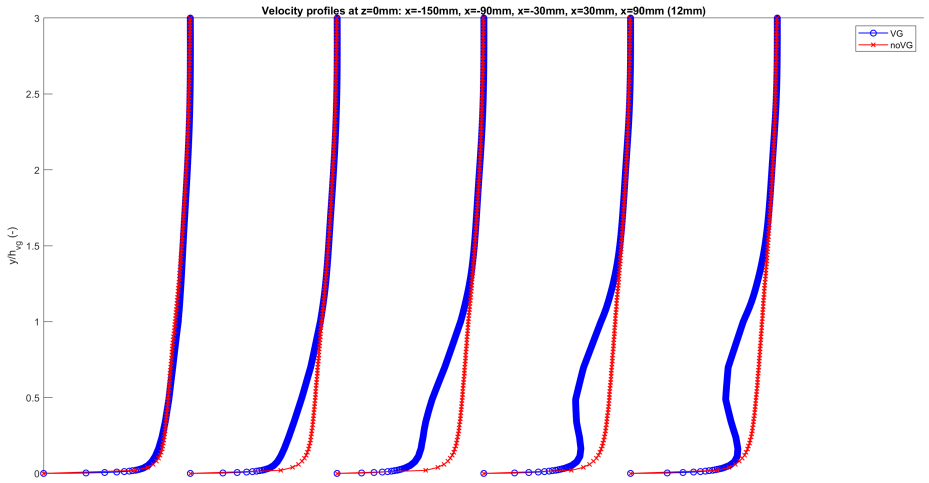

Figure 14: Velocity profiles comparison between the VG and noVG case for the experimental setup's domain at z=0mm ("12mm" inlet)

4.2.3 z=40mm

By looking at figures 15,16 and 17 it can be seen that the velocity profiles for the case with VG are already deformed, as the z=40mm coordinate line is already within the vortex. Just like for the other z-coordinates, by looking at the velocity profiles for z=40mm in Appendix B, it can be seen that the velocity gradient becomes steeper for the case with VG due to the presence of the vortex.

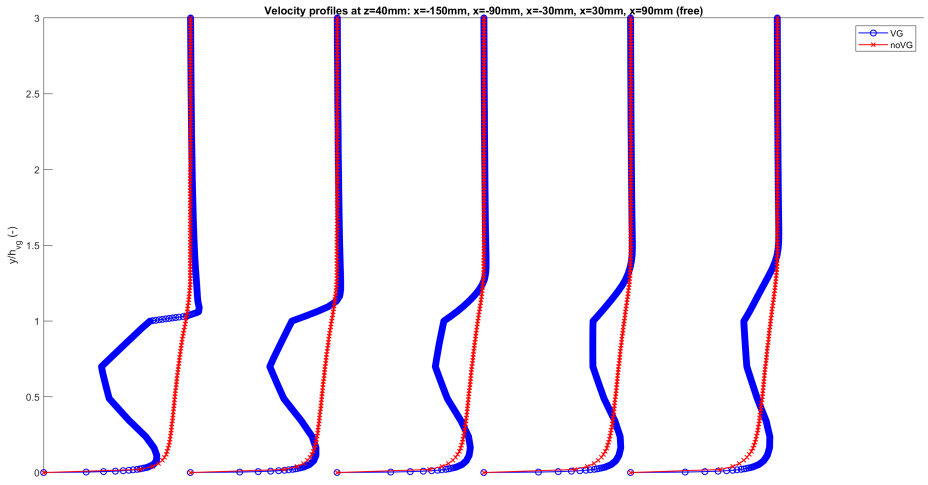

Figure 15: Velocity profiles comparison between the VG and noVG case for the experimental setup's domain at z=40mm ("free" inlet)

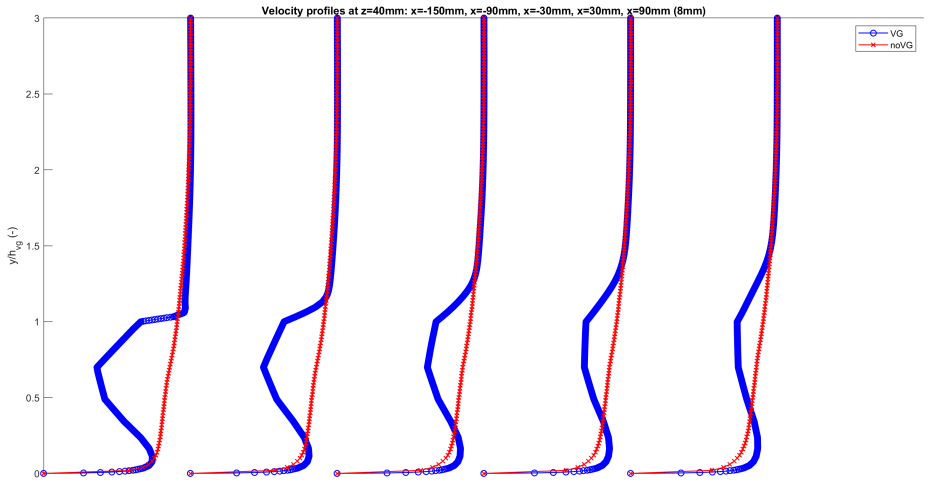

Figure 16: Velocity profiles comparison between the VG and noVG case for the experimental setup's domain at z=40mm ("8mm" inlet)

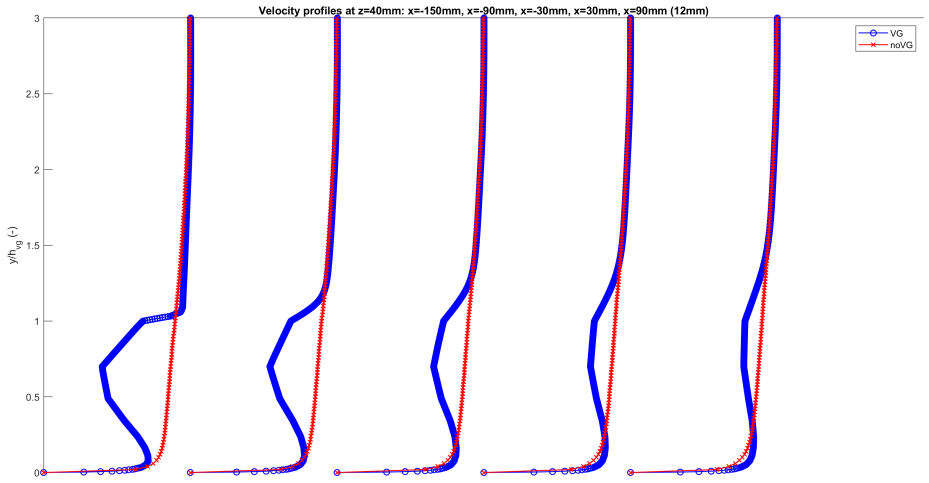

Figure 17: Velocity profiles comparison between the VG and noVG case for the experimental setup's domain at z=40mm ("12mm" inlet)

4.3 Boundary Layer properties

4.3.1 z=-40mm

In figures 18,19 and 20 it can be seen that after the z=-40mm coordinate is within the presence of the vortex, that δ, δ^*, and θ are getting bigger. δ for the "free" and the "8mm" inlet case becomes bigger for the case where there is a VG compared to the case without VG, and for the inlet case "12mm" is δ for the case without VG bigger than the case with VG. For all 3 different inlet cases, it can be seen that δ^* and θ are bigger for the case with VG than for the case without VG. It can be seen that the H value peaks, but then its value becomes lower again. The H value for when there is a VG becomes lower than the case for when there is no VG, only for the "free" inlet case. The H values for both the: with/without VG cases are within the turbulent flow region [22].

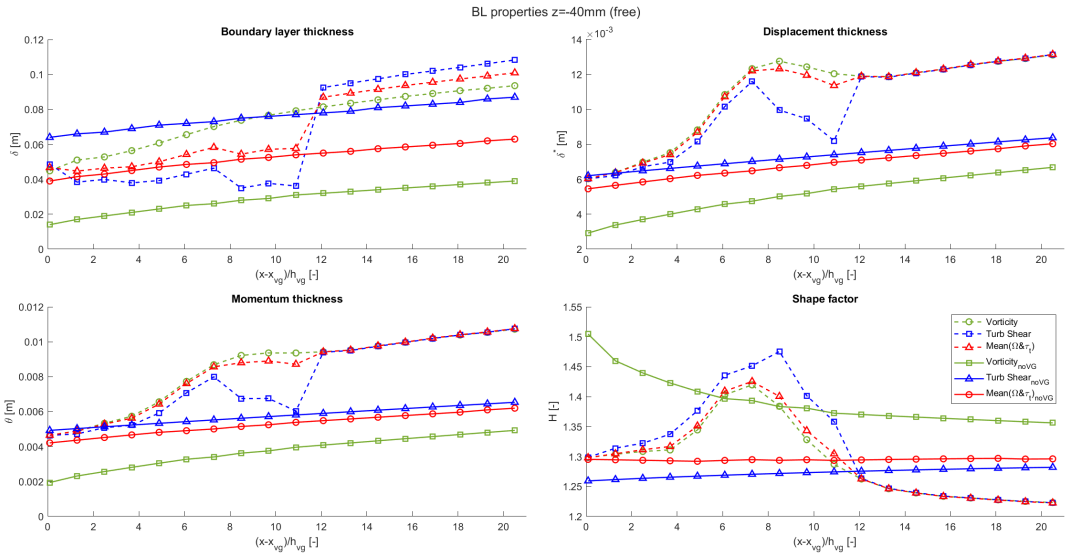

Figure 18: Boundary Layer properties for both the VG and noVG cases at z=-40mm ("free" inlet)

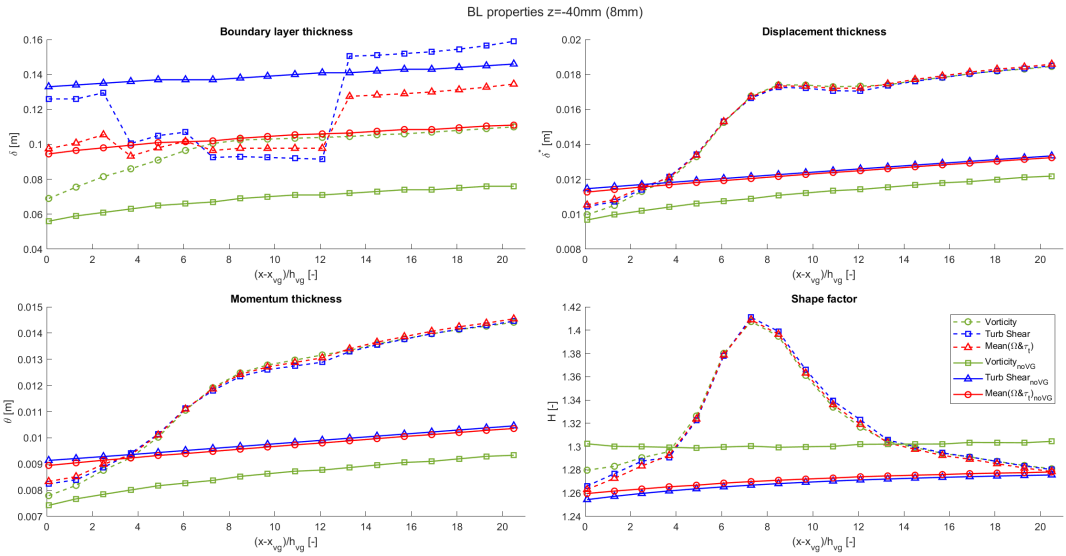

Figure 19: Boundary Layer properties for both the VG and noVG cases at z=-40mm ("8mm" inlet)

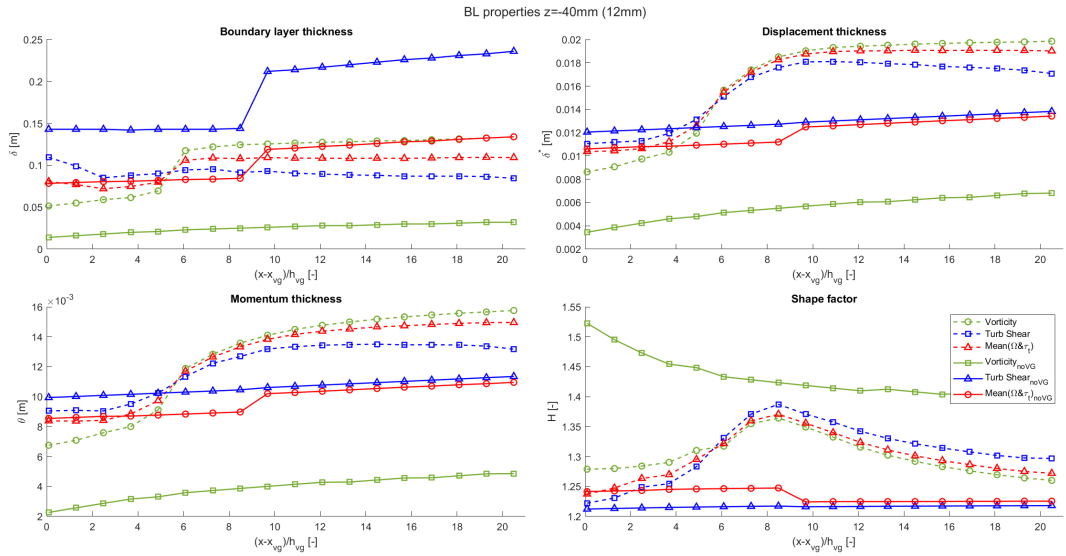

Figure 20: Boundary Layer properties for both the VG and noVG cases at z=-40mm ("12mm" inlet)

4.3.2 z=0mm

Looking at the results from figures 21, 22 and 23, it can be seen that δ^*, θ, and H almost instantly increases for the case with VG. This is as expected by looking at the velocity profiles for z=0mm. δ has an increase a bit later, further downstream. Just like for the results of z=-40mm, the δ for the "free" and "8mm" inlet cases becomes bigger for the case with VG compared to δ for the case without VG. δ^* and θ become bigger for the case with VG compared to the case without VG, for all inlet cases. It can be seen that H for the case with VG becomes less compared to the case without VG. But for the "8mm" and "12mm" inlet cases it can be seen that H for the case with VG becomes less than the H value for the case without VG further downstream of the flat plate, compared to the "free" inlet case. The H values for both the: with/without VG cases are within the turbulent flow region [22].

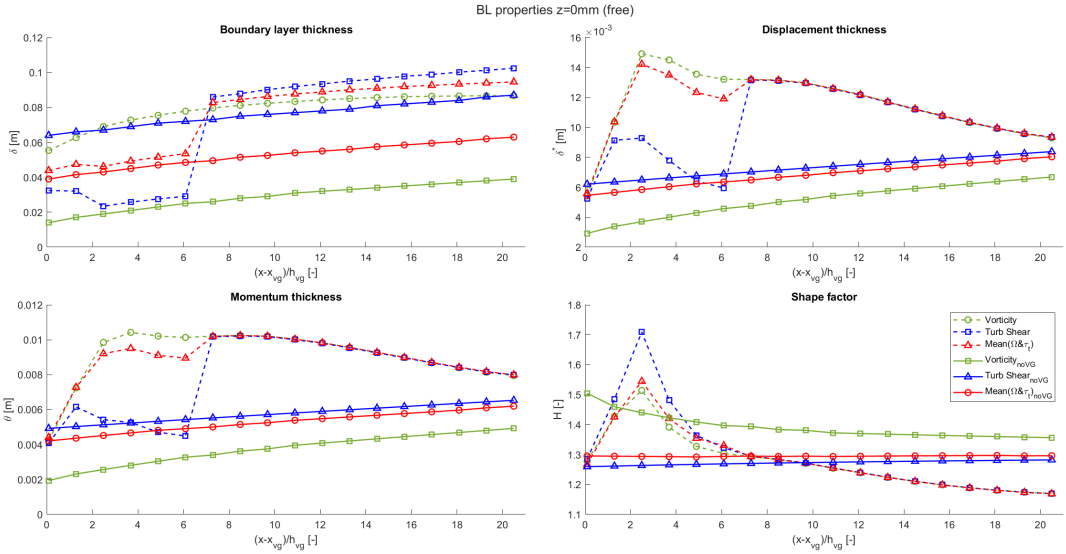

Figure 21: Boundary Layer properties for both the VG and noVG cases at z=0mm ("free" inlet)

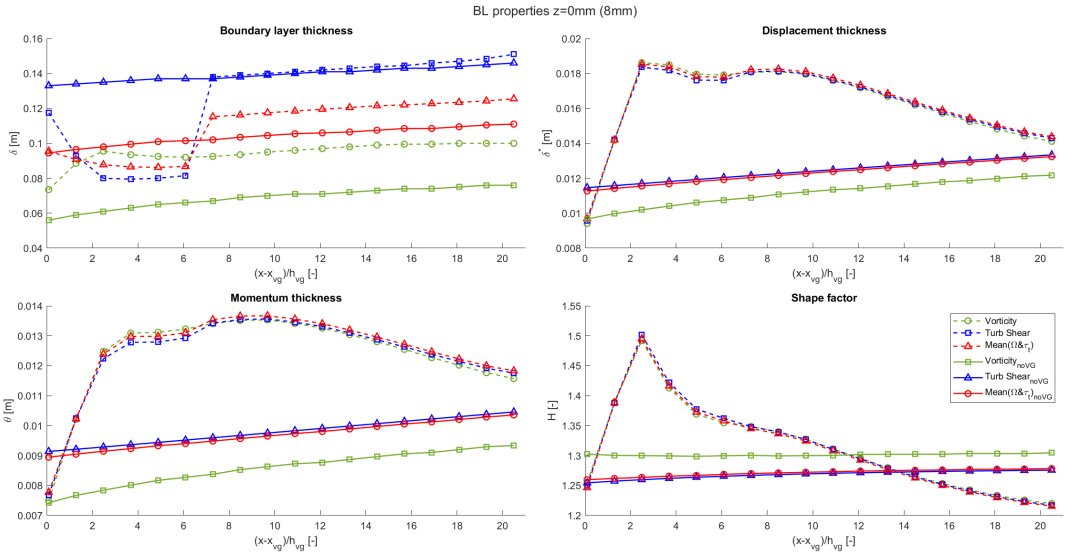

Figure 22: Boundary Layer properties for both the VG and noVG cases at z=0mm ("8mm" inlet)

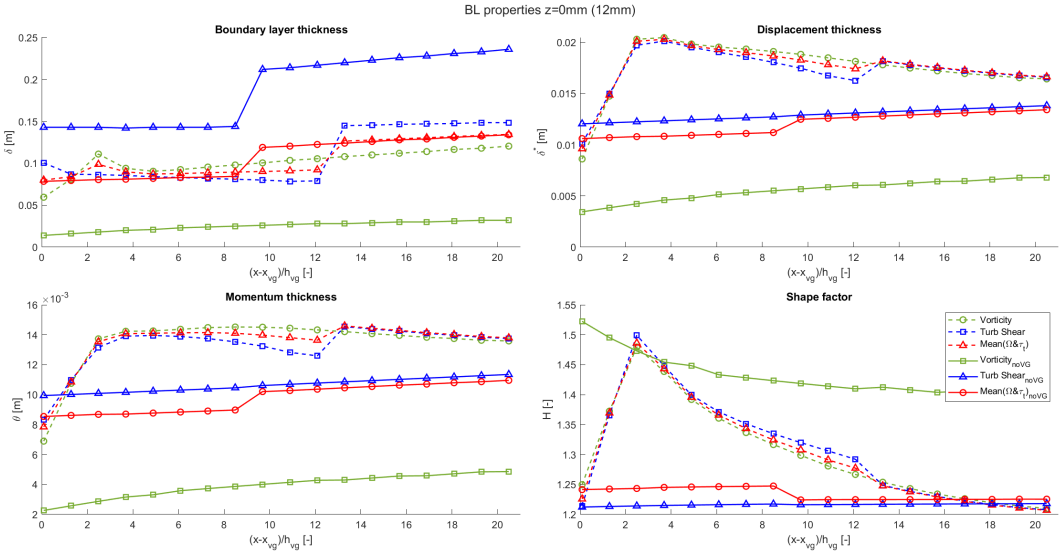

Figure 23: Boundary Layer properties for both the VG and noVG cases at z=0mm ("12mm" inlet)

4.3.3 z=40mm

It is seen in figures 24, 25 and 26, that δ for all inlet becomes bigger for the case with VG compared to the case without VG, but going further downstream the δ for the case with VG becomes less than the δ for the case without VG. The same can be said for the δ^* and θ. While δ^* and θ become lower for the case with VG compared to the case without VG, the H value of the case with VG becomes lower than the H value for the case without VG. This means that in the case with VG, more momentum is being transferred than mass flow being displaced compared to the case without VG. The H values for both the: with/without VG cases are within the turbulent flow region [22].

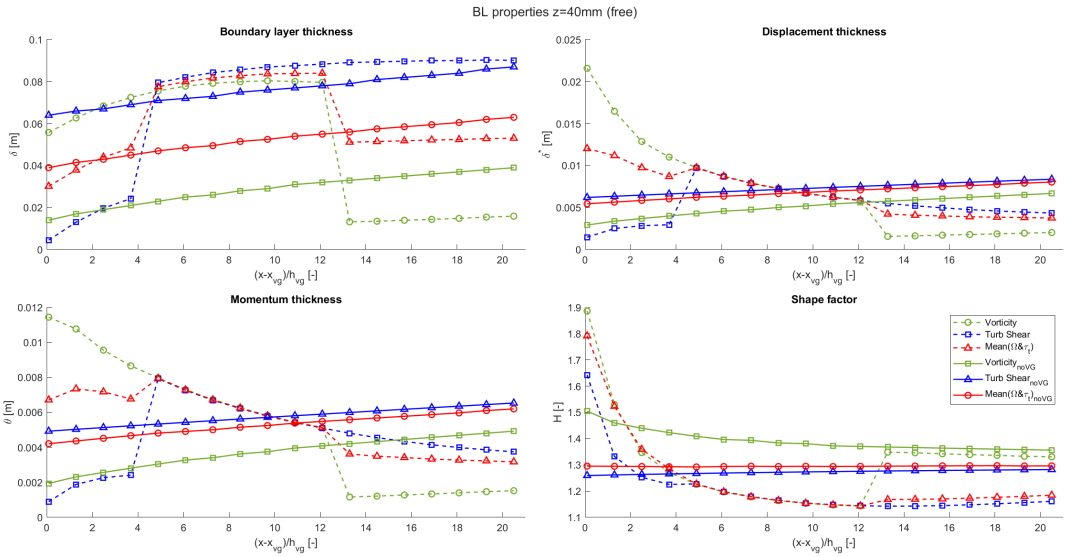

Figure 24: Boundary Layer properties for both the VG and noVG cases at z=40mm ("free" inlet)

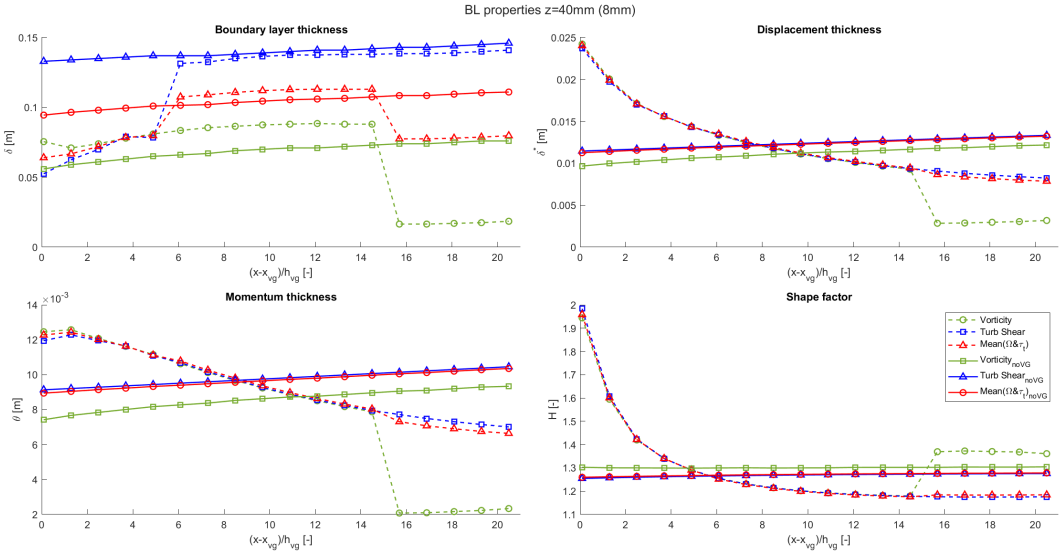

Figure 25: Boundary Layer properties for both the VG and noVG cases at z=40mm ("8mm" inlet)

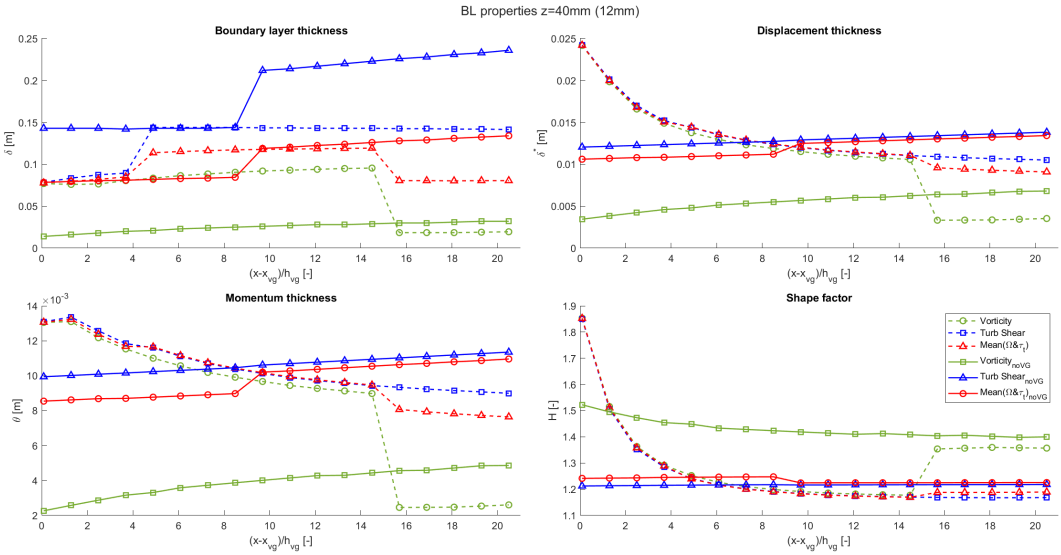

Figure 26: Boundary Layer properties for both the VG and noVG cases at z=40mm ("12mm" inlet)

4.4 Experiment comparison

4.4.1 Velocity Profiles z=-40mm

The velocity profile comparisons between VG and experiment for z=-40mm can be seen in figures 27, 28 and 29. It can be seen that there is not much difference between the velocity profiles. However, for x=-150mm there is a difference between the SU2 VG data and the experimental data. Where close to the wall, there is a slight curve back for the experimental data.

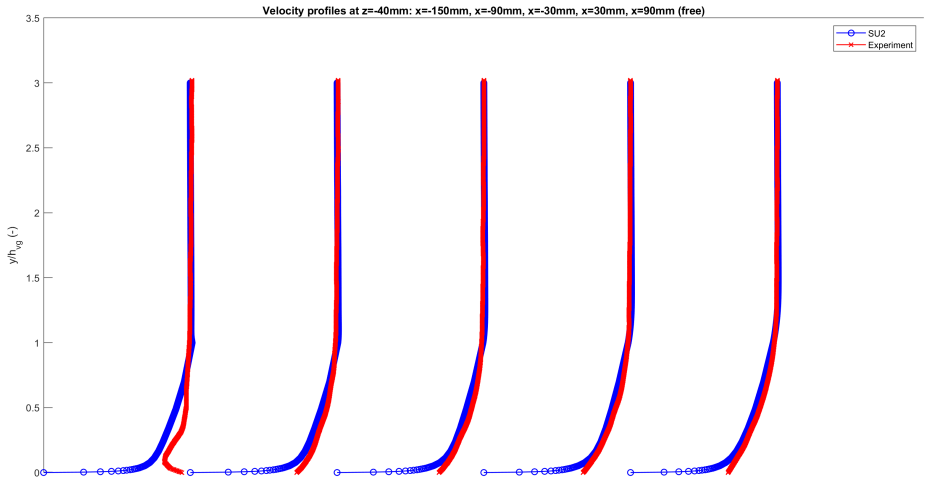

Figure 27: Velocity profiles comparison between SU2 and experimental data at z=-40mm ("free" inlet)

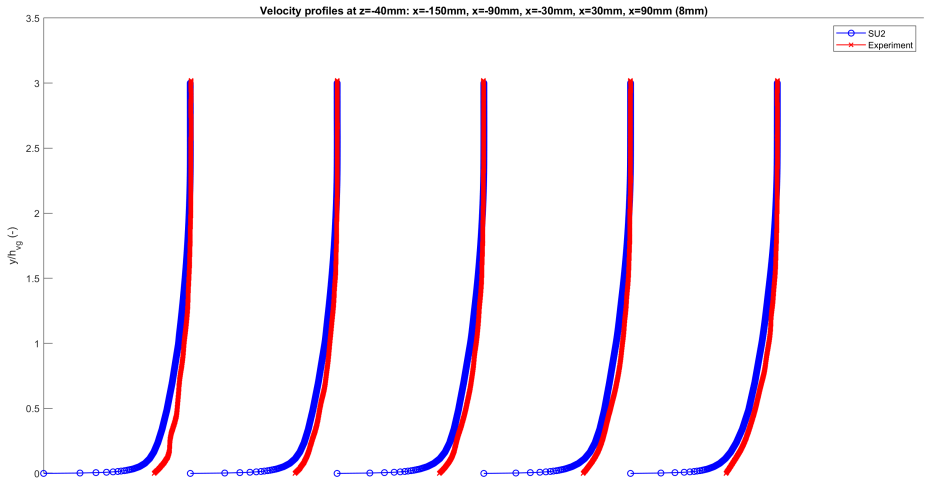

Figure 28: Velocity profiles comparison between SU2 and experimental data at z=-40mm ("8mm" inlet)

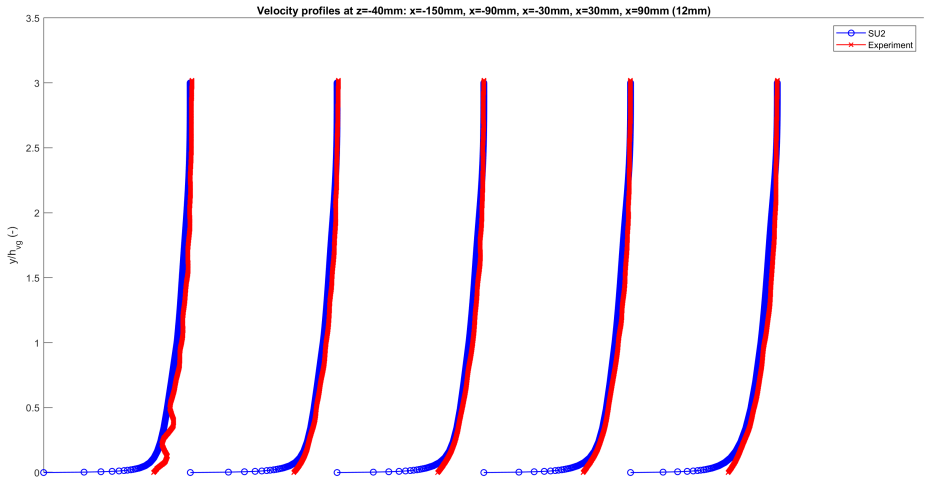

Figure 29: Velocity profiles comparison between SU2 and experimental data at z=-40mm ("12mm" inlet)

4.4.2 Velocity Profiles z=0mm

From figures 30, 31 and 32 can be seen that there is a difference between the velocity profiles generated by SU2 and the experimental data. While there is a difference, there is also a similarity between the shapes of the velocity profiles in which the velocity gradient close to the wall gets steeper, and then the velocity profile curves back and stabilizes back to U_∞.

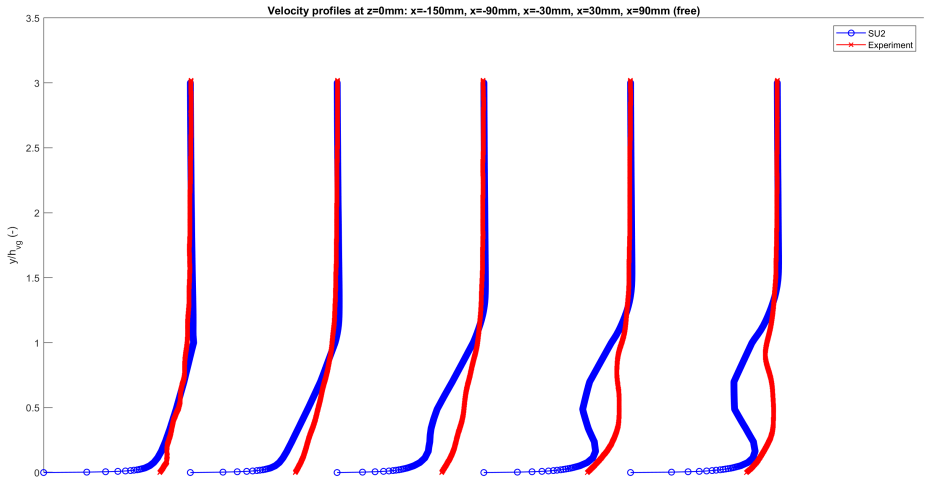

Figure 30: Velocity profiles comparison between SU2 and experimental data at z=0mm ("free" inlet)

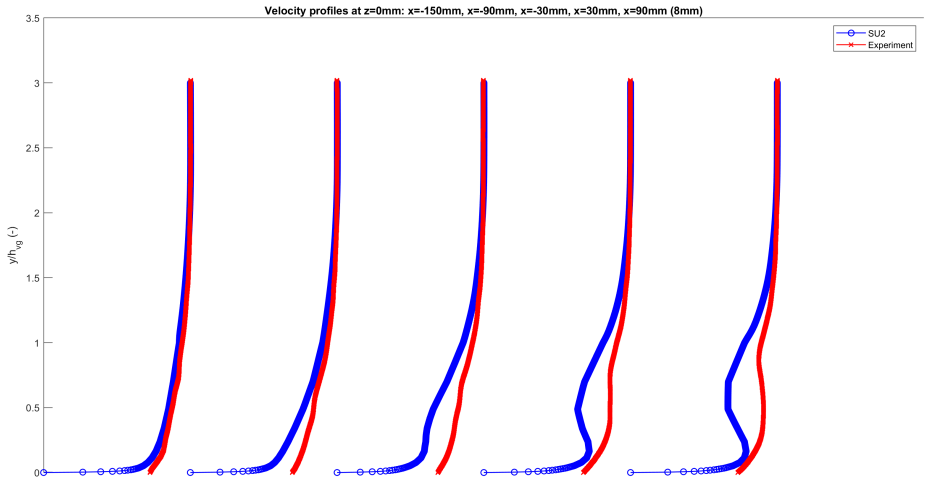

Figure 31: Velocity profiles comparison between SU2 and experimental data at z=0mm ("8mm" inlet)

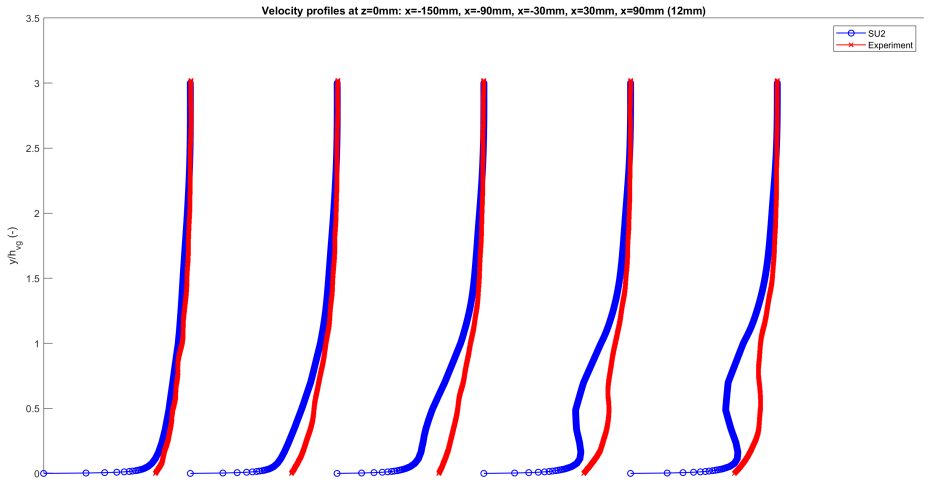

Figure 32: Velocity profiles comparison between SU2 and experimental data at z=0mm ("12mm" inlet)

4.4.3 Velocity Profiles z=40mm

It can be seen from figures 33, 34 and 35 that upstream the velocity profiles between the SU2 results and experimental data differ very much, but further downstream the shapes of the velocity profiles are more in line with each other. The velocity profiles at x=-30mm, x=30mm, and x=90mm are almost identical.

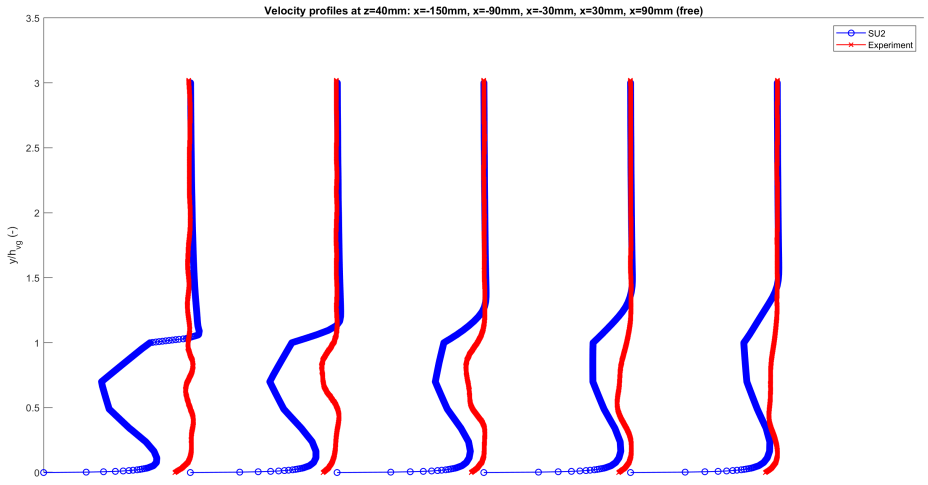

Figure 33: Velocity profiles comparison between SU2 and experimental data at z=40mm ("free" inlet)

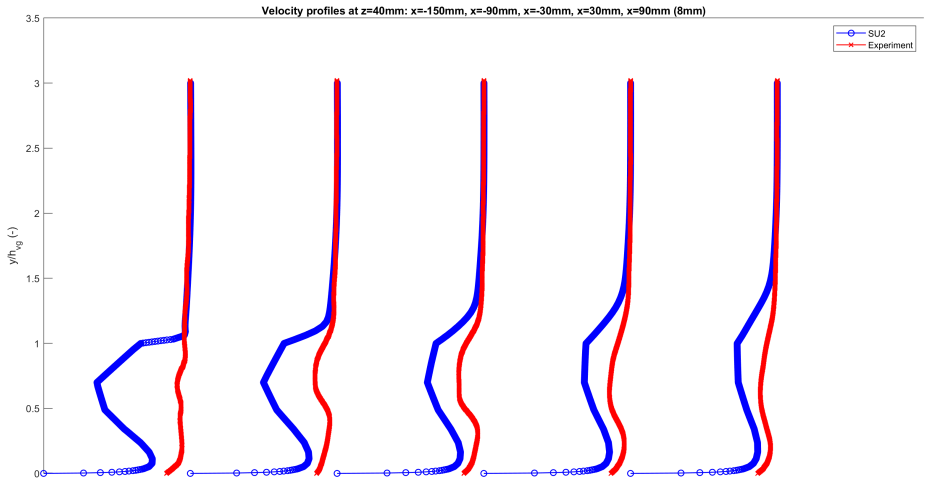

Figure 34: Velocity profiles comparison between SU2 and experimental data at z=40mm ("8mm" inlet)

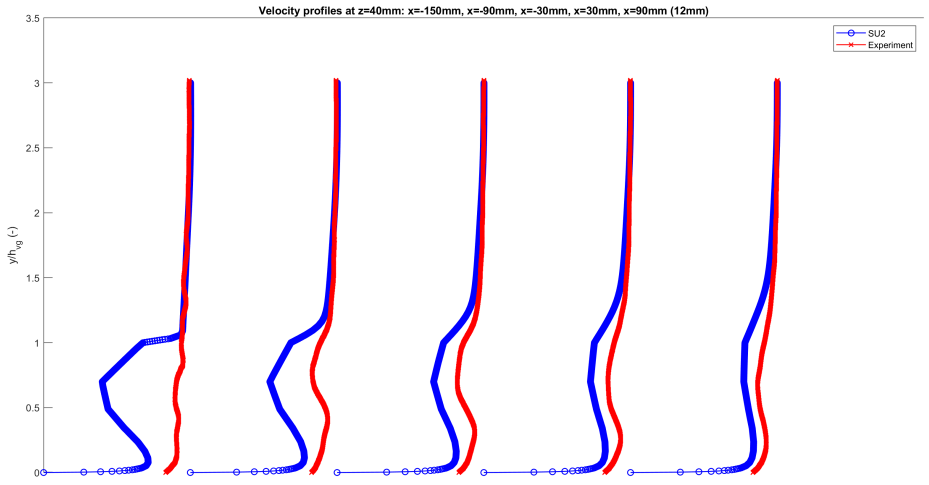

Figure 35: Velocity profiles comparison between SU2 and experimental data at z=40mm ("12mm" inlet)

4.4.4 Turbulent shear stress Profiles z=-40mm

The comparisons of the turbulent shear stress profiles between SU2 results and experimental data are shown in Appendix D. The results for z=-40mm are in sections 7.4.1, 7.4.2, and 7.4.3. From the figures in those sections it can be seen that for all inlet cases, the turbulent shear profiles from the SU2 results are different in magnitude compared to the experimental results, but there are some similarities in shape. The SU2 turbulent shear profile shapes are also in line with the theory as the turbulent shear stress eventually goes to 0. The best comparison plots for each inlet case can be seen in figures 36, 37, and 38.

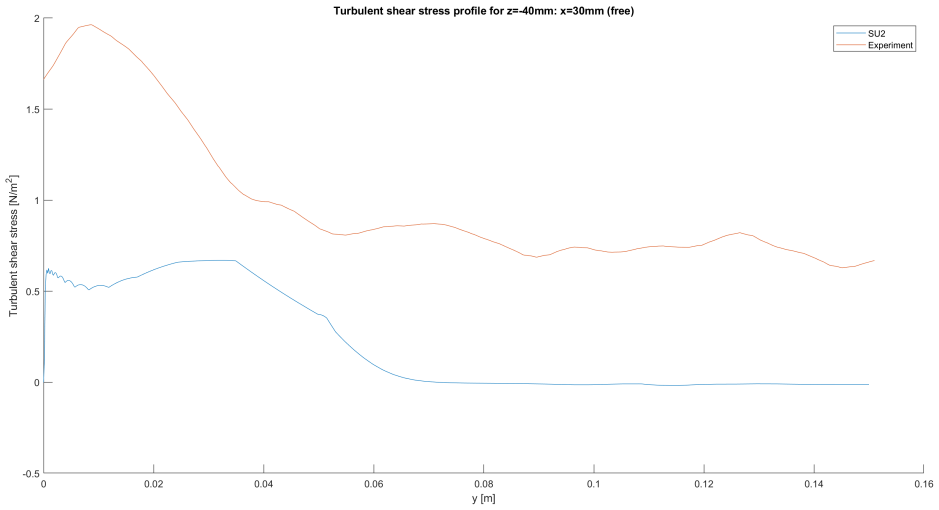

Figure 36: Turbulent shear profiles VG vs Experiment z=-40mm, x=30mm (free)

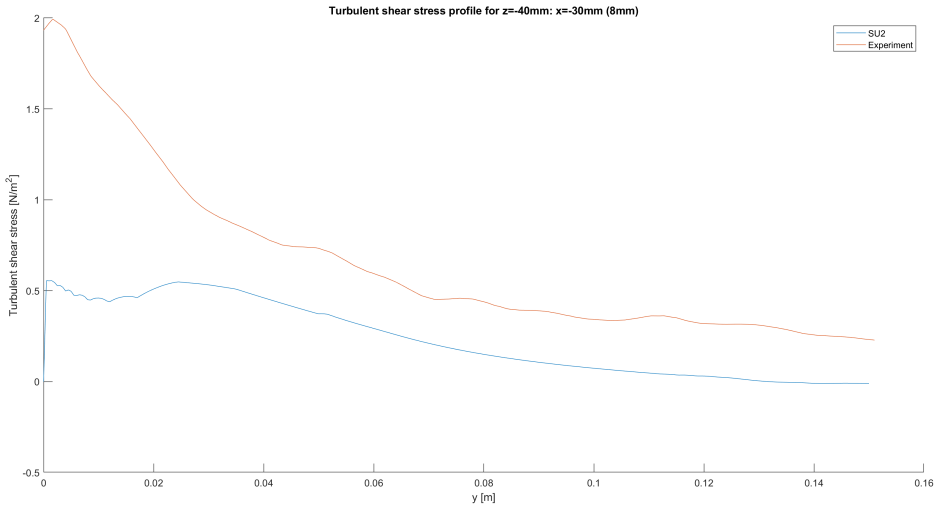

Figure 37: Turbulent shear profiles VG vs Experiment z=-40mm, x=-30mm (8mm)

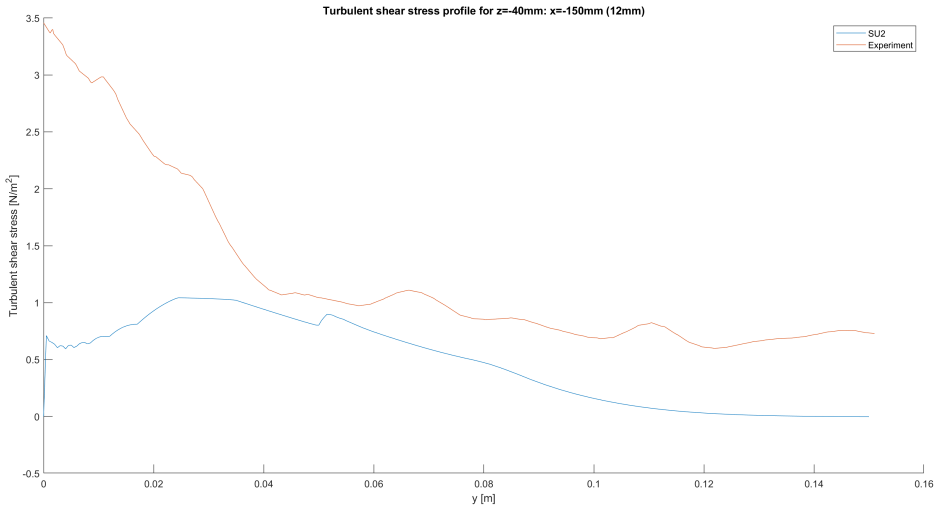

Figure 38: Turbulent shear profiles VG vs Experiment z=-40mm, x=-150mm (12mm)

4.4.5 Turbulent shear stress Profiles z=0mm

The turbulent shear stress profile comparisons for z=0mm can be found in sections 7.4.4, 7.4.5, and 7.4.6. From looking at these figures, there is a magnitude difference between the SU2 results and experimental data for all inlet cases. The turbulent shear stress profiles from the "8mm" inlet case are most similar to each other. For the "free" inlet case some turbulent shear stress profiles from SU2 results have a similar shape as the experimental results. For the "12mm" inlet case, is the difference in shape between the SU2 results and experimental results too big, and almost no similarity can be found. The SU2 results do however go to 0 for all inlet cases which is expected. The best comparison plots for each inlet case can be seen in figures 39, 40, and 41.

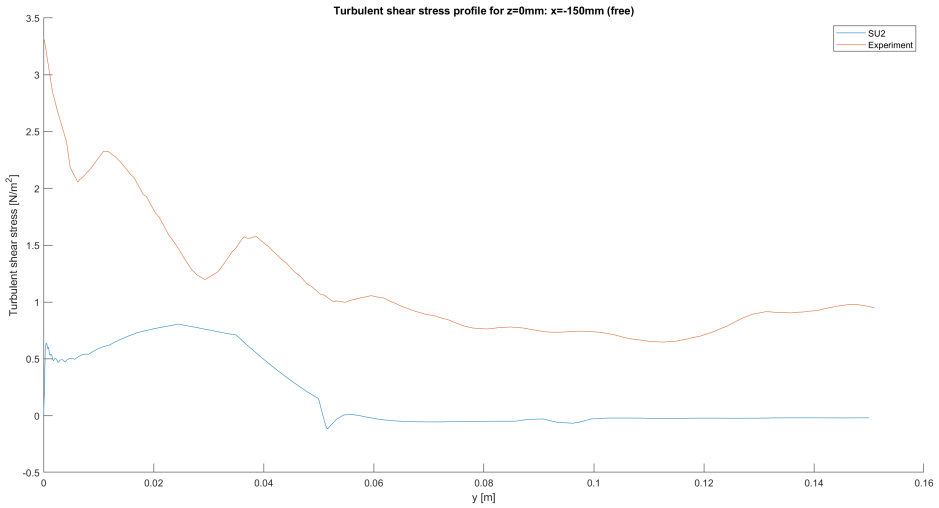

Figure 39: Turbulent shear profiles VG vs Experiment z=0mm, x=-150mm (free)

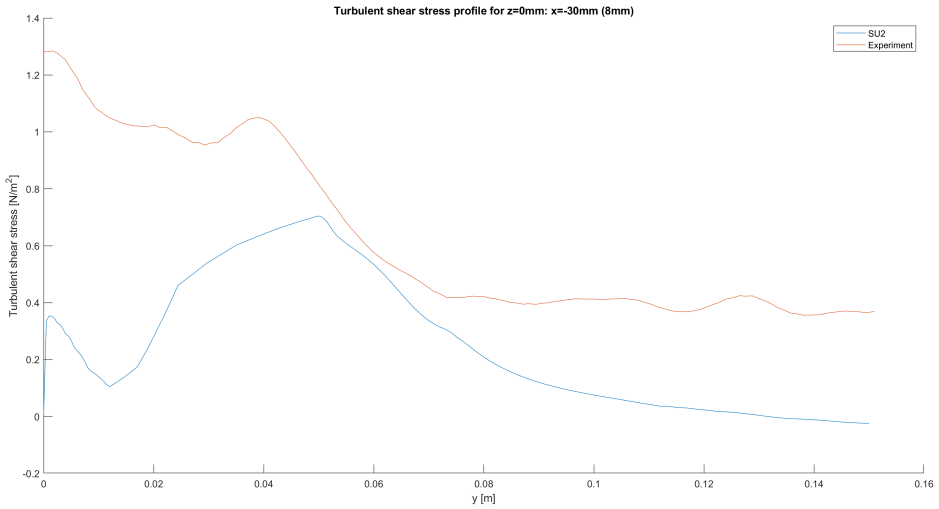

Figure 40: Turbulent shear profiles VG vs Experiment z=0mm, x=-30mm (8mm)

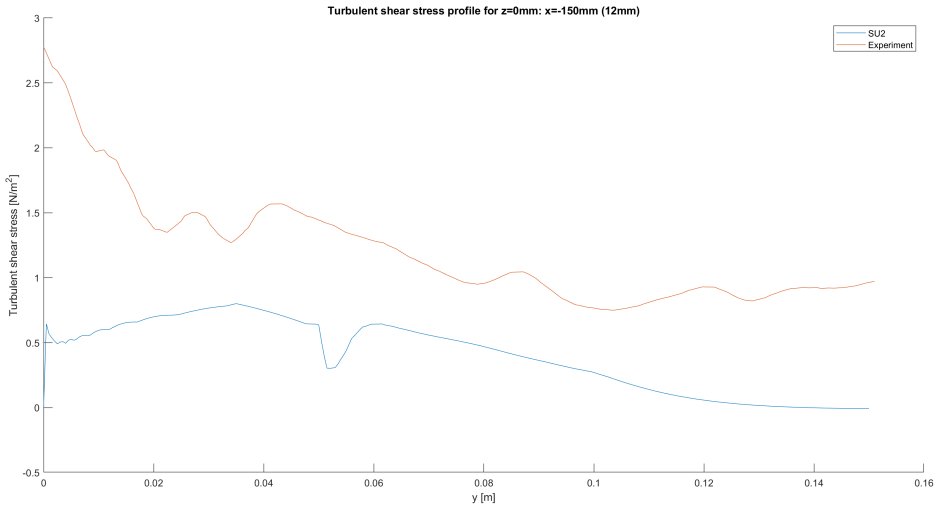

Figure 41: Turbulent shear profiles VG vs Experiment z=0mm, x=-150mm (12mm)

4.4.6 Turbulent shear stress Profiles z=40mm

The turbulent shear stress profile comparisons for z=40mm can be found in sections 7.4.7, 7.4.8, and 7.4.9. Again for all inlet cases, there is a difference in the magnitude of the turbulent shear stress profiles between the SU2 results and experimental results. However, for all inlet cases, almost all turbulent shear stress profiles from the SU2 results have similarities in shape compared to the experimental data. The SU2 results eventually go to zero which is expected. The best comparison plots for each inlet case can be seen in figures 42, 43, and 44.

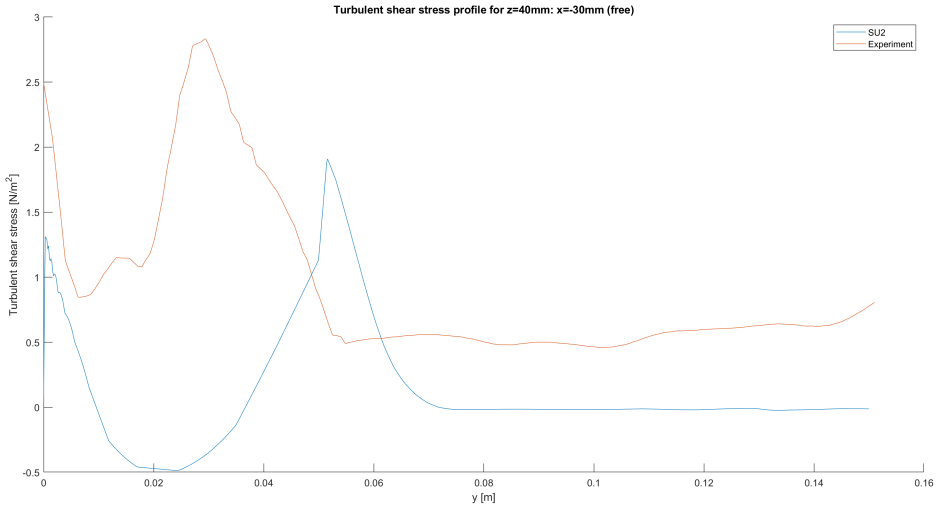

Figure 42: Turbulent shear profiles VG vs Experiment z=40mm, x=-30mm (free)

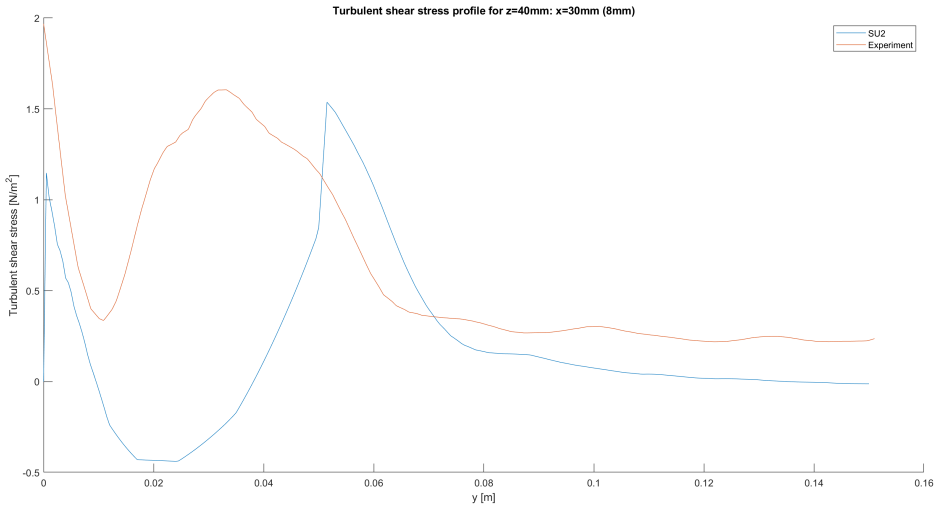

Figure 43: Turbulent shear profiles VG vs Experiment z=40mm, x=30mm (8mm)

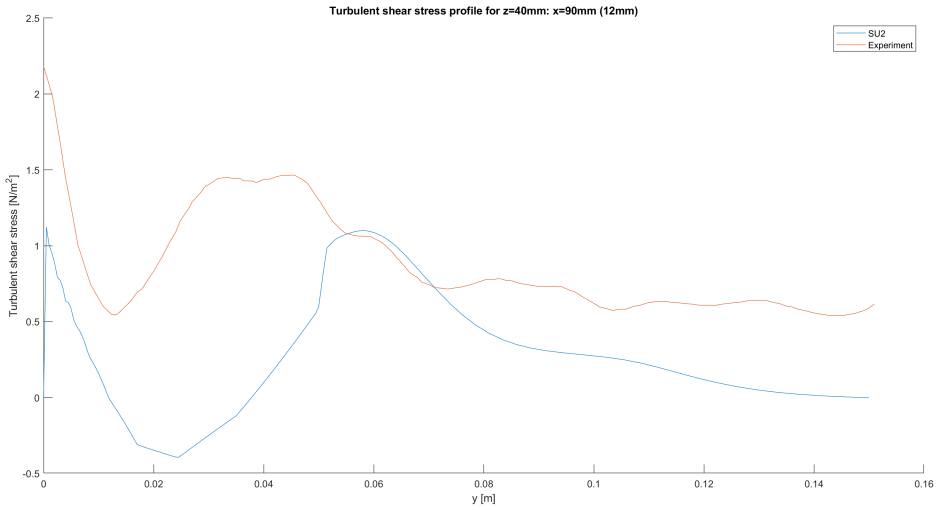

Figure 44: Turbulent shear profiles VG vs Experiment z=40mm, x=90mm (12mm)

5 Discussion

From looking at the results of Chapter 4, it can be seen that the vortex created by the VG affects the velocity profile and boundary layer properties of the flow.
It was seen that for the velocity profiles, the velocity gradient close to the wall became steeper when being closer to the vortex. As the velocity gradient close to the wall becomes steeper, then τ_w will increase which is an indication that the boundary layer has more momentum.
For δ, it could be seen that it increased due to the presence of the vortex, but for the "12mm" inlet case it seemed that the δ for the case with VG could not get higher than the case without VG. A possible explanation could be that due to the bigger tripping zigzag tape, the δ for the case without VG becomes bigger, which F.dos Santos et al concluded in their study [23], such that the effect of a VG has a small/no contribution to the increase of δ. This can also be seen from the H value comparisons for the "12mm" inlet case, where the H value with VG only becomes lower than the H value without VG far downstream of the flat plate.
δ^* and θ increased when in the presence of the vortex created by the VG. This was also seen in the studies from A.K.Ravishanara et al [8] and a confidential internship report of ECN from Steiner. J (Personal information, 2017). In section 4.3.3 it could be seen that the δ^* and θ for the case with the VG becomes lower than for the case without the VG when there is no presence anymore from the vortex. However looking at H, it could be seen that for the case with the VG, more momentum is being transferred than mass flow being displaced compared to the case without VG as the H value for the case with the VG

is lower. This would mean that the flow for the case with the VG would have more momentum being transferred to the boundary layer which would delay separation.
The velocity profiles from the SU2 results did have similar shapes compared to the experimental data, however, the velocity magnitude was a bit different and in section 4.4.3 it could be seen that close to the location of the VG the magnitude difference was really big. To understand why there is a bigger magnitude difference for z=40mm compared to the results from z=-40mm and z=0mm, further research needs to be done.
Finally, for the turbulent shear stress profile comparisons, it could be seen that there was a magnitude difference between SU2 results and experimental data. But also the shapes of the turbulent shear stress profiles from SU2 did not always have similarities compared to the experimental data. The difference in turbulent shear stress profiles could be explained since in this project only the xz-component of the Reynolds stress tensor is taken for the turbulent shear stress from SU2 results. It could be that the results from SU2 for the turbulent shear stress would be more in line with experimental data if the norm of the Reynolds stress tensor had been taken instead. To add to this, the turbulent shear stress is calculated using Boussinesq's approximation [24], which is shown to be not entirely accurate when working with Reynolds stresses [25]. However, the turbulent shear stress profiles do comply with the expectation that the turbulent shear stress eventually goes to 0.

6 Conclusion and further research

6.1 Conclusion

Within this project, the effect of a singular triangular vane VG on a turbulent flow over a flat plate was analyzed using SU2 as the CFD program. The primary objective was to find the effect of the VG on the boundary layer properties of the turbulent flow. The secondary objective was to compare the CFD results with experimental data from Y.Bay [9] to see if the velocity and turbulent shear stress profiles were in line with the real case. By looking at the results it can be concluded that the presence of the VG successfully changes the boundary layer properties of the flow, such that flow separation gets delayed. The velocity gradient near the wall is steeper and δ, δ^*, and θ are all higher and H becomes less when a VG is applied. This effect is more noticeable when the inflow is less turbulent/tripped. The turbulent shear stress profiles were in line with expectations from theory but were sometimes not similar in shape and magnitude compared to the experimental data. A possible explanation for this difference is that only the xz-component of the Reynolds stress, and Boussinesq approximation were used for the simulation results which is not accurate for magnitude. However, the turbulent shear stress profiles do comply with the theory that it eventually goes to 0. The velocity profiles from the simulation were similar in shape to the experimental data but were not similar in magnitude. To find the exact reason for this, further research needs to be done.

6.2 Further research

Further research that could be done to complement this project is to compare the effect of different shapes of singular vane VG's. Due to a different shape VG, the airflow can curl differently resulting in a different type of vortex which can have a different effect on the flow. Another interesting thing to research is to look at what happens to the turbulent flow when the β angle of the VG changes as this would change the path of the vortex created. Finally, further research can be done to look at the effect of changing the dimensions of a singular triangular vane VG on a turbulent flow over a flat plate, as this will also change the vortex created by the VG.

References

[1] aerospaceengineeringblog.com Boundary layer separation and pressure drag;. Accessed: 2024-04-05. https://aerospaceengineeringblog.com/boundary-layer-separation-and-pressure-drag/.

[2] Anderson JD. Fundamentals of Aerodynamics. McGraw-Hill series in aeronautical and aerospace engineering. McGraw-Hill Education; 2017.

[3] Energypost.eu What's stopping even bigger Wind Turbines? Blade speed and flexing? More likely manufacturing and installation capacity;. Accessed: 2024-02-13. https://energypost.eu/what-stops-us-from-building-even-bigger-wind-turbines-blade-speed-and-flexing-more-likely-manufacturing#:~:text=In%20theory%2C%20turbines%20can%20keep,rotates%2C%20which%20generates%20more%20electricity.

[4] Wikipedia Tip-speed ratio;. Accessed: 2024-02-13. https://en.wikipedia.org/wiki/Tip-speed_ratio.

[5] Zhang L, Li X, Yang K, Xue D. Effects of vortex generators on aerodynamic performance of thick wind turbine airfoils. Journal of Wind Engineering and Industrial Aerodynamics. 2016 9;156:84-92.

[6] Choudhry A, Arjomandi M, Kelso R. Methods to control dynamic stall for wind turbine applications. Renewable Energy. 2016 2;86:26-37.

[7] "Drela M. "XFOIL: An Analysis and Design System for Low Reynolds Number Airfoils". In: "Mueller TJ, editor. "Low Reynolds Number Aerodynamics". Berlin, Heidelberg: Springer Berlin Heidelberg; 1989. .

[8] Ravishanara AK, Özdemir H, Franco A. Towards a vortex generator model for integral boundary layer methods. AIAA Scitech 2019 Forum. 2019. Available from: https://arc.aiaa.org/doi/10.2514/6.2019-0803.

[9] Bay Y. "A detailed flow field analysis of a single vortex generator for flow separation control", PhD Thesis. University of Twente; to be published.

[10] Fernández-Gámiz U, Zamorano G, Zulueta E. Computational study of the vortex path variation with the VG height. Journal of Physics: Conference Series. 2014 jun;524(1):012024. Available from: https://dx.doi.org/10.1088/1742-6596/524/1/012024.

[11] Rubenstein DA, Yin W, Frame MD. Chapter 2 - Fundamentals of Fluid Mechanics. In: Rubenstein DA, Yin W, Frame MD, editors. Biofluid Mechanics (Second Edition). second edition ed. Biomedical Engineering. Boston: Academic Press; 2015. p. 15-62. Available from: https://www.sciencedirect.com/science/article/pii/B9780128009444000020.

[12] Kundu PK, Cohen IM, Dowling DR. Chapter 12 - Turbulence. In: Kundu PK, Cohen IM, Dowling DR, editors. Fluid Mechanics (Sixth Edition). sixth edition ed. Boston: Academic Press; 2016. p. 603-97. Available from: https://www.sciencedirect.com/science/article/pii/B9780124059351000125.

[13] Cousteix J. Aircraft Aerodynamic Boundary Layers. In: Meyers RA, editor. Encyclopedia of Physical Science and Technology (Third Edition). third edition ed. New York: Academic Press; 2003. p. 301-17. Available from: https://www.sciencedirect.com/science/article/pii/B0122274105009066.

[14] Menter F. In: Zonal Two Equation k-w Turbulence Models For Aerodynamic Flows;. Available from: https://arc.aiaa.org/doi/abs/10.2514/6.1993-2906.

[15] CFD online Turbulence free-stream boundary conditions;. Accessed: 2024-06-18. https://www.cfd-online.com/Wiki/Turbulence_free-stream_boundary_conditions.

[16] CFD online Turbulence length scale;. Accessed: 2024-06-18. https://www.cfd-online.com/Wiki/Turbulent_length_scale.

[17] SU2;. Accessed: 2024-07-10. https://su2code.github.io/.

[18] SU2 Inc Turbulent Flat Plate Github;. Accessed: 2024-07-10. https://github.com/su2code/Tutorials/tree/master/incompressible_flow/Inc_Turbulent_Flat_Plate.

[19] SU2 Markers and boundary conditions;. Accessed: 2024-07-10. https://su2code.github.io/docs_v7/Markers-and-BC/.

[20] Mathworks pchip command;. Accessed: 2024-07-10. https://nl.mathworks.com/help/matlab/ref/pchip.html.

[21] Ahrens J, Geveci B, Law C. ParaView: An End-User Tool for Large Data Visualization. In: Visualization Handbook. Elesvier; 2005. ISBN 978-0123875822.

[22] Gersten K. Hermann Schlichting and the Boundary-Layer Theory. In: Radespiel R, Rossow CC, Brinkmann BW, editors. Hermann Schlichting – 100 Years. Berlin, Heidelberg: Springer Berlin Heidelberg; 2009. p. 3-17.

[23] dos Santos FL, Venner C, Santana L. Tripping Device Effects on the Turbulent Boundary Layer Development; 2022. .

[24] CFD online Boussinesq eddy viscosity assumption;. Accessed: 2024-07-01. https://www.cfdonline.com/Wiki/Boussinesq_eddy_viscosity_assumption.

[25] Schmitt FG. About Boussinesq's turbulent viscosity hypothesis: historical remarks and a direct evaluation of its validity. Comptes Rendus Mécanique. 2007 Oct;335(9-10):617-27. Available from: https://hal.science/hal-00264386.

7 Appendices

7.1 Appendix A

7.1.1 SU2 configuration file for the case with VG

```
%%%%%%%%%%%%%%%%%%%%%%%%%%%%%%%%%%%%%%%%%%%%%%%%%%%%%%%%%%%%%%%%%%%%%%%%%%%%%%%%
%                                                                              %
% SU2 configuration file                                                       %
% Case description: Turbulent flow over flat plate with VG (incompressible)    %
% Author: Chris Beumer                                                         %
% Date: 2024.06.23                                                             %
% This is a modified cfg file from the SU2 tutorial: Turbulent flat plate      %
%%%%%%%%%%%%%%%%%%%%%%%%%%%%%%%%%%%%%%%%%%%%%%%%%%%%%%%%%%%%%%%%%%%%%%%%%%%%%%%%

% ------------- DIRECT, ADJOINT, AND LINEARIZED PROBLEM DEFINITION ------------%
%
% Physical governing equations (EULER, NAVIER_STOKES,
%                               WAVE_EQUATION, HEAT_EQUATION, FEM_ELASTICITY,
%                               POISSON_EQUATION)
SOLVER= INC_RANS
%
KIND_TURB_MODEL= SST
%
% Mathematical problem (DIRECT, CONTINUOUS_ADJOINT)
MATH_PROBLEM= DIRECT
%
% Restart solution (NO, YES)
RESTART_SOL= NO

% ---------------- INCOMPRESSIBLE FLOW CONDITION DEFINITION -------------------%
%
% Initial density for incompressible flows (1.2886 kg/m^3 by default)
INC_DENSITY_INIT= 1.204
%
% Initial velocity for incompressible flows (1.0,0,0 m/s by default)
INC_VELOCITY_INIT= (1.0, 0.0, 0.0 )
%
% List of inlet types for incompressible flows. List length must
% match number of inlet markers. Options: VELOCITY_INLET, PRESSURE_INLET.
INC_INLET_TYPE= VELOCITY_INLET
%
% Damping coefficient for iterative updates at pressure inlets. (0.1 by default)
INC_INLET_DAMPING= 0.1
%
% List of outlet types for incompressible flows. List length must
% match number of outlet markers. Options: PRESSURE_OUTLET, MASS_FLOW_OUTLET
INC_OUTLET_TYPE= PRESSURE_OUTLET PRESSURE_OUTLET
%
% Damping coefficient for iterative updates at mass flow outlets. (0.1 by default)
INC_OUTLET_DAMPING= 0.1

% --------------------------- VISCOSITY MODEL ---------------------------------%
%
% Viscosity model (SUTHERLAND, CONSTANT_VISCOSITY).
VISCOSITY_MODEL= CONSTANT_VISCOSITY
%
% Molecular Viscosity that would be constant (1.716E-5 by default)
MU_CONSTANT= 1.825e-05
```

```
% ---------------------- REFERENCE VALUE DEFINITION --------------------------%
%
% Reference origin for moment computation
REF_ORIGIN_MOMENT_X = 0.25
REF_ORIGIN_MOMENT_Y = 0.00
REF_ORIGIN_MOMENT_Z = 0.00
%
% Reference length for pitching, rolling, and yawing non-dimensional moment
REF_LENGTH= 1.0
%
% Reference area for force coefficients (0 implies automatic calculation)
REF_AREA= 0

% ------------------- BOUNDARY CONDITION DEFINITION -------------------------%
%
% Navier-Stokes wall boundary marker(s) (NONE = no marker)
MARKER_HEATFLUX= ( bottom, 0.0, vg, 0.0 )
%
%
% Read inlet profile from a file (YES,NO) default: NO
SPECIFIED_INLET_PROFILE= YES
%
%INLET_FILENAME= inlet.dat
%Velocity=20.5234
% Inlet boundary marker(s) (NONE = no marker)
% Format: ( inlet marker, total temperature, velocity magnitude, flow_direction_x,
%           flow_direction_y, flow_direction_z ... )
MARKER_INLET= ( inlet, 0.0, 20.5234, 1.0, 0.0, 0.0 )
%
% Outlet boundary marker(s) (NONE = no marker)
% Format: ( outlet marker, back pressure, ... )
MARKER_OUTLET= ( outlet, 0.0, left, 0.0 , right, 0.0, top, 0.0)
%
%
% Marker(s) of the surface to be plotted or designed
MARKER_PLOTTING= ( bottom, vg )
%
% Marker(s) of the surface where the functional (Cd, Cl, etc.) will be evaluated
MARKER_MONITORING= ( bottom, vg )

% ------------- COMMON PARAMETERS DEFINING THE NUMERICAL METHOD ---------------%
%
% Numerical method for spatial gradients (GREEN_GAUSS, LEAST_SQUARES,
%                                         WEIGHTED_LEAST_SQUARES)
NUM_METHOD_GRAD= GREEN_GAUSS
%
% Courant-Friedrichs-Lewy condition of the finest grid
CFL_NUMBER= 100.0
%
% Adaptive CFL number (NO, YES)
CFL_ADAPT= YES
%
% Parameters of the adaptive CFL number (factor down, factor up, CFL min value,
%                                        CFL max value )
CFL_ADAPT_PARAM= ( 0.1, 2.0, 100.0, 1e3 )
%
% Runge-Kutta alpha coefficients
RK_ALPHA_COEFF= ( 0.66667, 0.66667, 1.000000 )
%
% Number of total iterations
ITER= 99999

% ------------------------ LINEAR SOLVER DEFINITION --------------------------%
%
% Linear solver for implicit formulations (BCGSTAB, FGMRES)
LINEAR_SOLVER= FGMRES
```

```
%
% Preconditioner of the Krylov linear solver (JACOBI, LINELET, LU_SGS)
LINEAR_SOLVER_PREC= ILU
%
% Linael solver ILU preconditioner fill-in level (0 by default)
LINEAR_SOLVER_ILU_FILL_IN= 0
%
% Minimum error of the linear solver for implicit formulations
LINEAR_SOLVER_ERROR= 1E-12
%
% Max number of iterations of the linear solver for the implicit formulation
LINEAR_SOLVER_ITER= 20

% ----------------------- SLOPE LIMITER DEFINITION ---------------------------%
%
% Coefficient for the limiter
VENKAT_LIMITER_COEFF= 0.1
%
% Coefficient for the sharp edges limiter
ADJ_SHARP_LIMITER_COEFF= 3.0
%
% Reference coefficient (sensitivity) for detecting sharp edges.
REF_SHARP_EDGES= 3.0
%
% Remove sharp edges from the sensitivity evaluation (NO, YES)
SENS_REMOVE_SHARP= NO

% ------------------------- MULTIGRID PARAMETERS -----------------------------%
%
% Multi-Grid Levels (0 = no multi-grid)
MGLEVEL= 0
%
% Multi-grid cycle (V_CYCLE, W_CYCLE, FULLMG_CYCLE)
MGCYCLE= V_CYCLE
%
% Multi-grid pre-smoothing level
MG_PRE_SMOOTH= ( 1, 1, 1, 1 )
%
% Multi-grid post-smoothing level
MG_POST_SMOOTH= ( 0, 0, 0, 0 )
%
% Jacobi implicit smoothing of the correction
MG_CORRECTION_SMOOTH= ( 0, 0, 0, 0 )
%
% Damping factor for the residual restriction
MG_DAMP_RESTRICTION= 0.8
%
% Damping factor for the correction prolongation
MG_DAMP_PROLONGATION= 0.8

% -------------------- FLOW NUMERICAL METHOD DEFINITION ----------------------%
%
% Convective numerical method (JST, LAX-FRIEDRICH, CUSP, ROE, AUSM, HLLC,
%                              TURKEL_PREC, MSW)
CONV_NUM_METHOD_FLOW= FDS
%
% Monotonic Upwind Scheme for Conservation Laws (TVD) in the flow equations.
%           Required for 2nd order upwind schemes (NO, YES)
MUSCL_FLOW= YES
%
% Slope limiter (NONE, VENKATAKRISHNAN, VENKATAKRISHNAN_WANG,
%                BARTH_JESPERSEN, VAN_ALBADA_EDGE)
SLOPE_LIMITER_FLOW= NONE
%
% Time discretization (RUNGE-KUTTA_EXPLICIT, EULER_IMPLICIT, EULER_EXPLICIT)
TIME_DISCRE_FLOW= EULER_IMPLICIT
```

```
% ------------------- TURBULENT NUMERICAL METHOD DEFINITION ------------------%
%
% Convective numerical method (SCALAR_UPWIND)
CONV_NUM_METHOD_TURB= SCALAR_UPWIND
%
% Monotonic Upwind Scheme for Conservation Laws (TVD) in the turbulence equations.
%           Required for 2nd order upwind schemes (NO, YES)
MUSCL_TURB= NO
%
% Slope limiter (VENKATAKRISHNAN, MINMOD)
SLOPE_LIMITER_TURB= VENKATAKRISHNAN
%
% Time discretization (EULER_IMPLICIT)
TIME_DISCRE_TURB= EULER_IMPLICIT

% -------------------------- CONVERGENCE PARAMETERS --------------------------%
%
% Convergence criteria (CAUCHY, RESIDUAL)
CONV_FIELD= RMS_PRESSURE
%
% Min value of the residual (log10 of the residual)
CONV_RESIDUAL_MINVAL= -14
%
% Start convergence criteria at iteration number
CONV_STARTITER= 10
%
% Number of elements to apply the criteria
CONV_CAUCHY_ELEMS= 100
%
% Epsilon to control the series convergence
CONV_CAUCHY_EPS= 1E-6
%

% ------------------------ INPUT/OUTPUT INFORMATION ------------------------%
%
% Mesh input file
MESH_FILENAME= utvg_mesh.pw.su2
%
% Mesh input file format (SU2, CGNS, NETCDF_ASCII)
MESH_FORMAT= SU2
%
% Mesh output file
MESH_OUT_FILENAME= mesh_out_vg_m.su2
%
% Restart flow input file
SOLUTION_FILENAME= solution_flow.dat
%
% Restart adjoint input file
SOLUTION_ADJ_FILENAME= solution_adj.dat
%
% Output file format (PARAVIEW, TECPLOT, SLT)
TABULAR_FORMAT= CSV
%
% Output file convergence history (w/o extension)
CONV_FILENAME= history
%
% Output file restart flow
RESTART_FILENAME= restart_flow.dat
%
% Output file restart adjoint
RESTART_ADJ_FILENAME= restart_adj.dat
%
% Output file flow (w/o extension) variables
VOLUME_FILENAME= flow
%
```

```
% Output file adjoint (w/o extension) variables
VOLUME_ADJ_FILENAME= adjoint
%
% Output objective function gradient (using continuous adjoint)
GRAD_OBJFUNC_FILENAME= of_grad.dat
%
% Output file surface flow coefficient (w/o extension)
SURFACE_FILENAME= surface_flow
%
% Output file surface adjoint coefficient (w/o extension)
SURFACE_ADJ_FILENAME= surface_adjoint
%
%
% Screen output
SCREEN_OUTPUT= (INNER_ITER, WALL_TIME, RMS_PRESSURE, RMS_NU_TILDE, LIFT, DRAG)


% ------------------------ DESIGN VARIABLE PARAMETERS --------------------------%
%
%
% Kind of deformation (NO_DEFORMATION, SCALE_GRID, TRANSLATE_GRID, ROTATE_GRID,
%                      FFD_SETTING, FFD_NACELLE,
%                      FFD_CONTROL_POINT, FFD_CAMBER, FFD_THICKNESS, FFD_TWIST
%                      FFD_CONTROL_POINT_2D, FFD_CAMBER_2D, FFD_THICKNESS_2D,
%                      FFD_TWIST_2D, HICKS_HENNE, SURFACE_BUMP, SURFACE_FILE)
DV_KIND= SCALE_GRID
%
DV_PARAM= ( 1.0 )
%
% Value of the deformation
DV_VALUE= 0.001
```

7.1.2 Experimental measurements of inlet profile

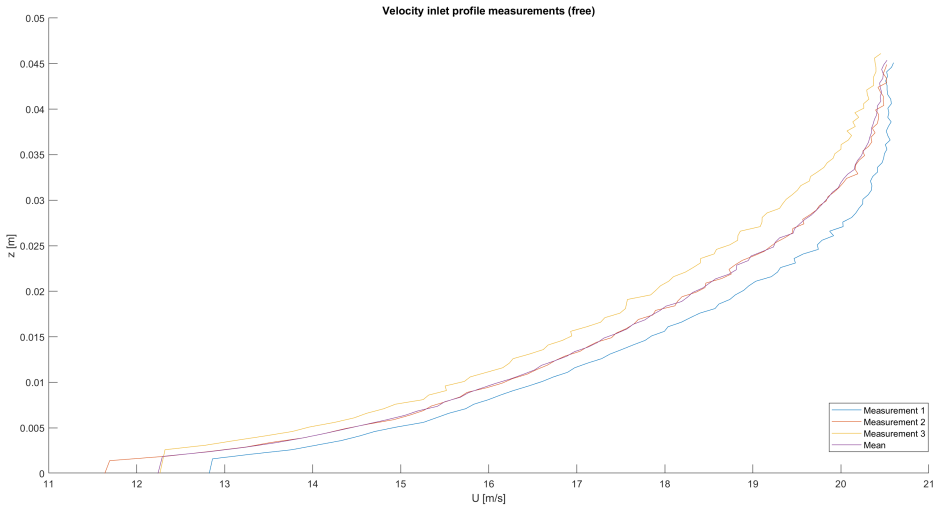

Figure 45: Experimental inlet profile measurements (free)

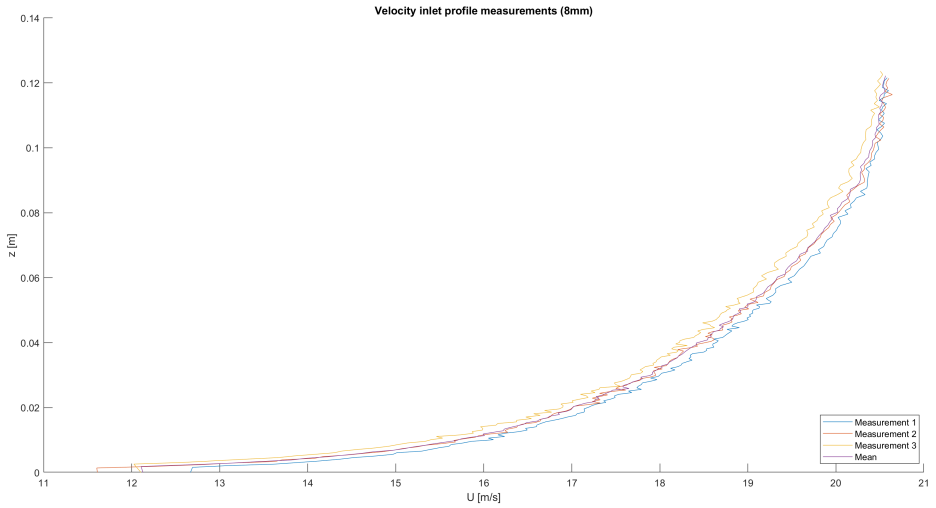

Figure 46: Experimental inlet profile measurements (8mm)

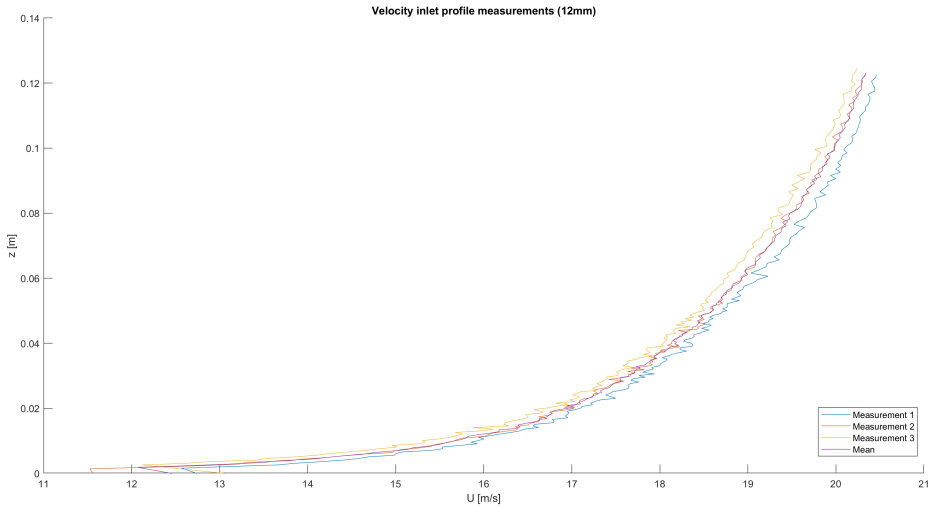

Figure 47: Experimental inlet profile measurements (12mm)

7.1.3 Interpolated/Extrapolated inlet profiles

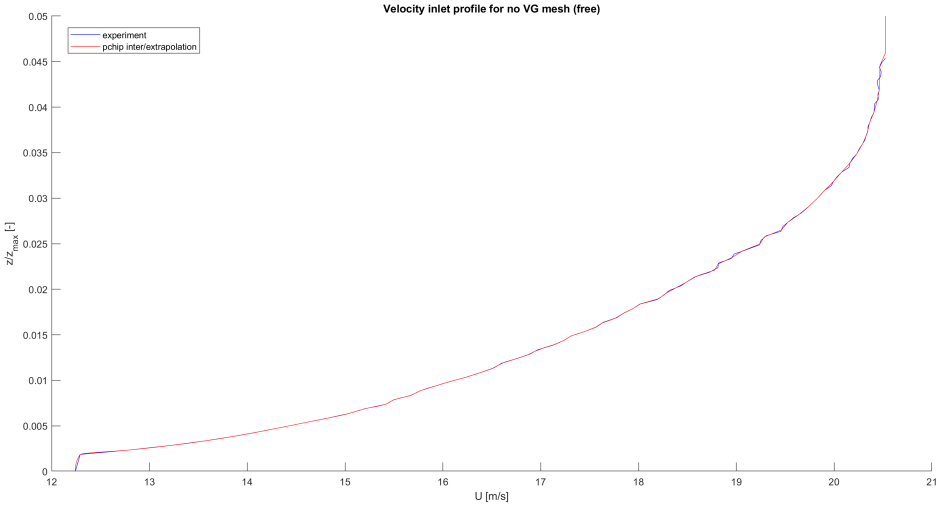

Figure 48: Interpolated/extrapolated inlet profile no VG case (free)

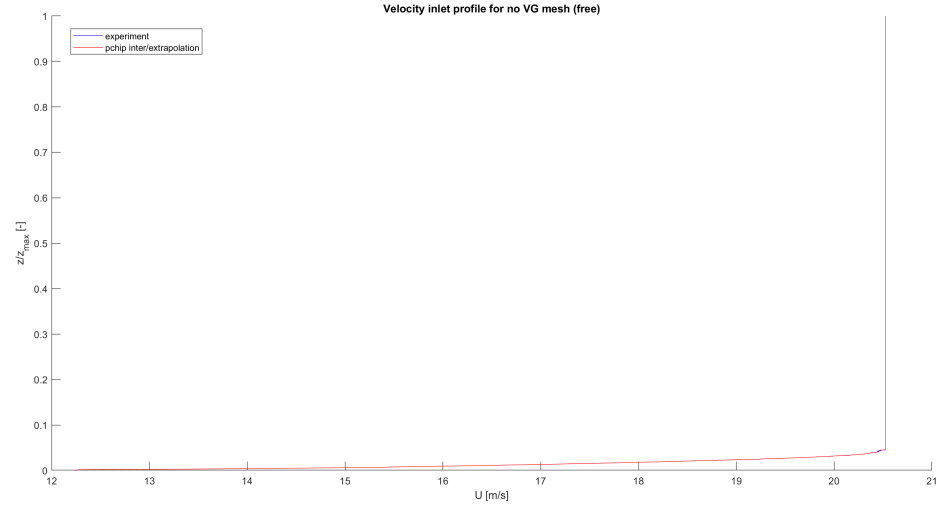

Figure 49: Zoomed out interpolated/extrapolated inlet profile no VG case (free)

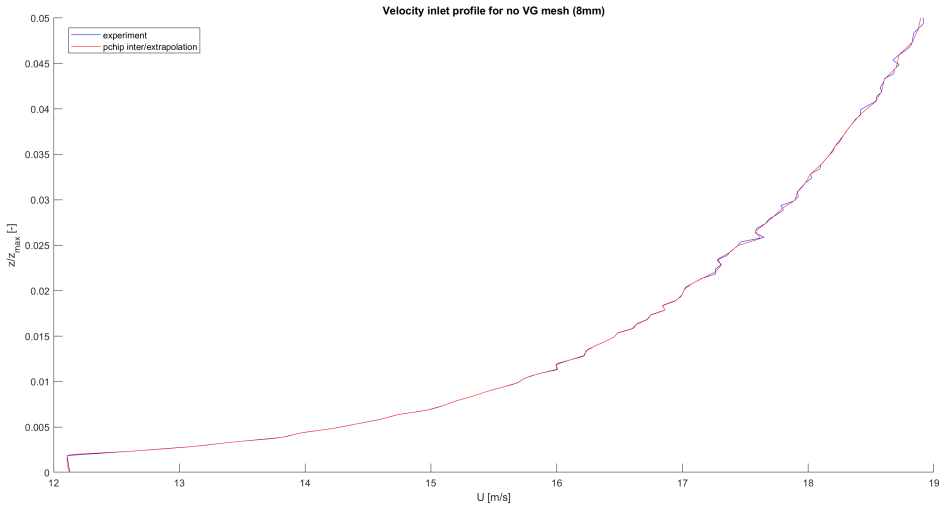

Figure 50: Interpolated/Extrapolated inlet profile no VG case (8mm)

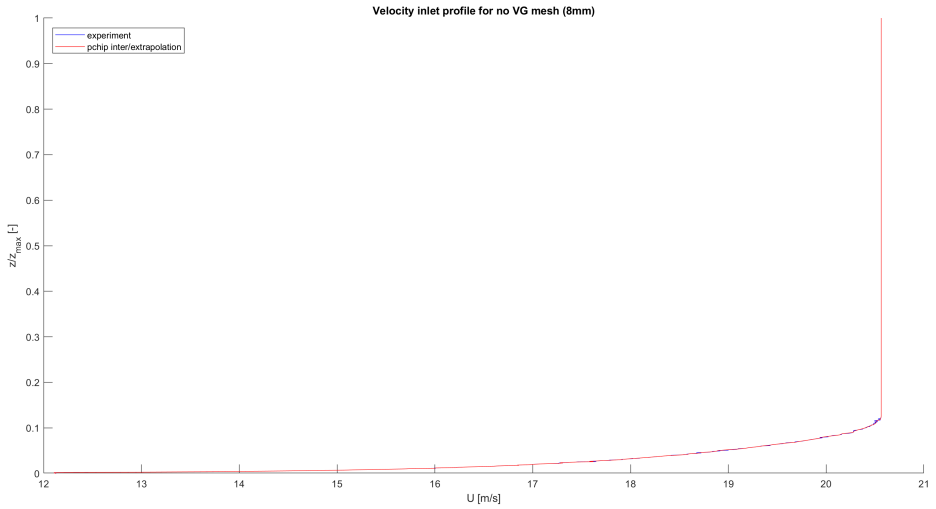

Figure 51: Zoomed out interpolated/extrapolated inlet profile no VG case (8mm)

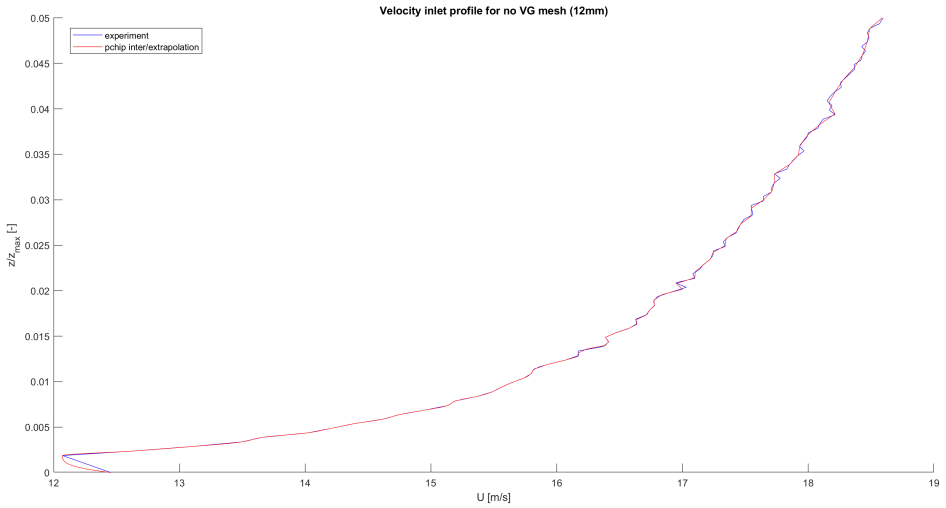

Figure 52: Interpolated/Extrapolated inlet profile no VG case (12mm)

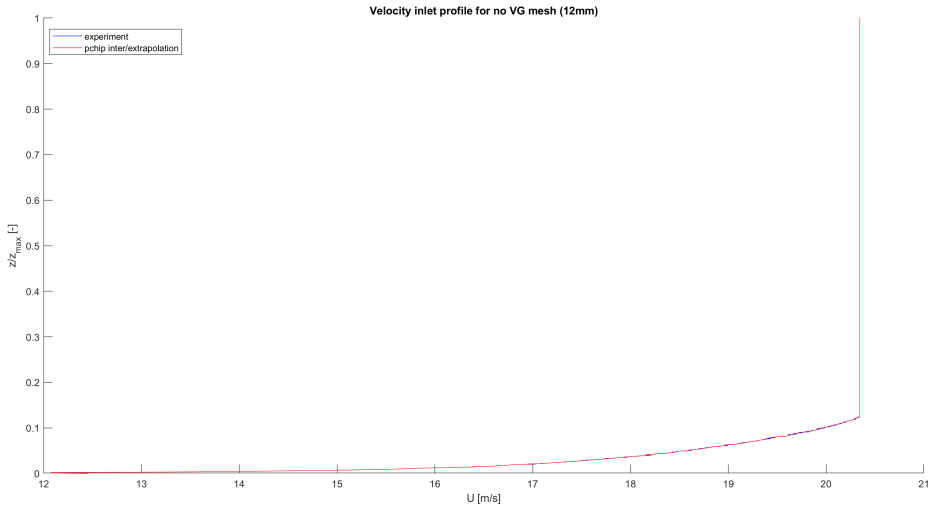

Figure 53: Zoomed out interpolated/extrapolated inlet profile no VG case (12mm)

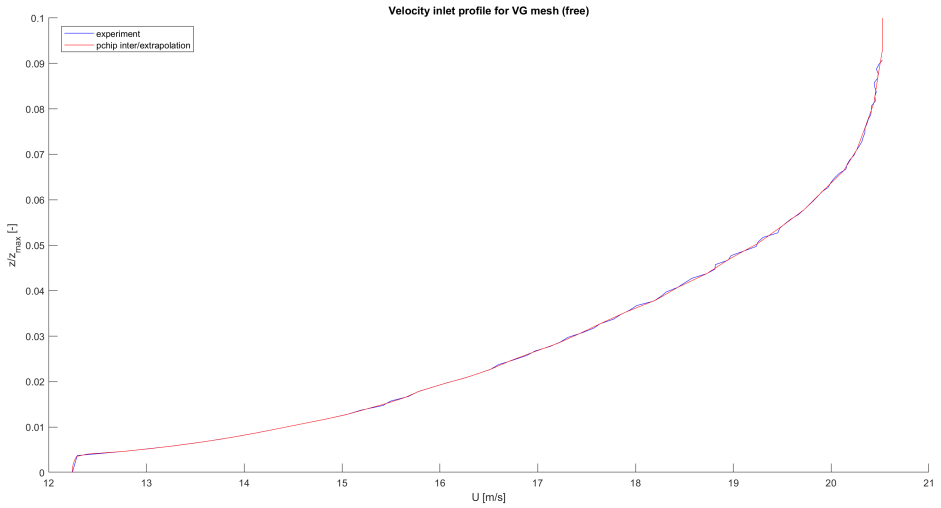

Figure 54: Interpolated/Extrapolated inlet profile VG case (free)

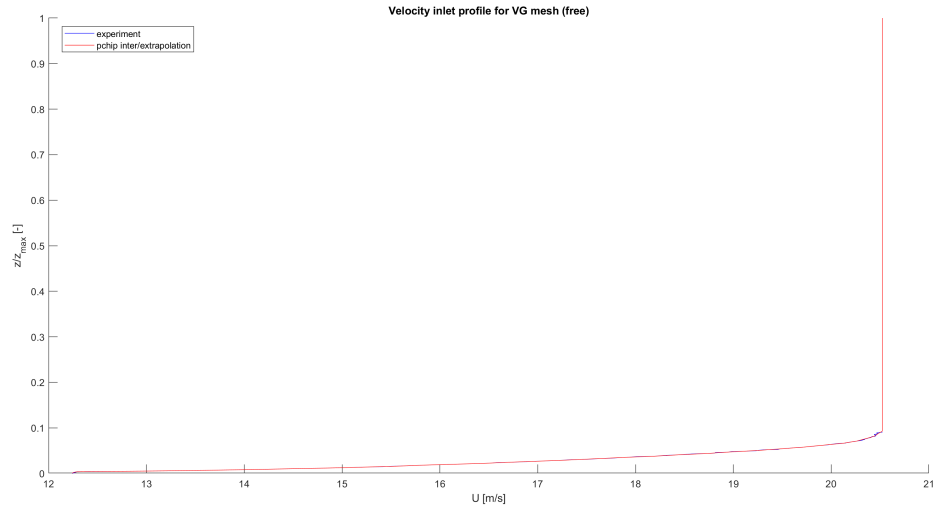

Figure 55: Zoomed out interpolated/extrapolated inlet profile VG case (free)

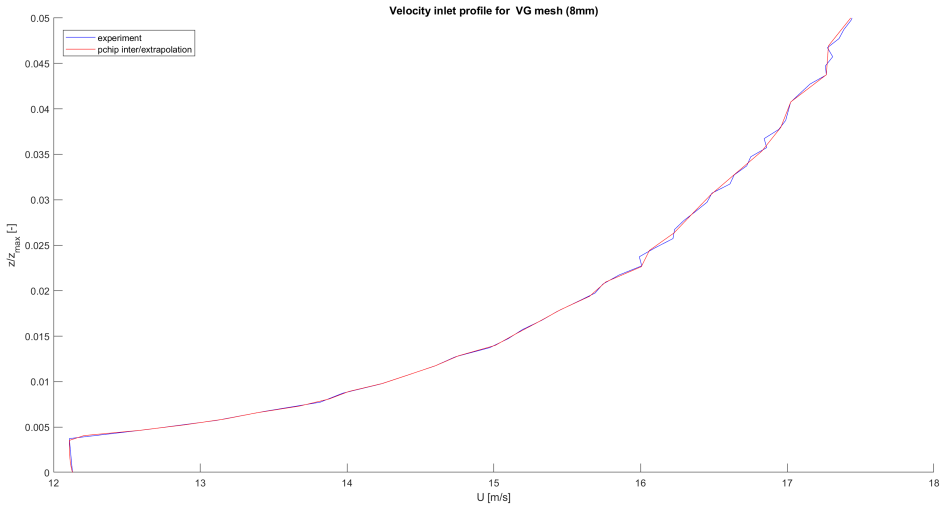

Figure 56: Interpolated/extrapolated inlet profile VG case (8mm)

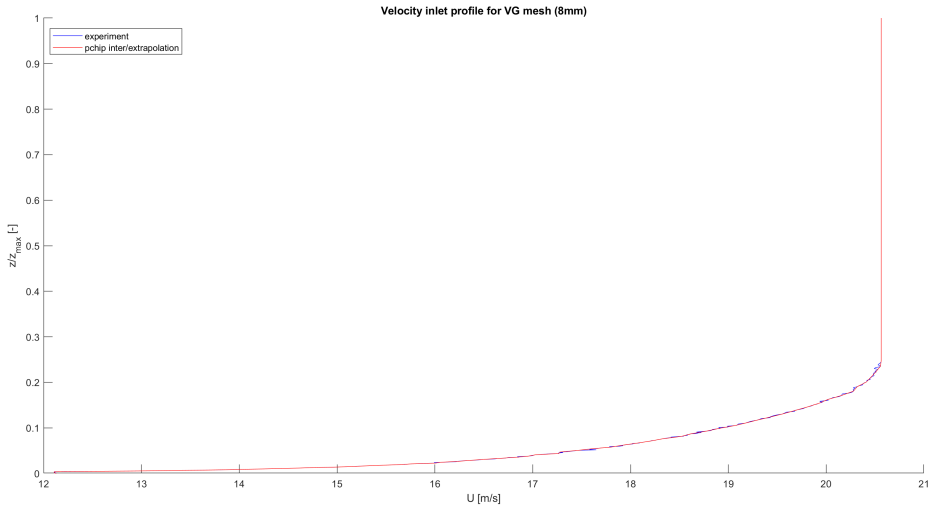

Figure 57: Zoomed out interpolated/extrapolated inlet profile VG case (8mm)

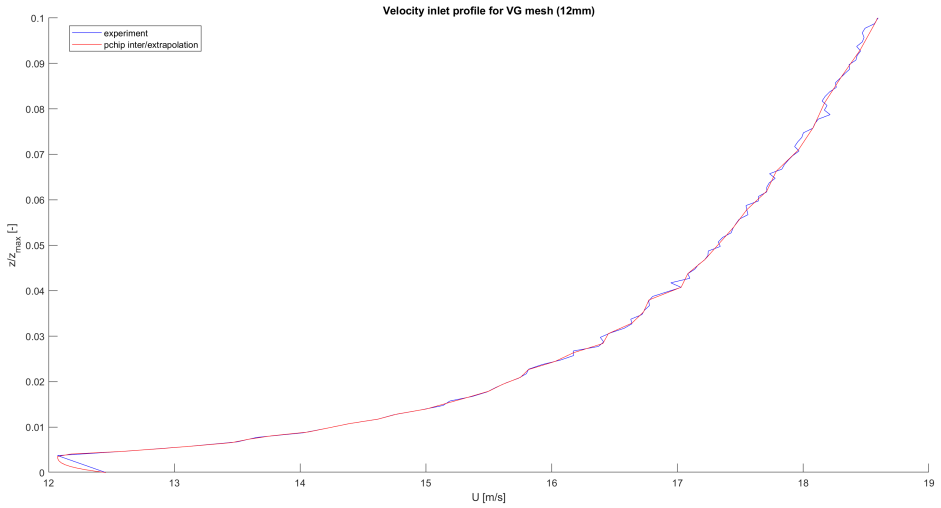

Figure 58: Interpolated/extrapolated inlet profile VG case (12mm)

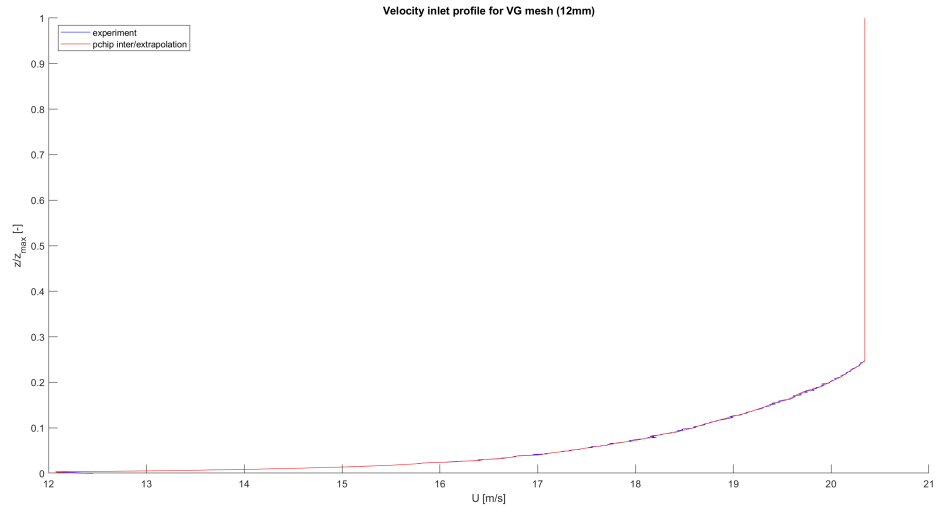

Figure 59: Zoomed out interpolated/extrapolated inlet profile VG case (12mm)

7.2 Appendix B

7.2.1 Velocity profiles z=-40mm (free)

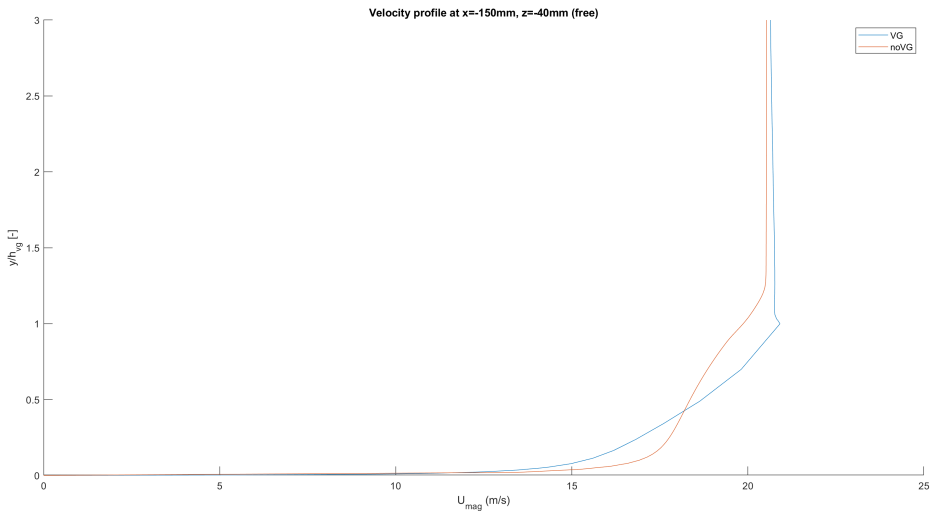

Figure 60: Velocity profile z=-40mm, x=-150mm (free)

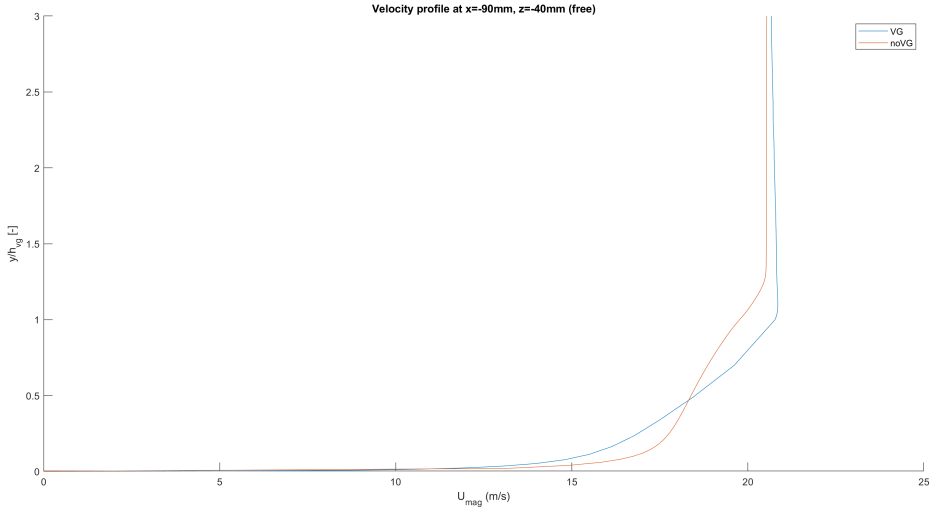

Figure 61: Velocity profile z=-40mm, x=-90mm (free)

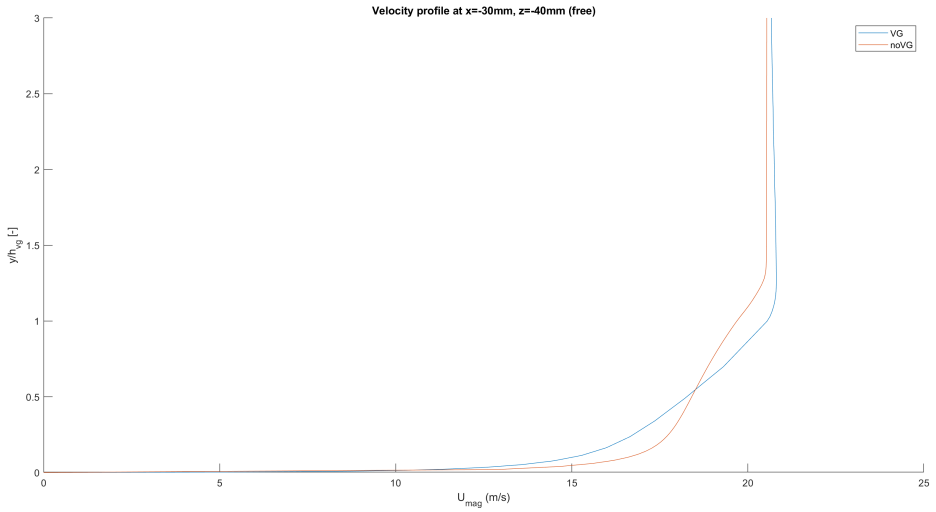

Figure 62: Velocity profile z=-40mm, x=-30mm (free)

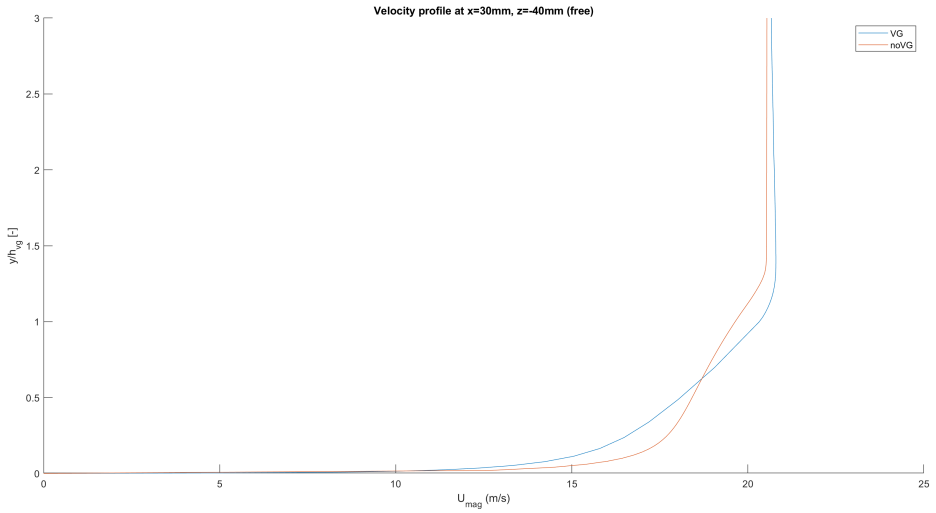

Figure 63: Velocity profile z=-40mm, x=30mm (free)

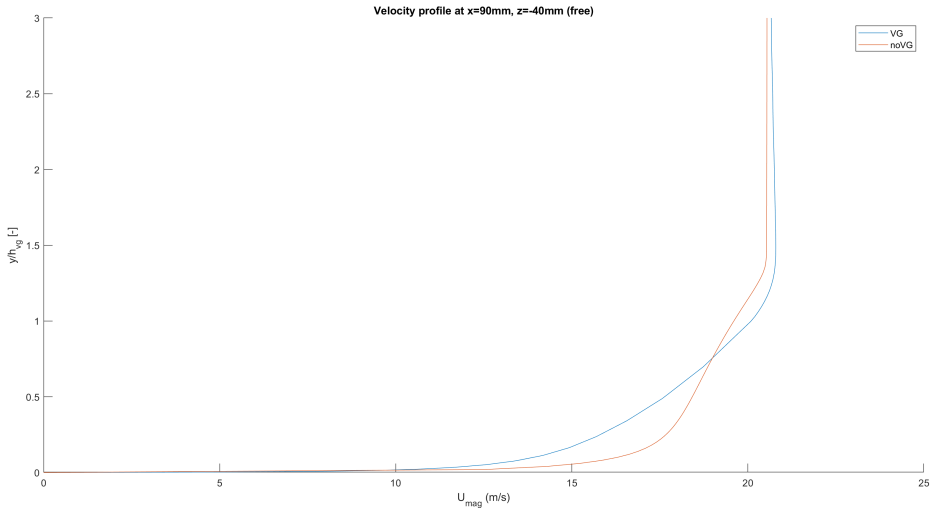

Figure 64: Velocity profile z=-40mm, x=90mm (free)

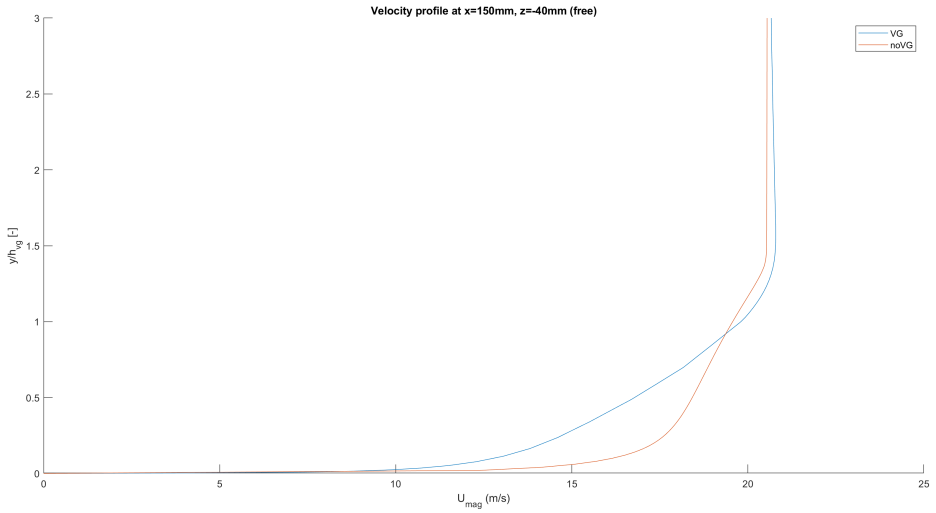

Figure 65: Velocity profile z=-40mm, x=150mm (free)

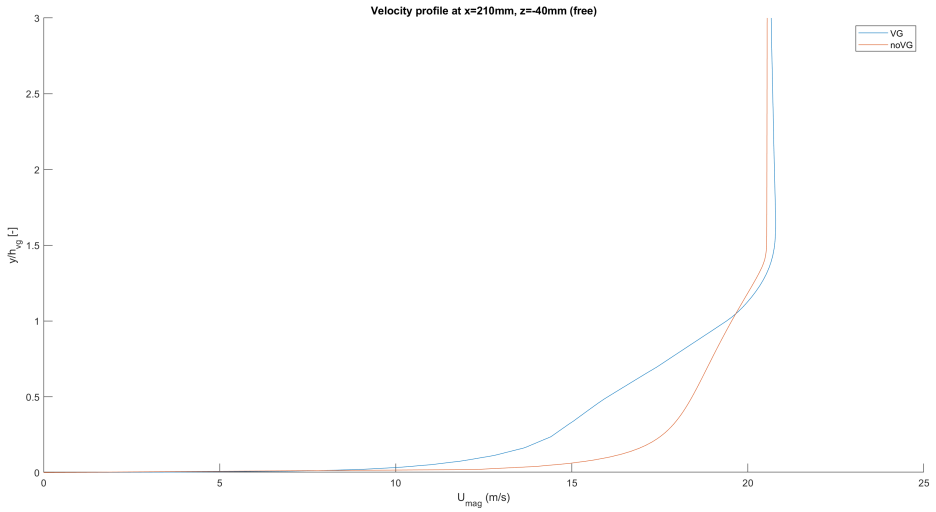

Figure 66: Velocity profile z=-40mm, x=210mm (free)

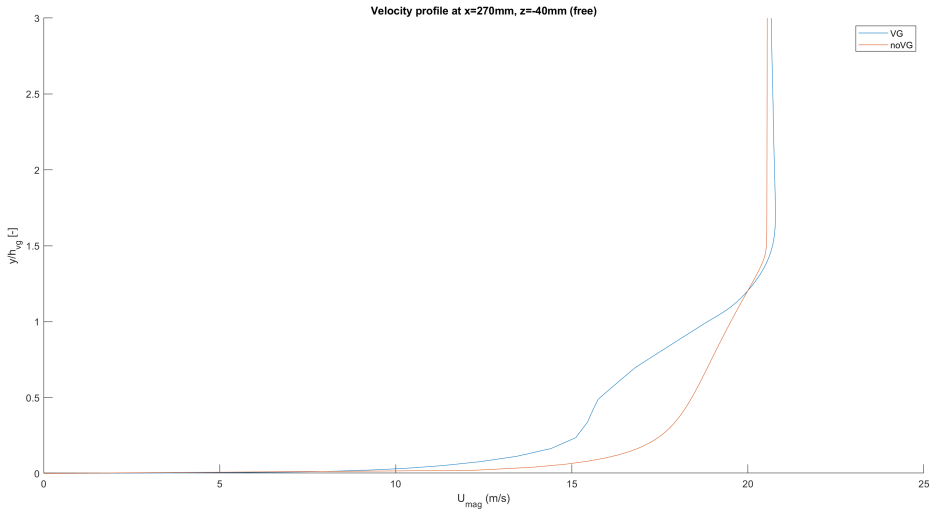

Figure 67: Velocity profile z=-40mm, x=270mm (free)

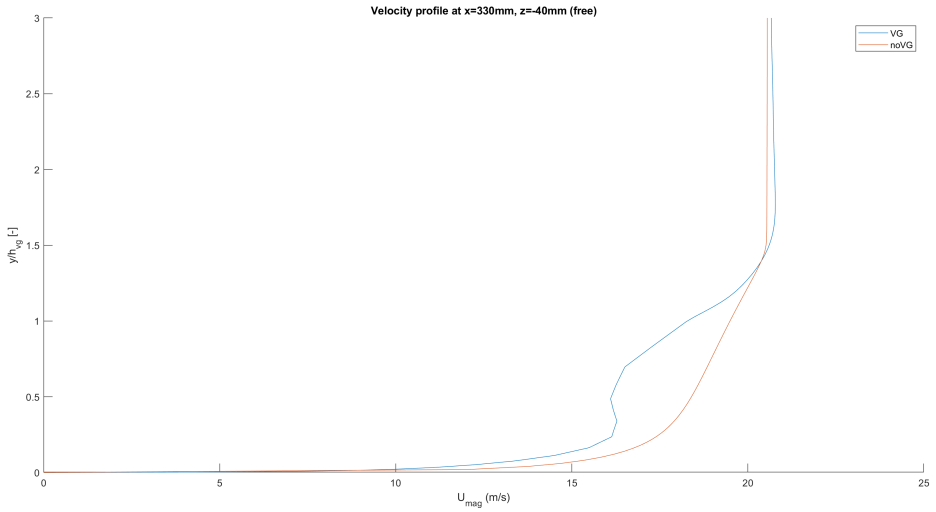

Figure 68: Velocity profile z=-40mm, x=330mm (free)

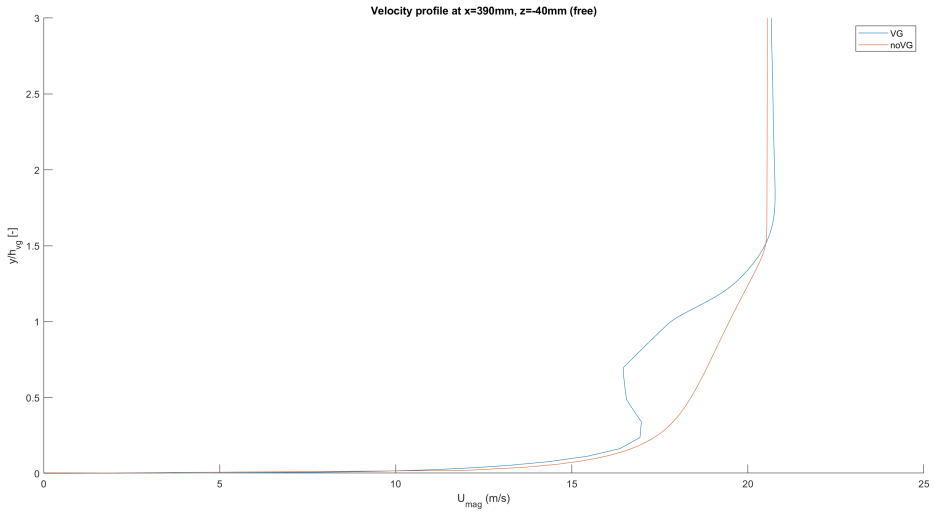

Figure 69: Velocity profile z=-40mm, x=390mm (free)

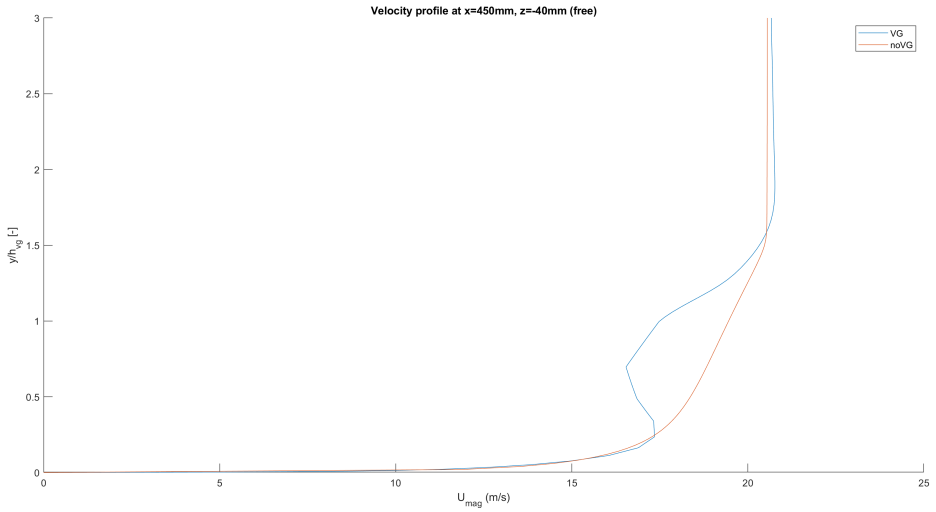

Figure 70: Velocity profile z=-40mm, x=450mm (free)

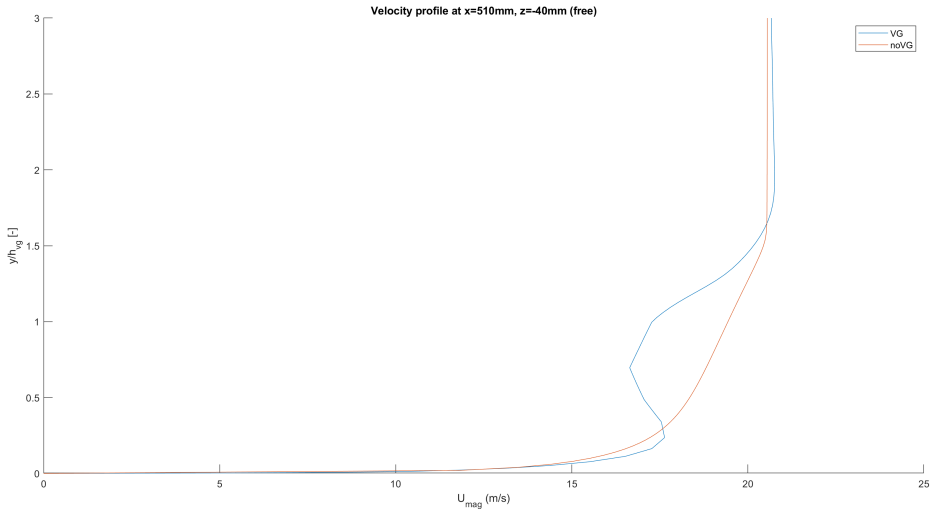

Figure 71: Velocity profile z=-40mm, x=510mm (free)

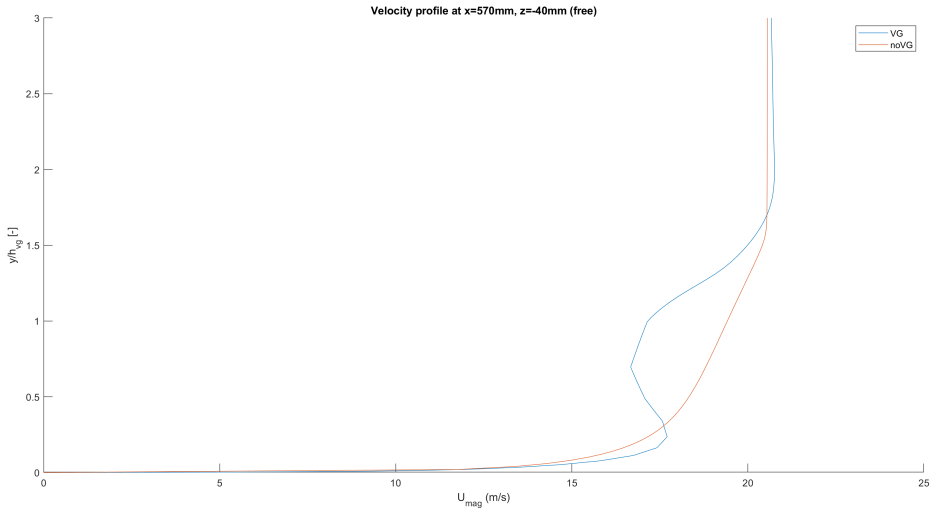

Figure 72: Velocity profile z=-40mm, x=570mm (free)

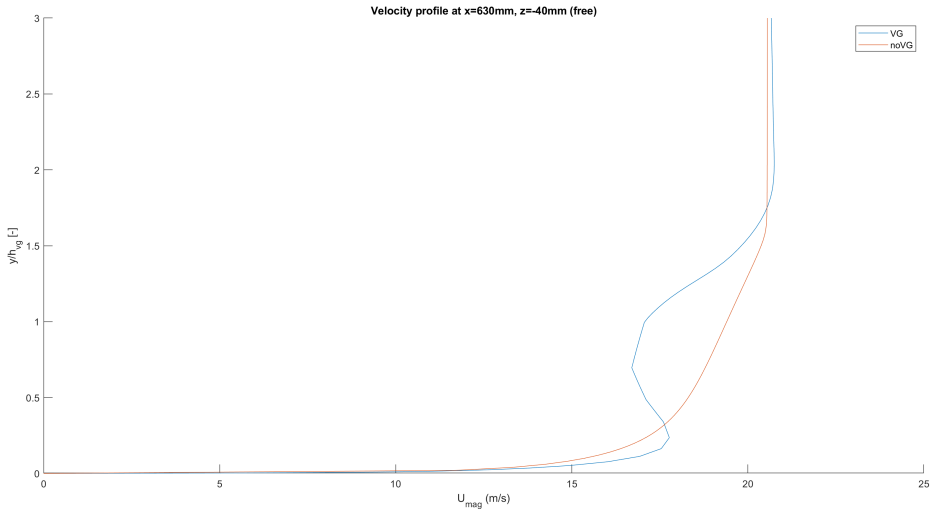

Figure 73: Velocity profile z=-40mm, x=630mm (free)

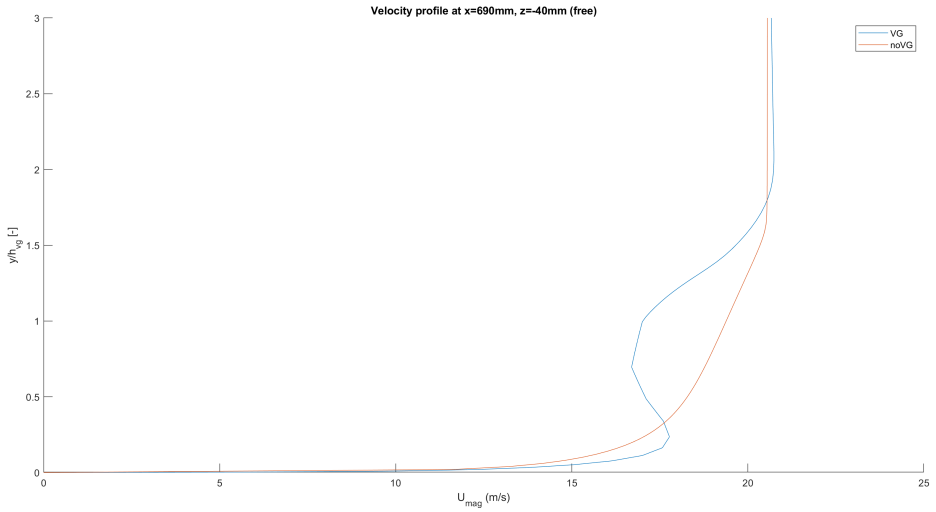

Figure 74: Velocity profile z=-40mm, x=690mm (free)

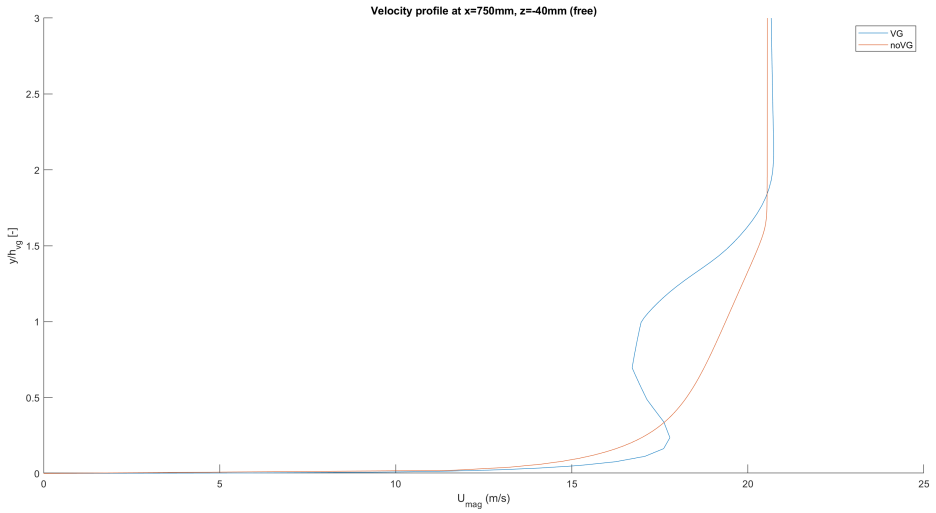

Figure 75: Velocity profile z=-40mm, x=750mm (free)

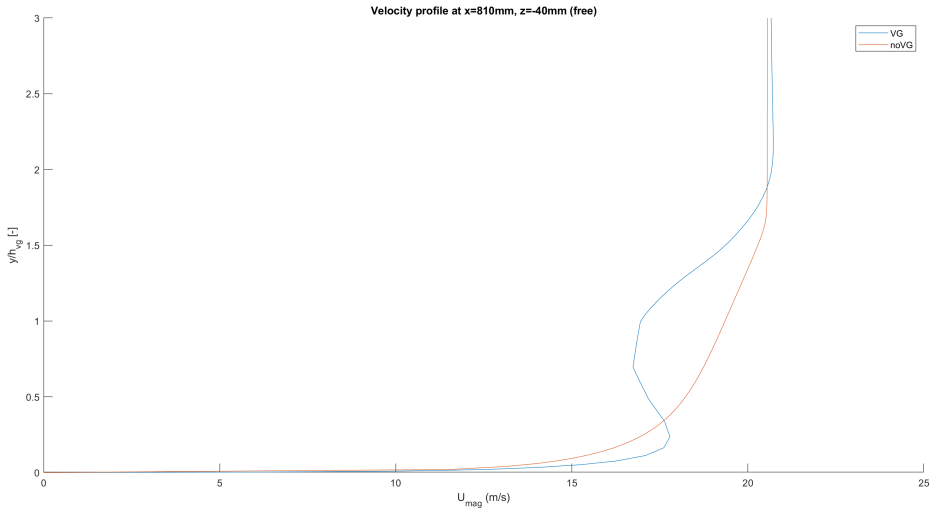

Figure 76: Velocity profile z=-40mm, x=810mm (free)

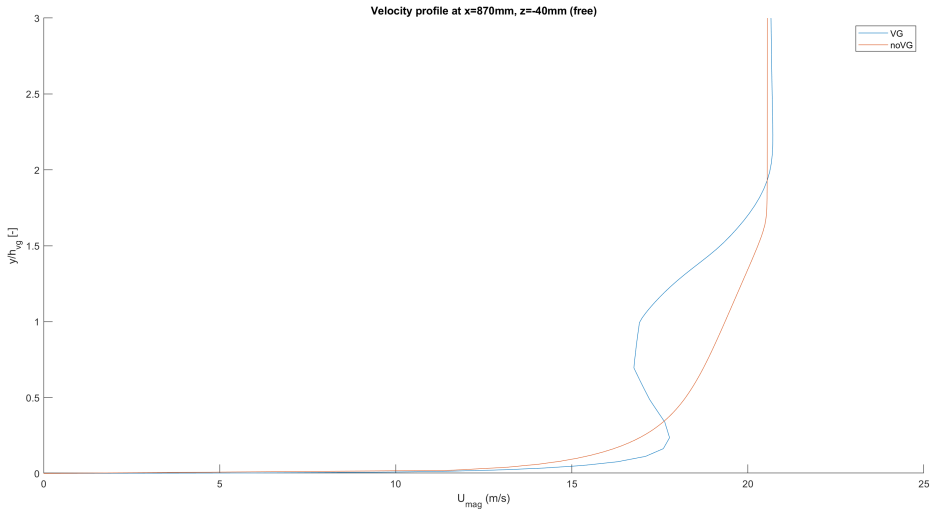

Figure 77: Velocity profile z=-40mm, x=870mm (free)

7.2.2 Velocity profiles z=-40mm (8mm)

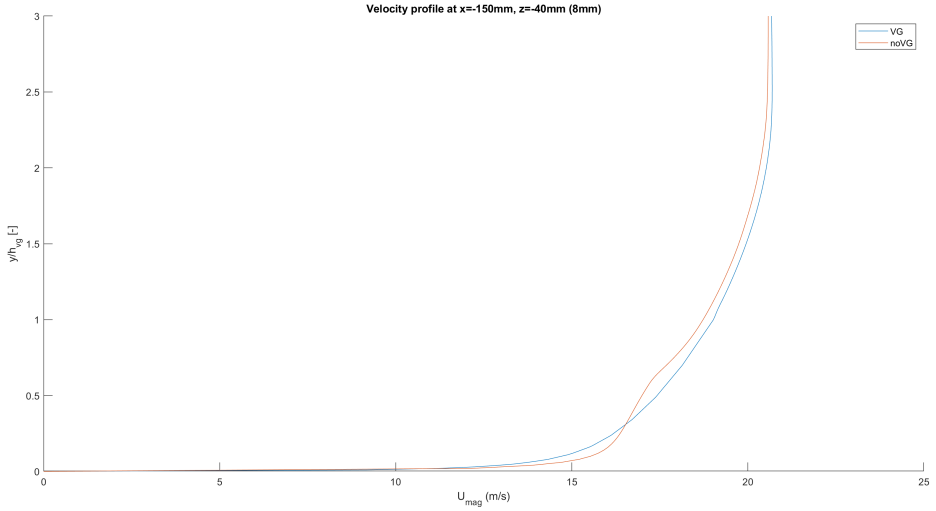

Figure 78: Velocity profile z=-40mm, x=-150mm (8mm)

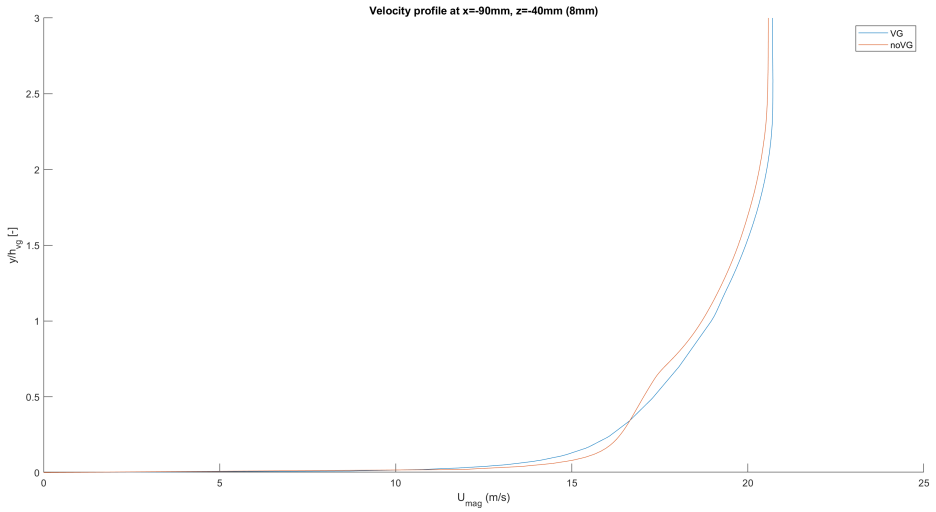

Figure 79: Velocity profile z=-40mm, x=-90mm (8mm)

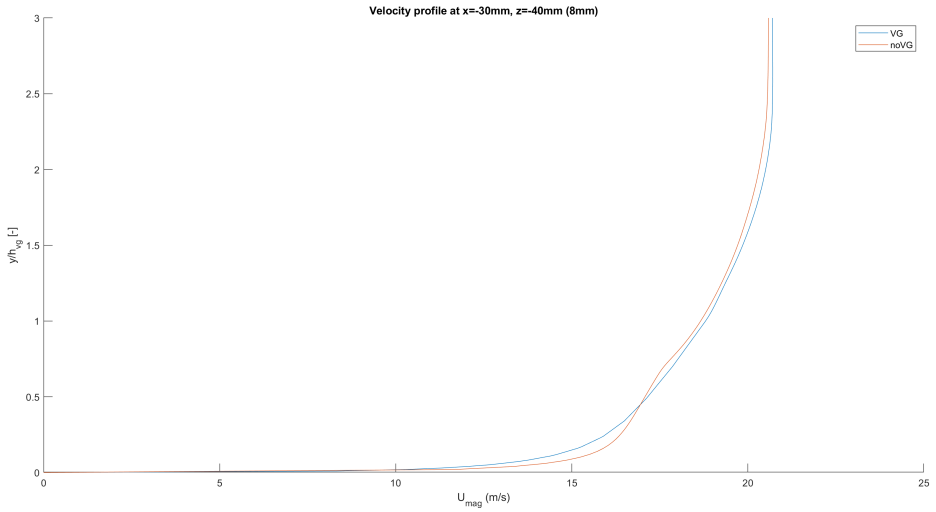

Figure 80: Velocity profile z=-40mm, x=-30mm (8mm)

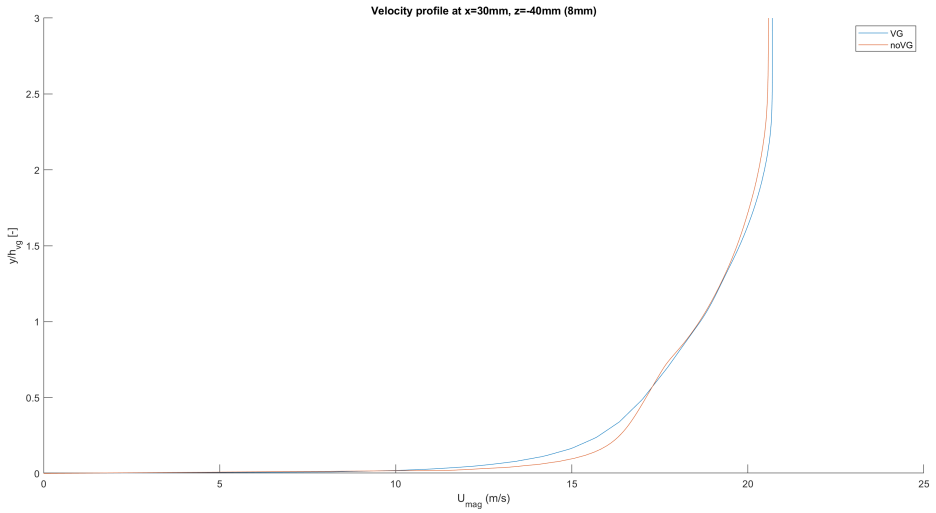

Figure 81: Velocity profile z=-40mm, x=30mm (8mm)

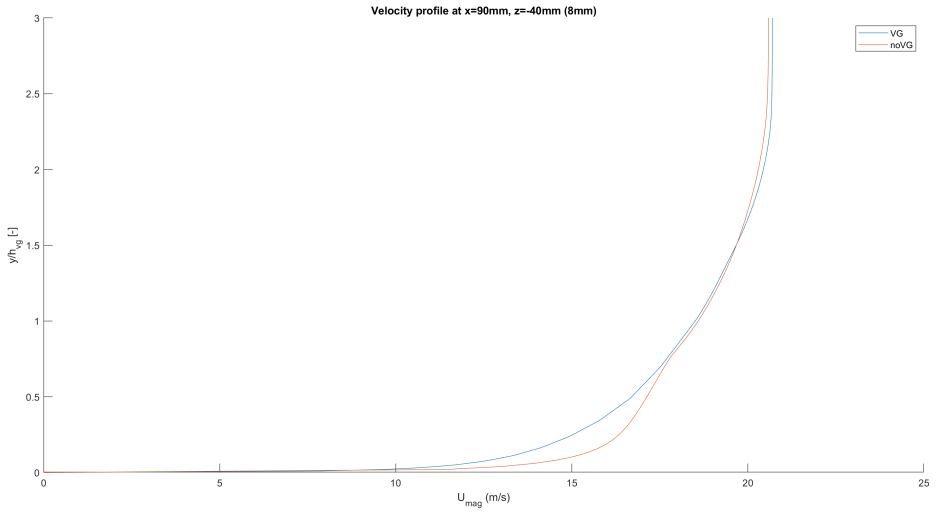

Figure 82: Velocity profile z=-40mm, x=90mm (8mm)

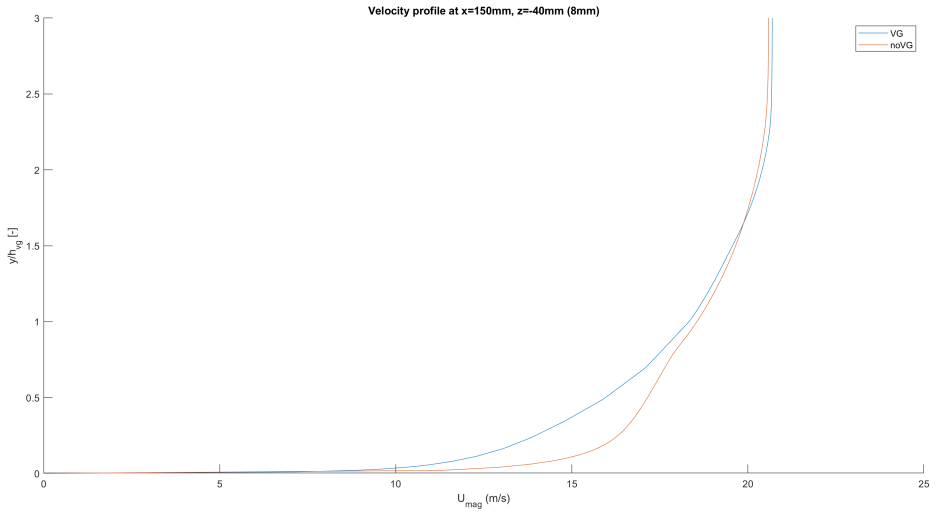

Figure 83: Velocity profile z=-40mm, x=150mm (8mm)

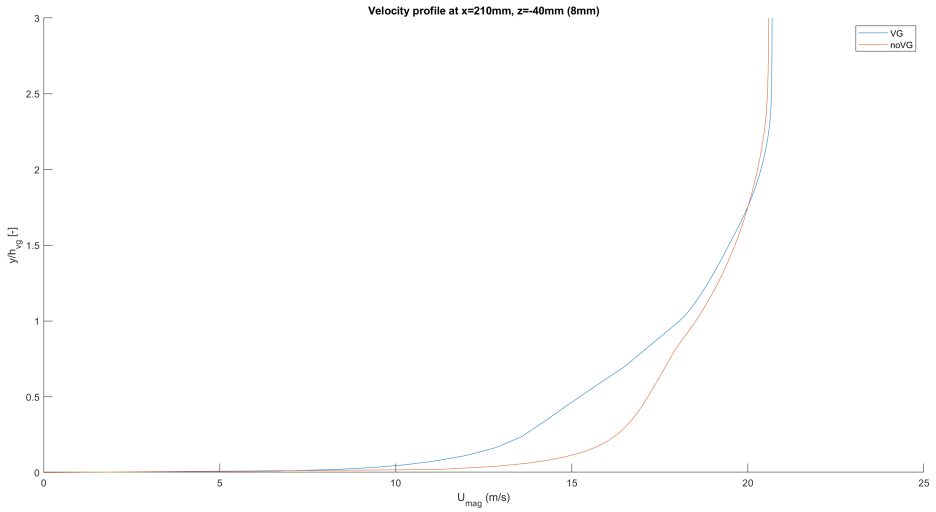

Figure 84: Velocity profile z=-40mm, x=210mm (8mm)

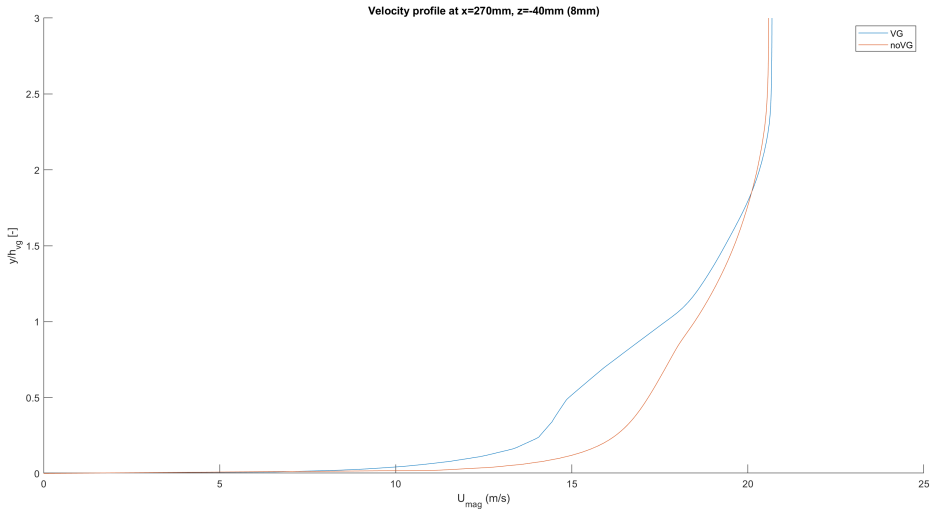

Figure 85: Velocity profile z=-40mm, x=270mm (8mm)

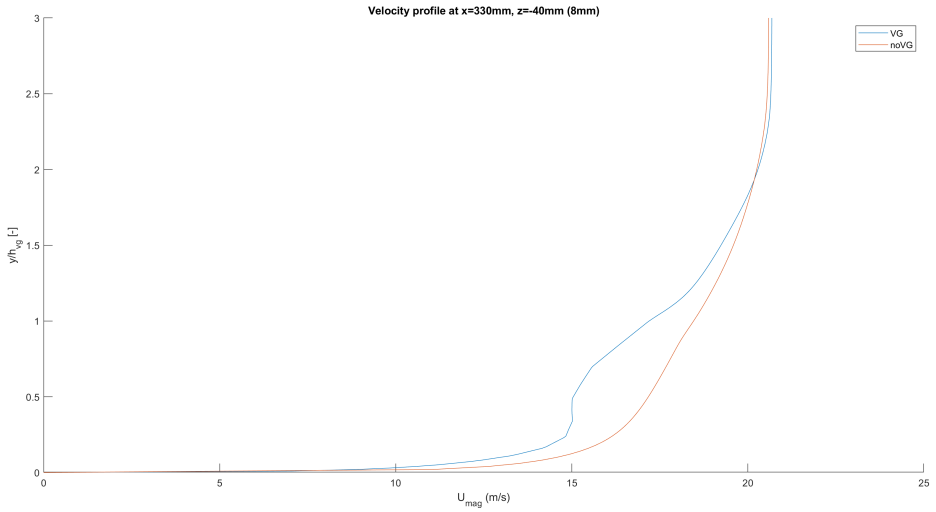

Figure 86: Velocity profile z=-40mm, x=330mm (8mm)

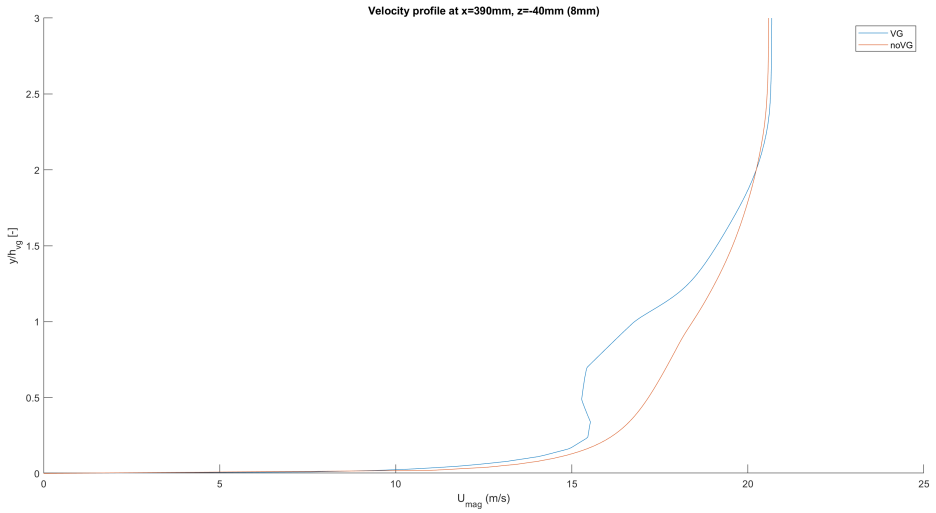

Figure 87: Velocity profile z=-40mm, x=390mm (8mm)

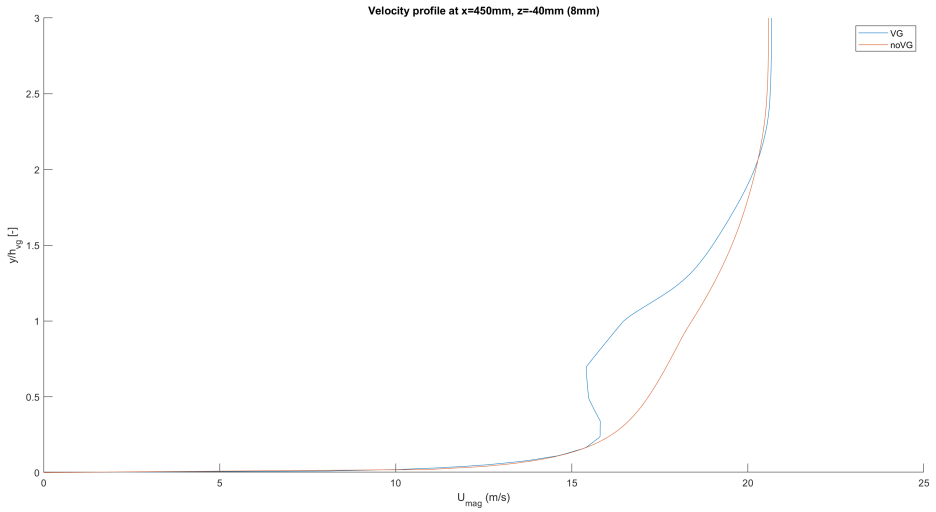

Figure 88: Velocity profile z=-40mm, x=450mm (8mm)

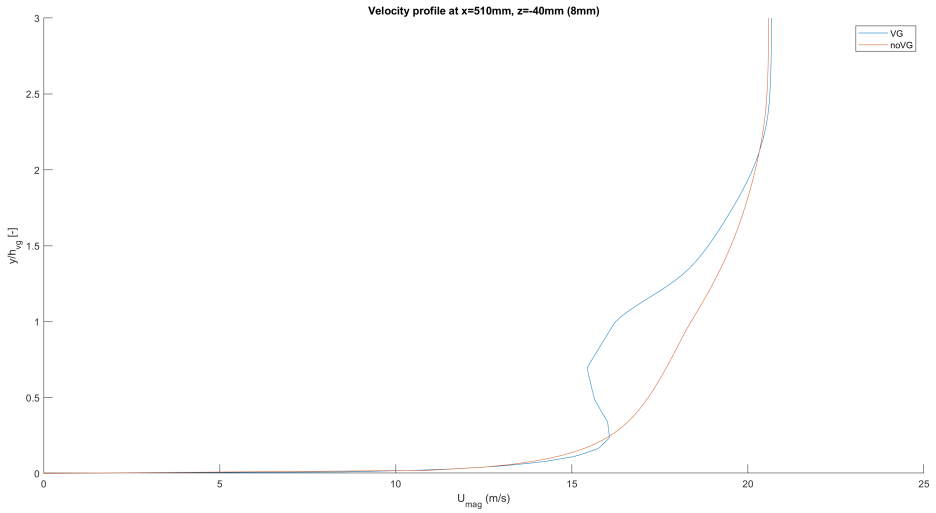

Figure 89: Velocity profile z=-40mm, x=510mm (8mm)

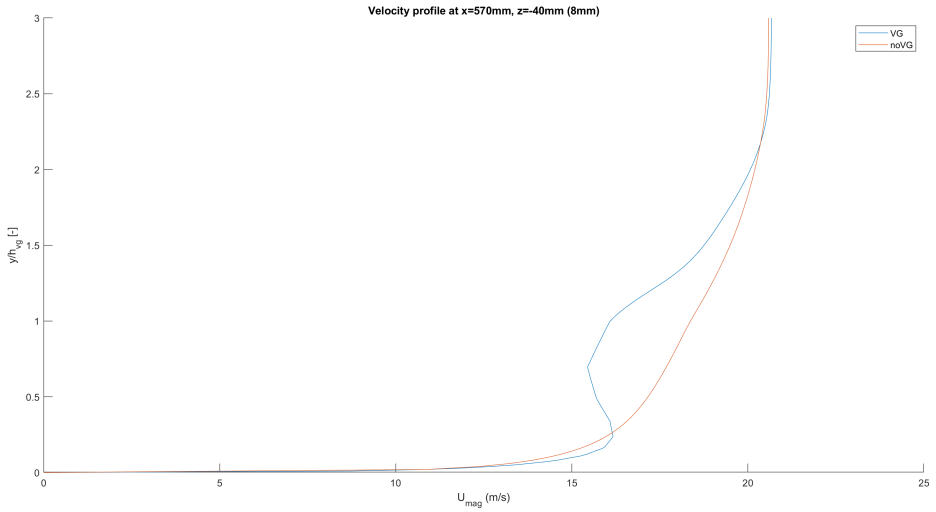

Figure 90: Velocity profile z=-40mm, x=570mm (8mm)

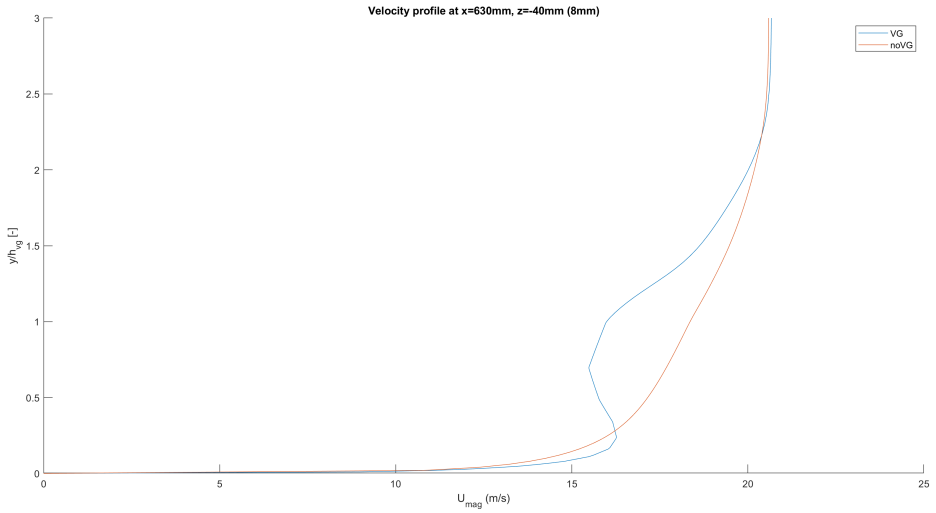

Figure 91: Velocity profile z=-40mm, x=630mm (8mm)

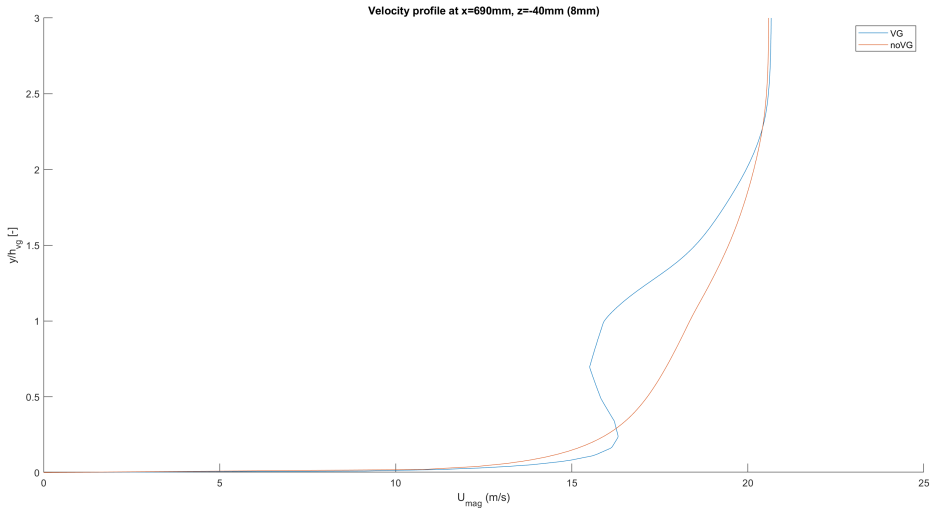

Figure 92: Velocity profile z=-40mm, x=690mm (8mm)

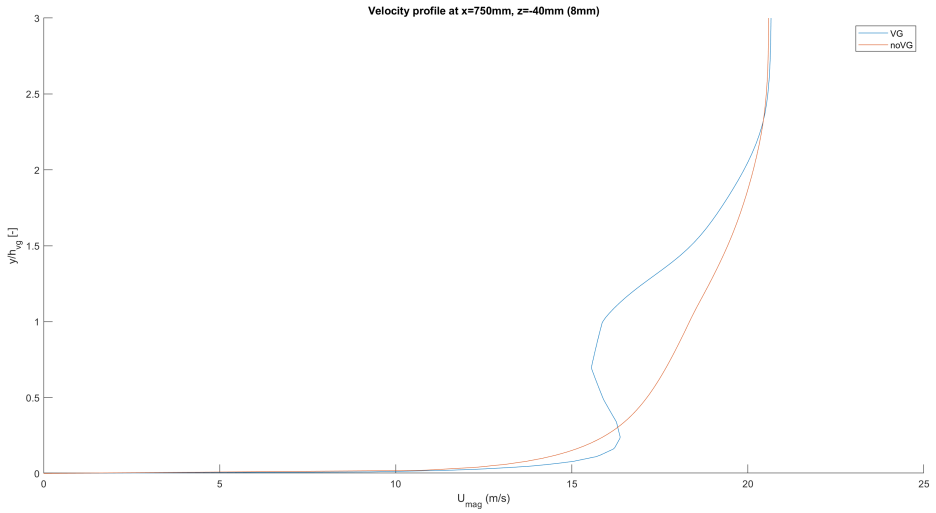

Figure 93: Velocity profile z=-40mm, x=750mm (8mm)

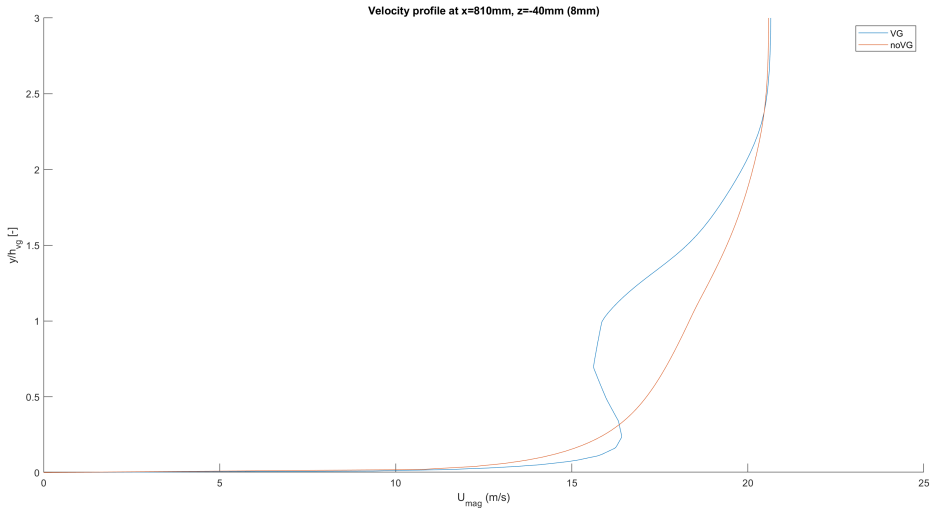

Figure 94: Velocity profile z=-40mm, x=810mm (8mm)

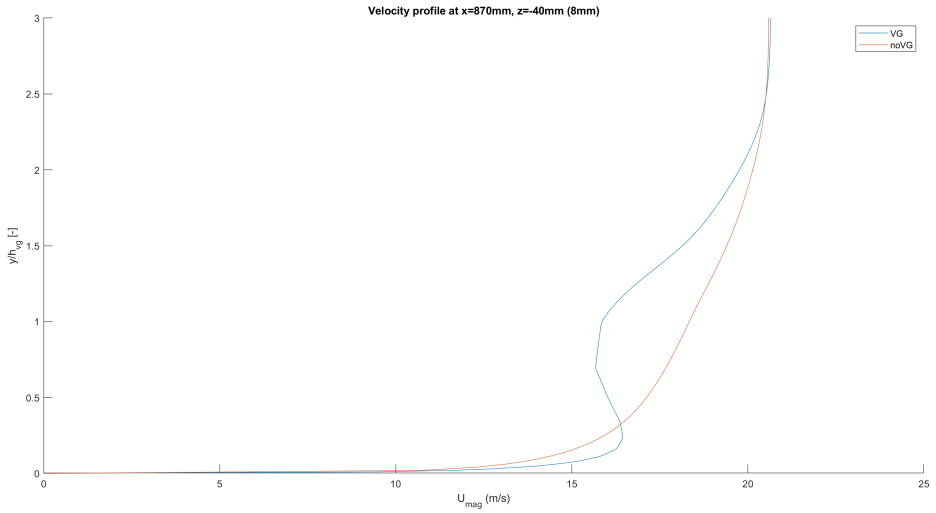

Figure 95: Velocity profile z=-40mm, x=870mm (8mm)

7.2.3 Velocity profiles z=-40mm (12mm)

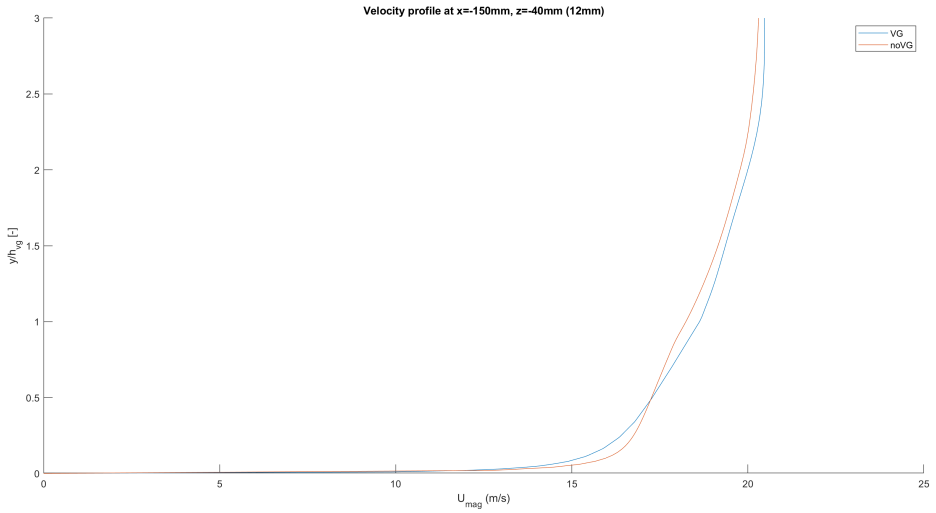

Figure 96: Velocity profile z=-40mm, x=-150mm (12mm)

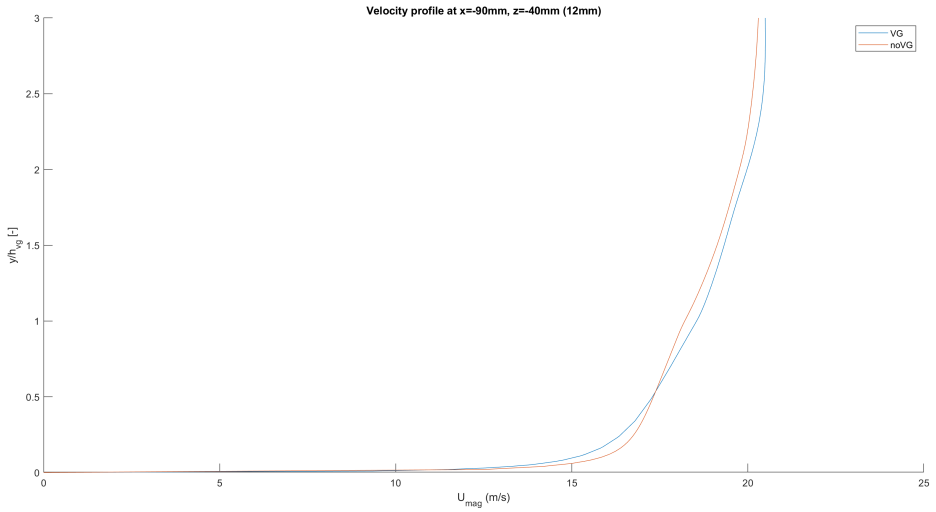

Figure 97: Velocity profile z=-40mm, x=-90mm (12mm)

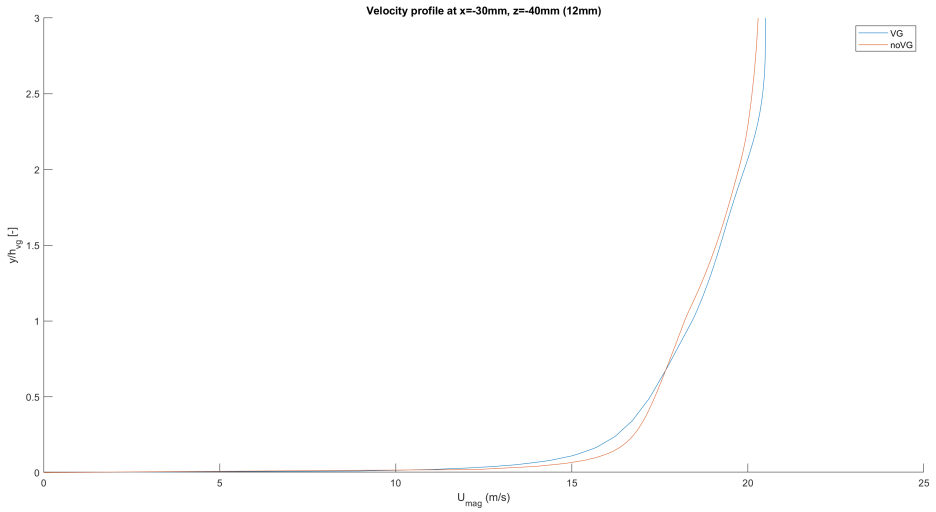

Figure 98: Velocity profile z=-40mm, x=-30mm (12mm)

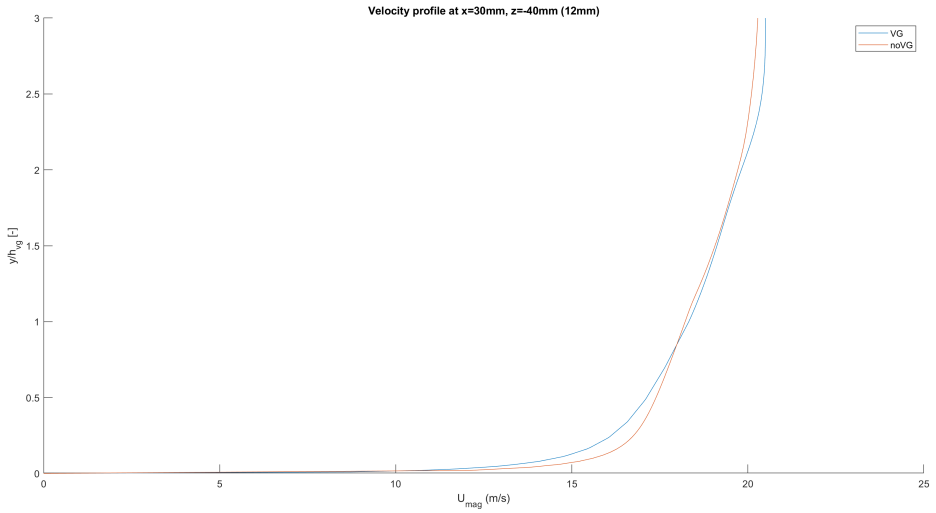

Figure 99: Velocity profile z=-40mm, x=30mm (12mm)

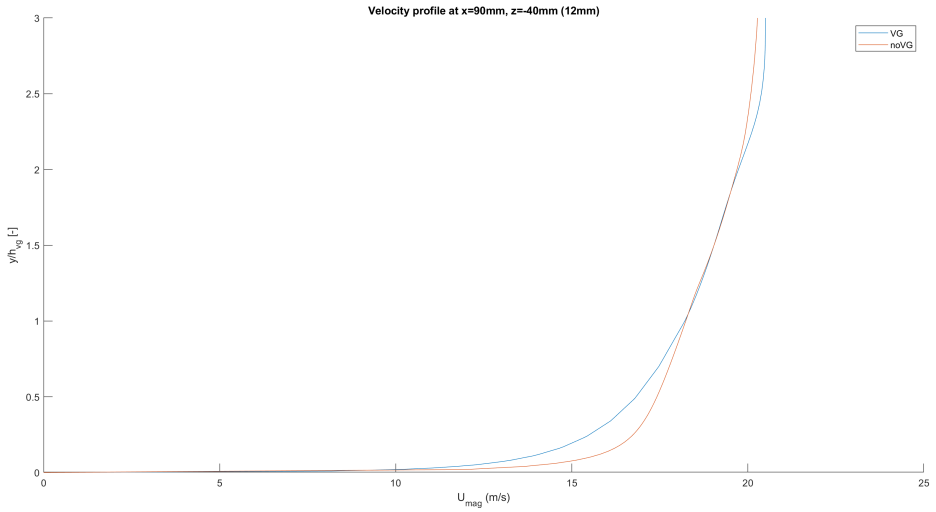

Figure 100: Velocity profile z=-40mm, x=90mm (12mm)

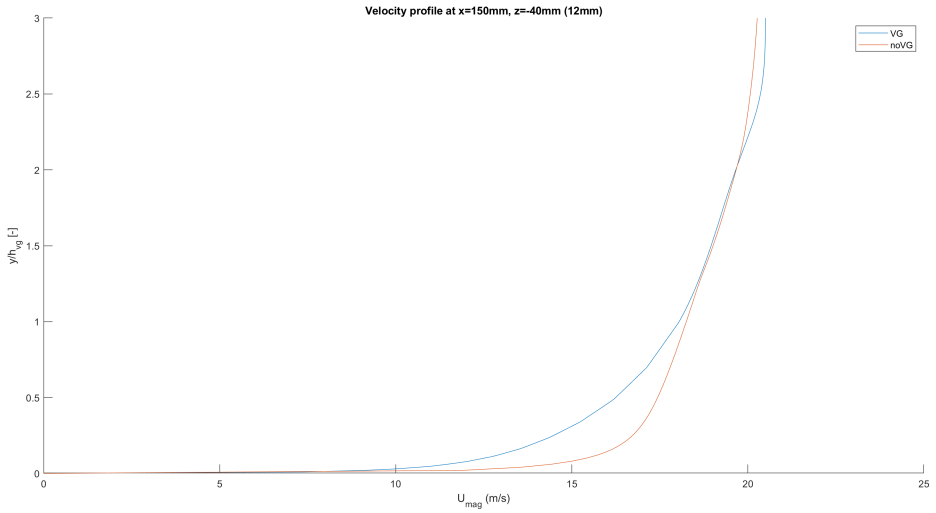

Figure 101: Velocity profile z=-40mm, x=150mm (12mm)

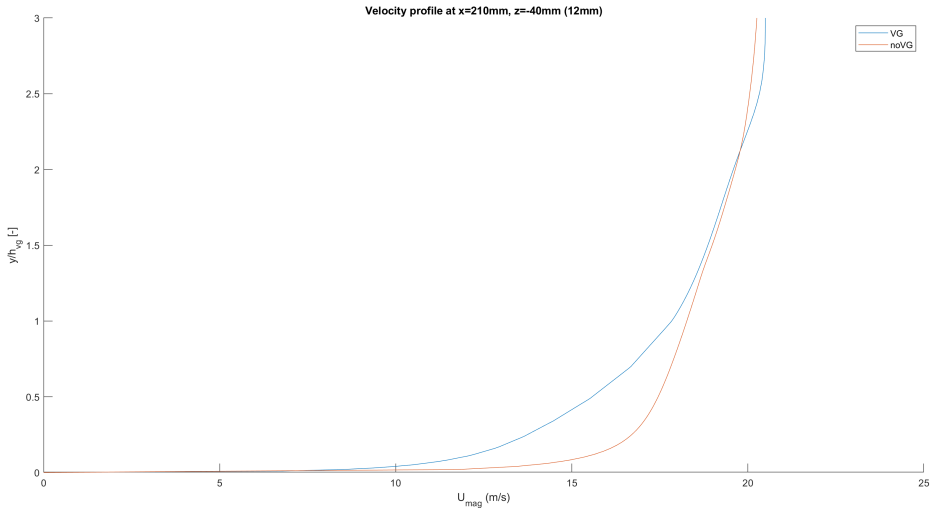

Figure 102: Velocity profile z=-40mm, x=210mm (12mm)

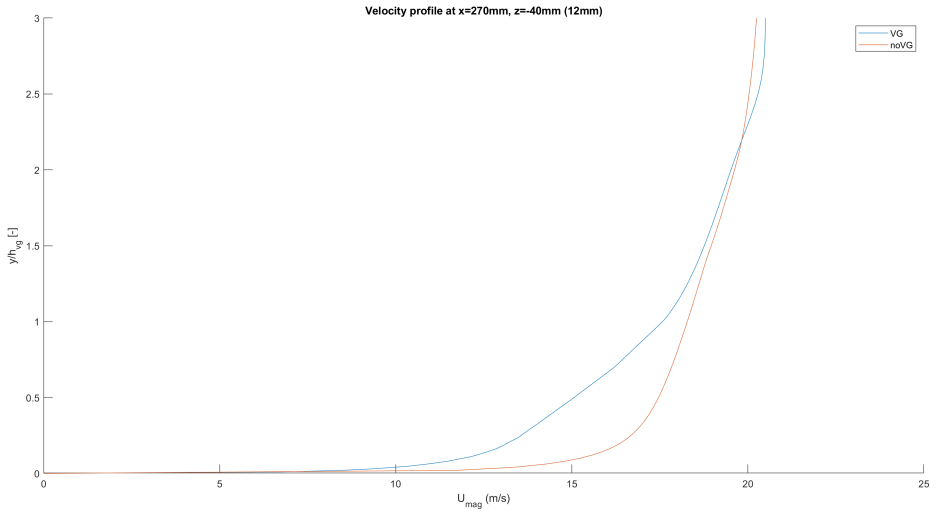

Figure 103: Velocity profile z=-40mm, x=270mm (12mm)

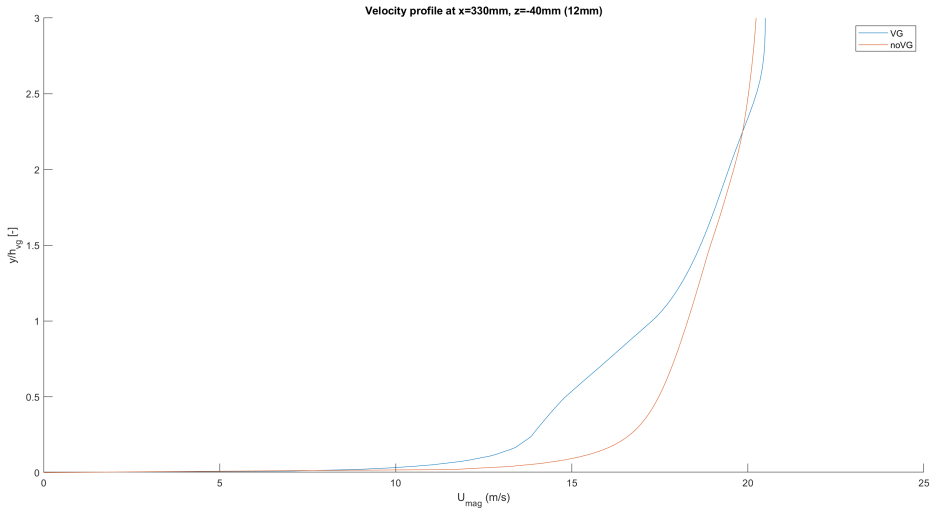

Figure 104: Velocity profile z=-40mm, x=330mm (12mm)

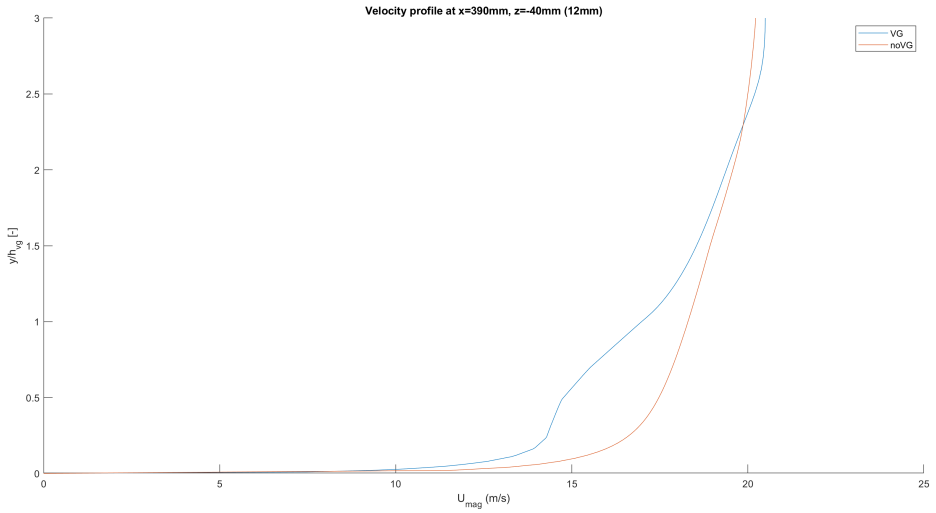

Figure 105: Velocity profile z=-40mm, x=390mm (12mm)

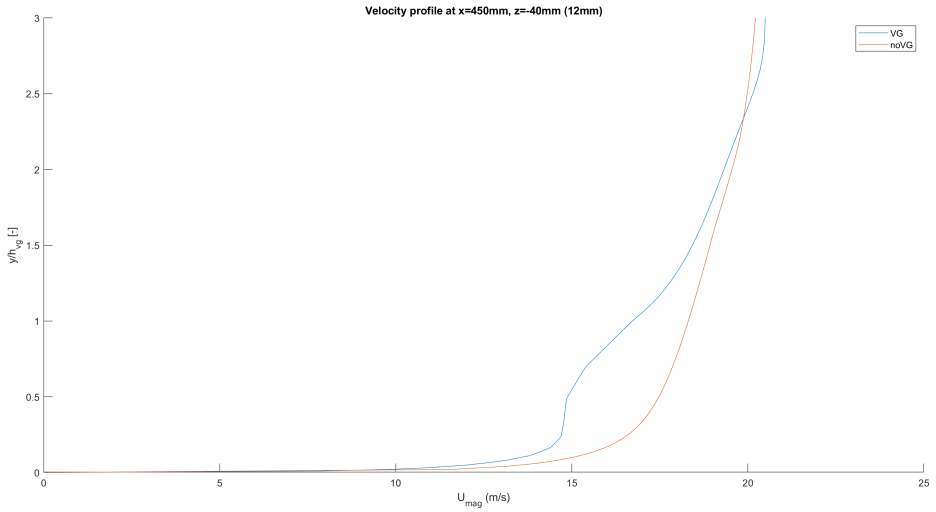

Figure 106: Velocity profile z=-40mm, x=450mm (12mm)

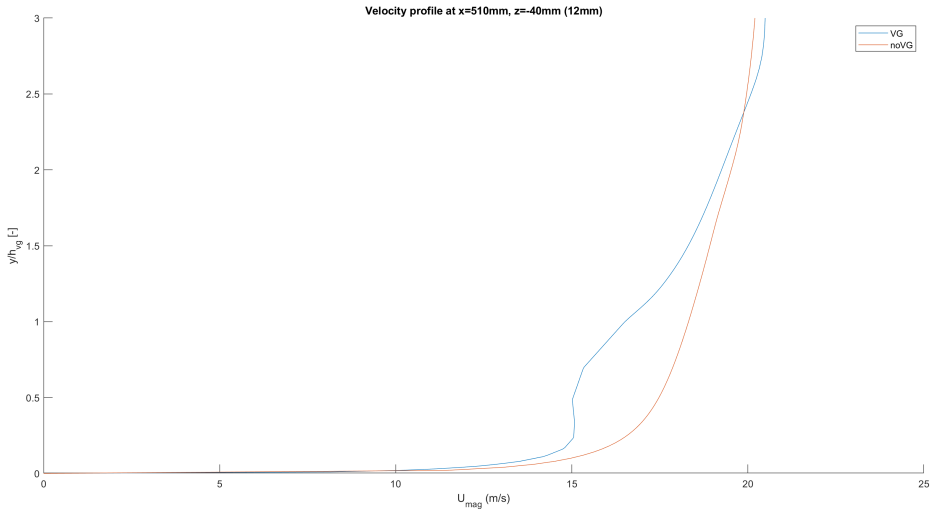

Figure 107: Velocity profile z=-40mm, x=510mm (12mm)

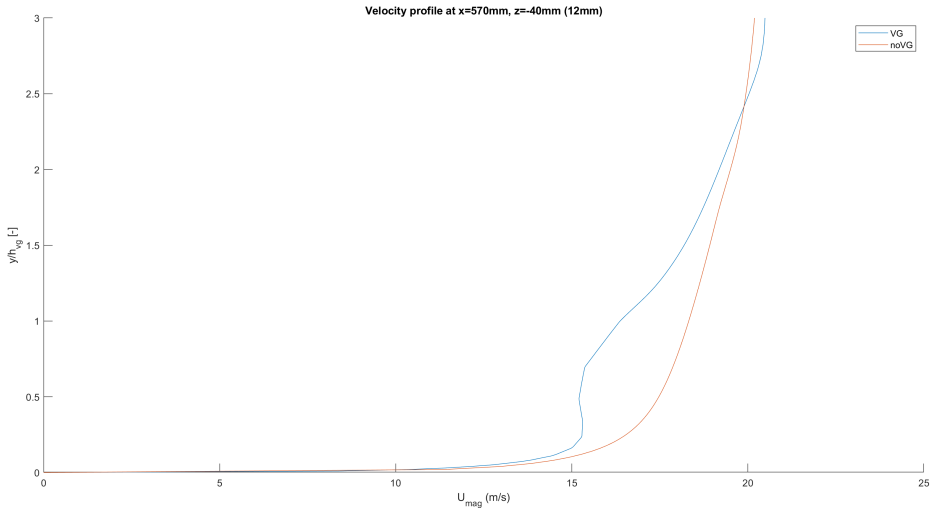

Figure 108: Velocity profile z=-40mm, x=570mm (12mm)

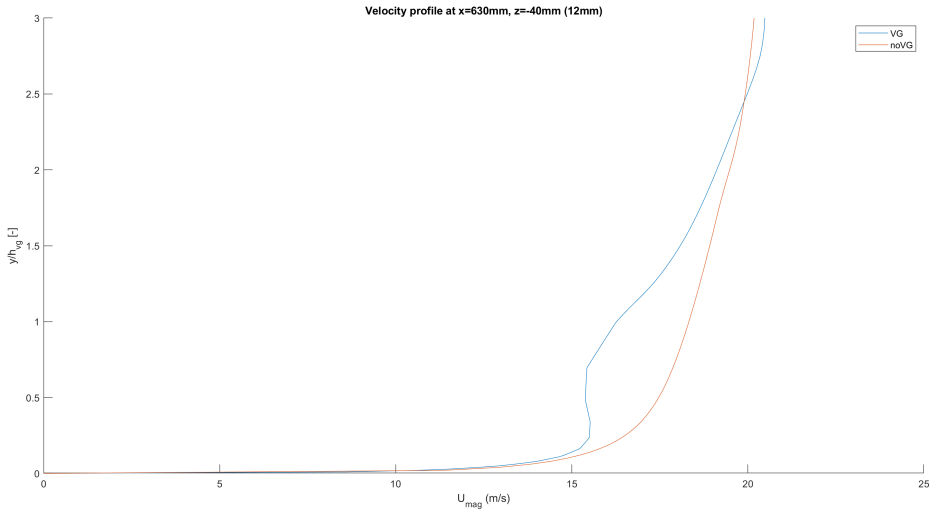

Figure 109: Velocity profile z=-40mm, x=630mm (12mm)

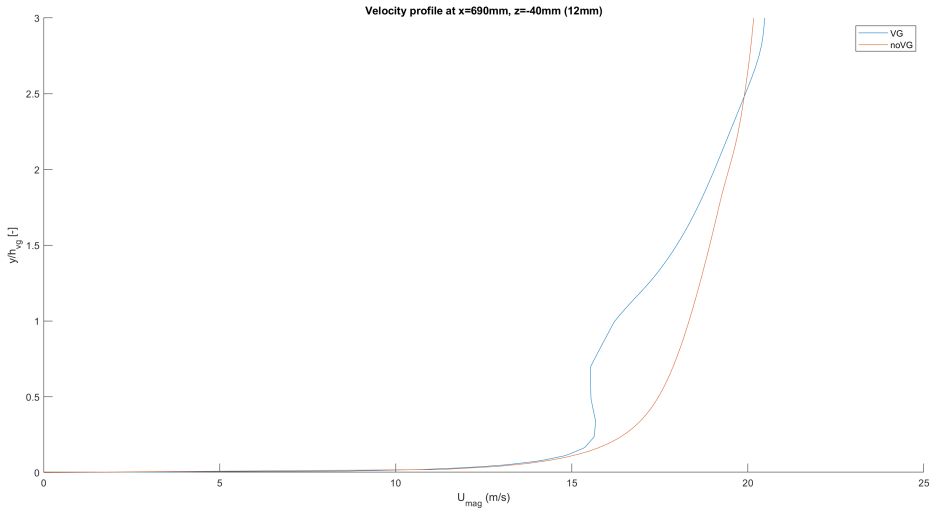

Figure 110: Velocity profile z=-40mm, x=690mm (12mm)

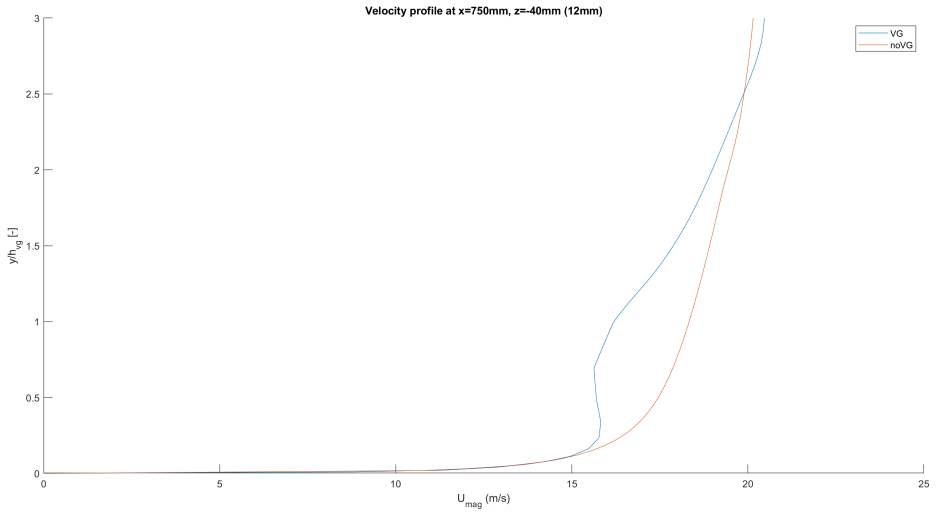

Figure 111: Velocity profile z=-40mm, x=750mm (12mm)

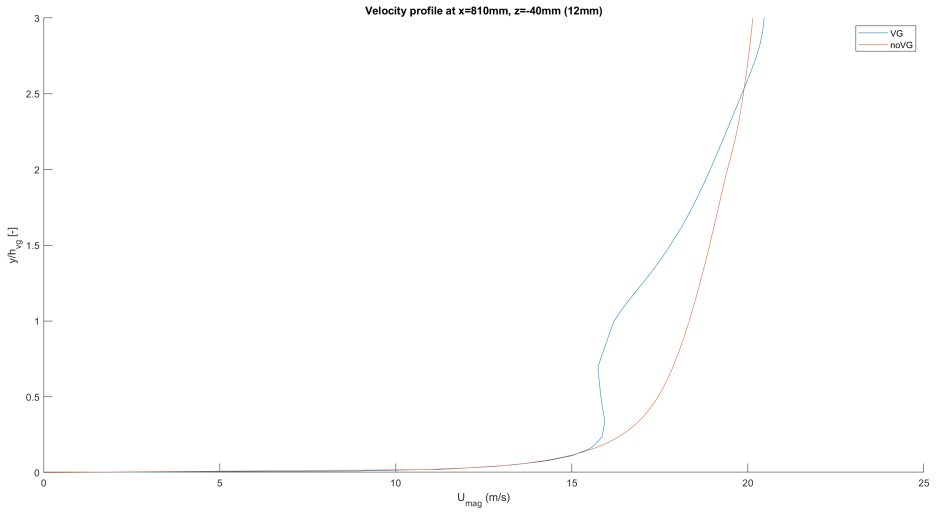

Figure 112: Velocity profile z=-40mm, x=810mm (12mm)

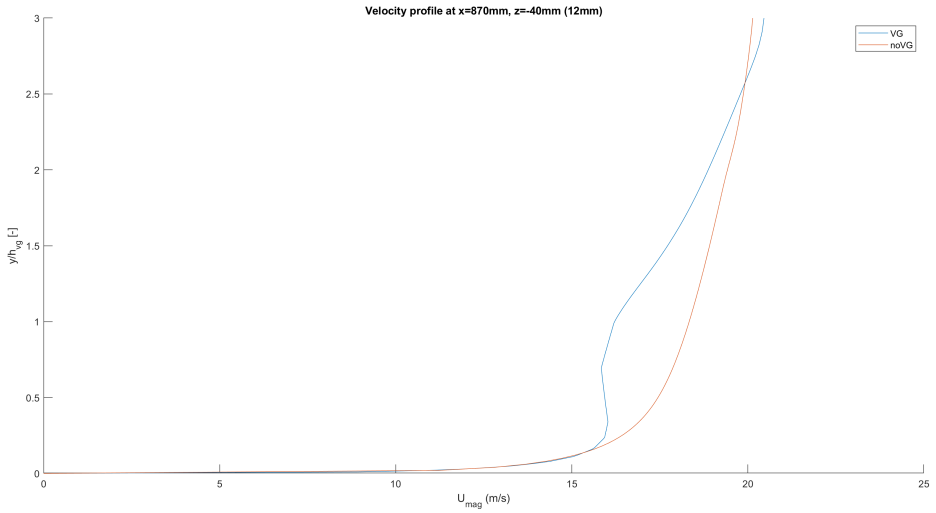

Figure 113: Velocity profile z=-40mm, x=870mm (12mm)

7.2.4 Velocity profiles z=0mm (free)

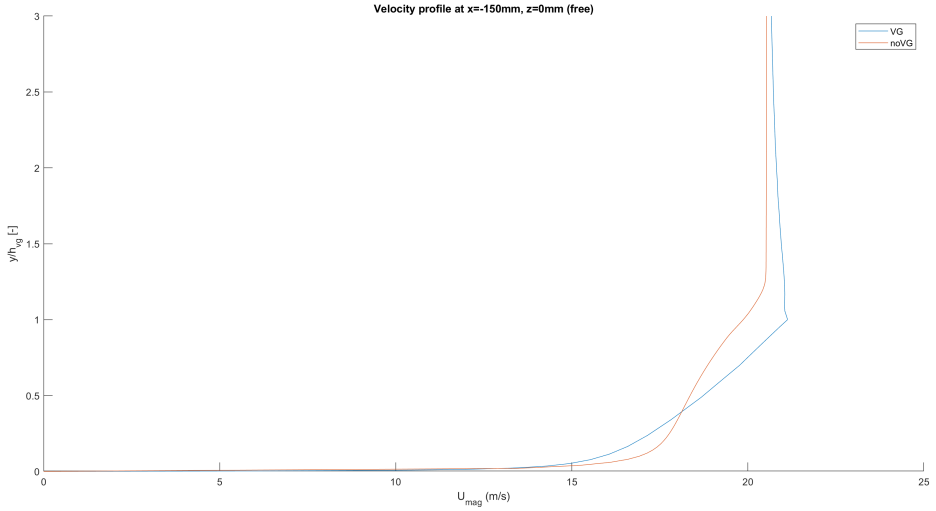

Figure 114: Velocity profile z=0mm, x=-150mm (free)

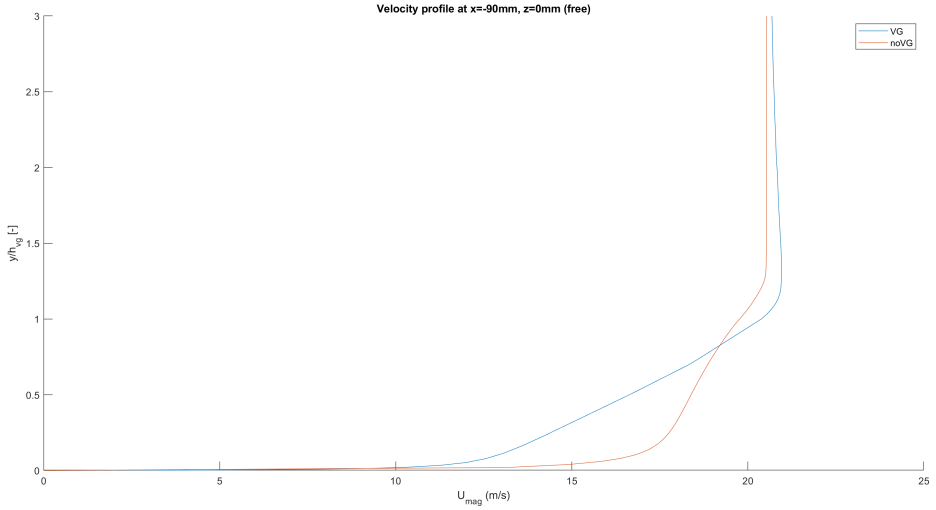

Figure 115: Velocity profile z=0mm, x=-90mm (free)

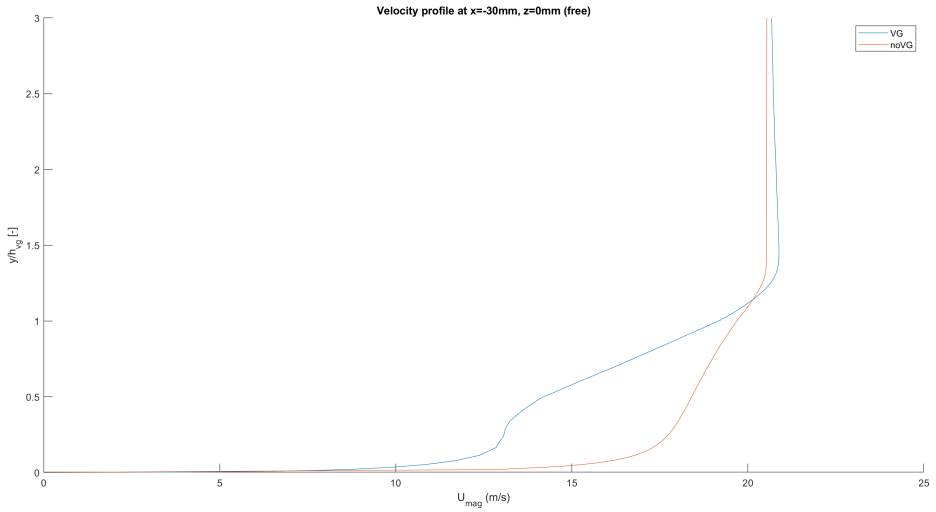

Figure 116: Velocity profile z=0mm, x=-30mm (free)

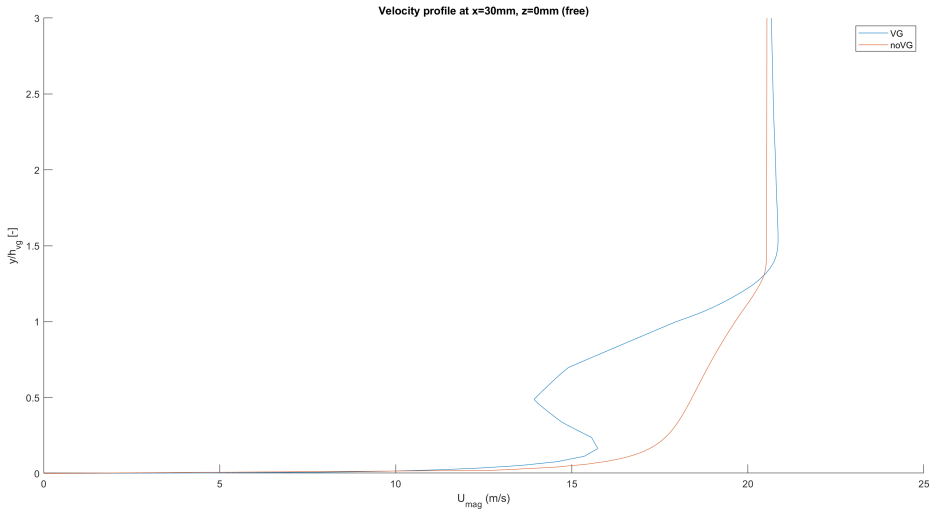

Figure 117: Velocity profile z=0mm, x=30mm (free)

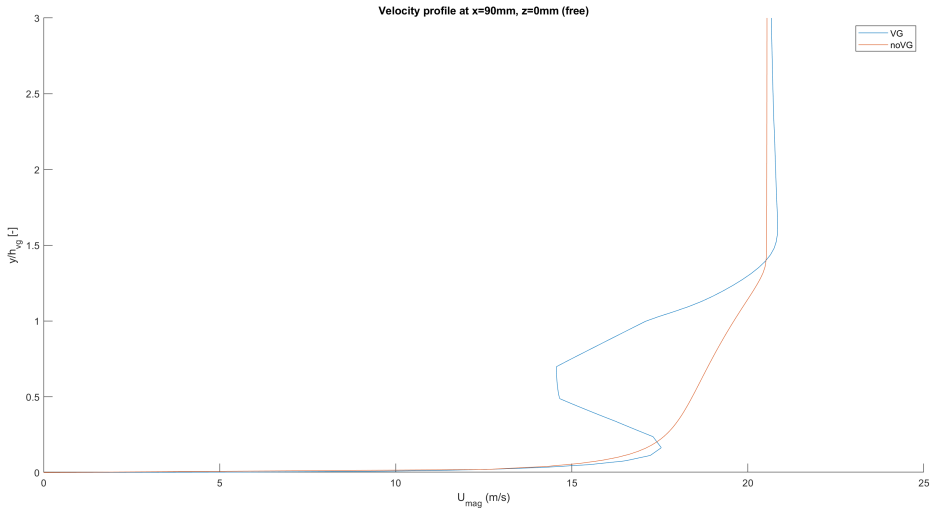

Figure 118: Velocity profile z=0mm, x=90mm (free)

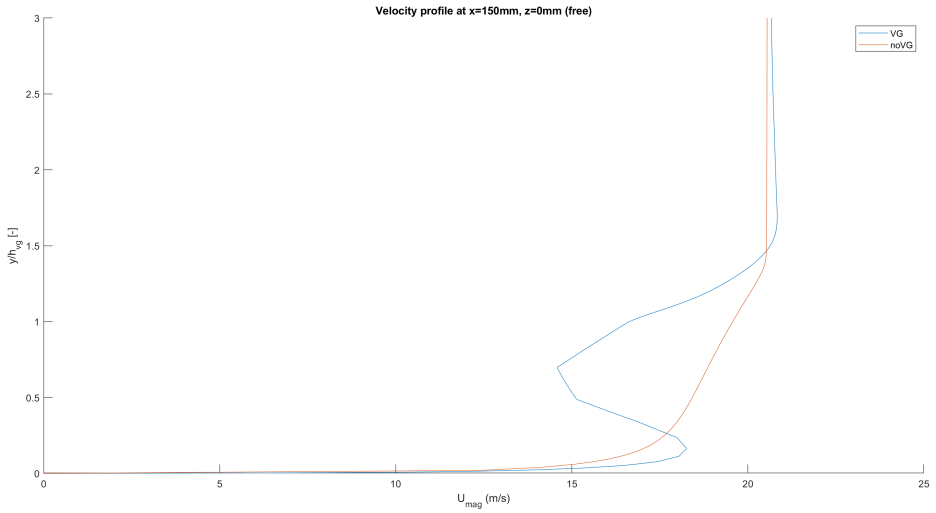

Figure 119: Velocity profile z=0mm, x=150mm (free)

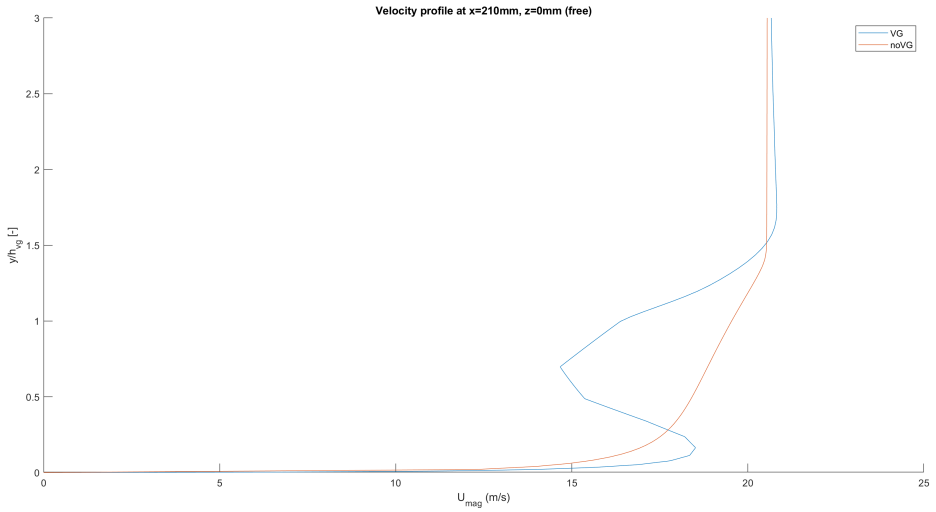

Figure 120: Velocity profile z=0mm, x=210mm (free)

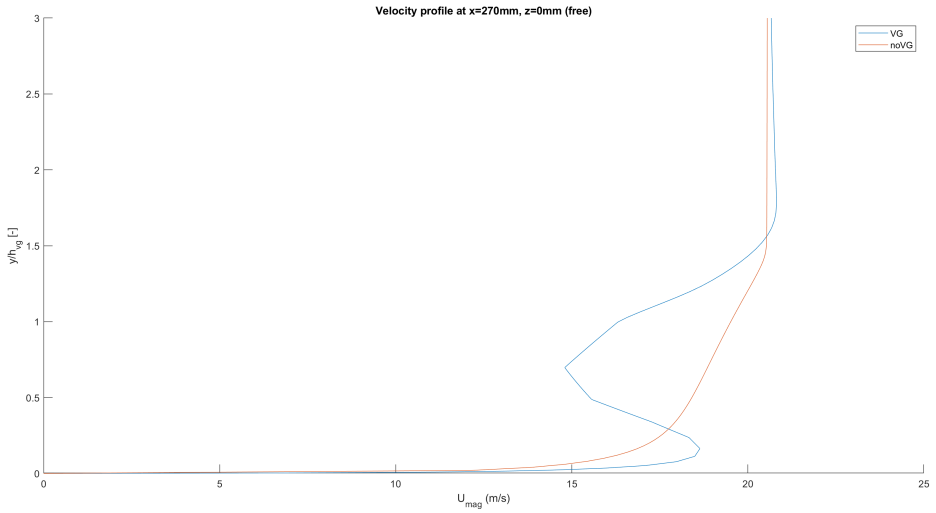

Figure 121: Velocity profile z=0mm, x=270mm (free)

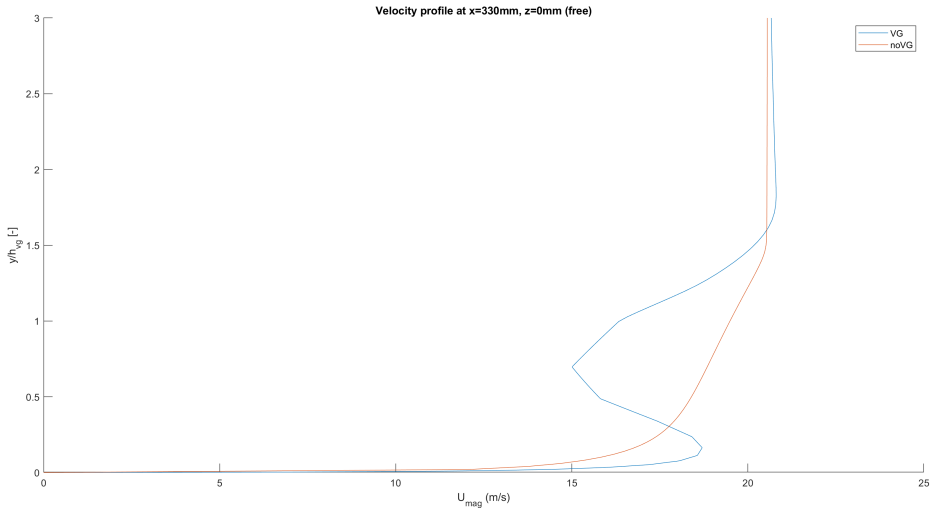

Figure 122: Velocity profile z=0mm, x=330mm (free)

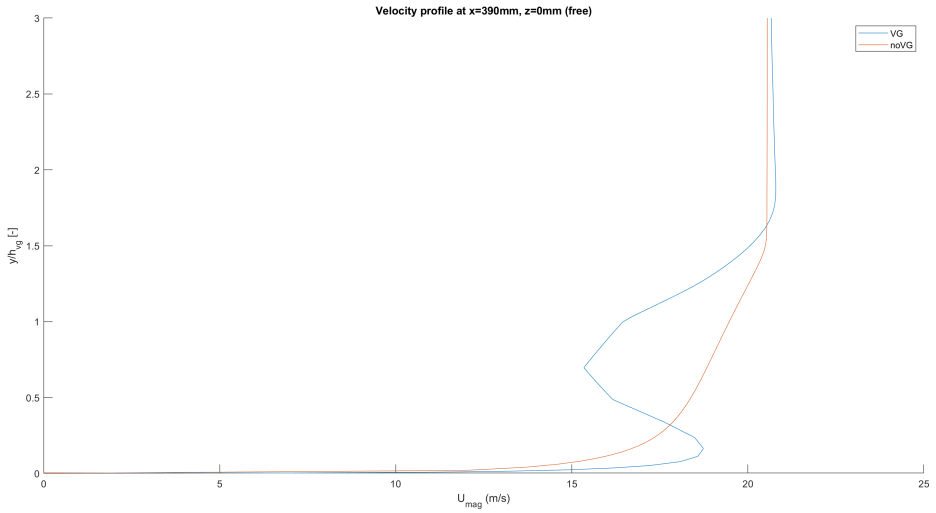

Figure 123: Velocity profile z=0mm, x=390mm (free)

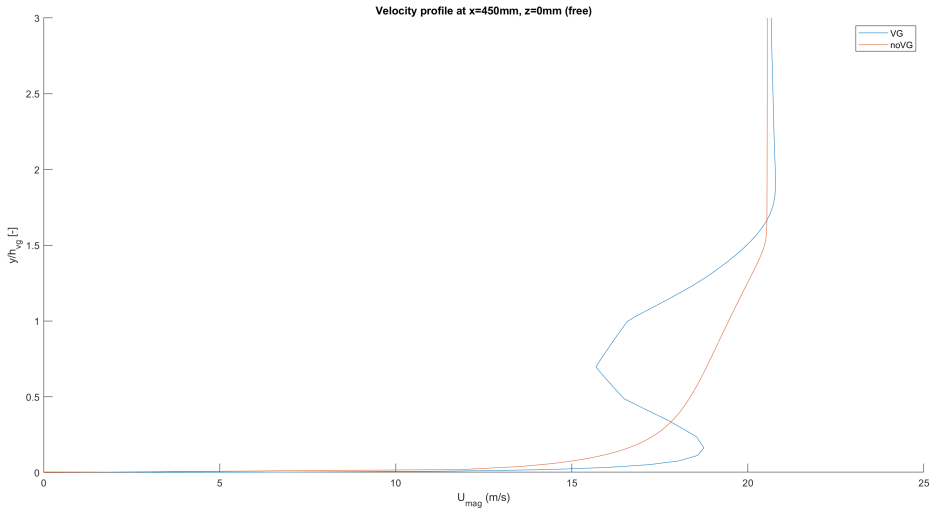

Figure 124: Velocity profile z=0mm, x=450mm (free)

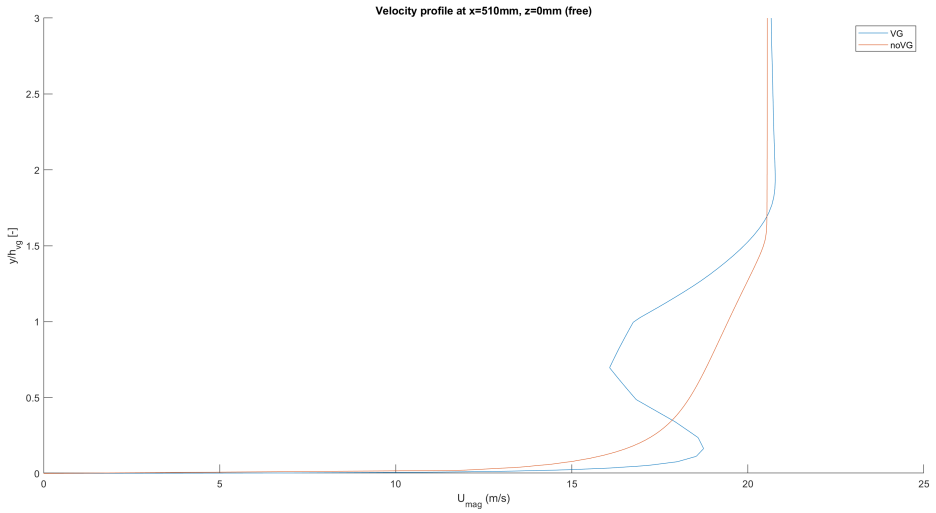

Figure 125: Velocity profile z=0mm, x=510mm (free)

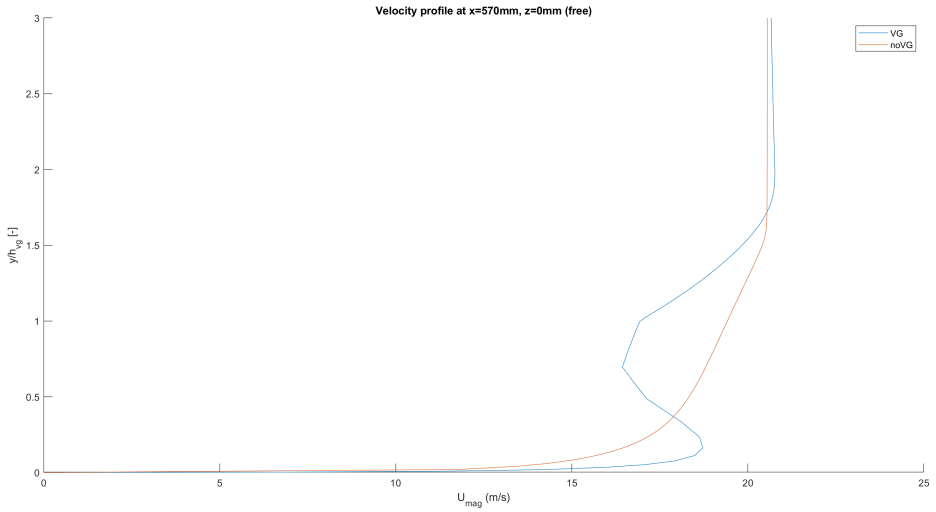

Figure 126: Velocity profile z=0mm, x=570mm (free)

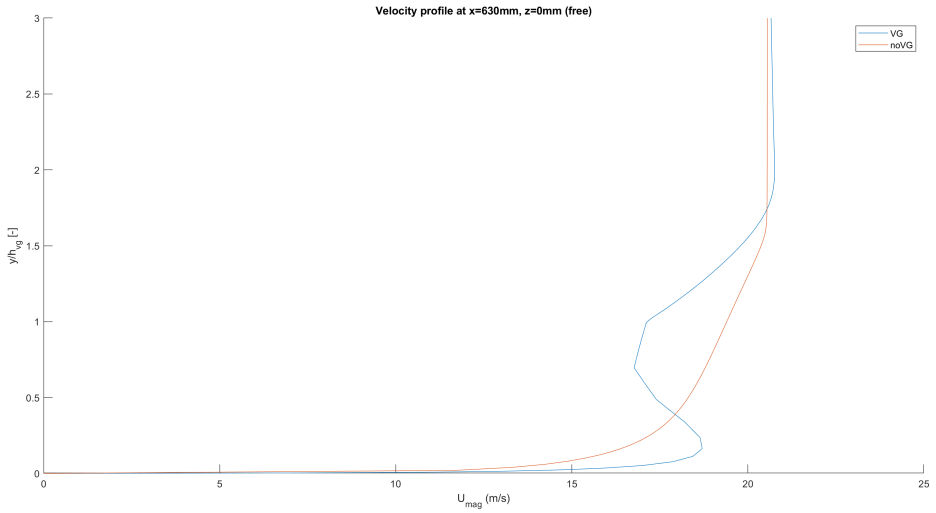

Figure 127: Velocity profile z=0mm, x=630mm (free)

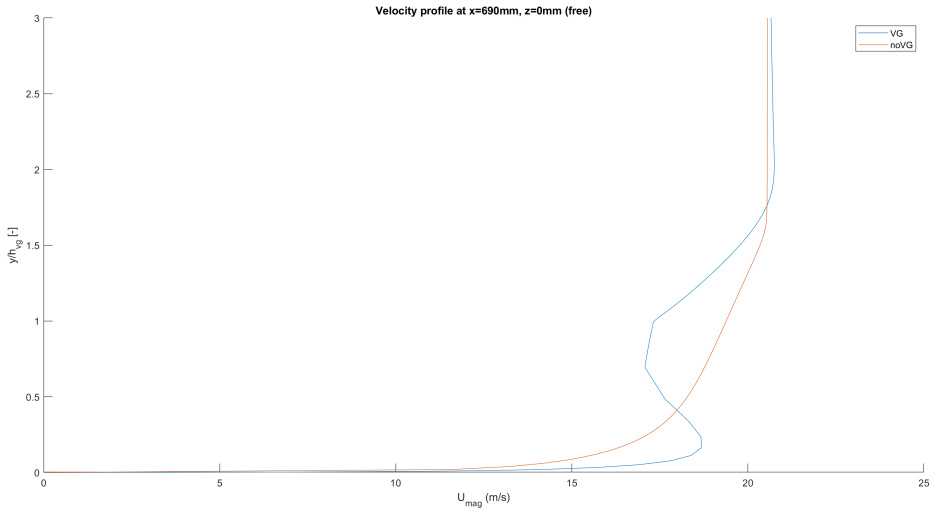

Figure 128: Velocity profile z=0mm, x=690mm (free)

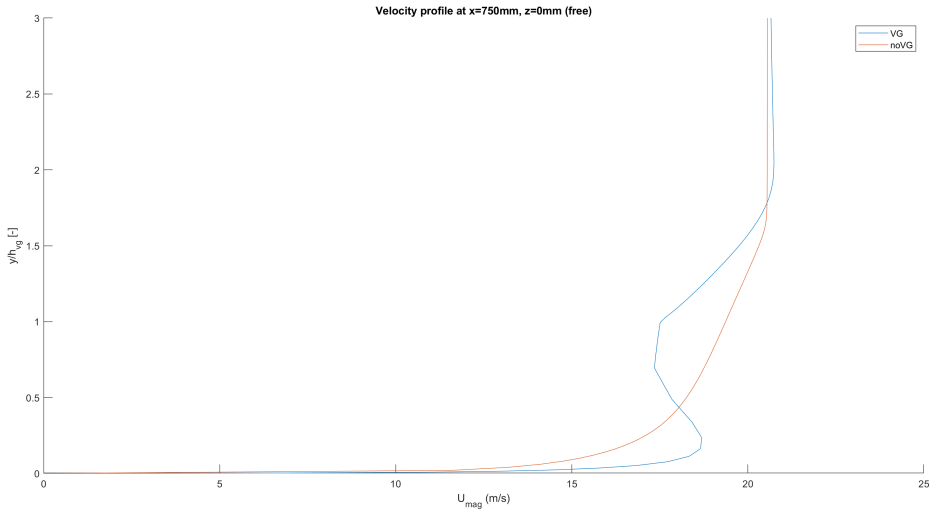

Figure 129: Velocity profile z=0mm, x=750mm (free)

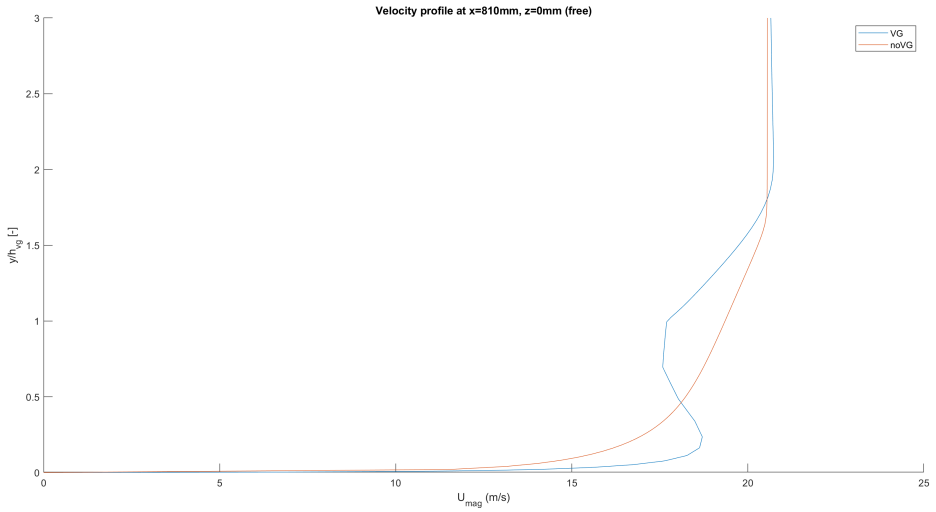

Figure 130: Velocity profile z=0mm, x=810mm (free)

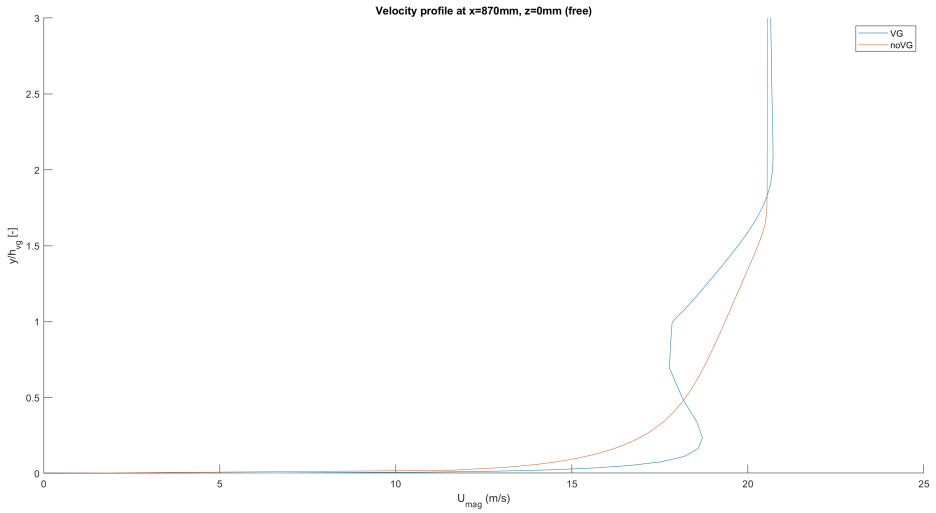

Figure 131: Velocity profile z=0mm, x=870mm (free)

7.2.5 Velocity profiles z=0mm (8mm)

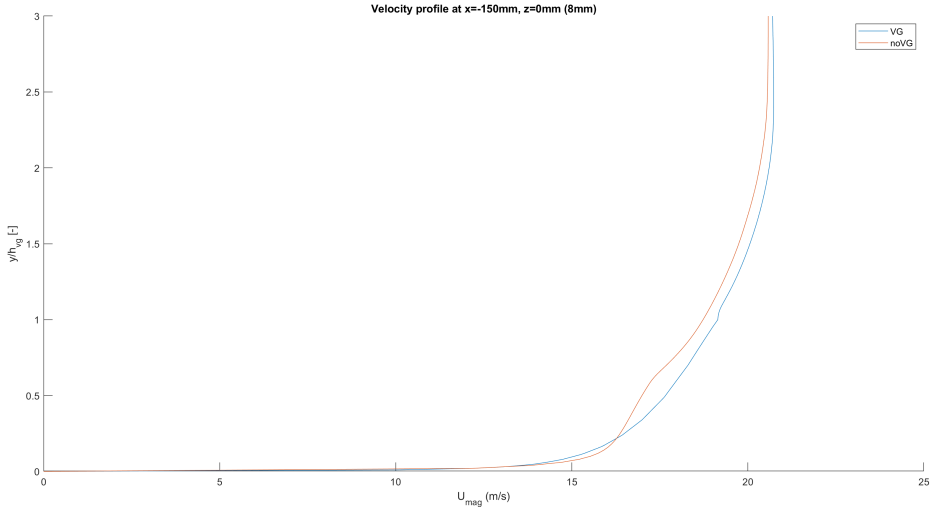

Figure 132: Velocity profile z=0mm, x=-150mm (8mm)

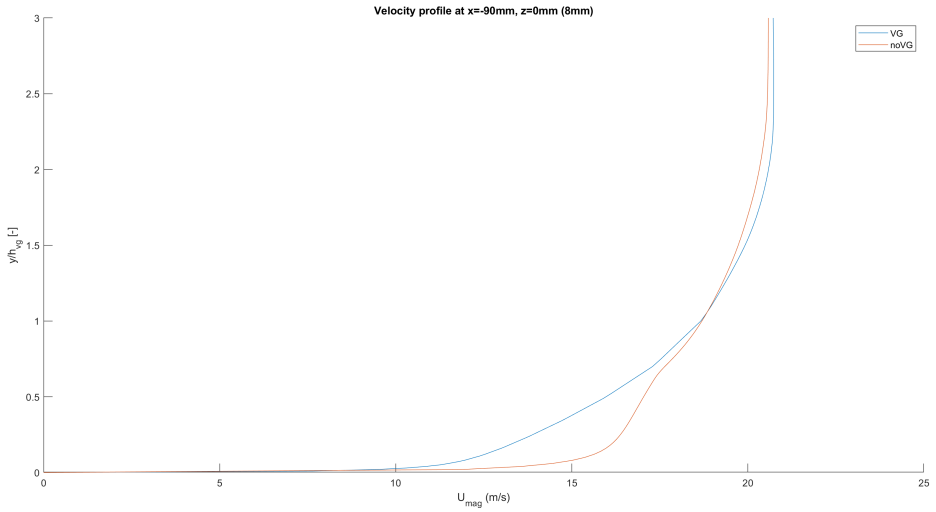

Figure 133: Velocity profile z=0mm, x=-90mm (8mm)

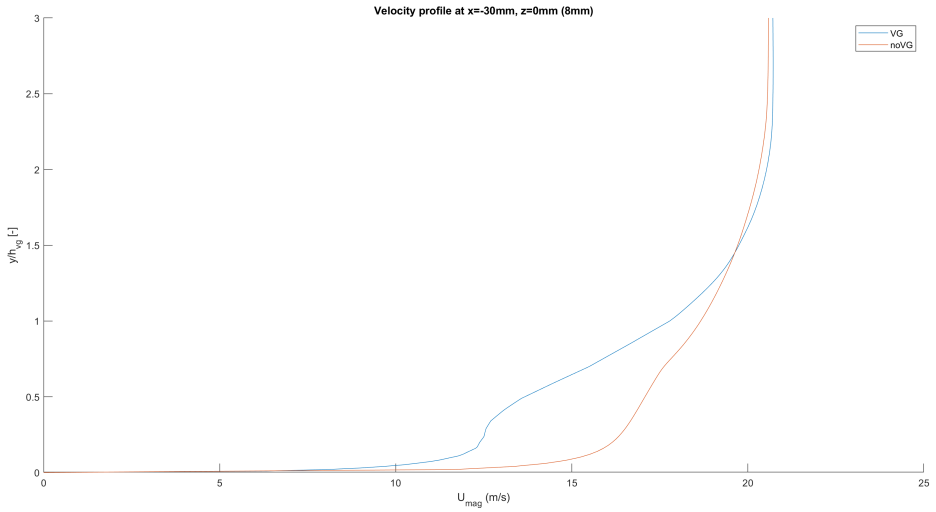

Figure 134: Velocity profile z=0mm, x=-30mm (8mm)

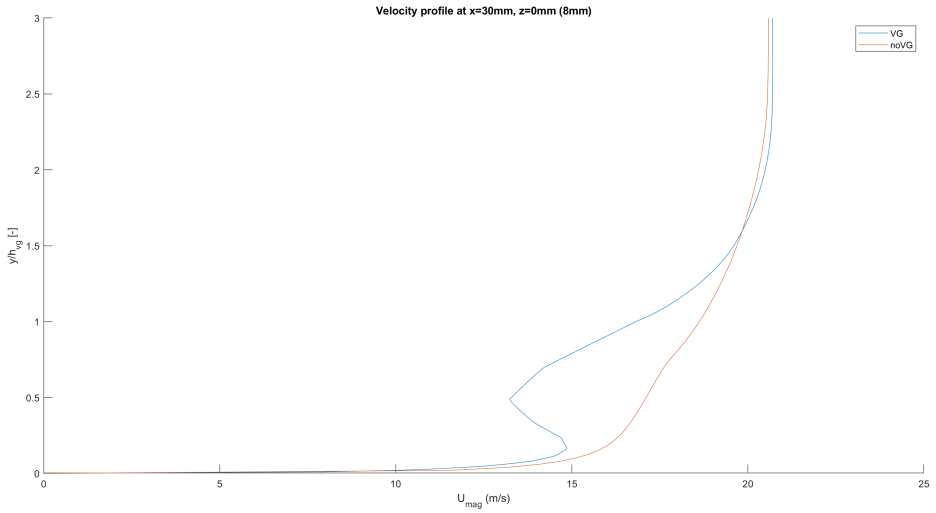

Figure 135: Velocity profile z=0mm, x=30mm (8mm)

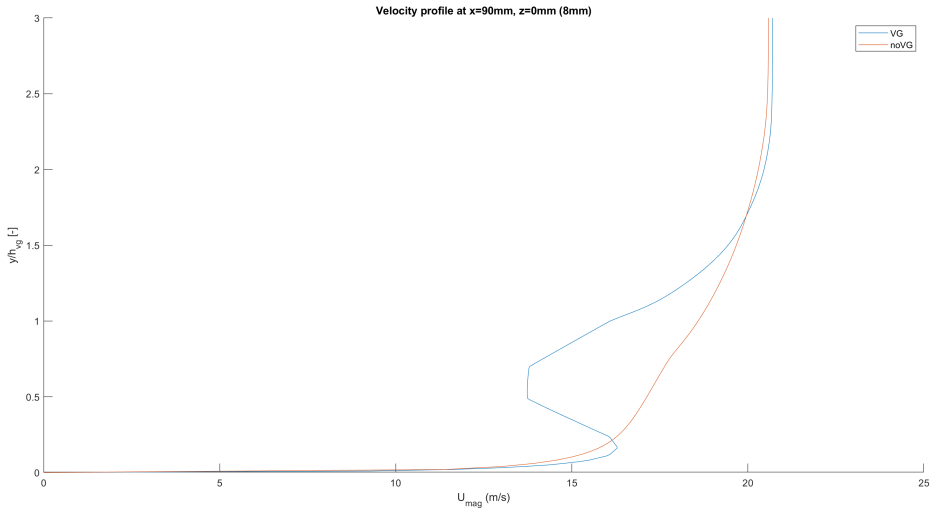

Figure 136: Velocity profile z=0mm, x=90mm (8mm)

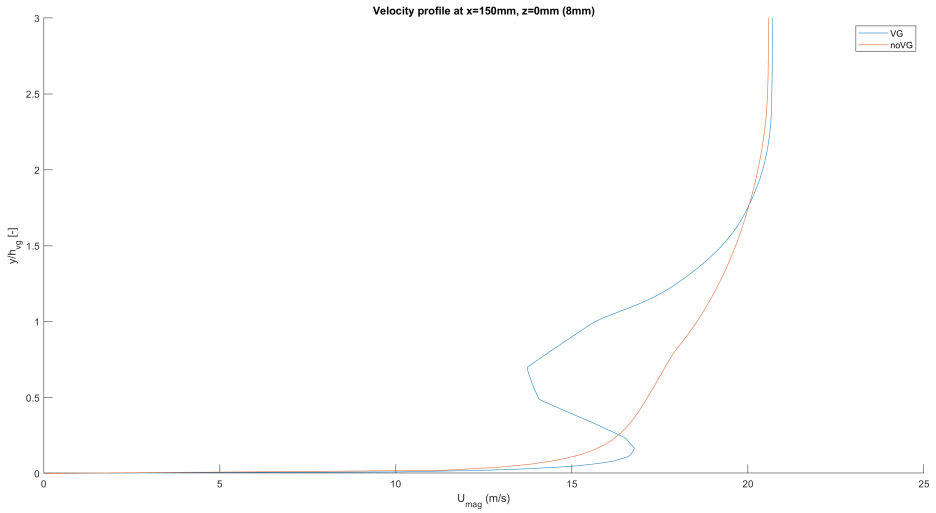

Figure 137: Velocity profile z=0mm, x=150mm (8mm)

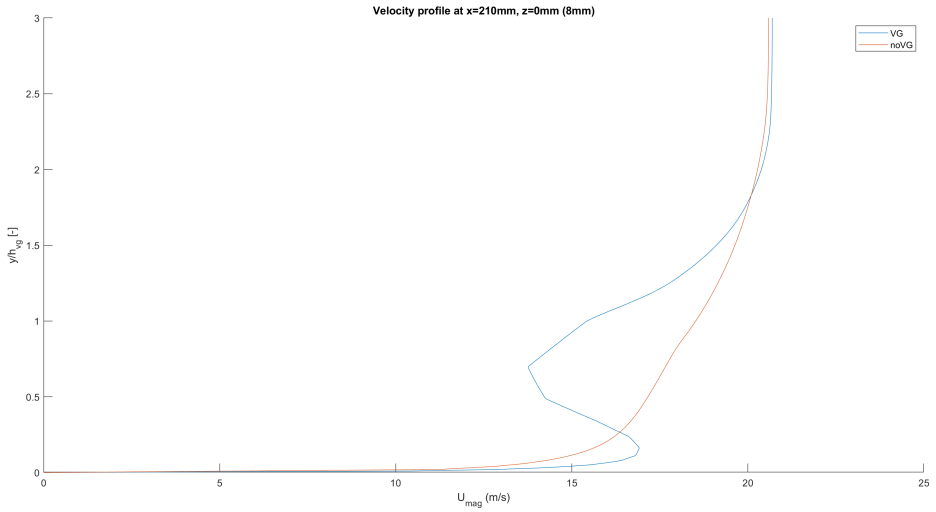

Figure 138: Velocity profile z=0mm, x=210mm (8mm)

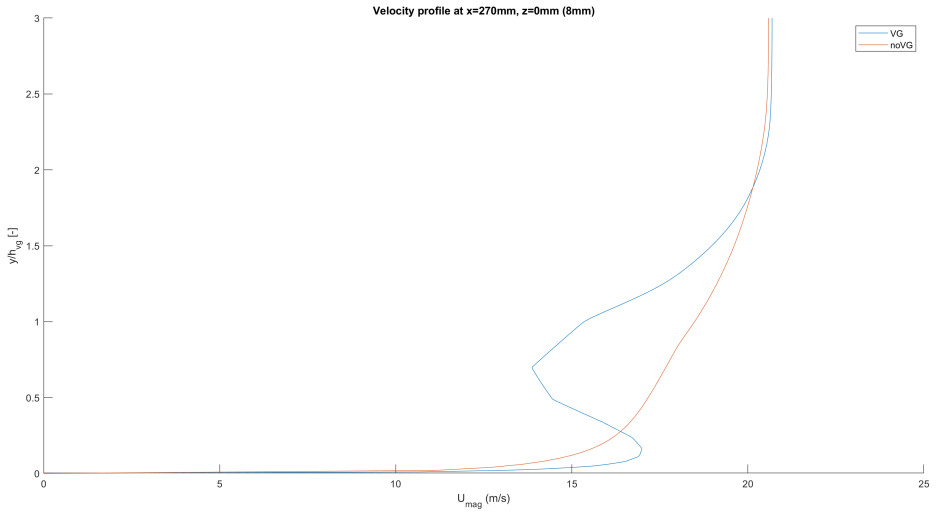

Figure 139: Velocity profile z=0mm, x=270mm (8mm)

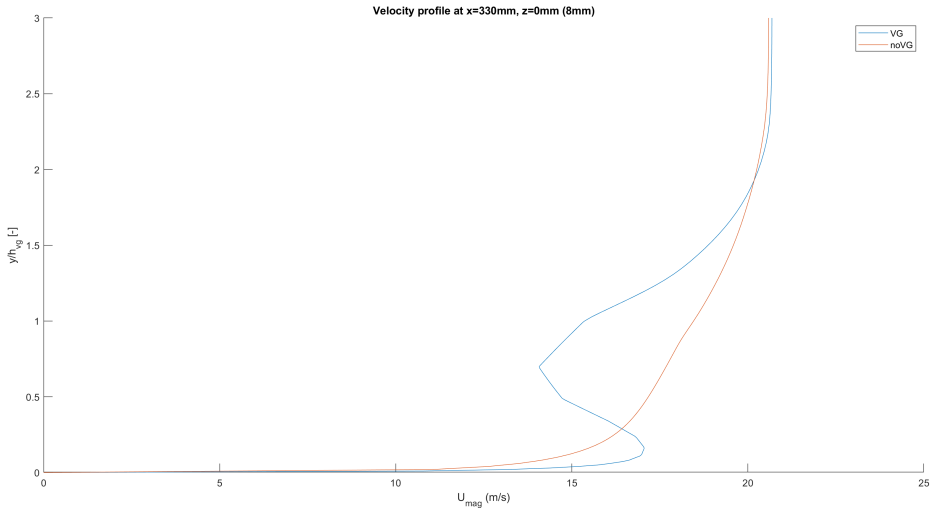

Figure 140: Velocity profile z=0mm, x=330mm (8mm)

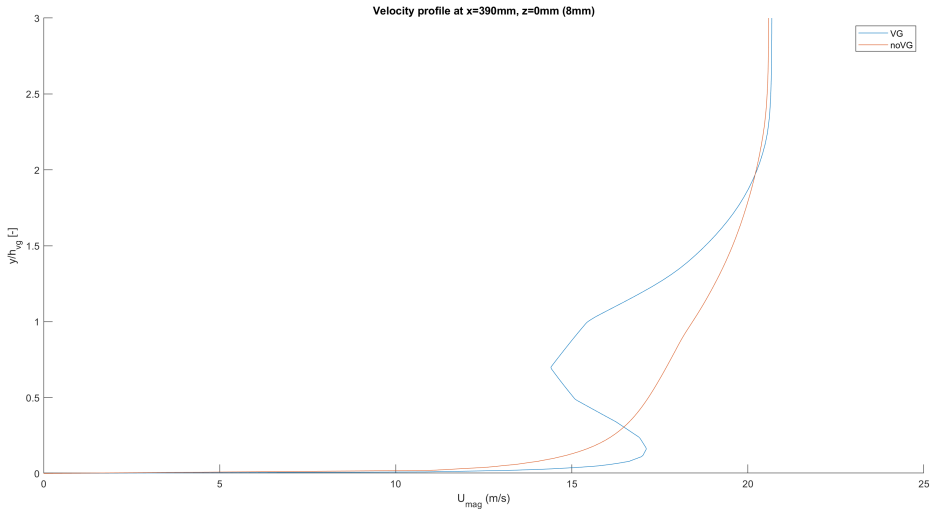

Figure 141: Velocity profile z=0mm, x=390mm (8mm)

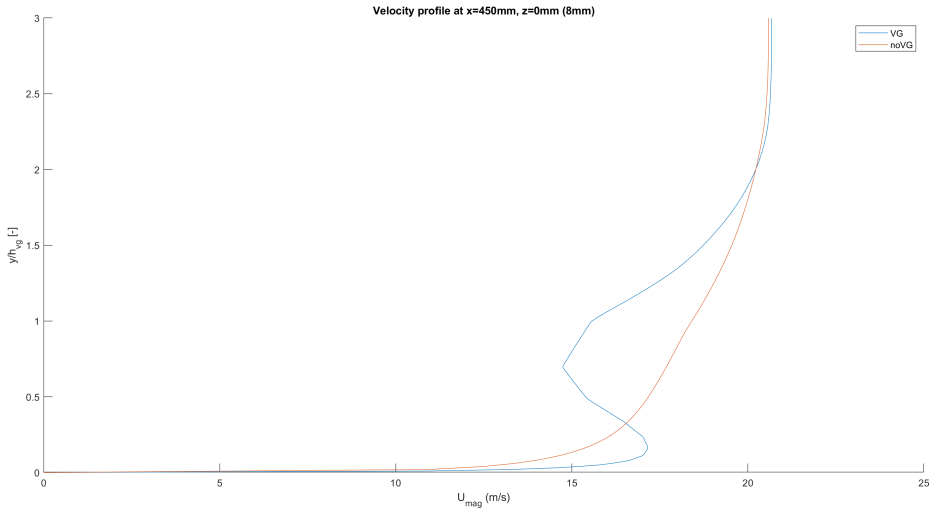

Figure 142: Velocity profile z=0mm, x=450mm (8mm)

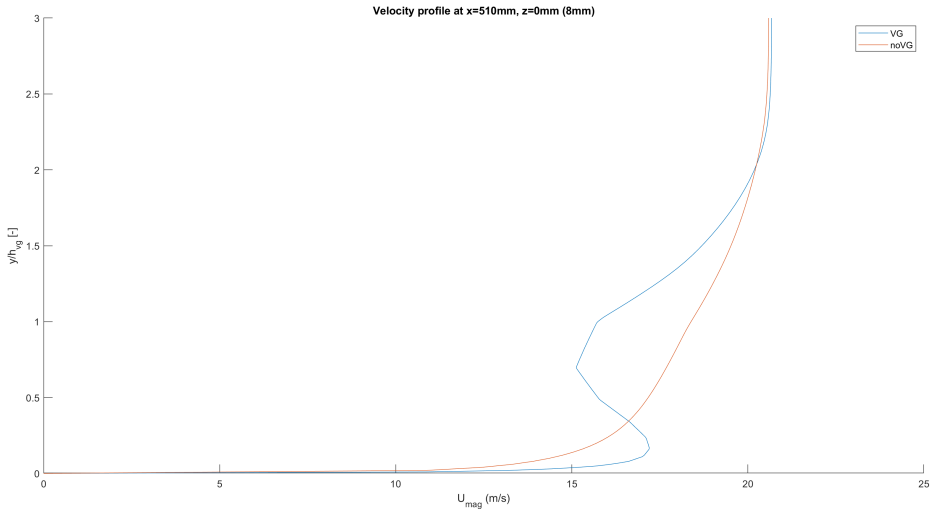

Figure 143: Velocity profile z=0mm, x=510mm (8mm)

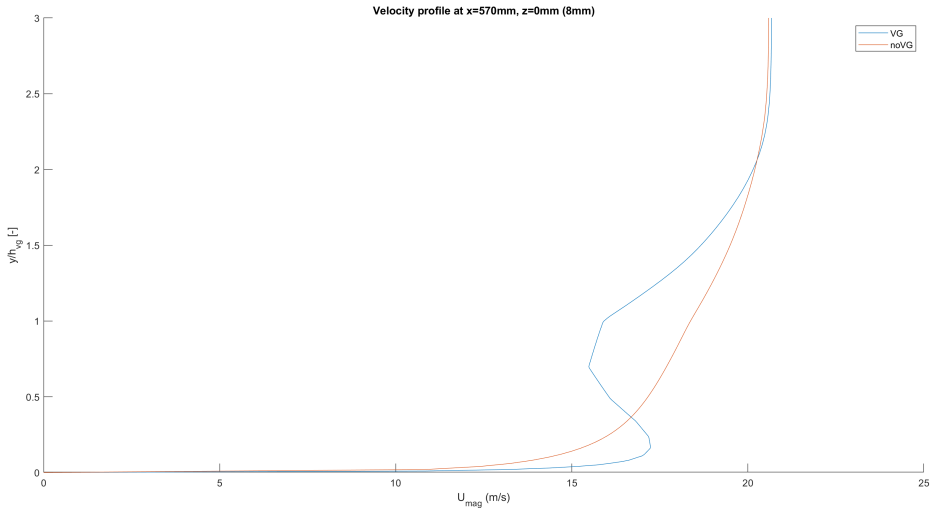

Figure 144: Velocity profile z=0mm, x=570mm (8mm)

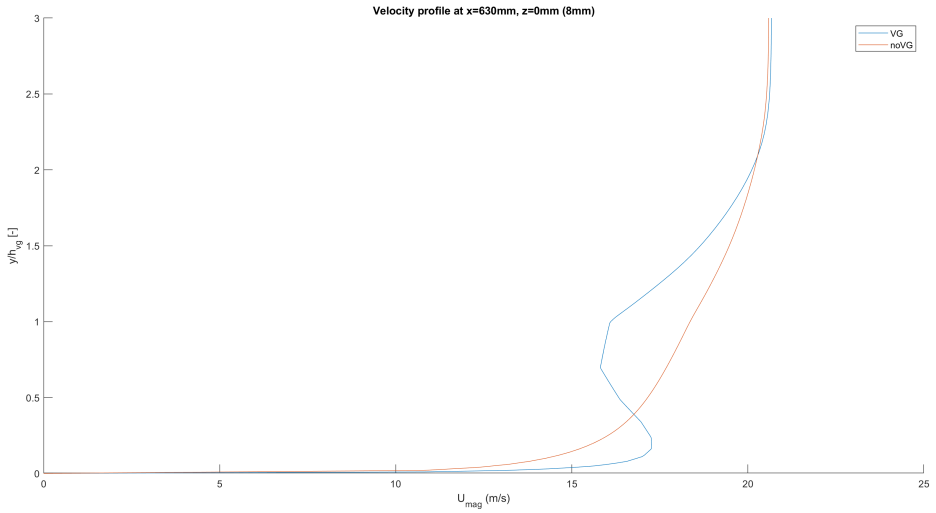

Figure 145: Velocity profile z=0mm, x=630mm (8mm)

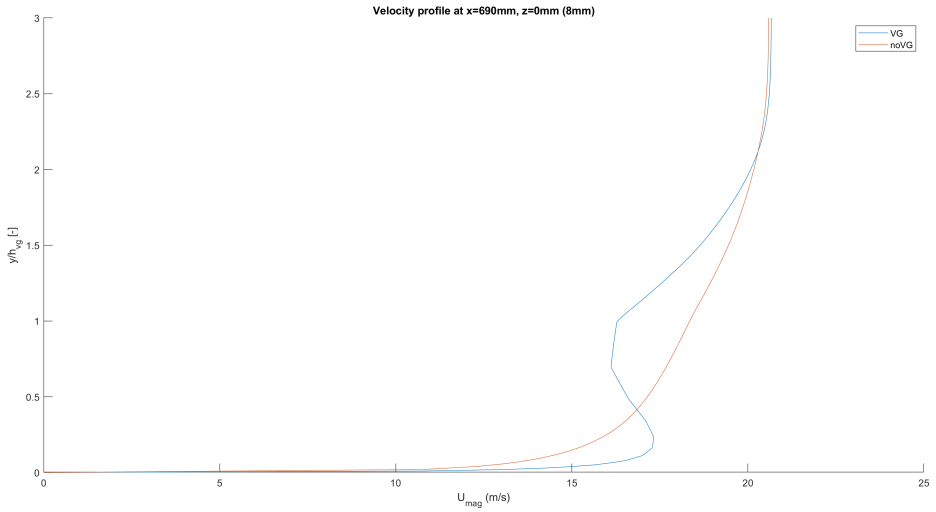

Figure 146: Velocity profile z=0mm, x=690mm (8mm)

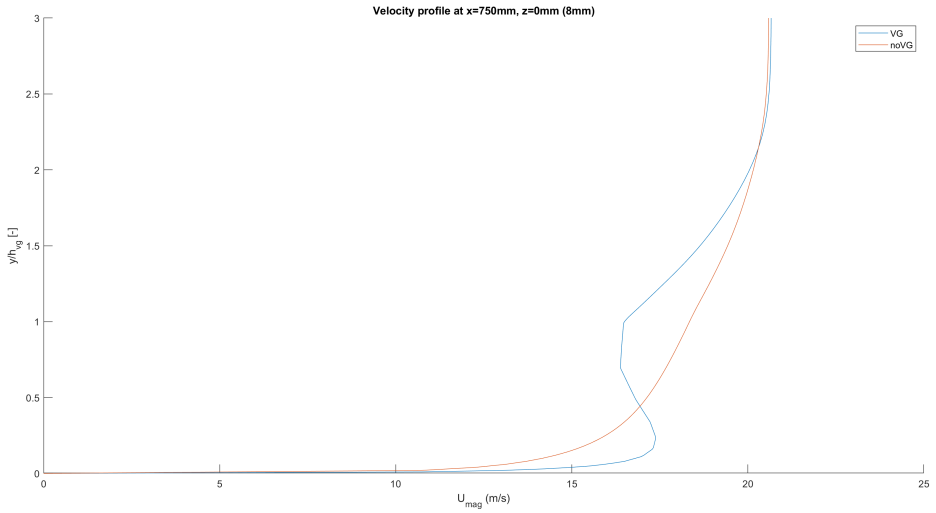

Figure 147: Velocity profile z=0mm, x=750mm (8mm)

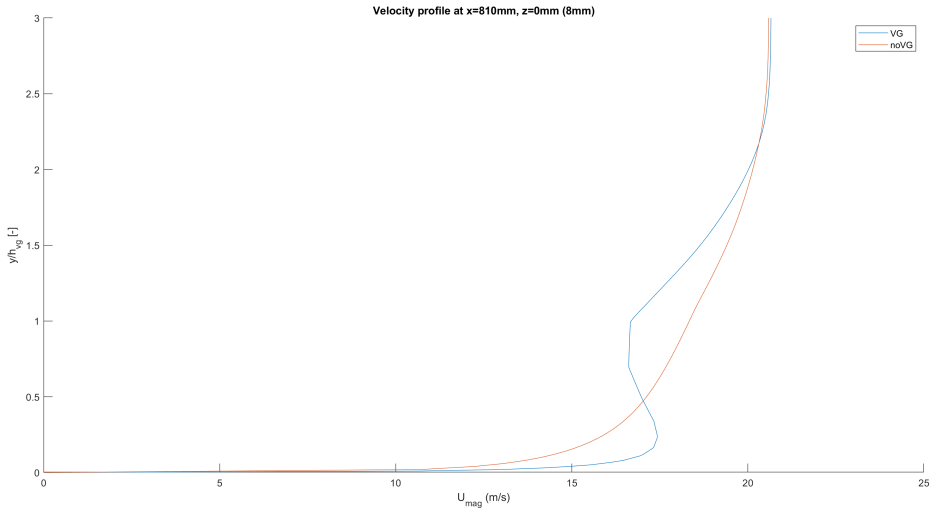

Figure 148: Velocity profile z=0mm, x=810mm (8mm)

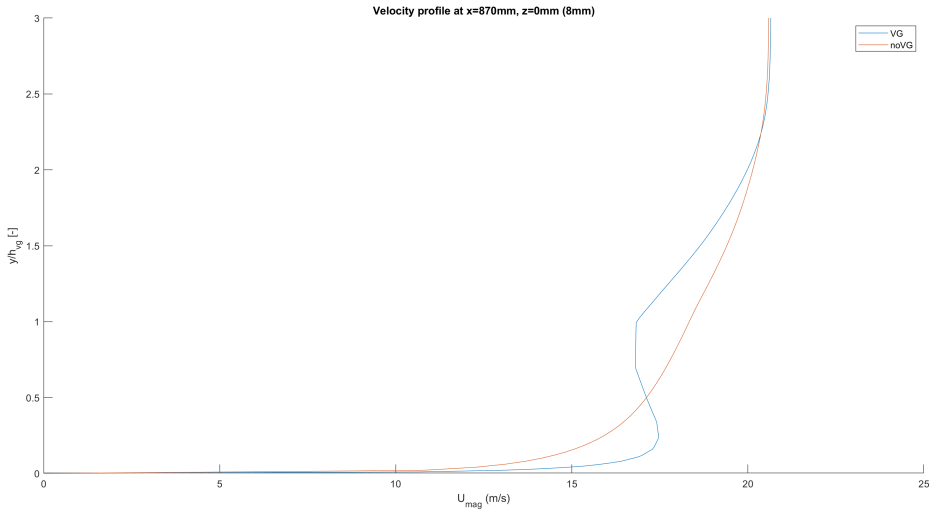

Figure 149: Velocity profile z=0mm, x=870mm (8mm)

7.2.6 Velocity profiles z=0mm (12mm)

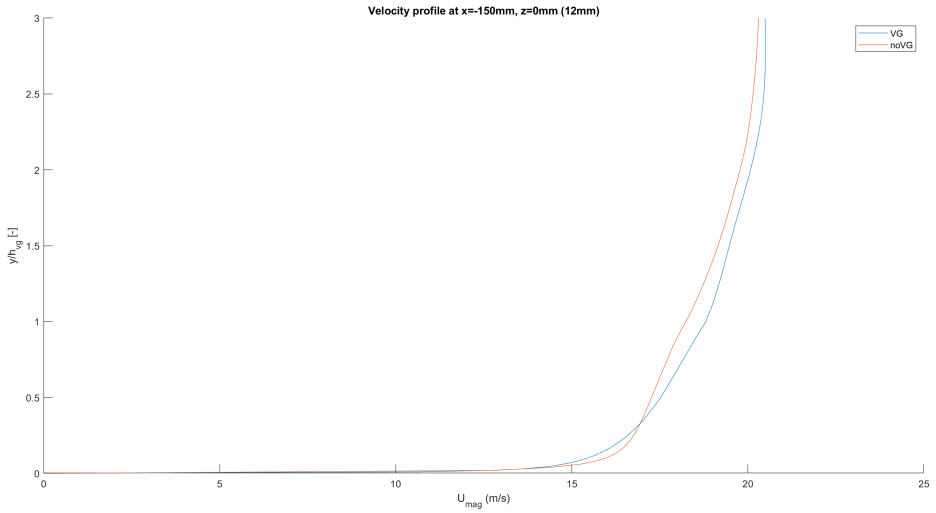

Figure 150: Velocity profile z=0mm, x=-150mm (12mm)

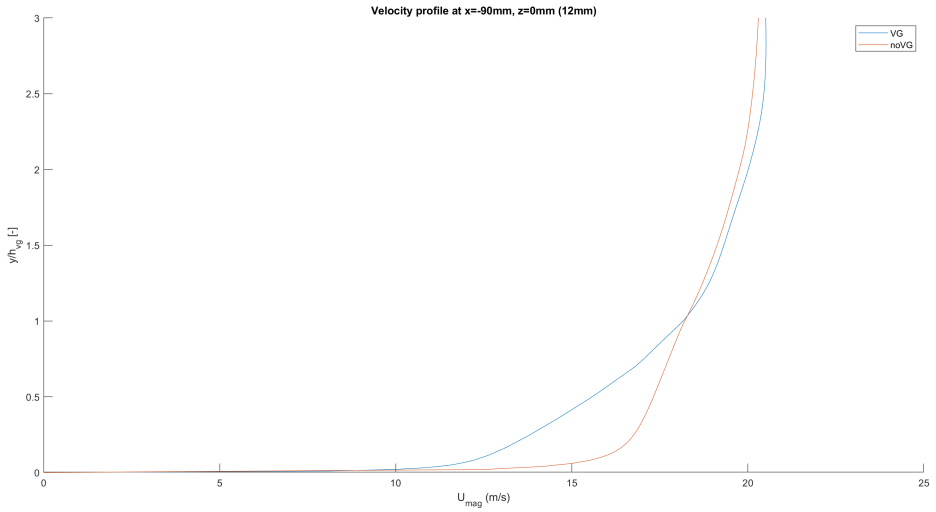

Figure 151: Velocity profile z=0mm, x=-90mm (12mm)

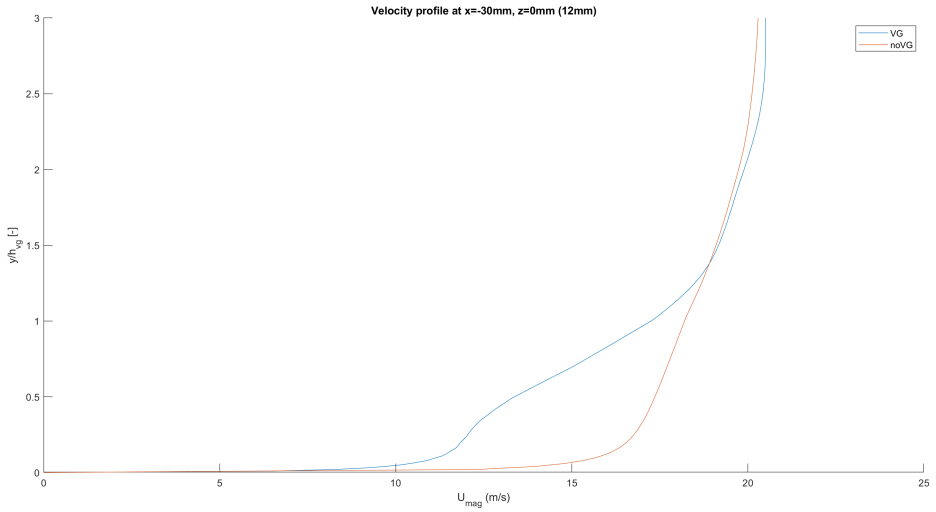

Figure 152: Velocity profile z=0mm, x=-30mm (12mm)

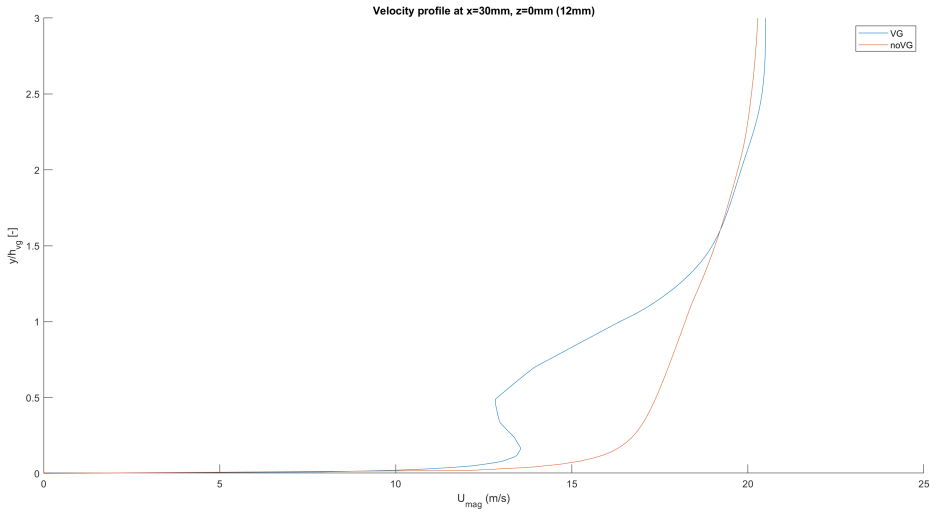

Figure 153: Velocity profile z=0mm, x=30mm (12mm)

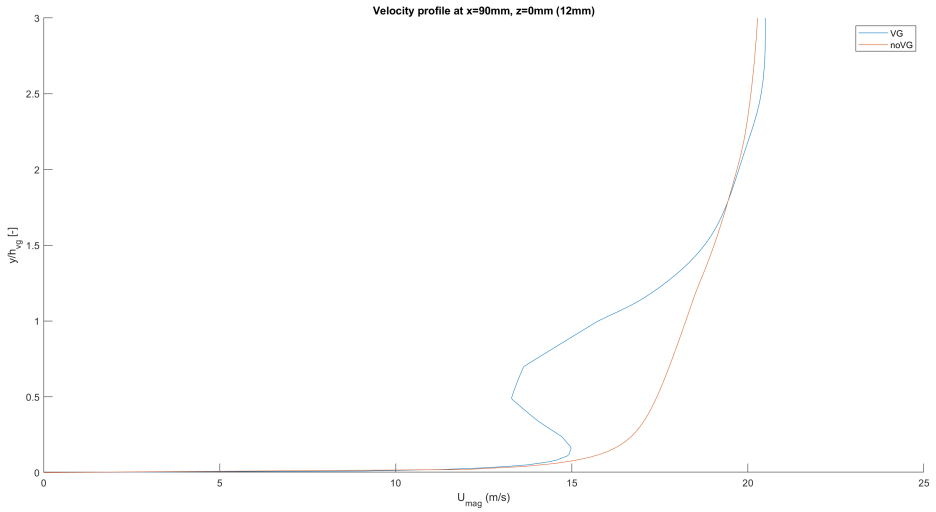

Figure 154: Velocity profile z=0mm, x=90mm (12mm)

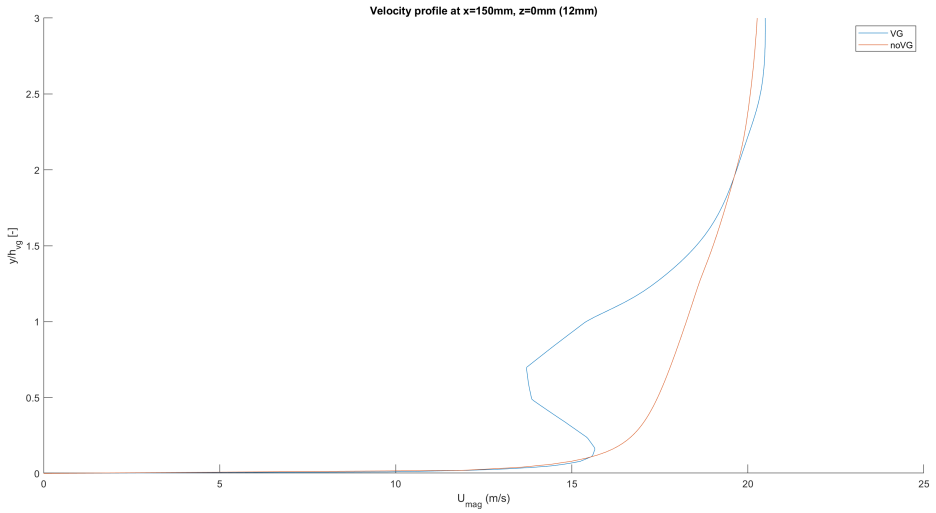

Figure 155: Velocity profile z=0mm, x=150mm (12mm)

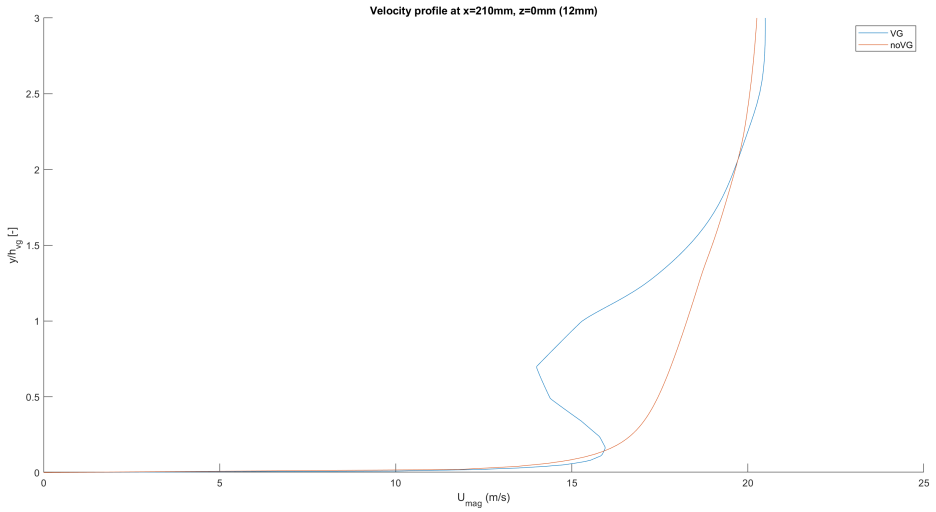

Figure 156: Velocity profile z=0mm, x=210mm (12mm)

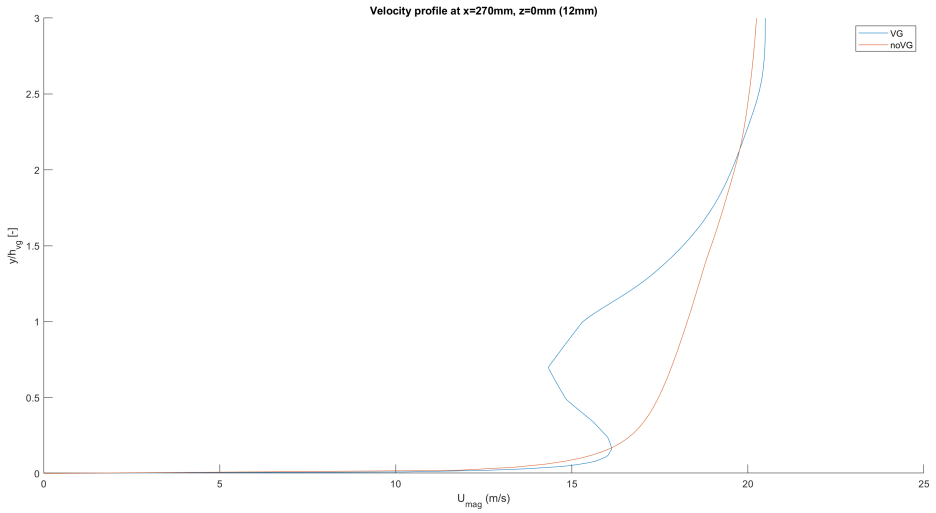

Figure 157: Velocity profile z=0mm, x=270mm (12mm)

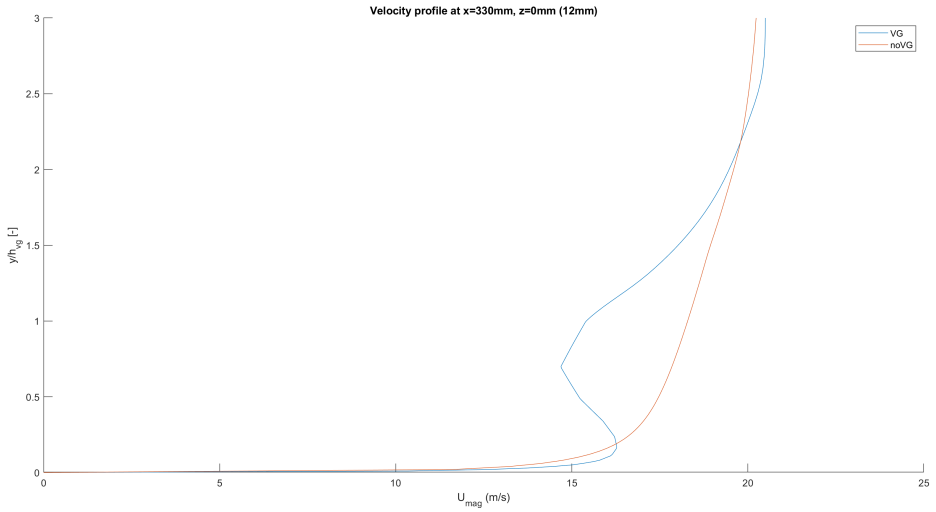

Figure 158: Velocity profile z=0mm, x=330mm (12mm)

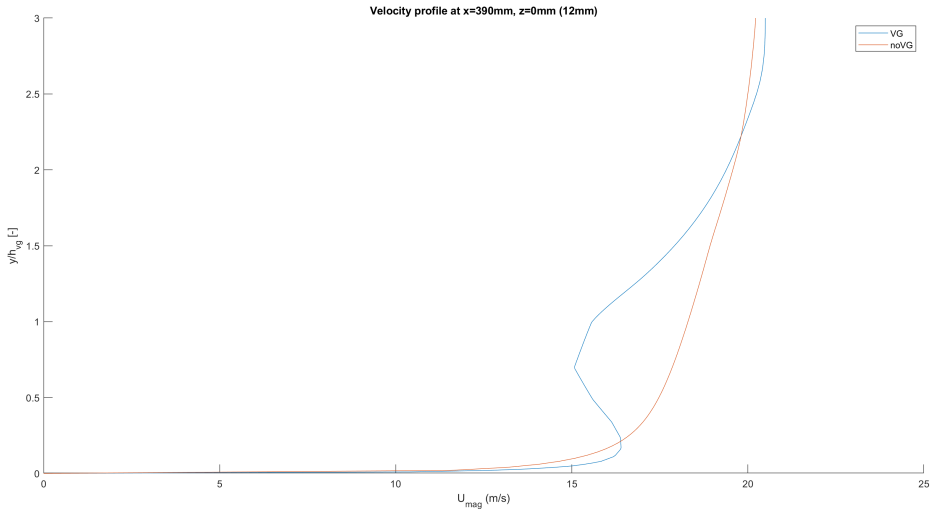

Figure 159: Velocity profile z=0mm, x=390mm (12mm)

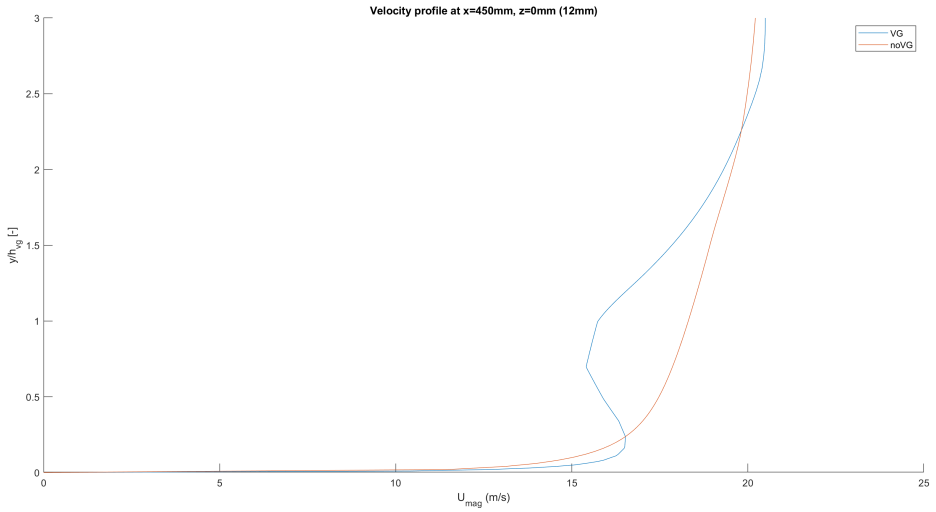

Figure 160: Velocity profile z=0mm, x=450mm (12mm)

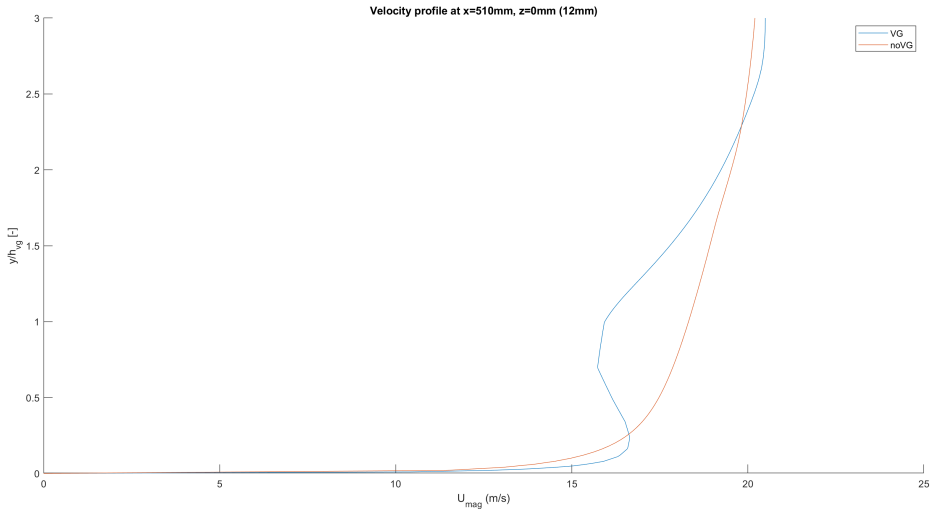

Figure 161: Velocity profile z=0mm, x=510mm (12mm)

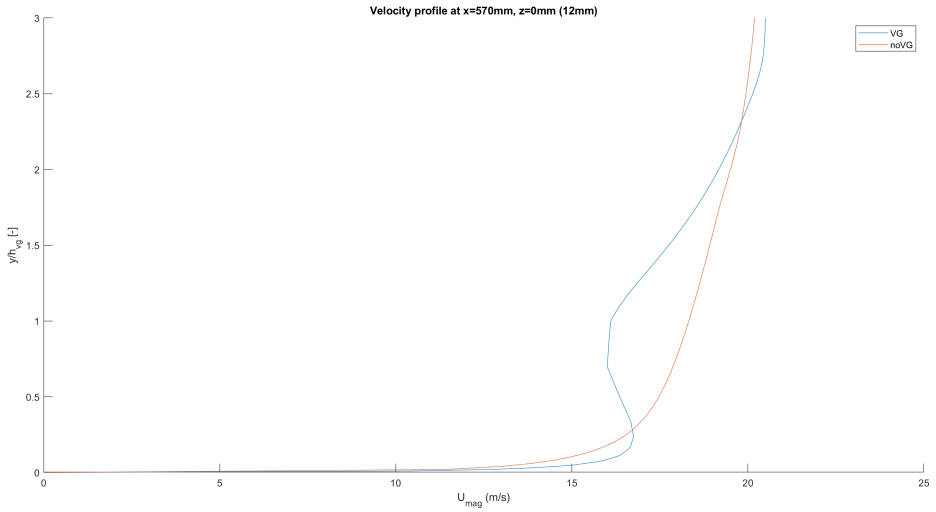

Figure 162: Velocity profile z=0mm, x=570mm (12mm)

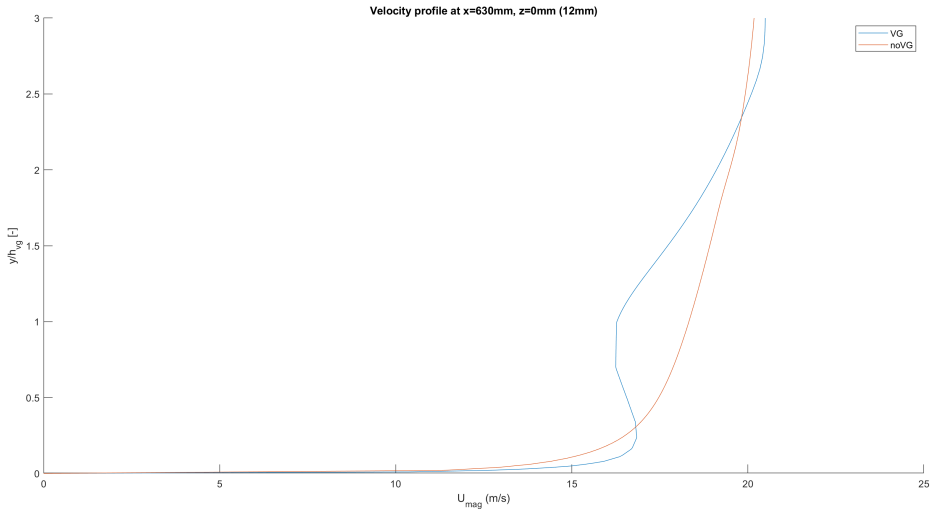

Figure 163: Velocity profile z=0mm, x=630mm (12mm)

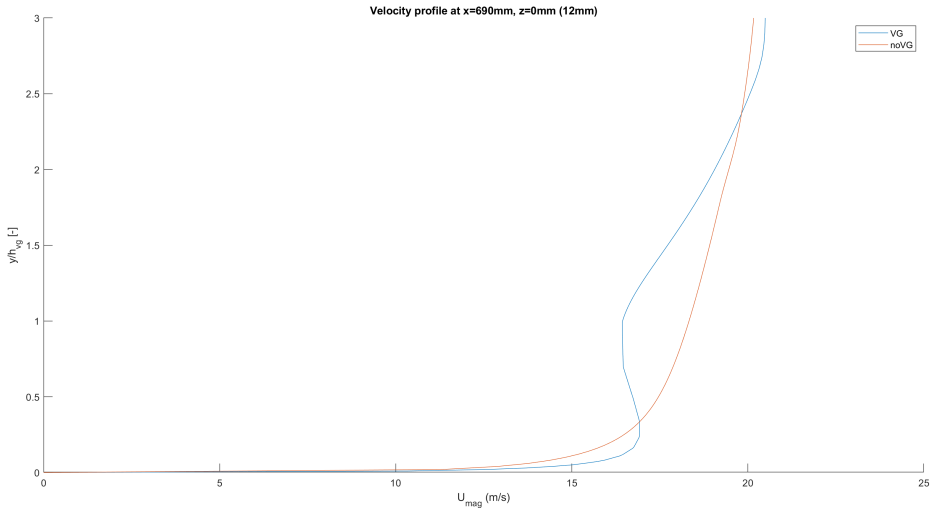

Figure 164: Velocity profile z=0mm, x=690mm (12mm)

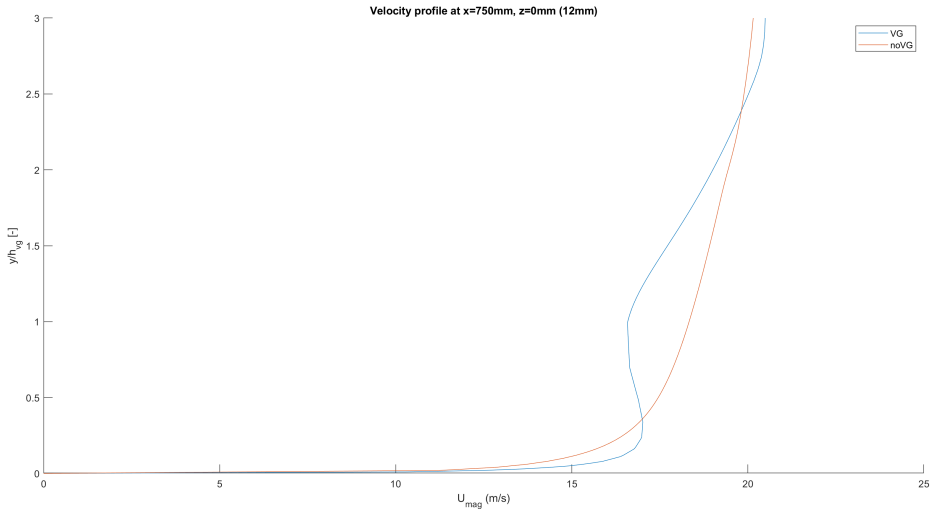

Figure 165: Velocity profile z=0mm, x=750mm (12mm)

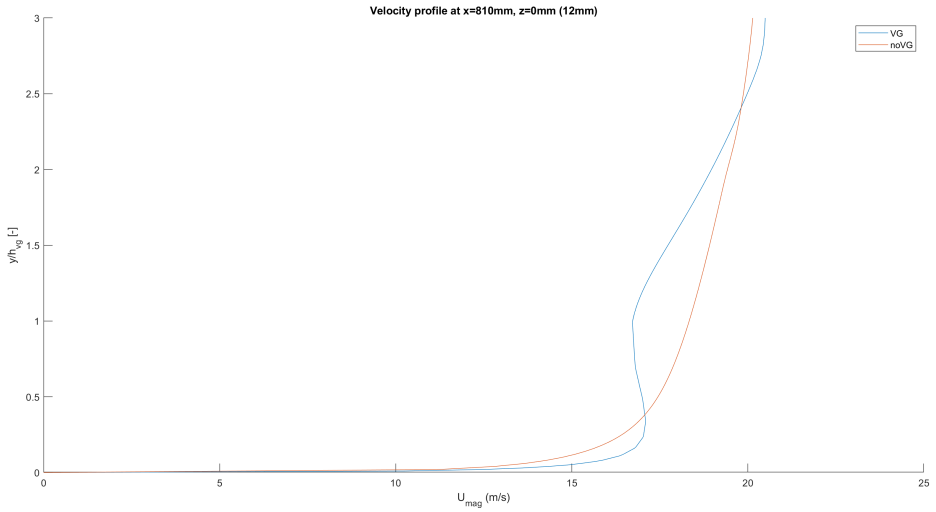

Figure 166: Velocity profile z=0mm, x=810mm (12mm)

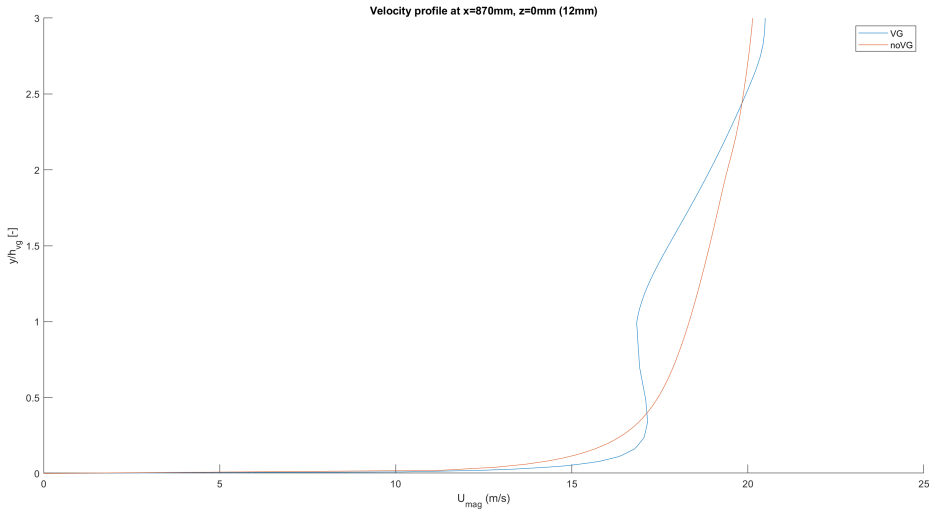

Figure 167: Velocity profile z=0mm, x=870mm (12mm)

7.2.7 Velocity profiles z=40mm (free)

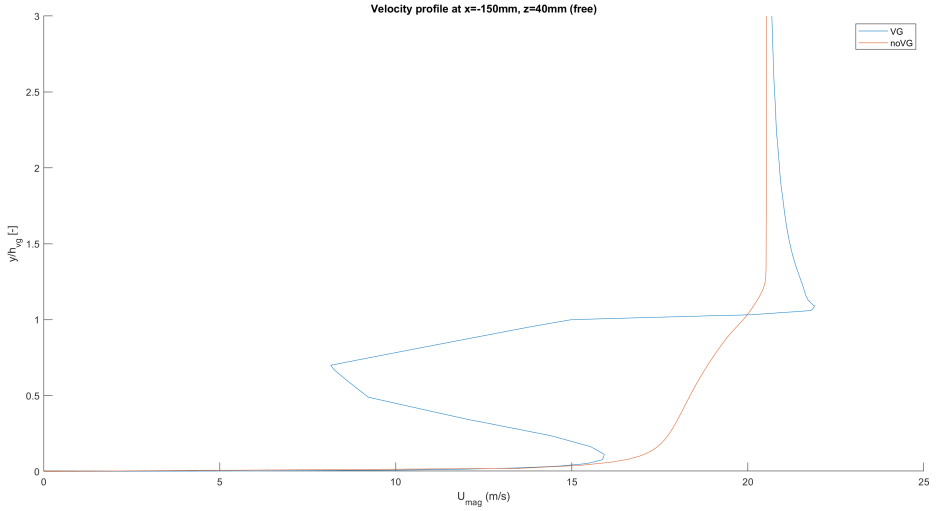

Figure 168: Velocity profile z=40mm, x=-150mm (free)

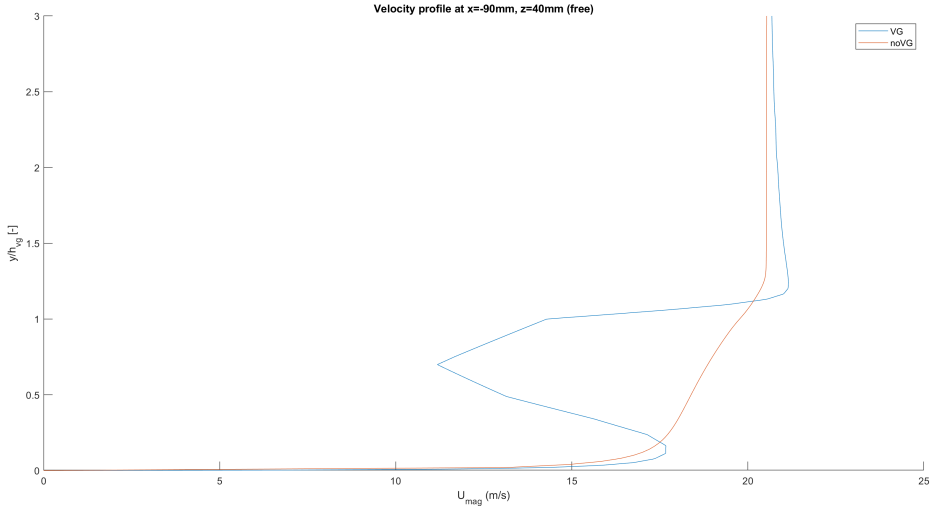

Figure 169: Velocity profile z=40mm, x=-90mm (free)

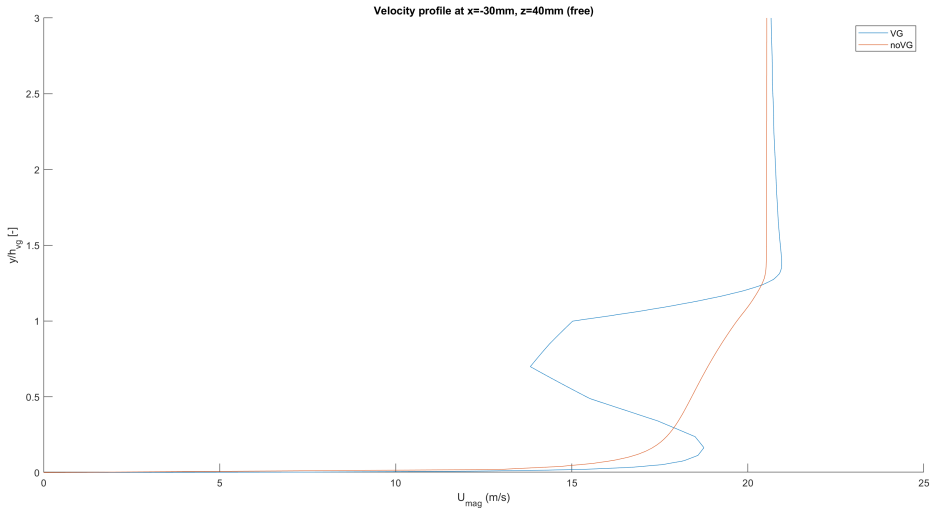

Figure 170: Velocity profile z=40mm, x=-30mm (free)

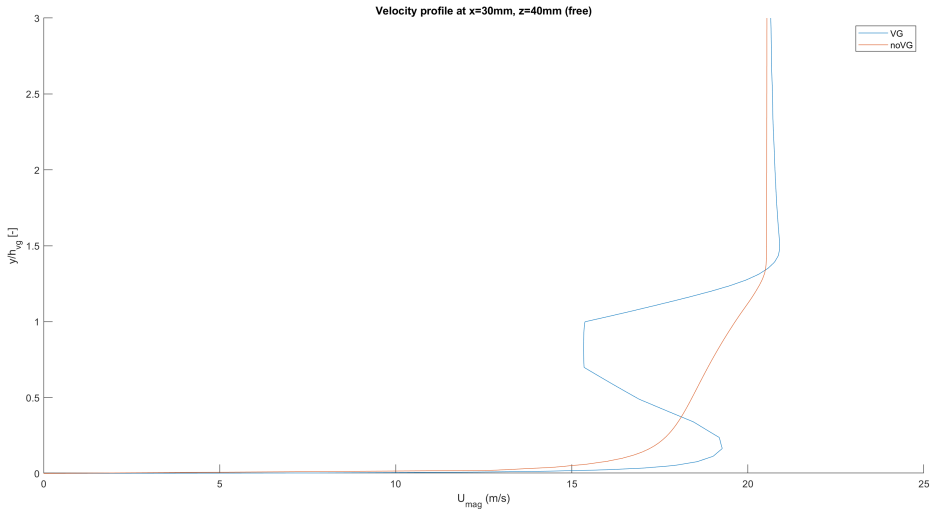

Figure 171: Velocity profile z=40mm, x=30mm (free)

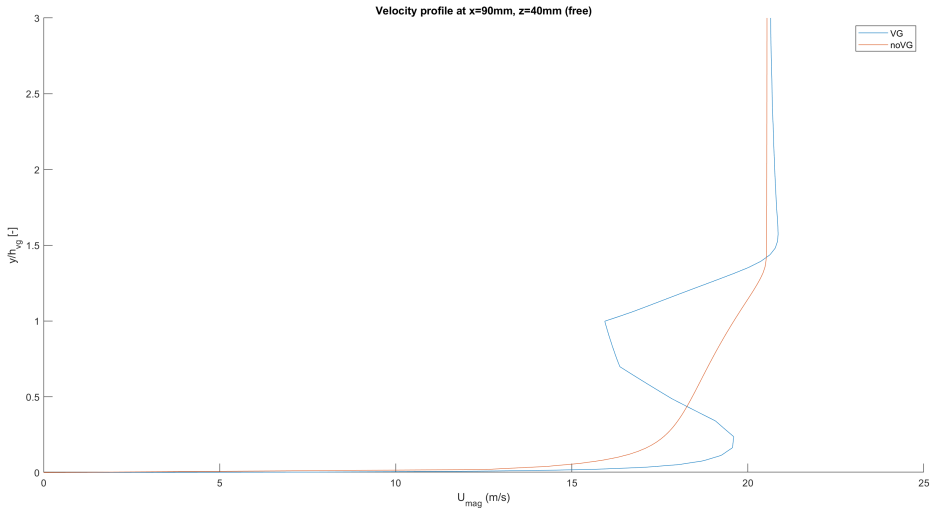

Figure 172: Velocity profile z=40mm, x=90mm (free)

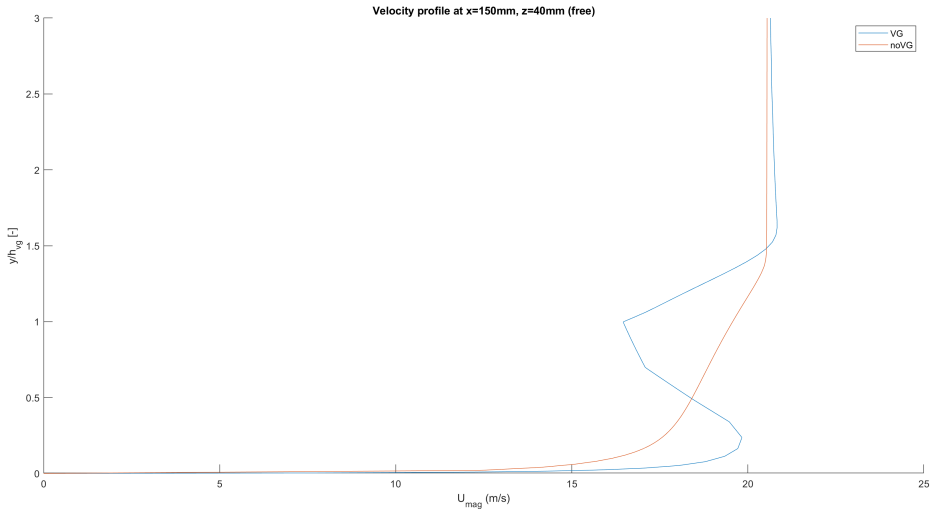

Figure 173: Velocity profile z=40mm, x=150mm (free)

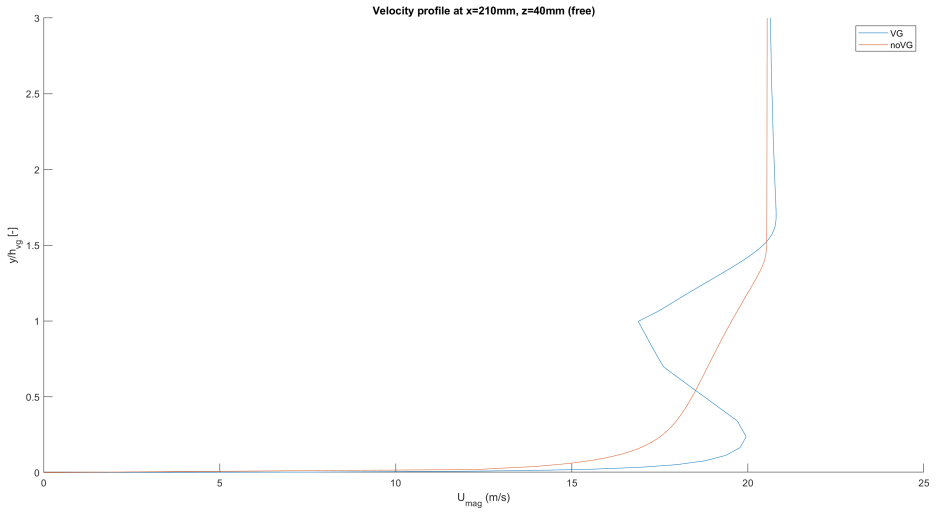

Figure 174: Velocity profile z=40mm, x=210mm (free)

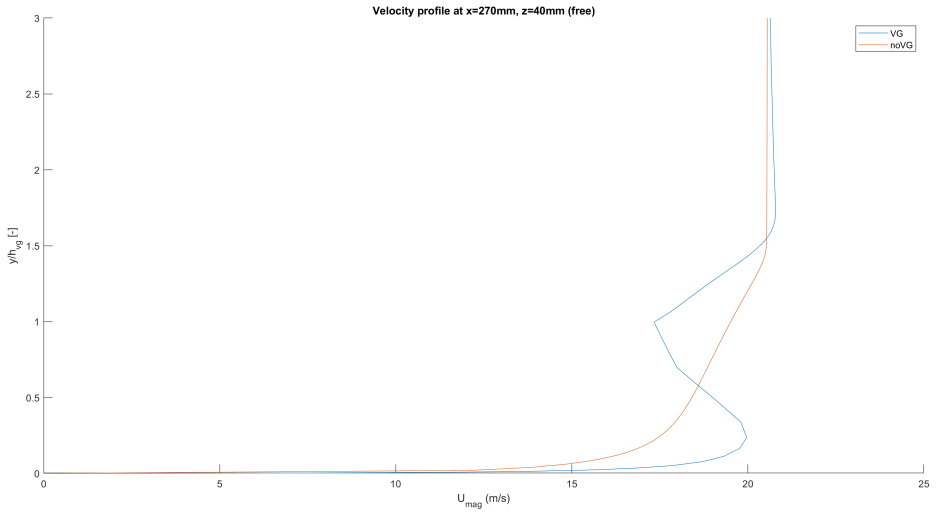

Figure 175: Velocity profile z=40mm, x=270mm (free)

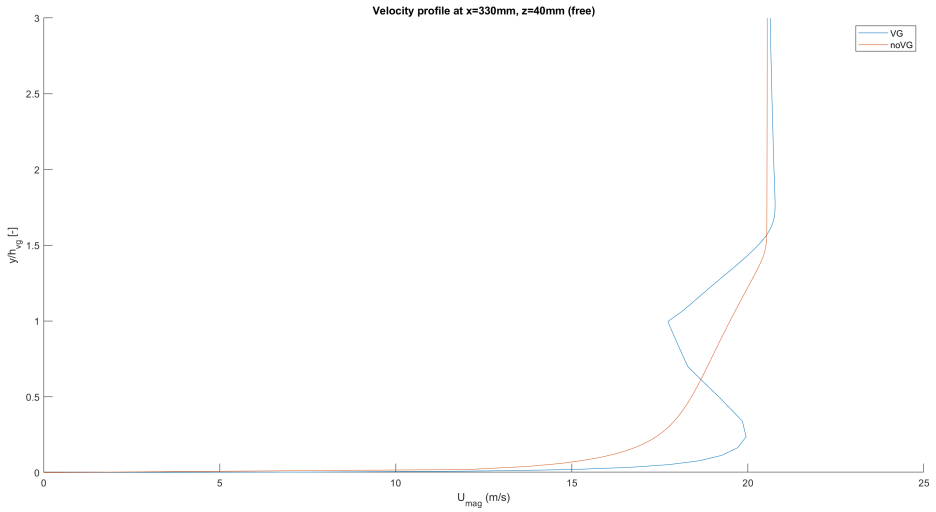

Figure 176: Velocity profile z=40mm, x=330mm (free)

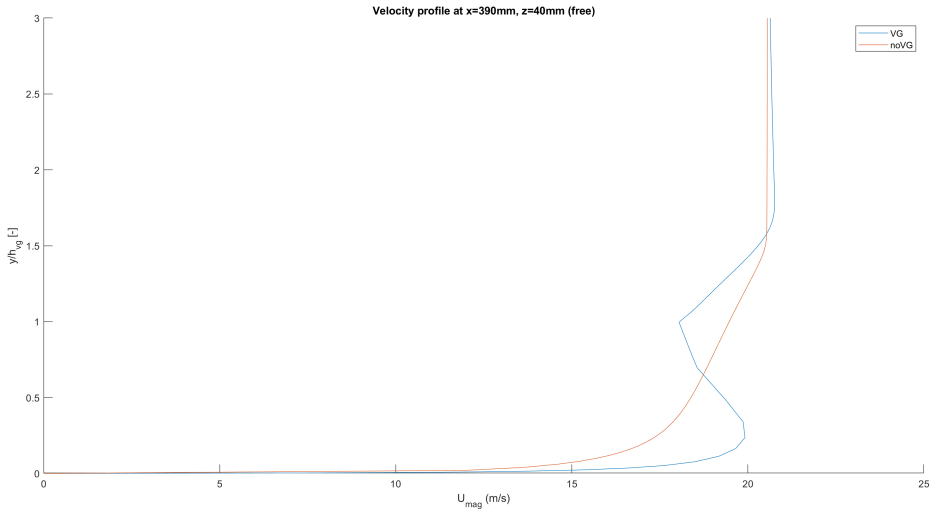

Figure 177: Velocity profile z=40mm, x=390mm (free)

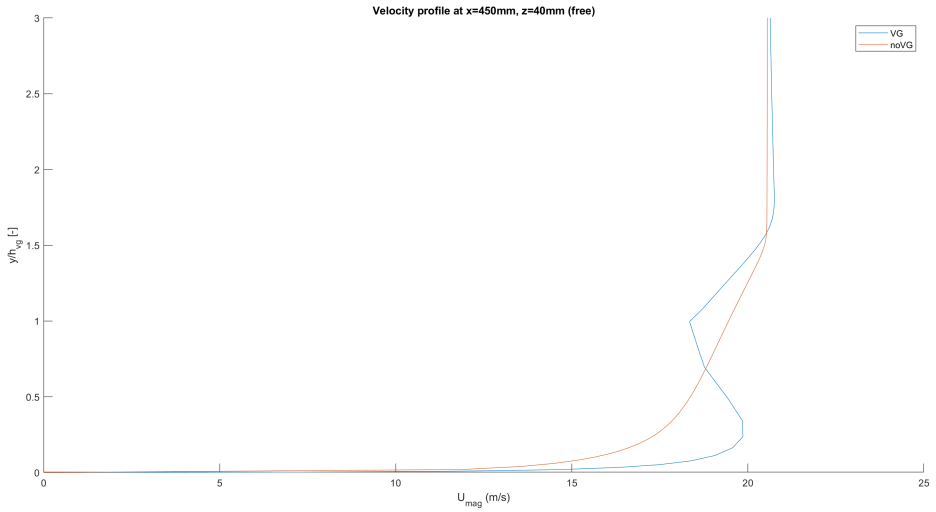

Figure 178: Velocity profile z=40mm, x=450mm (free)

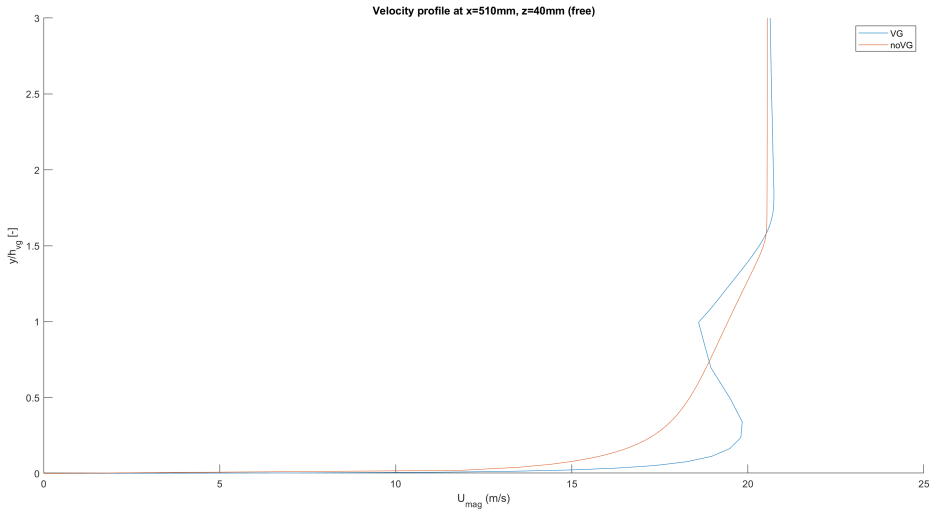

Figure 179: Velocity profile z=40mm, x=510mm (free)

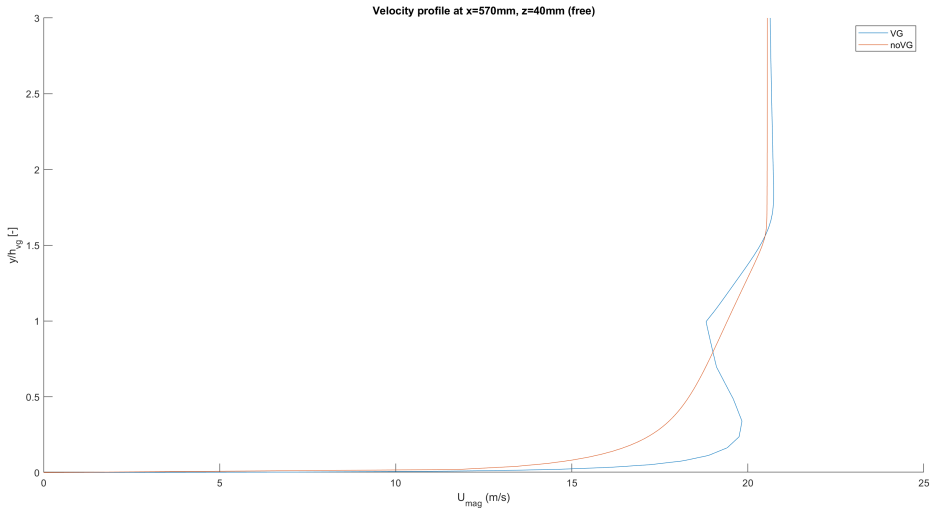

Figure 180: Velocity profile z=40mm, x=570mm (free)

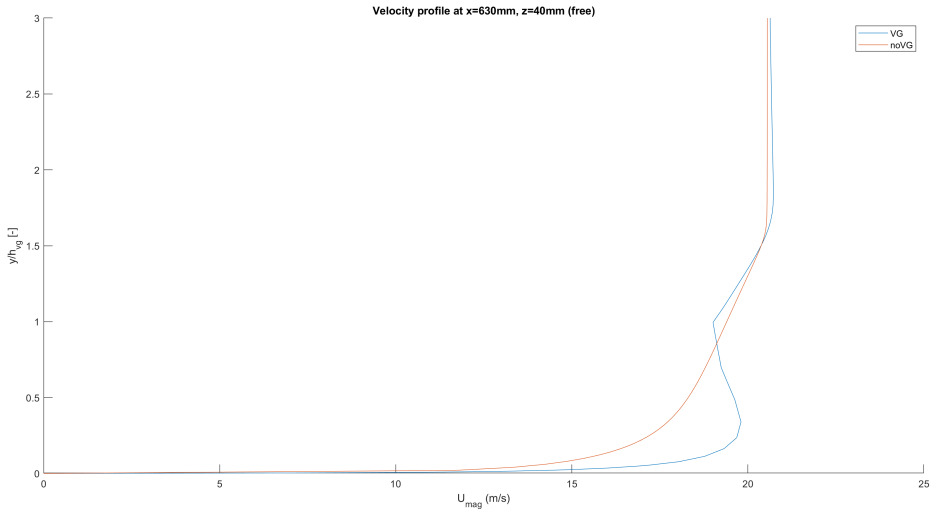

Figure 181: Velocity profile z=40mm, x=630mm (free)

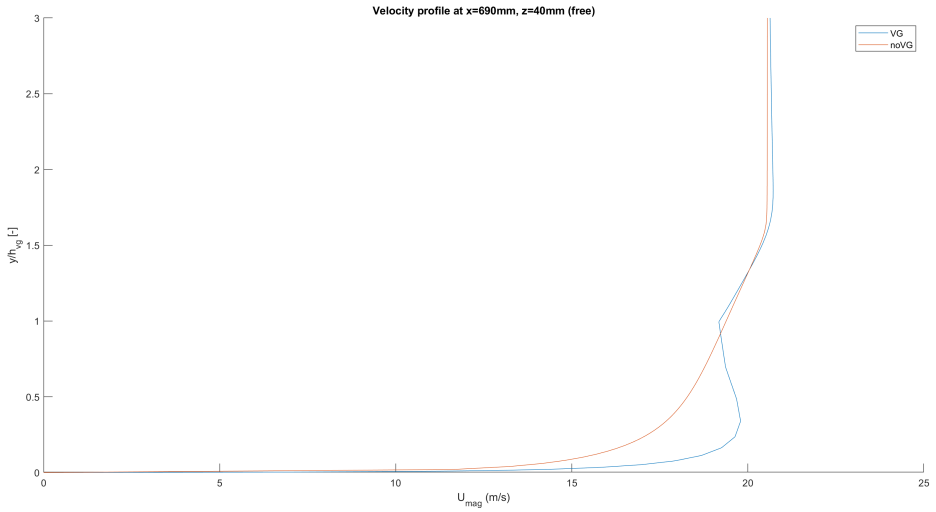

Figure 182: Velocity profile z=40mm, x=690mm (free)

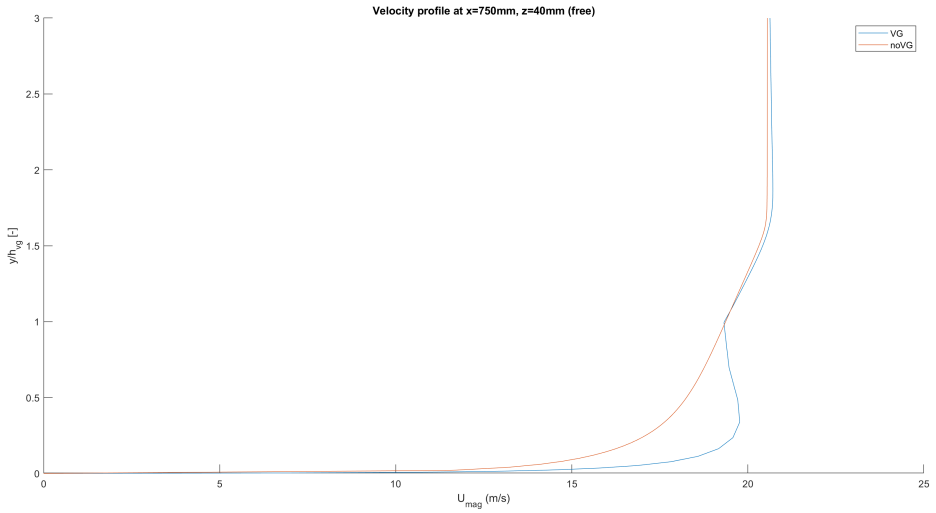

Figure 183: Velocity profile z=40mm, x=750mm (free)

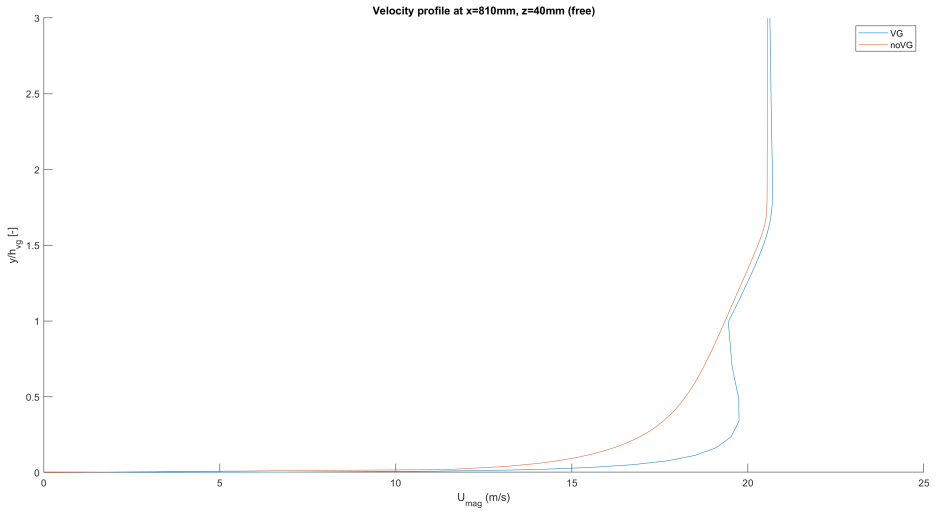

Figure 184: Velocity profile z=40mm, x=810mm (free)

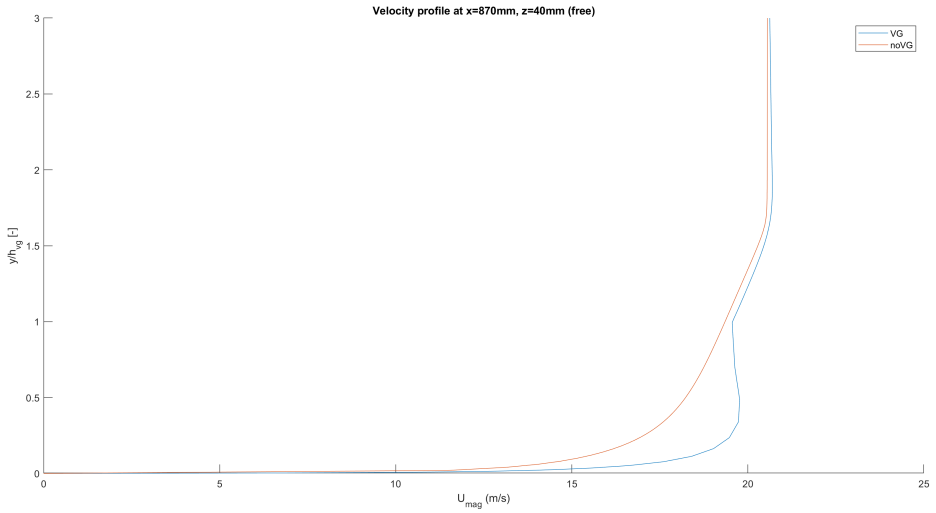

Figure 185: Velocity profile z=40mm, x=870mm (free)

7.2.8 Velocity profiles z=40mm (8mm)

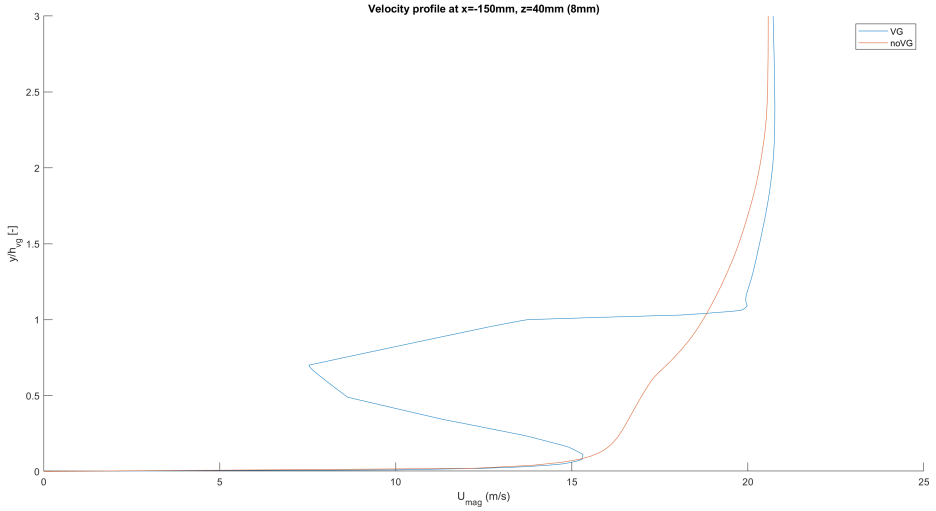

Figure 186: Velocity profile z=40mm, x=-150mm (8mm)

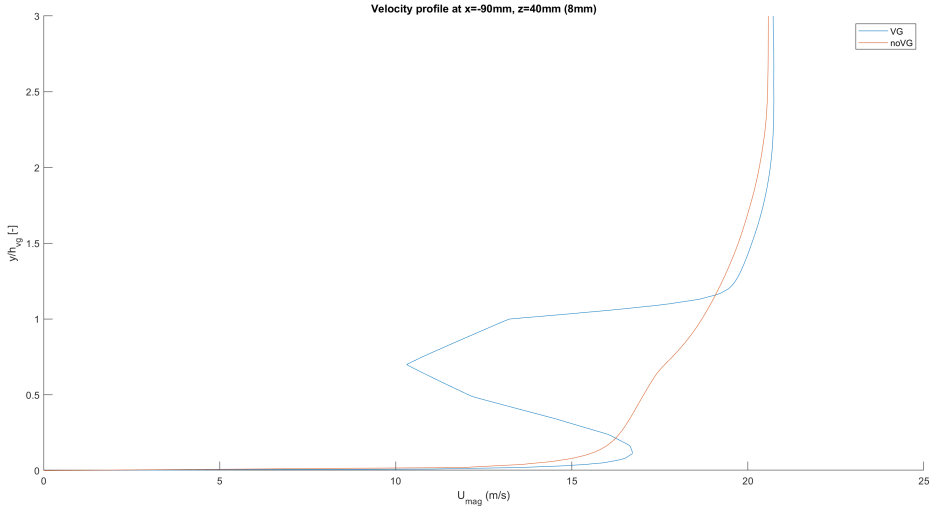

Figure 187: Velocity profile z=40mm, x=-90mm (8mm)

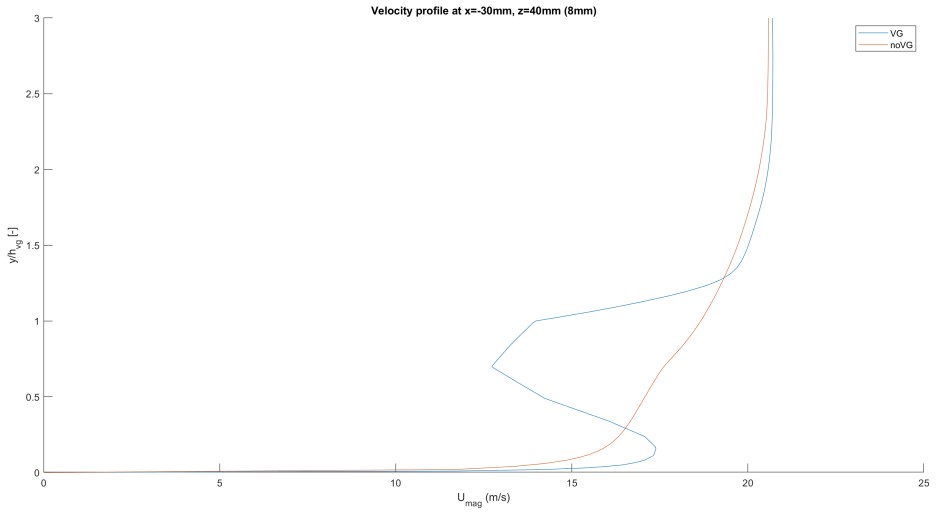

Figure 188: Velocity profile z=40mm, x=-30mm (8mm)

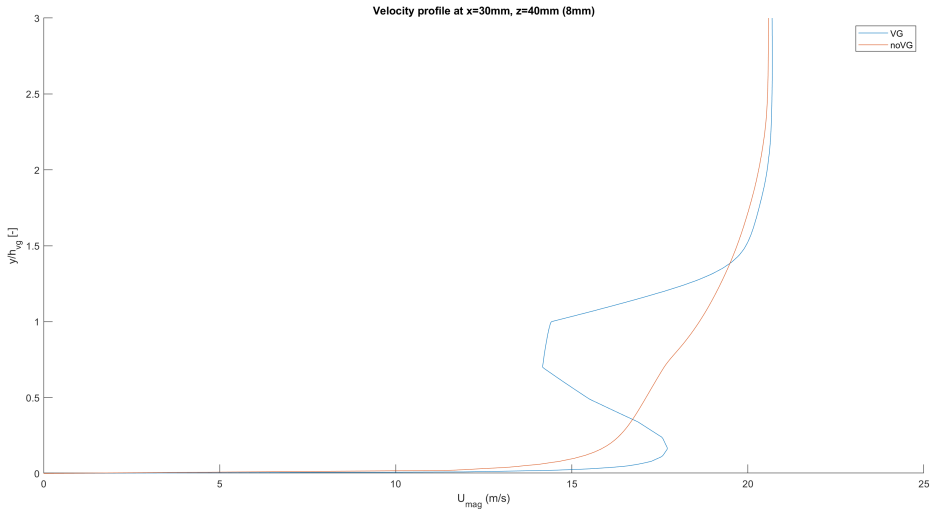

Figure 189: Velocity profile z=40mm, x=30mm (8mm)

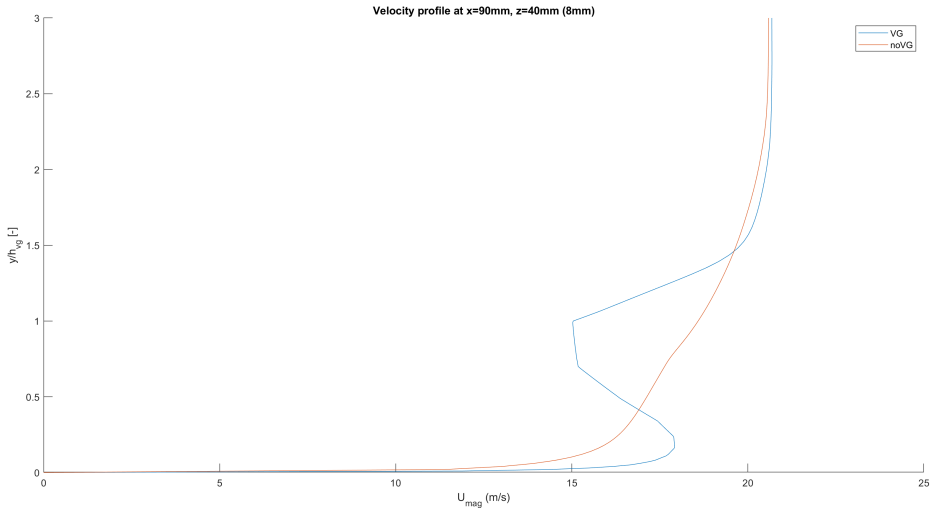

Figure 190: Velocity profile z=40mm, x=90mm (8mm)

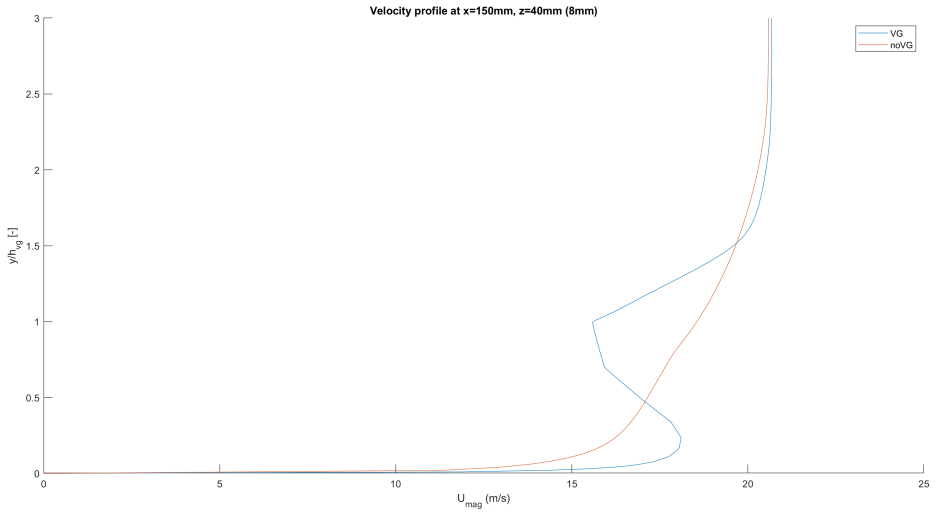

Figure 191: Velocity profile z=40mm, x=150mm (8mm)

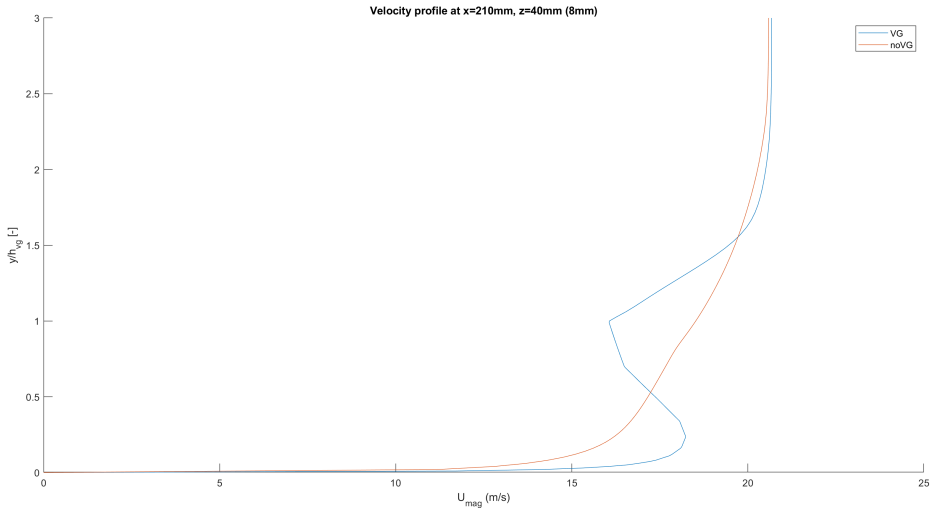

Figure 192: Velocity profile z=40mm, x=210mm (8mm)

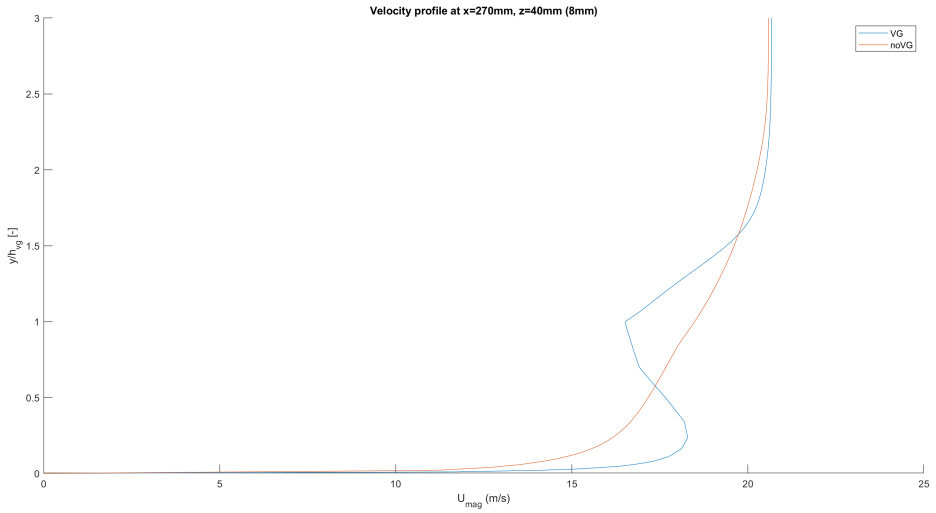

Figure 193: Velocity profile z=40mm, x=270mm (8mm)

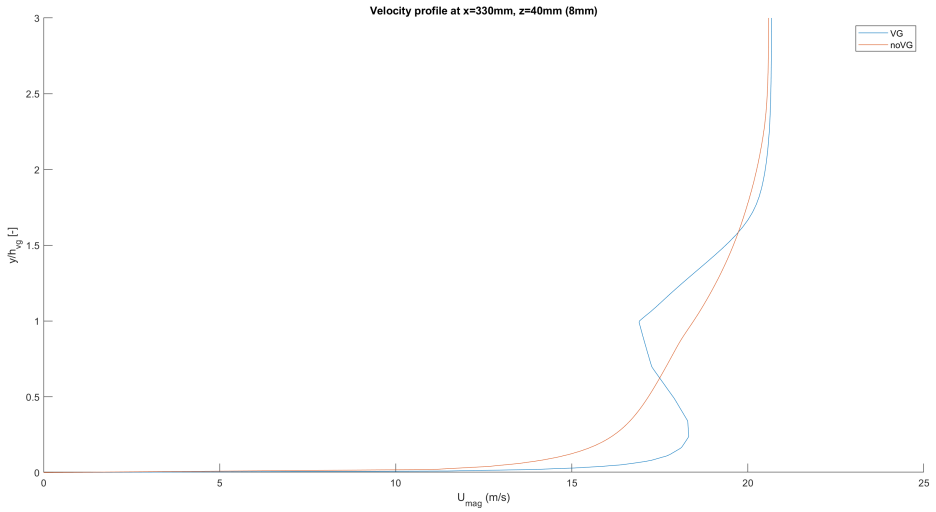

Figure 194: Velocity profile z=40mm, x=330mm (8mm)

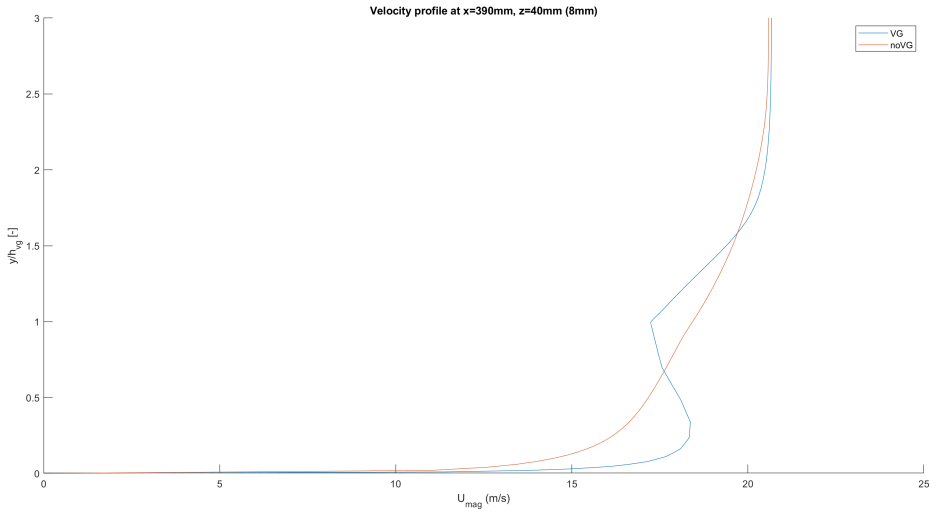

Figure 195: Velocity profile z=40mm, x=390mm (8mm)

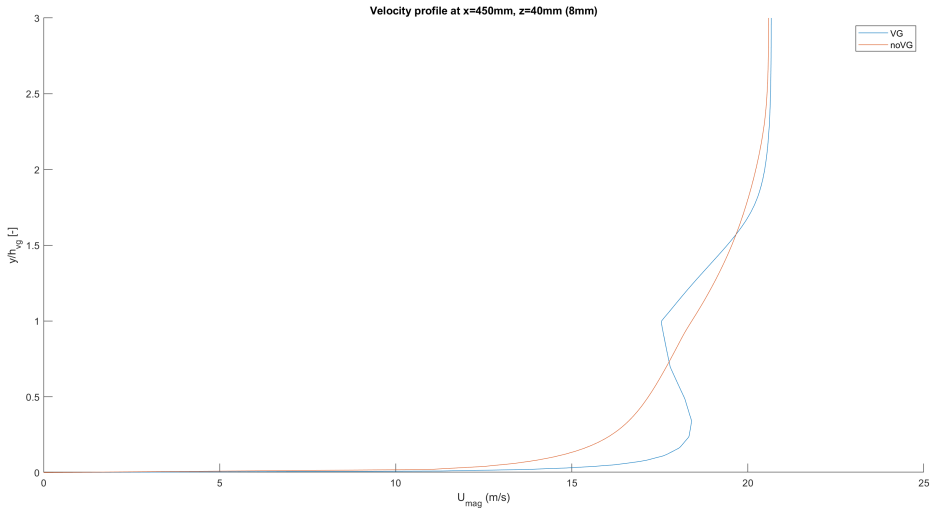

Figure 196: Velocity profile z=40mm, x=450mm (8mm)

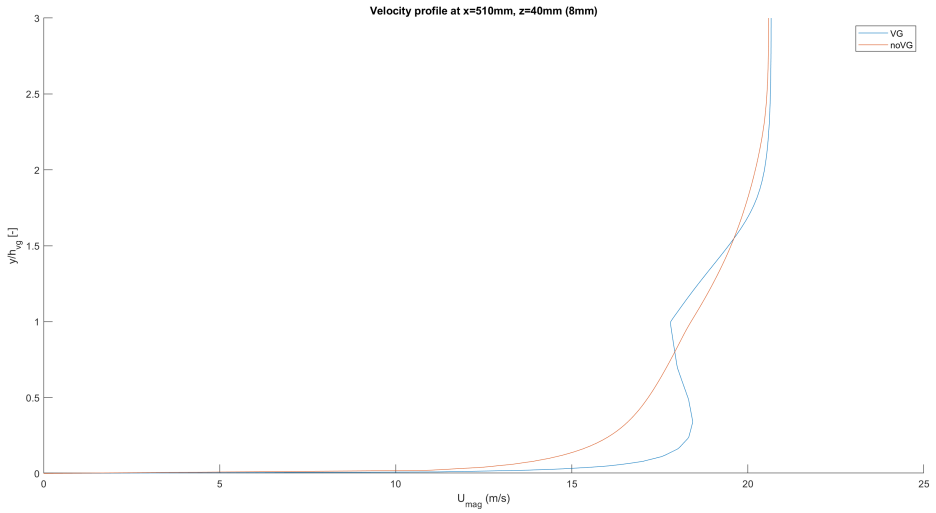

Figure 197: Velocity profile z=40mm, x=510mm (8mm)

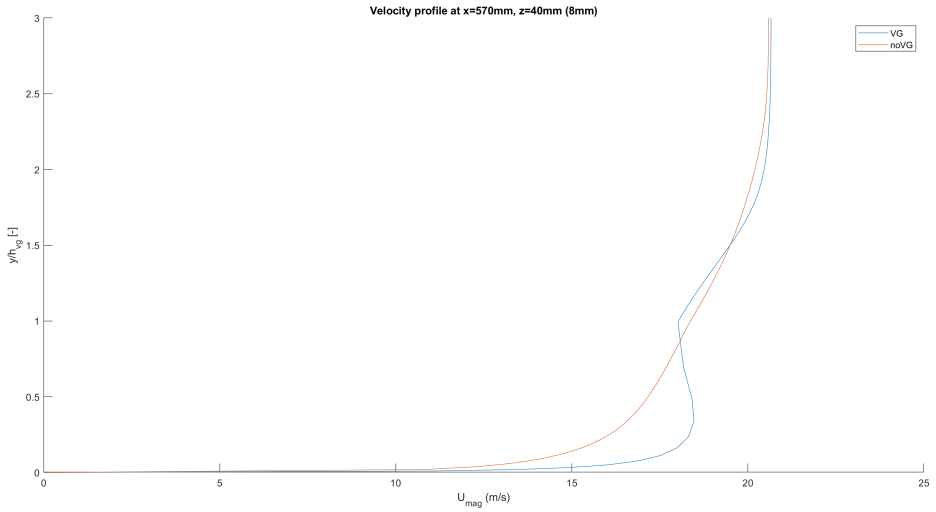

Figure 198: Velocity profile z=40mm, x=570mm (8mm)

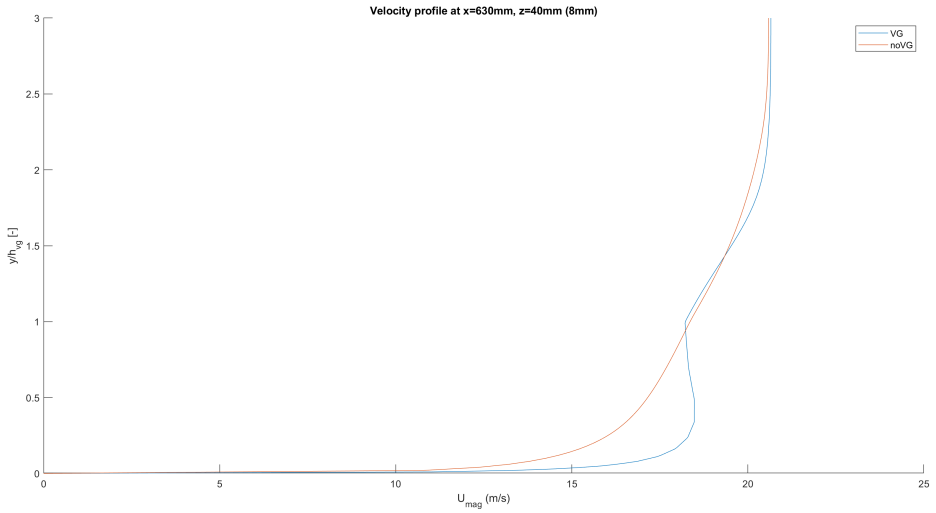

Figure 199: Velocity profile z=40mm, x=630mm (8mm)

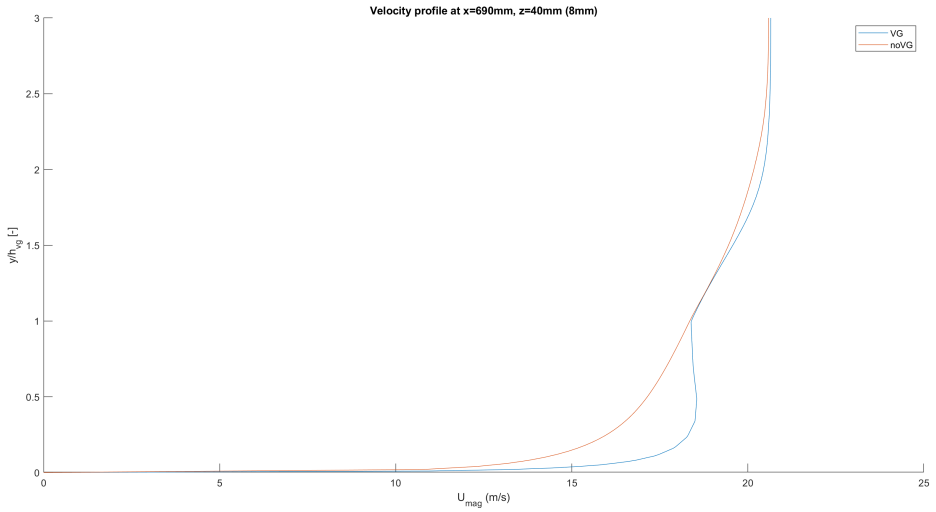

Figure 200: Velocity profile z=40mm, x=690mm (8mm)

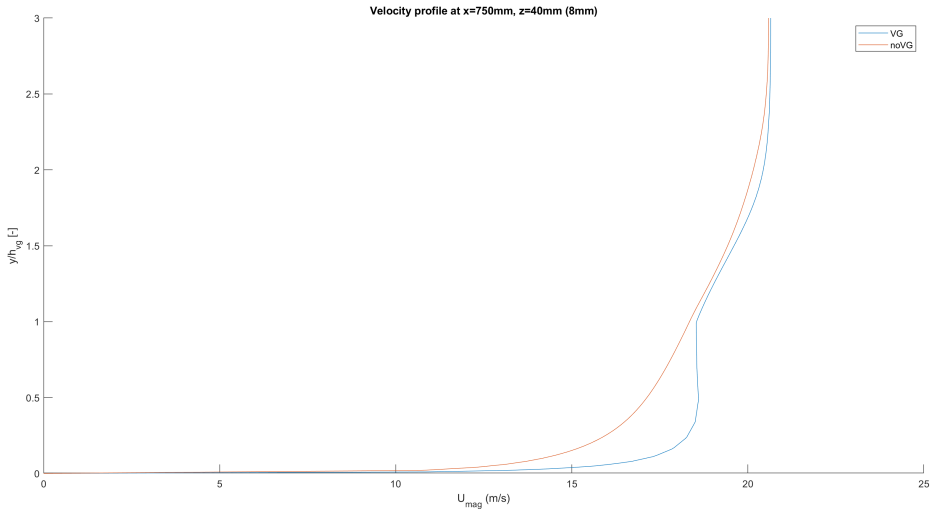

Figure 201: Velocity profile z=40mm, x=750mm (8mm)

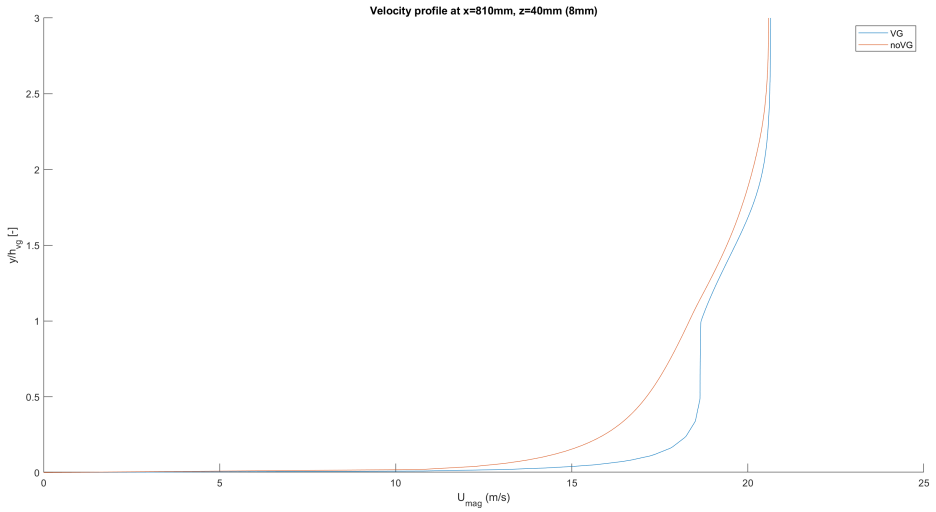

Figure 202: Velocity profile z=40mm, x=810mm (8mm)

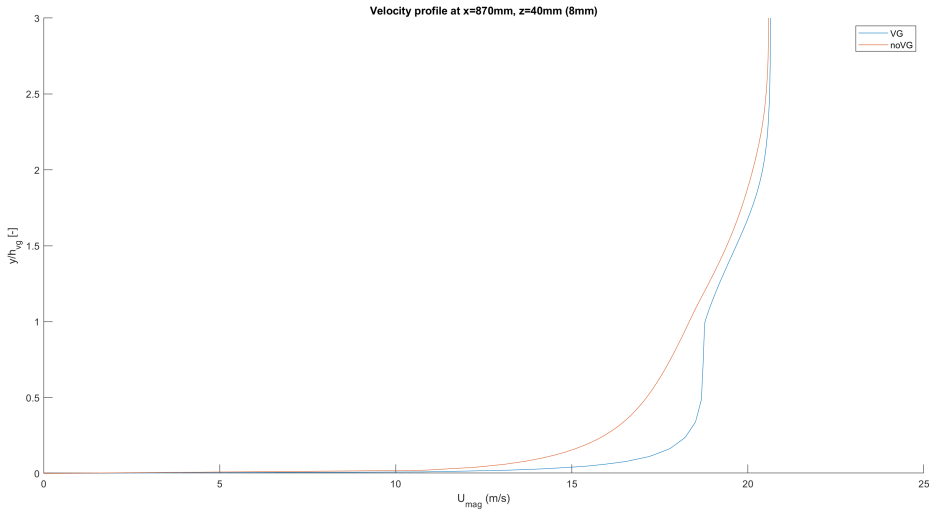

Figure 203: Velocity profile z=40mm, x=870mm (8mm)

7.2.9 Velocity profiles z=40mm (12mm)

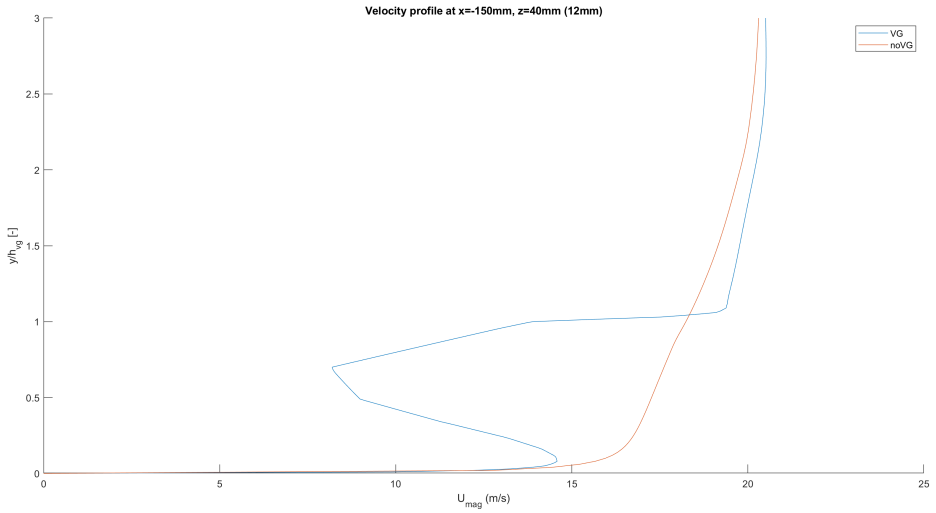

Figure 204: Velocity profile z=40mm, x=-150mm (12mm)

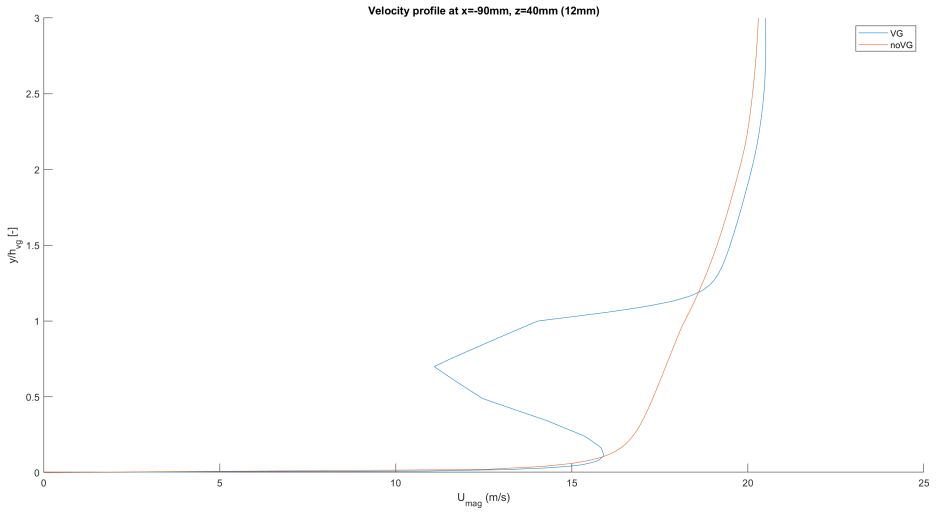

Figure 205: Velocity profile z=40mm, x=-90mm (12mm)

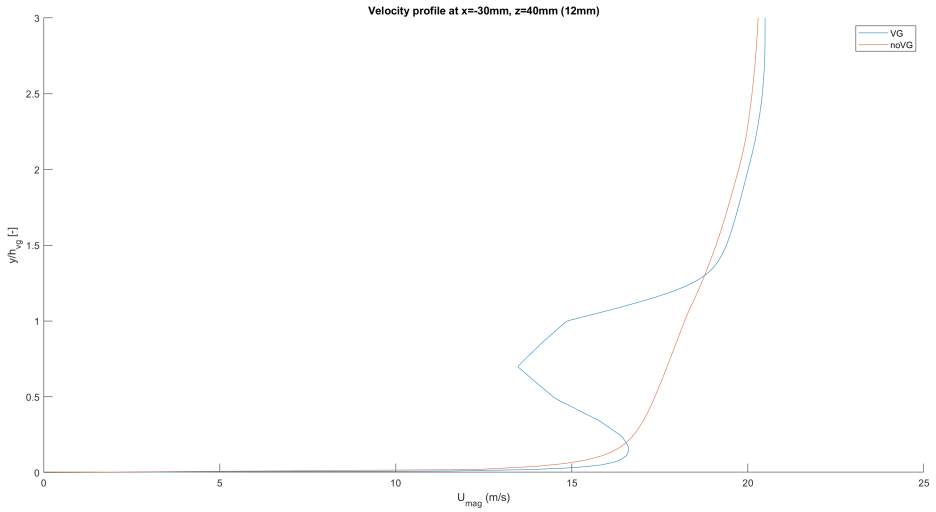

Figure 206: Velocity profile z=40mm, x=-30mm (12mm)

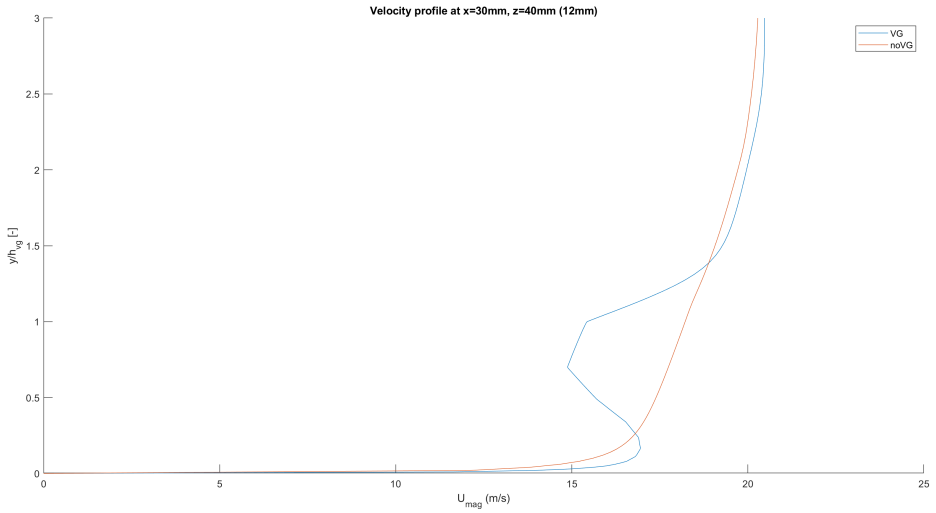

Figure 207: Velocity profile z=40mm, x=30mm (12mm)

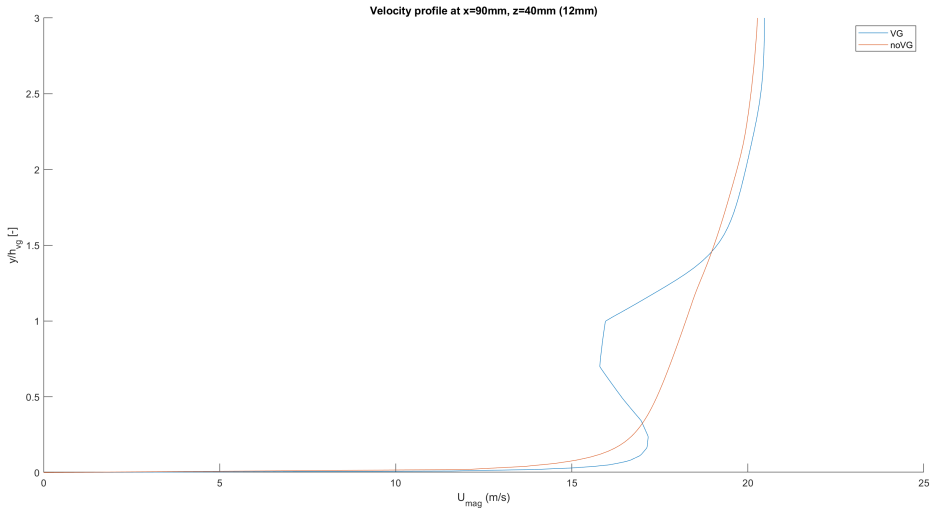

Figure 208: Velocity profile z=40mm, x=90mm (12mm)

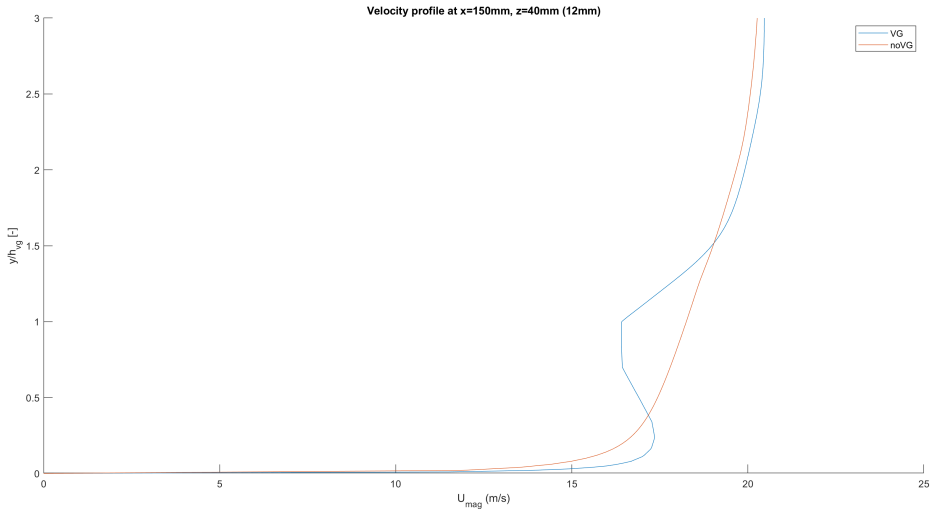

Figure 209: Velocity profile z=40mm, x=150mm (12mm)

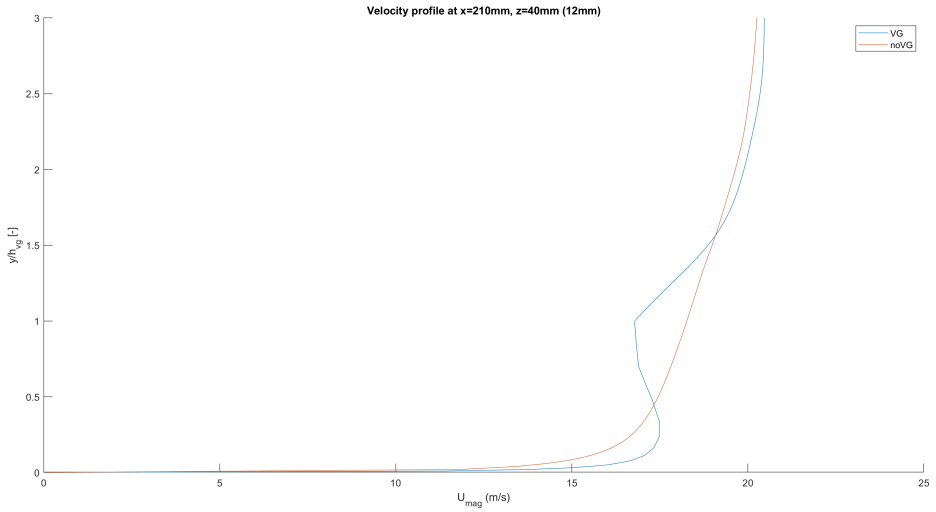

Figure 210: Velocity profile z=40mm, x=210mm (12mm)

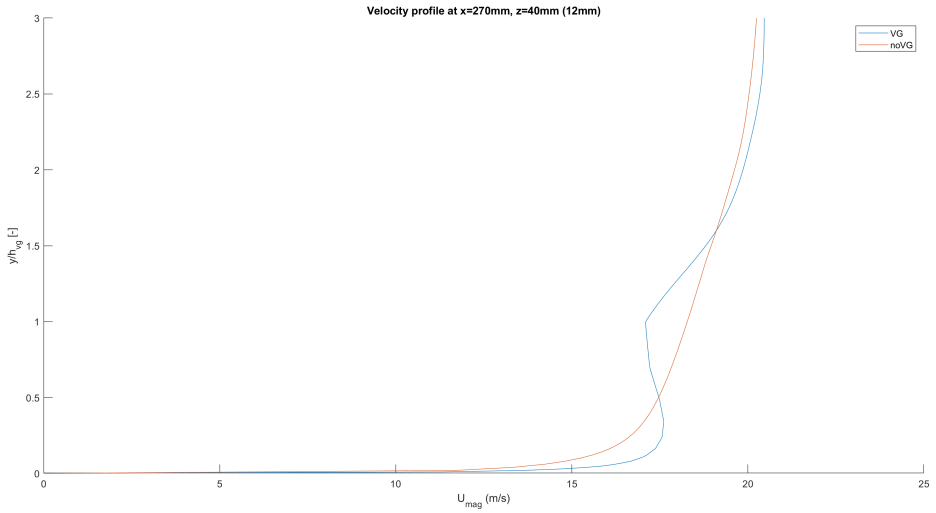

Figure 211: Velocity profile z=40mm, x=270mm (12mm)

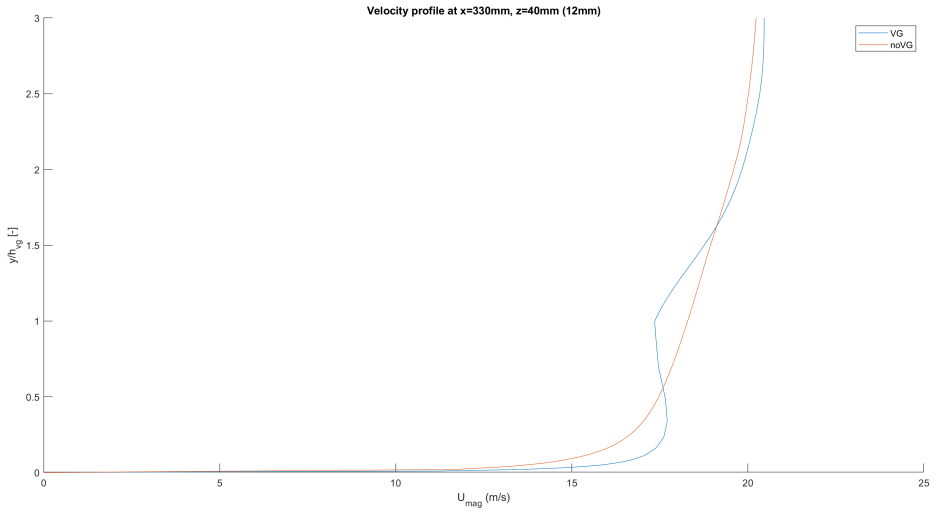

Figure 212: Velocity profile z=40mm, x=330mm (12mm)

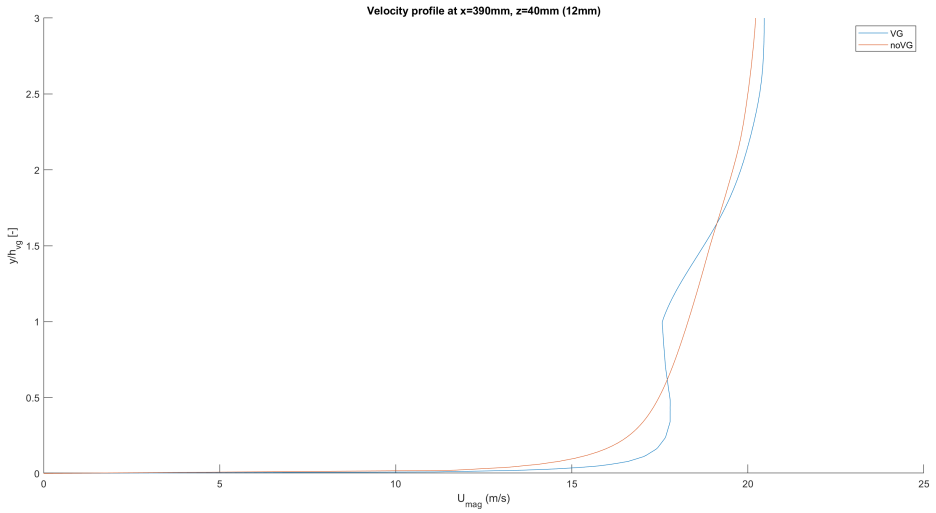

Figure 213: Velocity profile z=40mm, x=390mm (12mm)

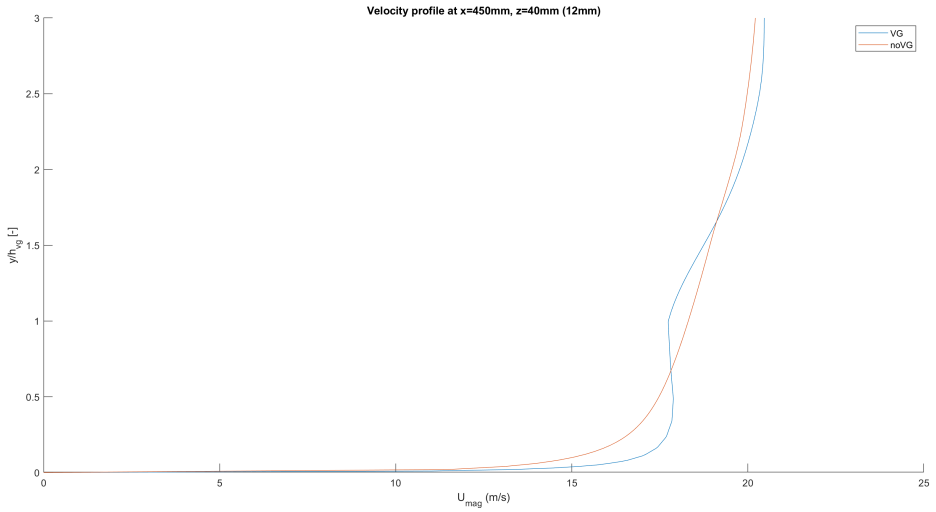

Figure 214: Velocity profile z=40mm, x=450mm (12mm)

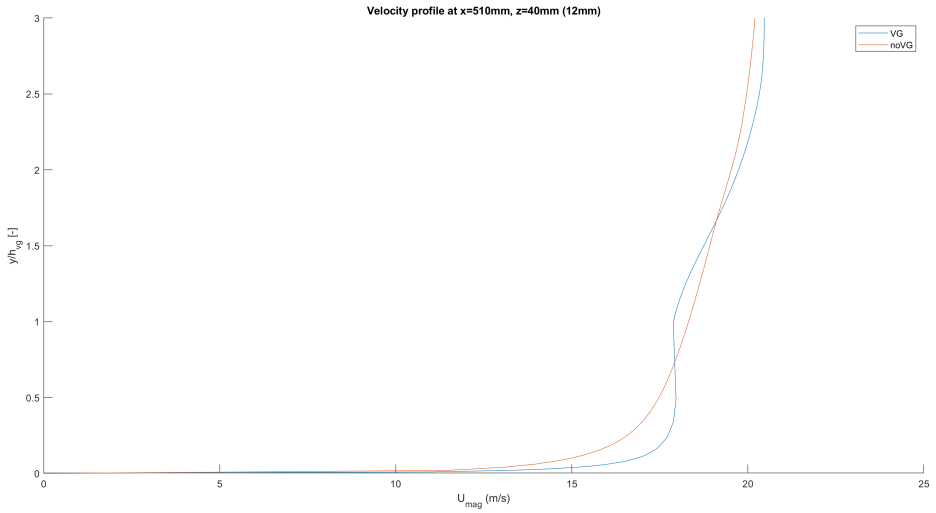

Figure 215: Velocity profile z=40mm, x=510mm (12mm)

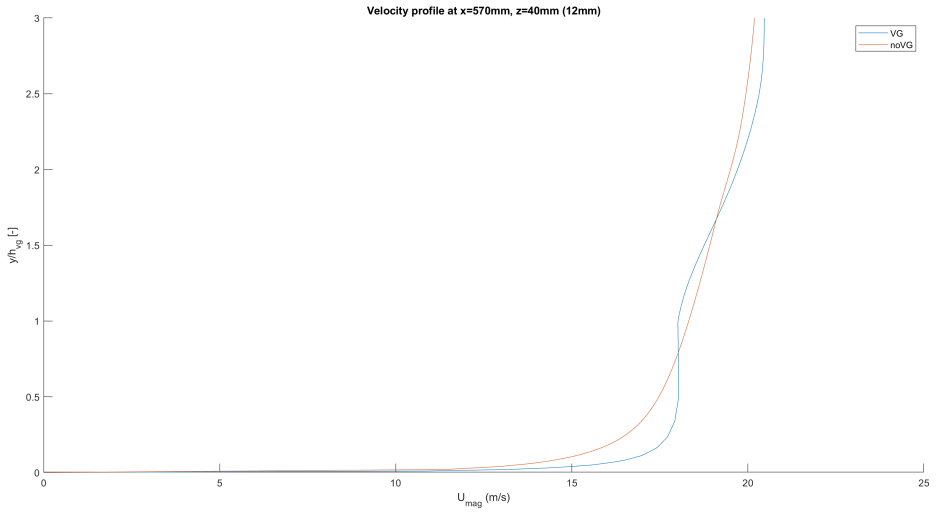

Figure 216: Velocity profile z=40mm, x=570mm (12mm)

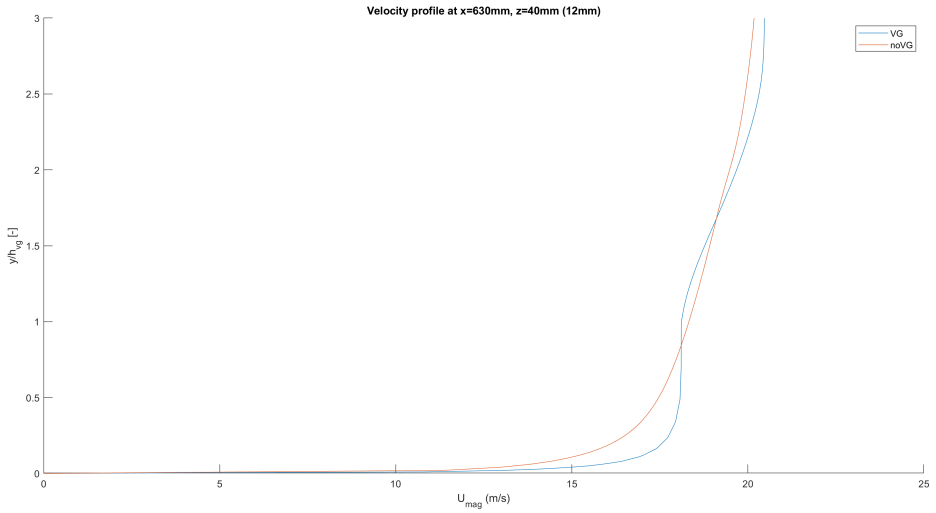

Figure 217: Velocity profile z=40mm, x=630mm (12mm)

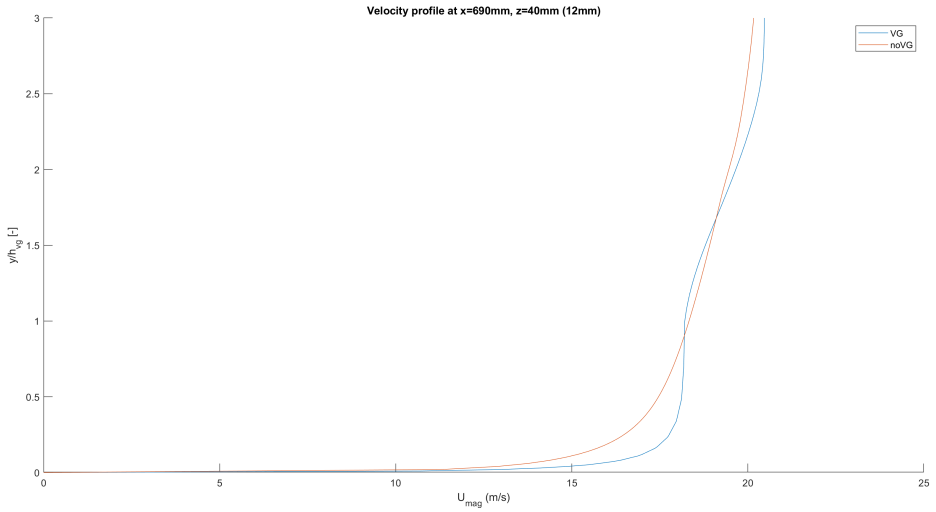

Figure 218: Velocity profile z=40mm, x=690mm (12mm)

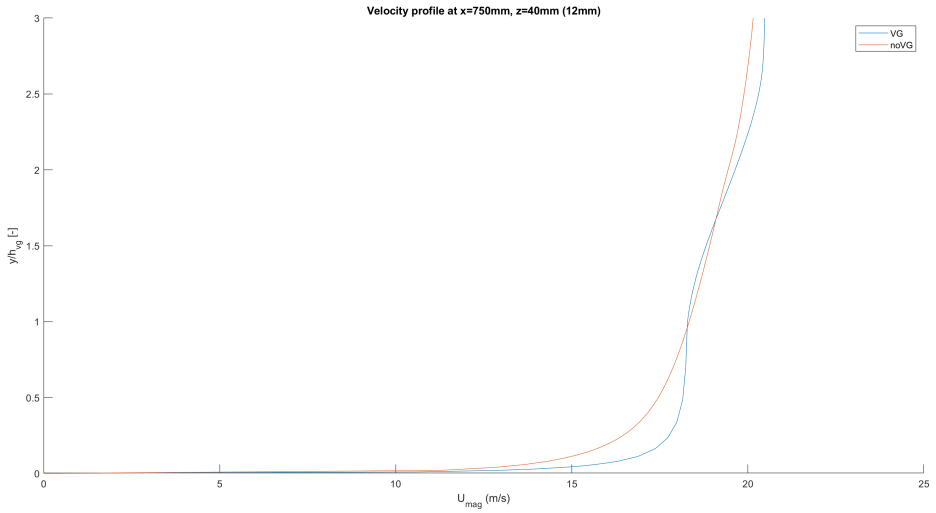

Figure 219: Velocity profile z=40mm, x=750mm (12mm)

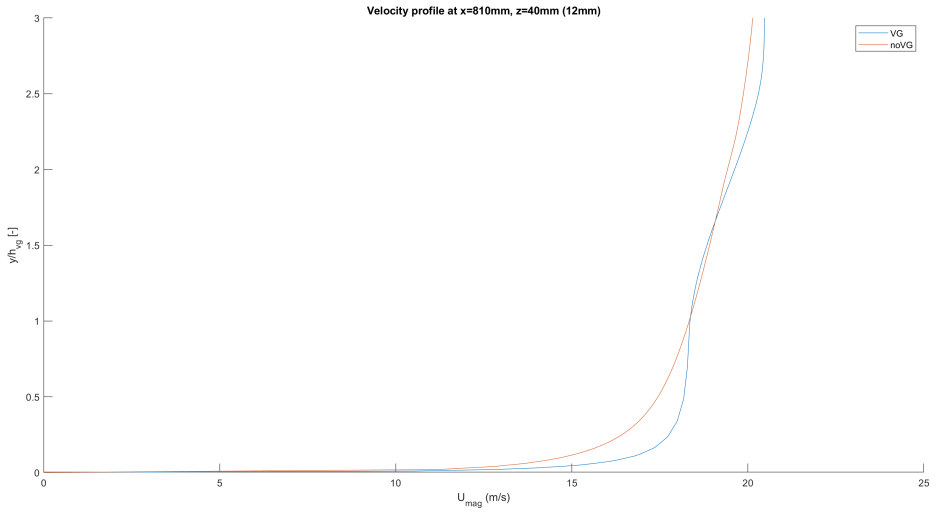

Figure 220: Velocity profile z=40mm, x=810mm (12mm)

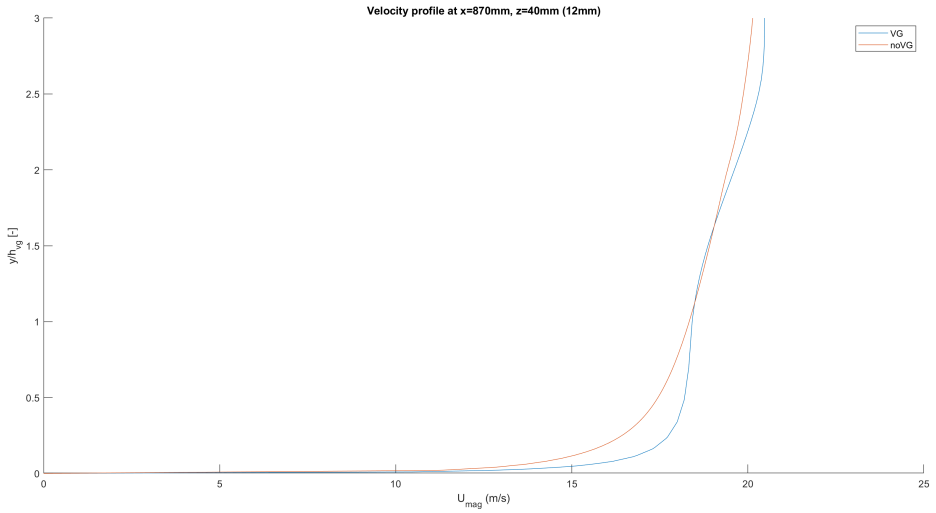

Figure 221: Velocity profile z=40mm, x=870mm (12mm)

7.3 Appendix C

7.3.1 Velocity profiles VG vs Experiment z=-40mm (free)

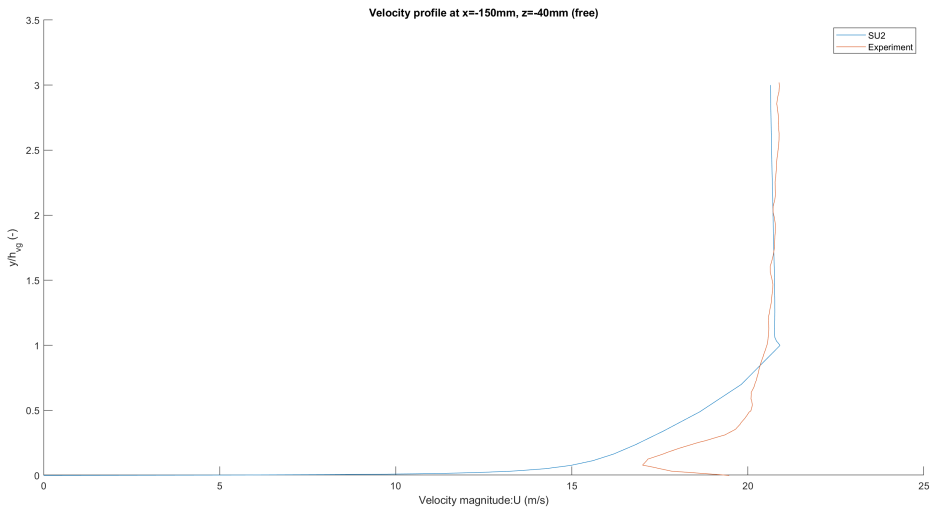

Figure 222: Velocity profiles VG vs Experiment z=-40mm, x=-150mm (free)

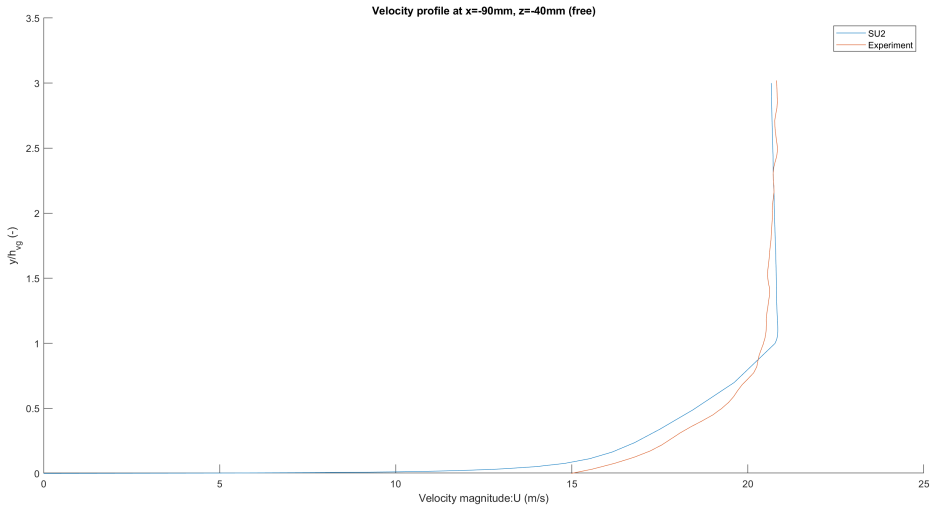

Figure 223: Velocity profiles VG vs Experiment z=-40mm, x=-90mm (free)

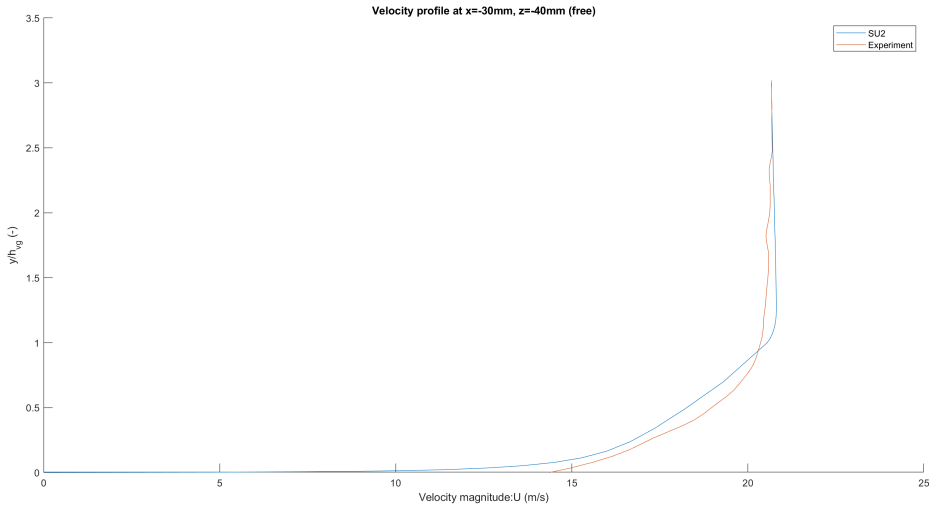

Figure 224: Velocity profiles VG vs Experiment z=-40mm, x=-30mm (free)

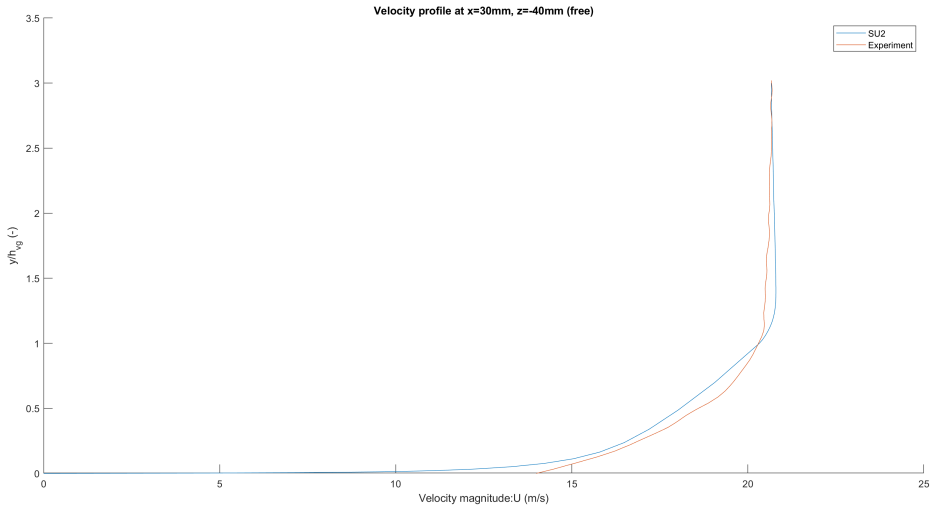

Figure 225: Velocity profiles VG vs Experiment z=-40mm, x=30mm (free)

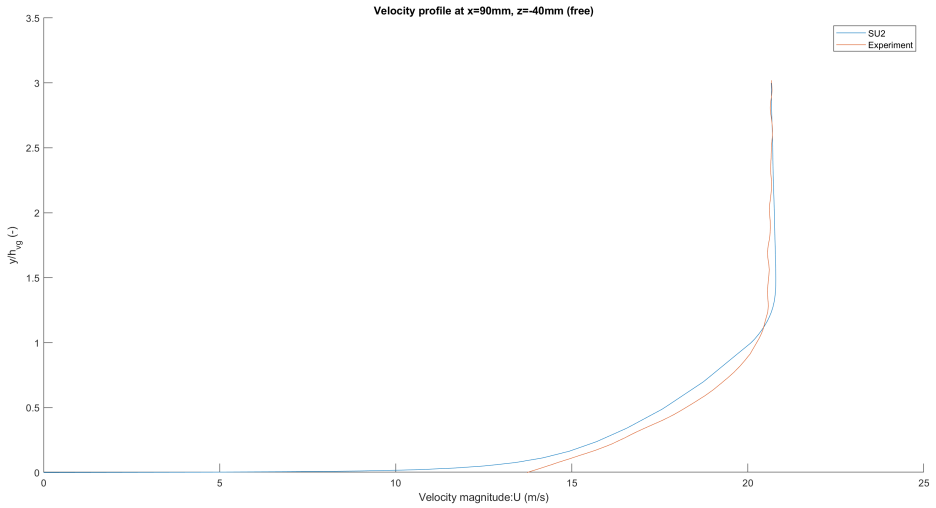

Figure 226: Velocity profiles VG vs Experiment z=-40mm, x=90mm (free)

7.3.2 Velocity profiles VG vs Experiment z=-40mm (8mm)

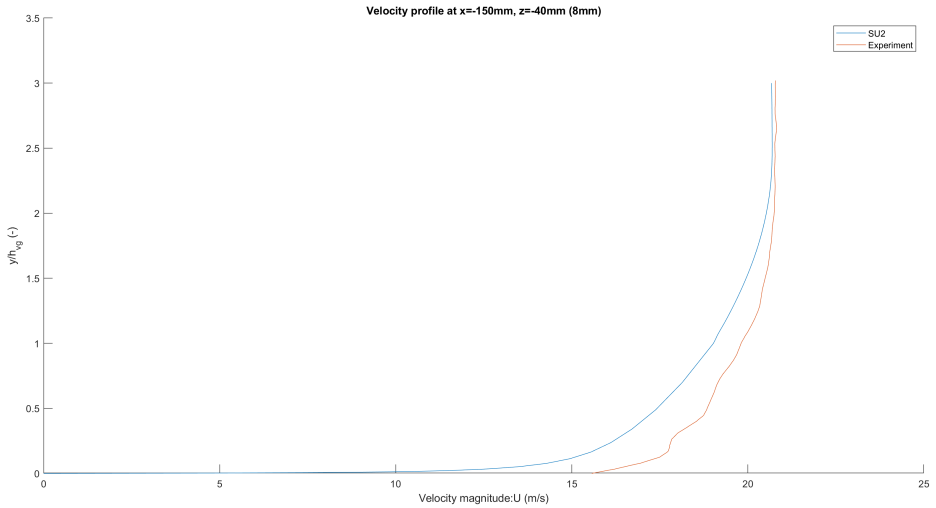

Figure 227: Velocity profiles VG vs Experiment z=-40mm, x=-150mm (8mm)

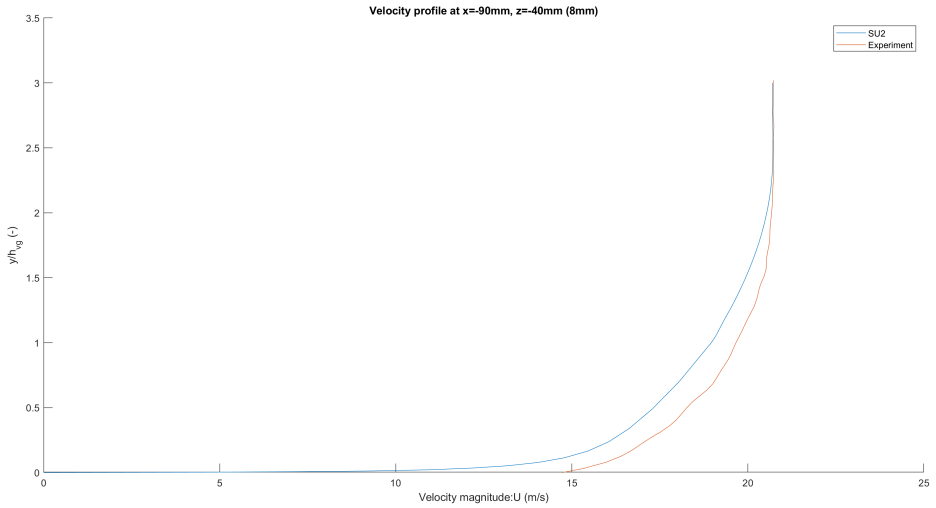

Figure 228: Velocity profiles VG vs Experiment z=-40mm, x=-90mm (8mm)

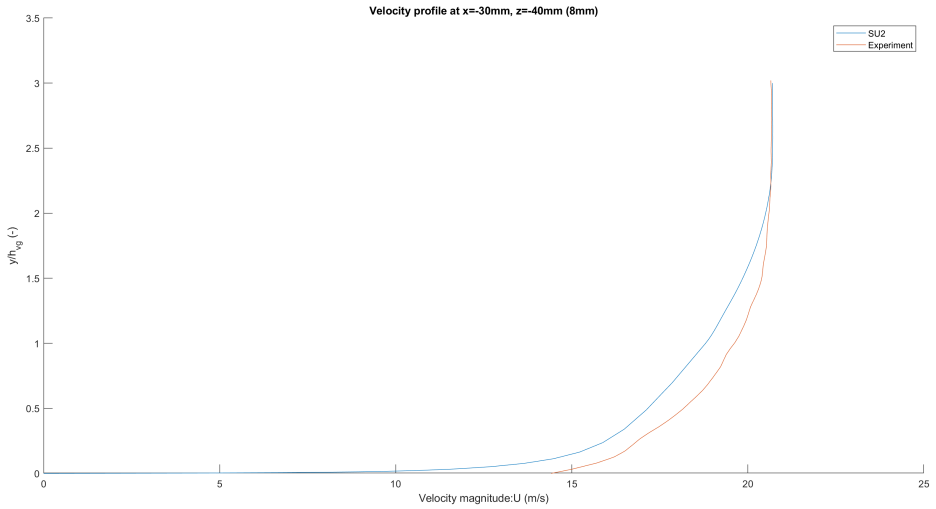

Figure 229: Velocity profiles VG vs Experiment z=-40mm, x=-30mm (8mm)

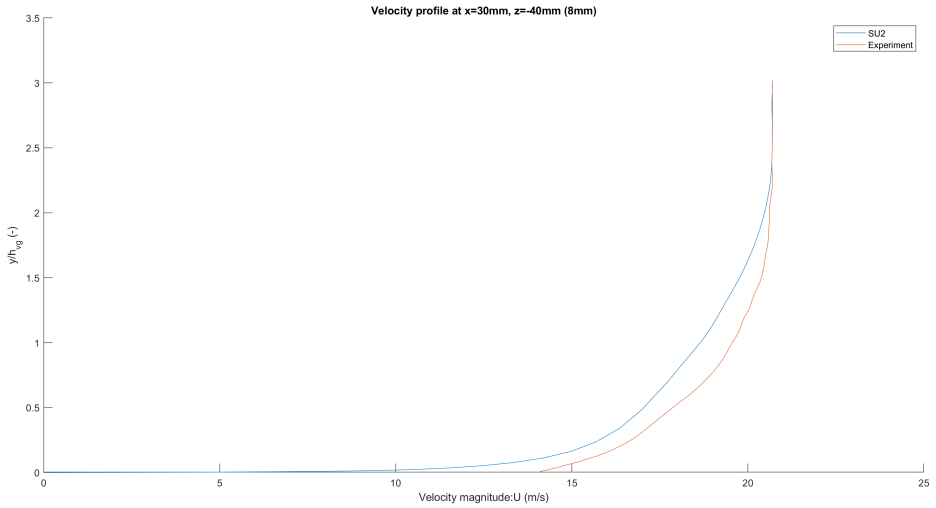

Figure 230: Velocity profiles VG vs Experiment z=-40mm, x=30mm (8mm)

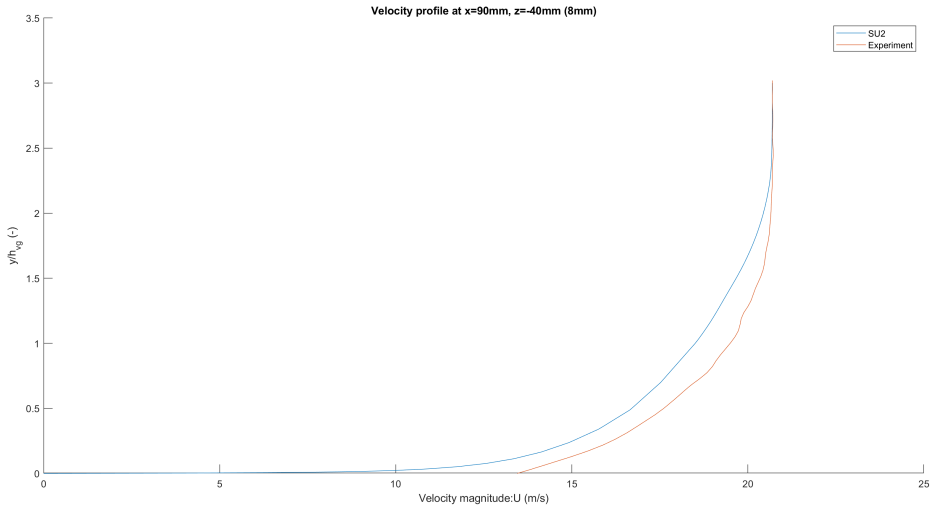

Figure 231: Velocity profiles VG vs Experiment z=-40mm, x=90mm (8mm)

7.3.3 Velocity profiles VG vs Experiment z=-40mm (12mm)

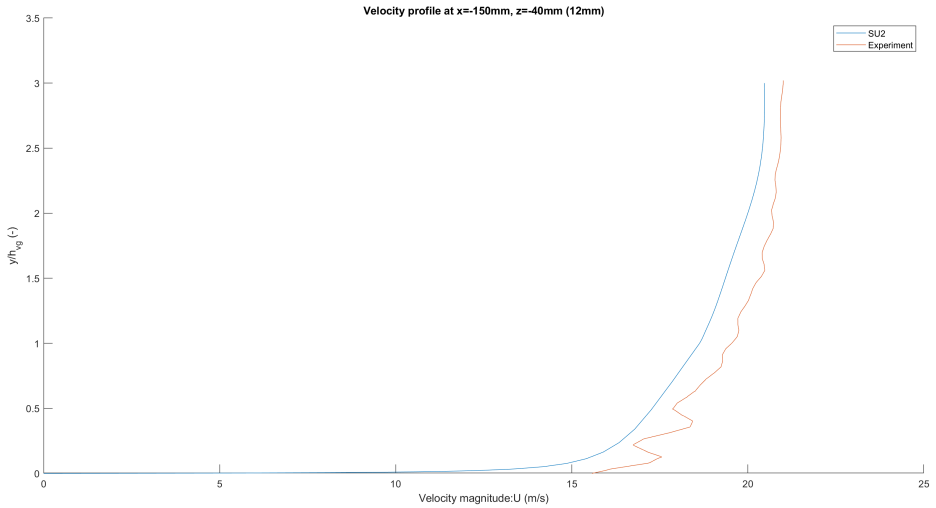

Figure 232: Velocity profiles VG vs Experiment z=-40mm, x=-150mm (12mm)

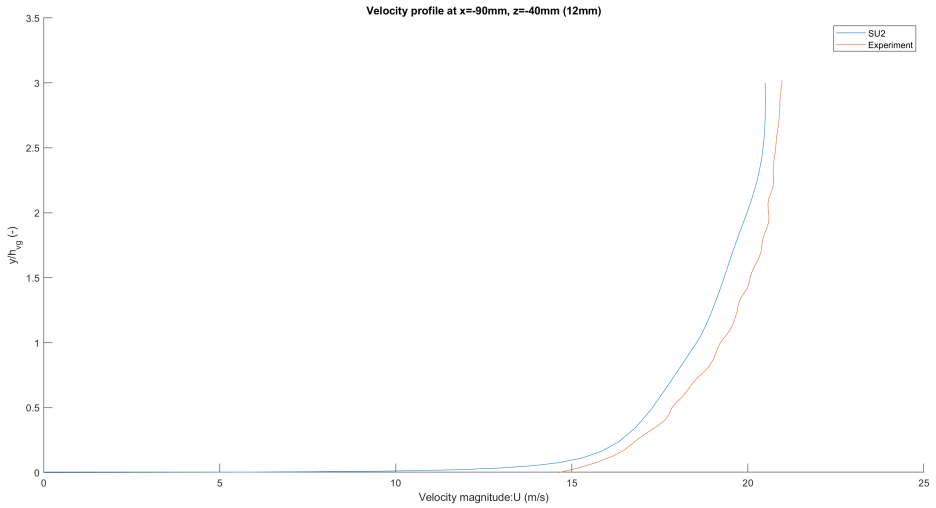

Figure 233: Velocity profiles VG vs Experiment z=-40mm, x=-90mm (12mm)

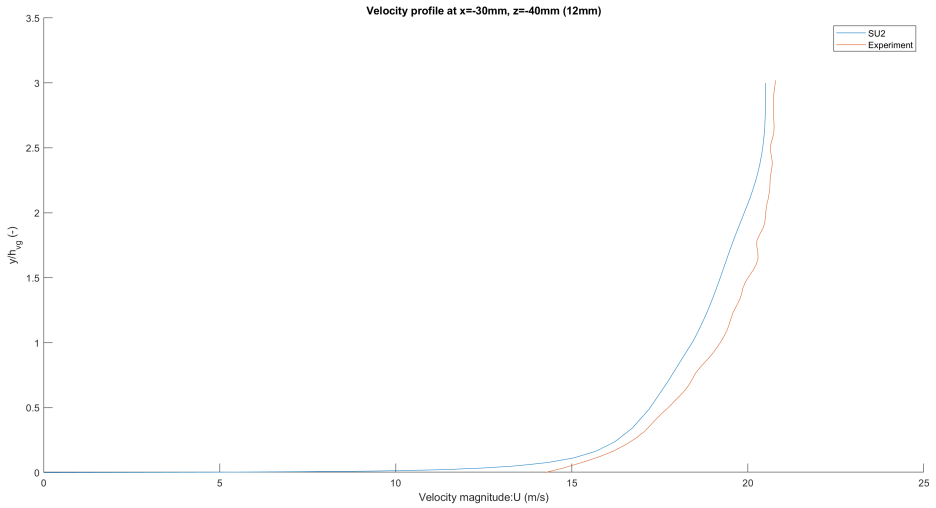

Figure 234: Velocity profiles VG vs Experiment z=-40mm, x=-30mm (12mm)

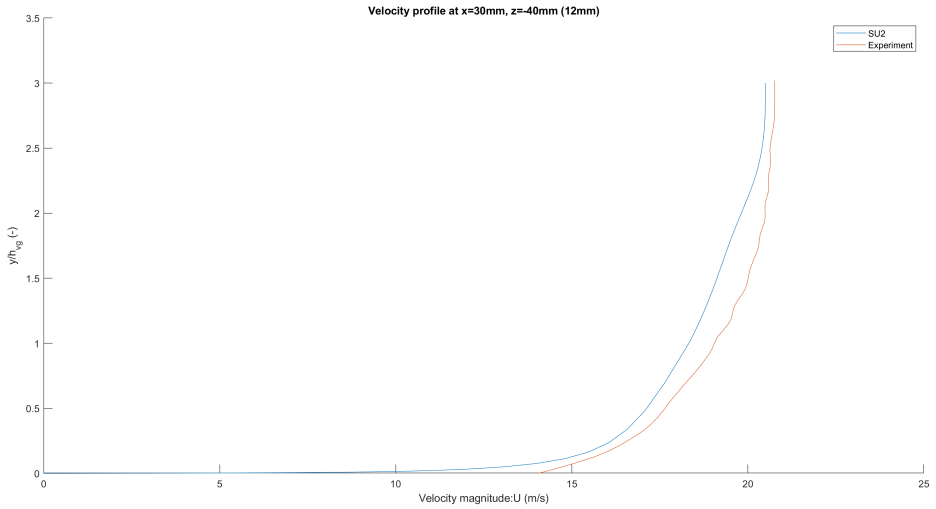

Figure 235: Velocity profiles VG vs Experiment z=-40mm, x=30mm (12mm)

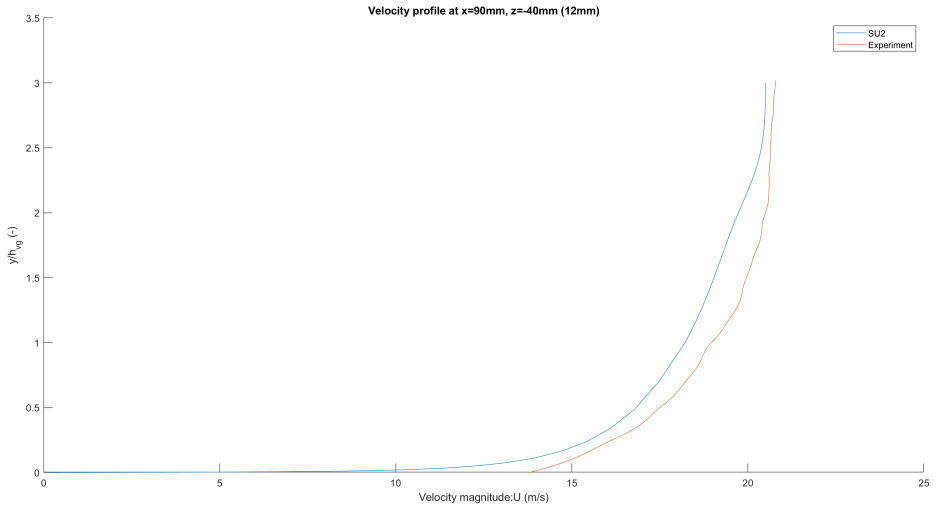

Figure 236: Velocity profiles VG vs Experiment z=-40mm, x=90mm (12mm)

7.3.4 Velocity profiles VG vs Experiment z=0mm (free)

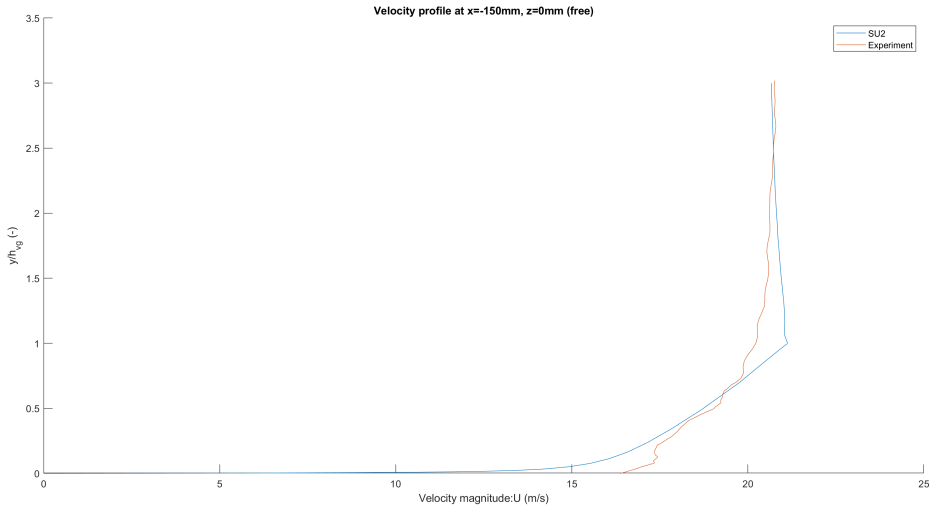

Figure 237: Velocity profiles VG vs Experiment z=0mm, x=-150mm (free)

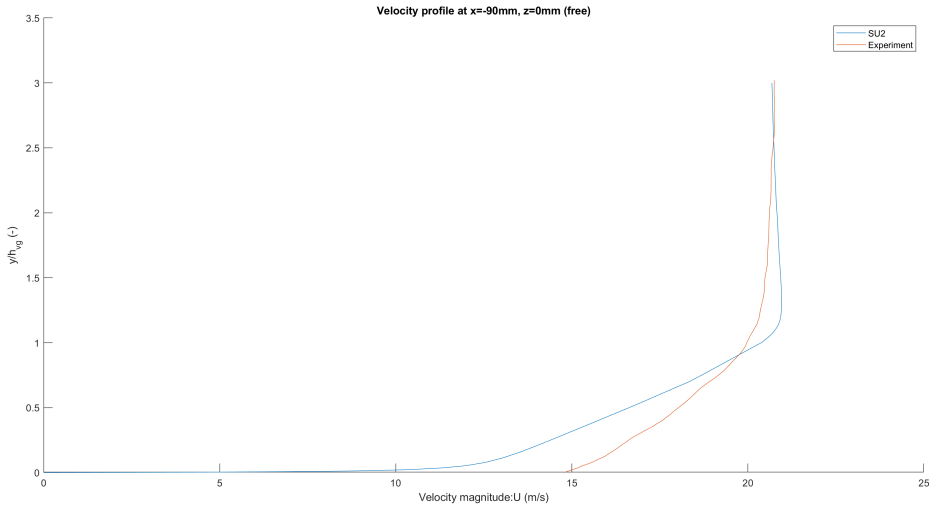

Figure 238: Velocity profiles VG vs Experiment z=0mm, x=-90mm (free)

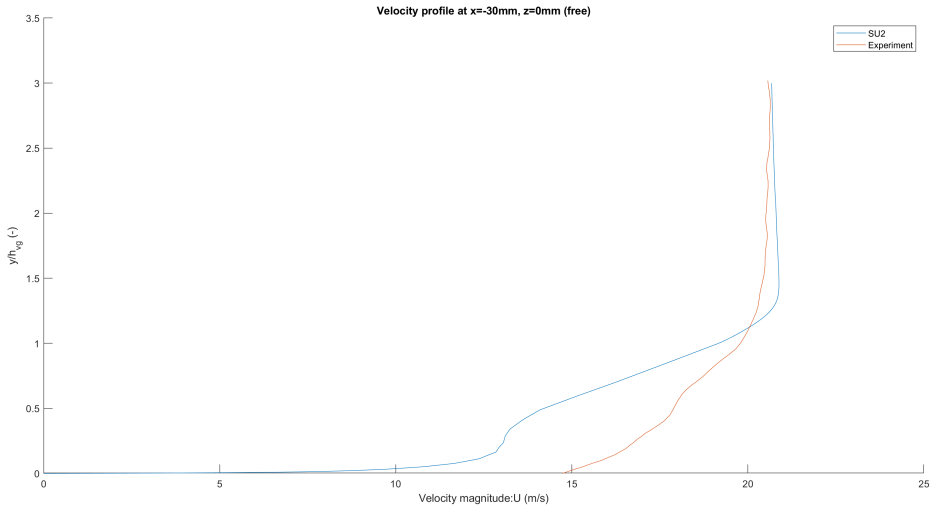

Figure 239: Velocity profiles VG vs Experiment z=0mm, x=-30mm (free)

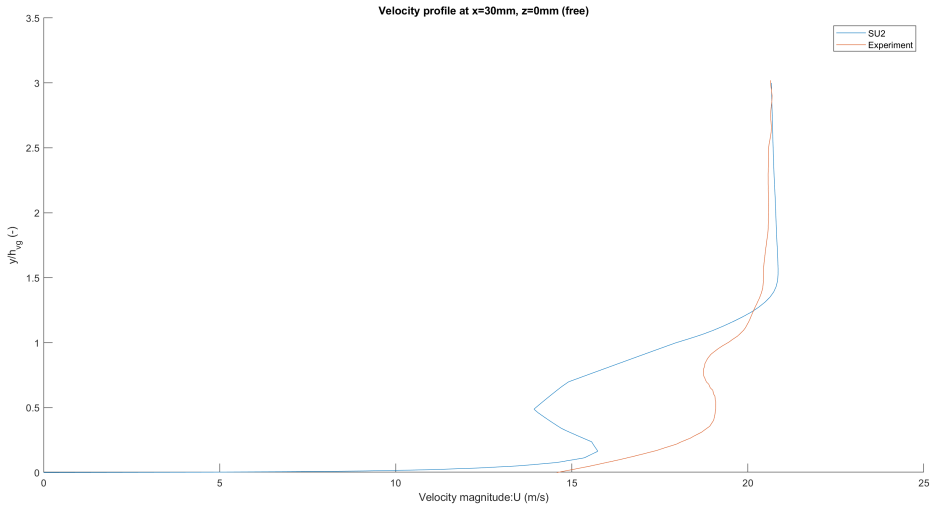

Figure 240: Velocity profiles VG vs Experiment z=0mm, x=30mm (free)

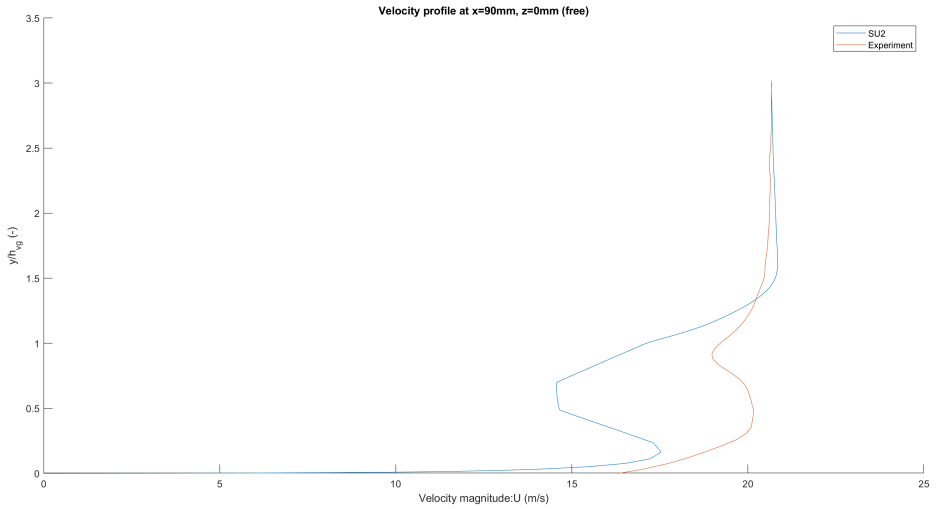

Figure 241: Velocity profiles VG vs Experiment z=0mm, x=90mm (free)

7.3.5 Velocity profiles VG vs Experiment z=0mm (8mm)

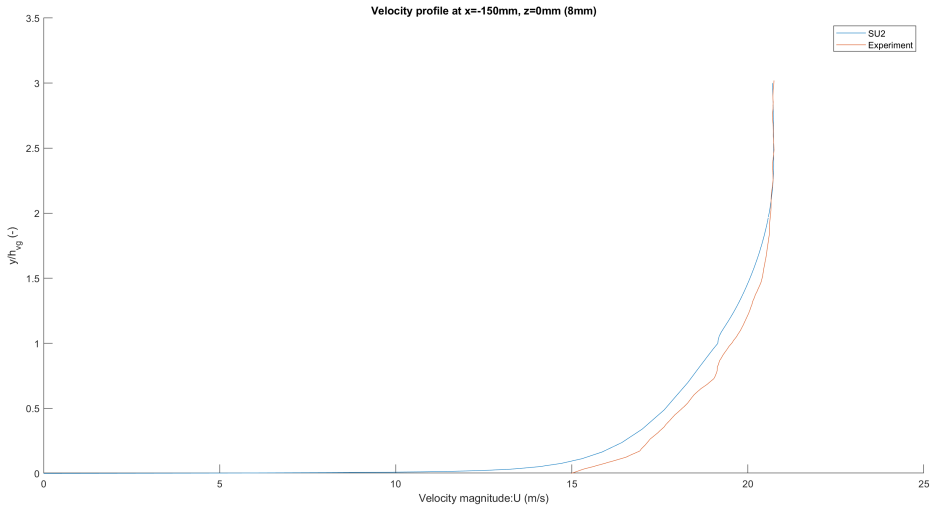

Figure 242: Velocity profiles VG vs Experiment z=0mm, x=-150mm (8mm)

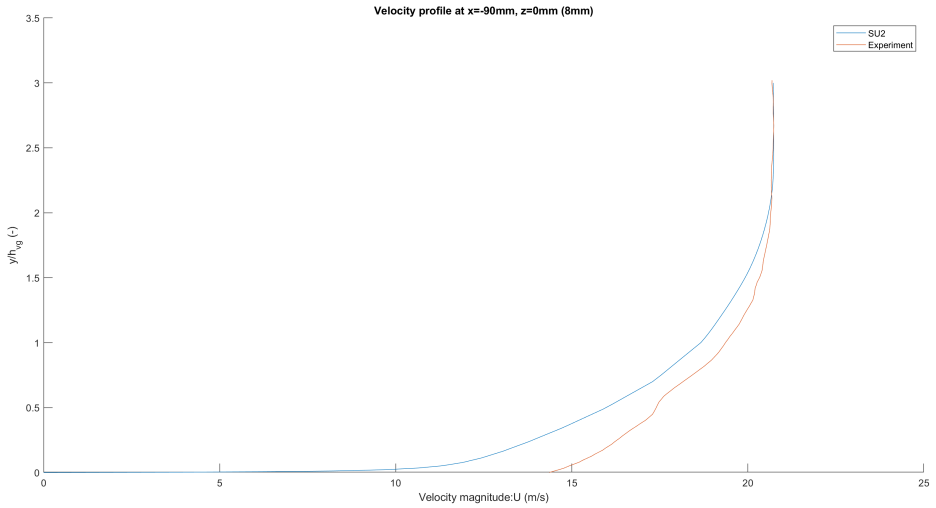

Figure 243: Velocity profiles VG vs Experiment z=0mm, x=-90mm (8mm)

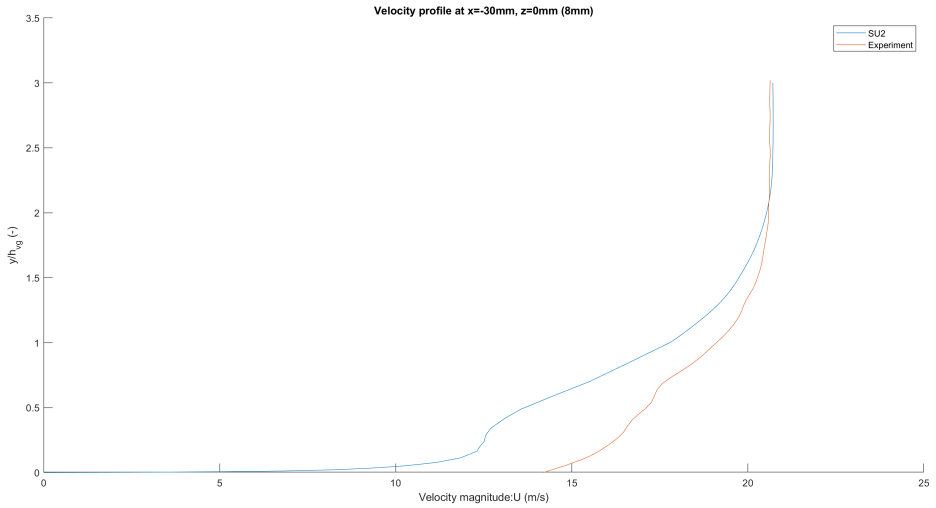

Figure 244: Velocity profiles VG vs Experiment z=0mm, x=-30mm (8mm)

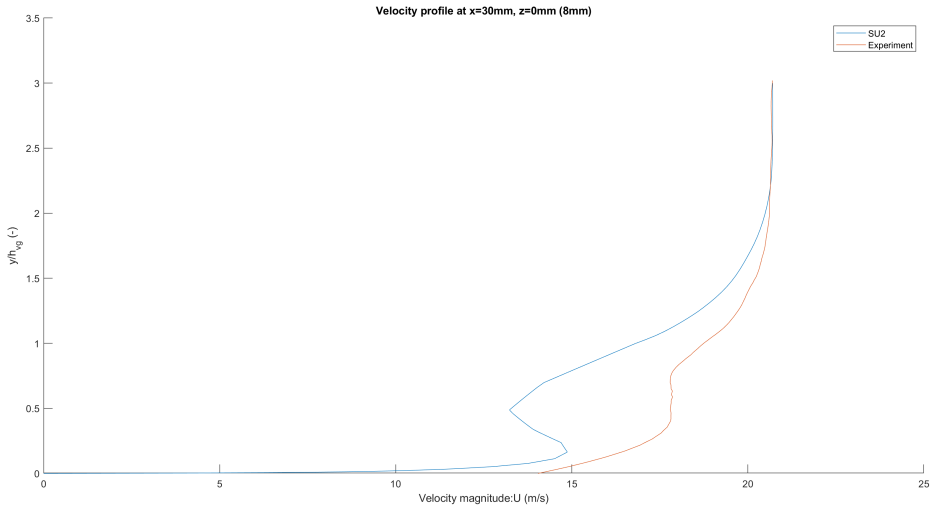

Figure 245: Velocity profiles VG vs Experiment z=0mm, x=30mm (8mm)

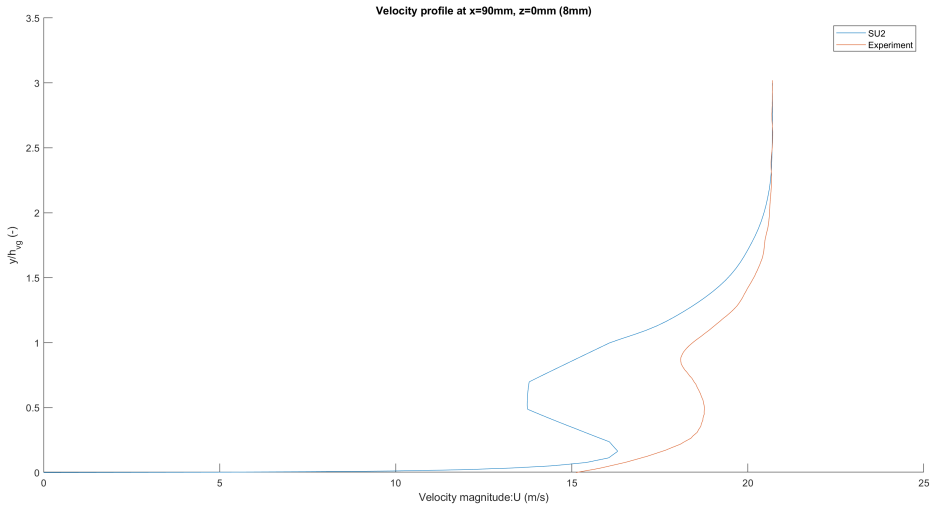

Figure 246: Velocity profiles VG vs Experiment z=0mm, x=90mm (8mm)

7.3.6 Velocity profiles VG vs Experiment z=0mm (12mm)

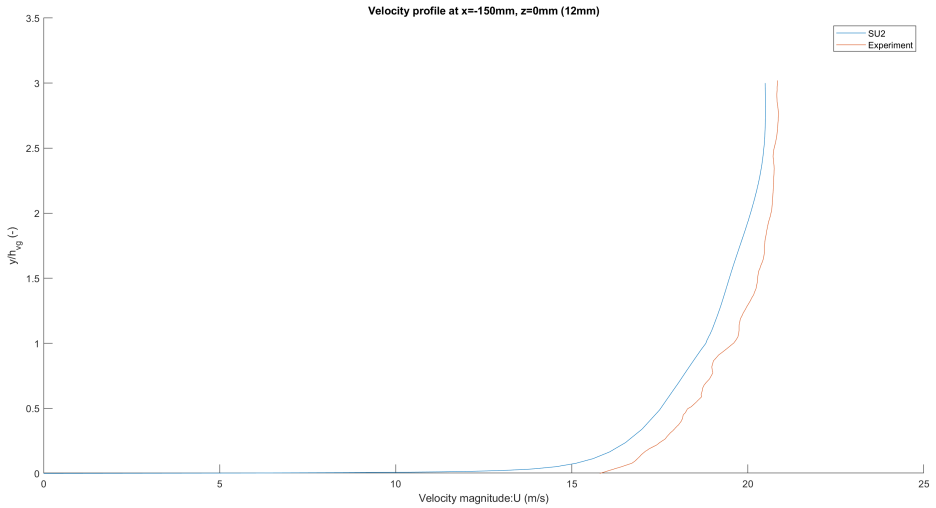

Figure 247: Velocity profiles VG vs Experiment z=0mm, x=-150mm (12mm)

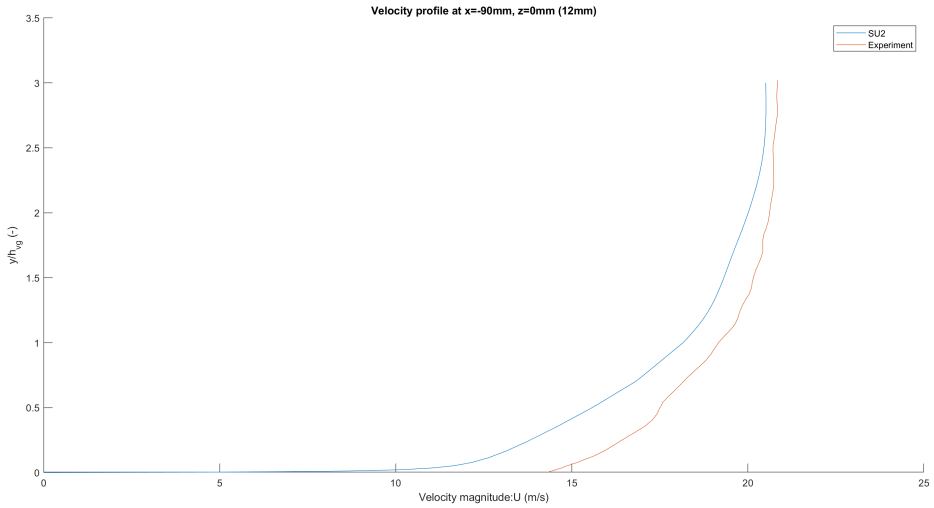

Figure 248: Velocity profiles VG vs Experiment z=0mm, x=-90mm (12mm)

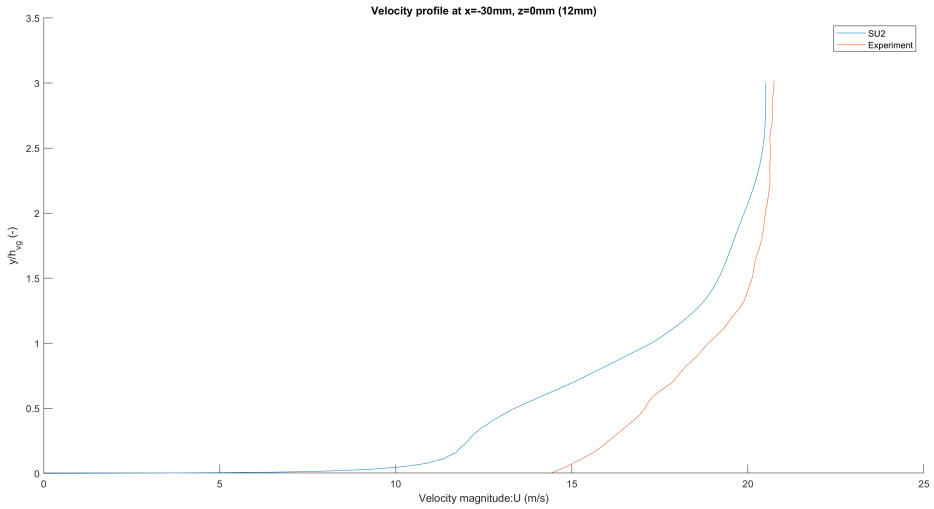

Figure 249: Velocity profiles VG vs Experiment z=0mm, x=-30mm (12mm)

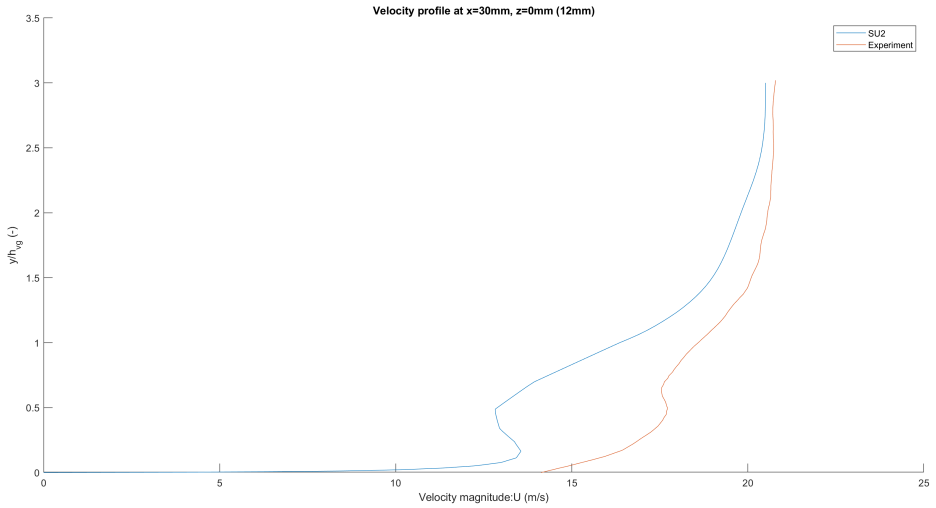

Figure 250: Velocity profiles VG vs Experiment z=0mm, x=30mm (12mm)

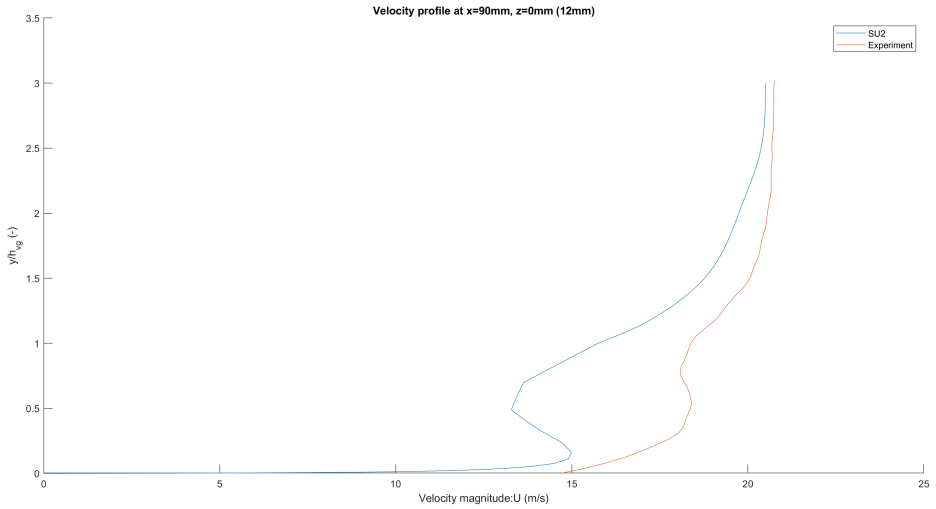

Figure 251: Velocity profiles VG vs Experiment z=0mm, x=90mm (12mm)

7.3.7 Velocity profiles VG vs Experiment z=40mm (free)

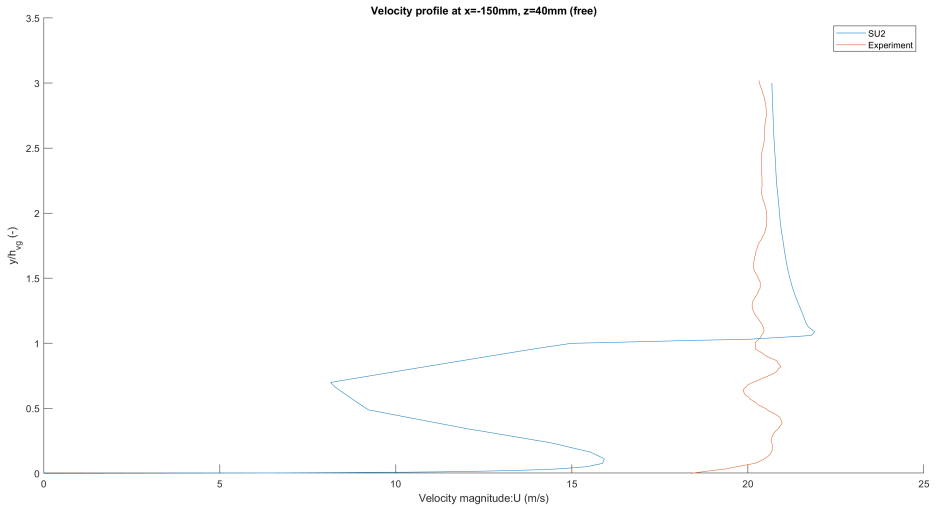

Figure 252: Velocity profiles VG vs Experiment z=40mm, x=-150mm (free)

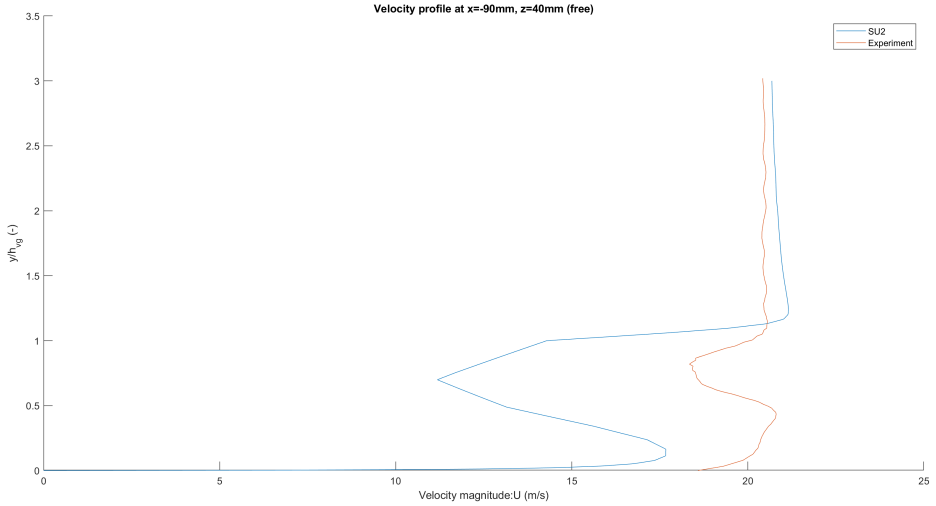

Figure 253: Velocity profiles VG vs Experiment z=40mm, x=-90mm (free)

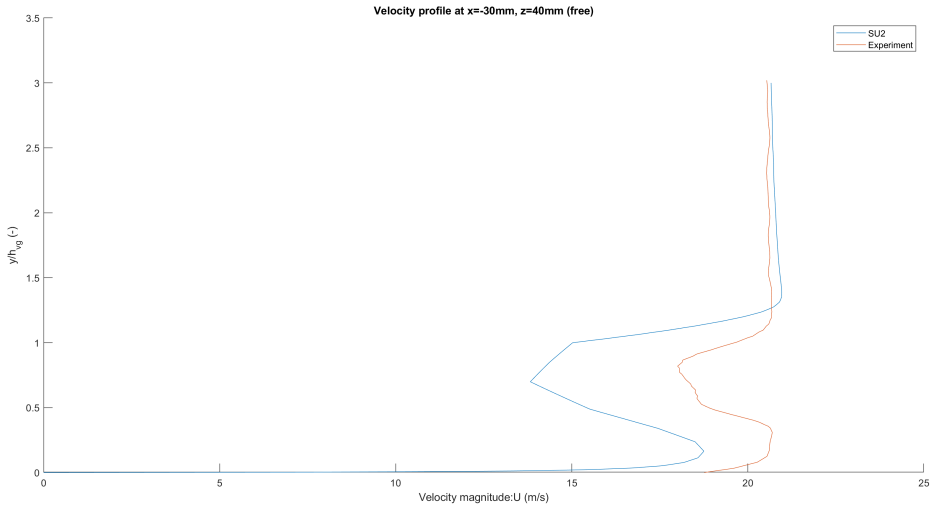

Figure 254: Velocity profiles VG vs Experiment z=40mm, x=-30mm (free)

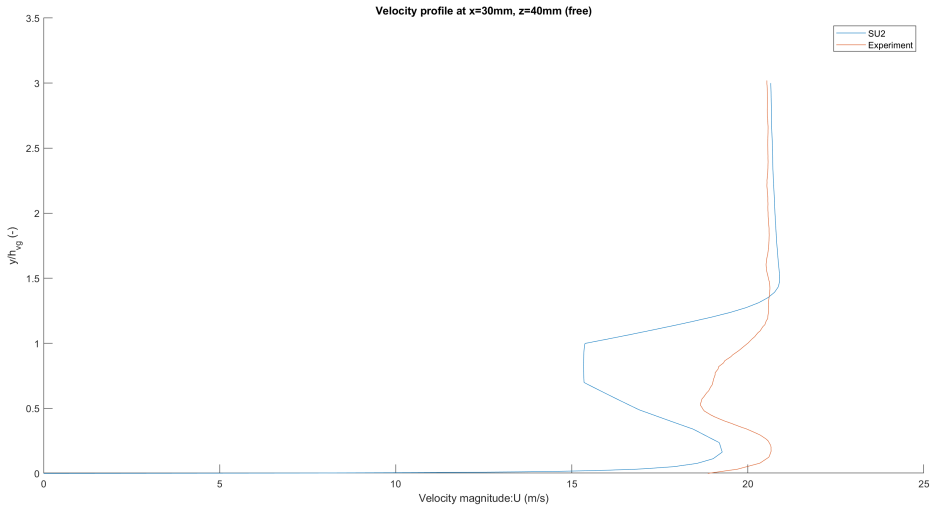

Figure 255: Velocity profiles VG vs Experiment z=40mm, x=30mm (free)

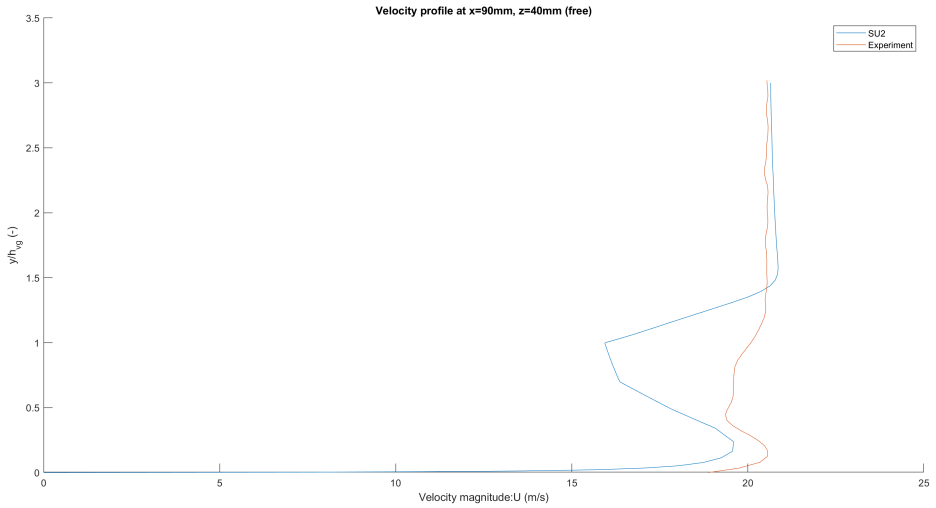

Figure 256: Velocity profiles VG vs Experiment z=40mm, x=90mm (free)

7.3.8 Velocity profiles VG vs Experiment z=40mm (8mm)

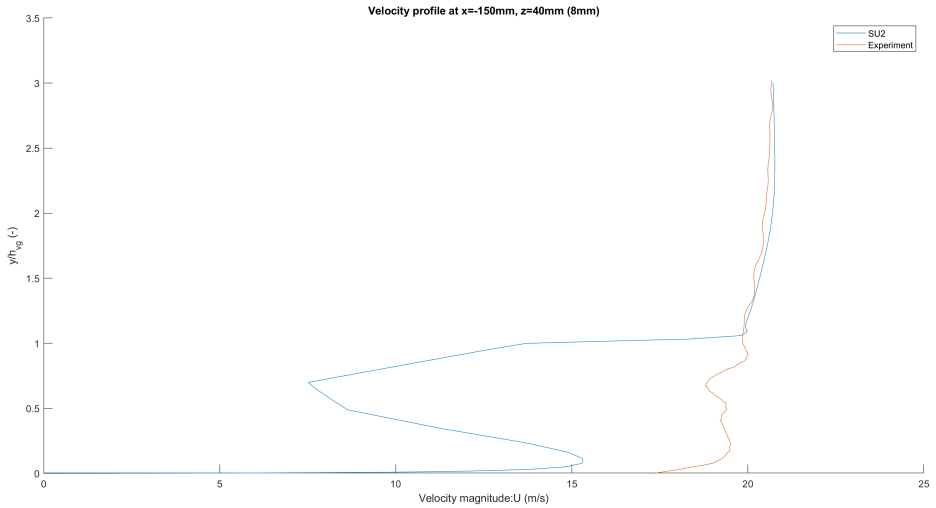

Figure 257: Velocity profiles VG vs Experiment z=40mm, x=-150mm (8mm)

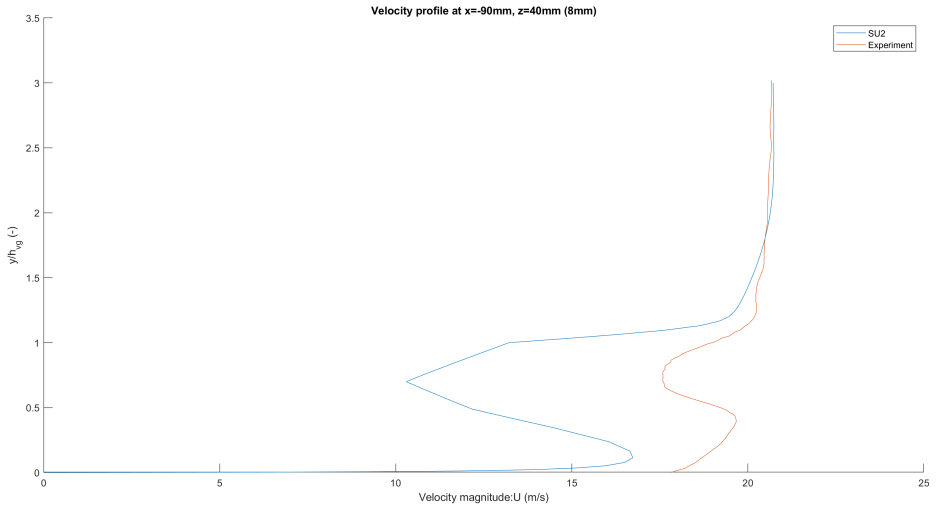

Figure 258: Velocity profiles VG vs Experiment z=40mm, x=-90mm (8mm)

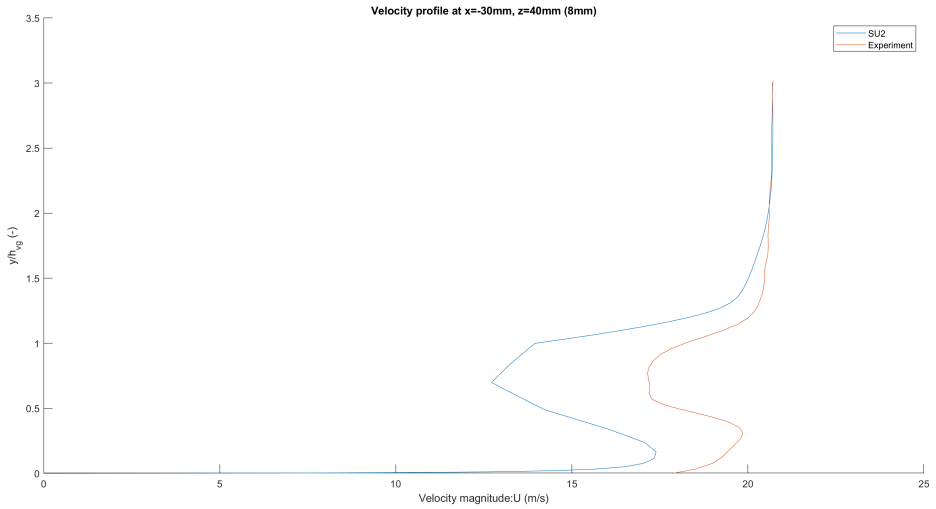

Figure 259: Velocity profiles VG vs Experiment z=40mm, x=-30mm (8mm)

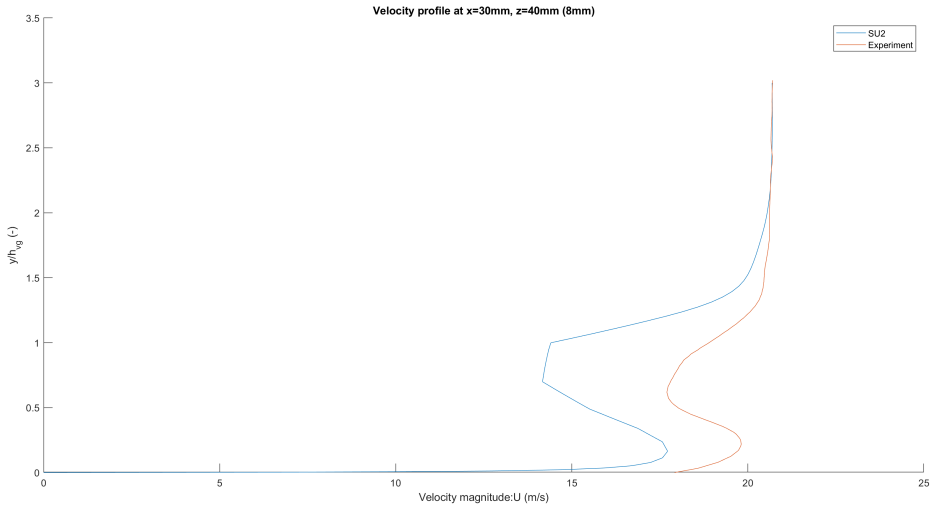

Figure 260: Velocity profiles VG vs Experiment z=40mm, x=30mm (8mm)

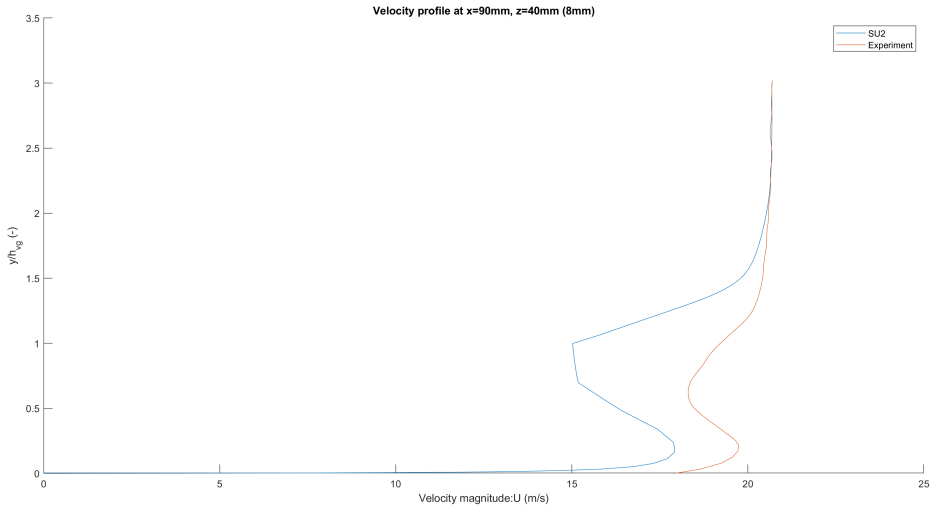

Figure 261: Velocity profiles VG vs Experiment z=40mm, x=90mm (8mm)

7.3.9 Velocity profiles VG vs Experiment z=40mm (12mm)

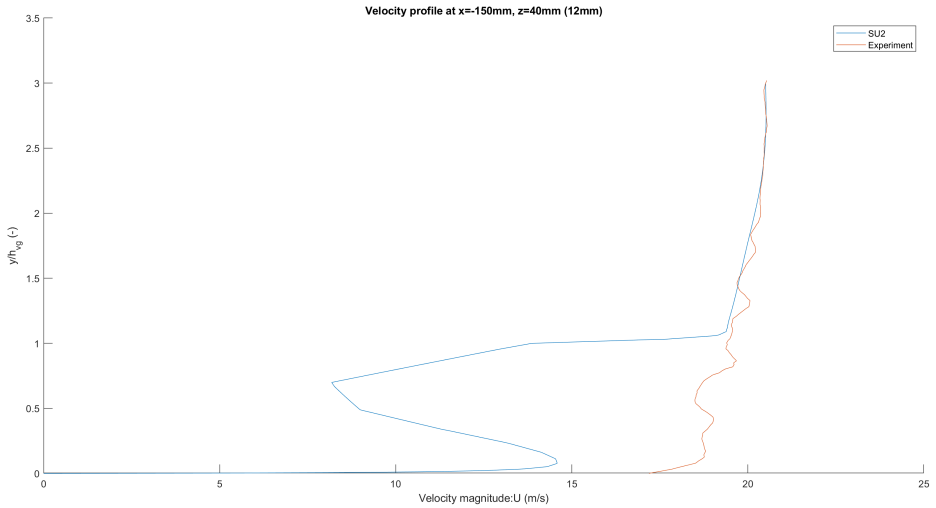

Figure 262: Velocity profiles VG vs Experiment z=40mm, x=-150mm (12mm)

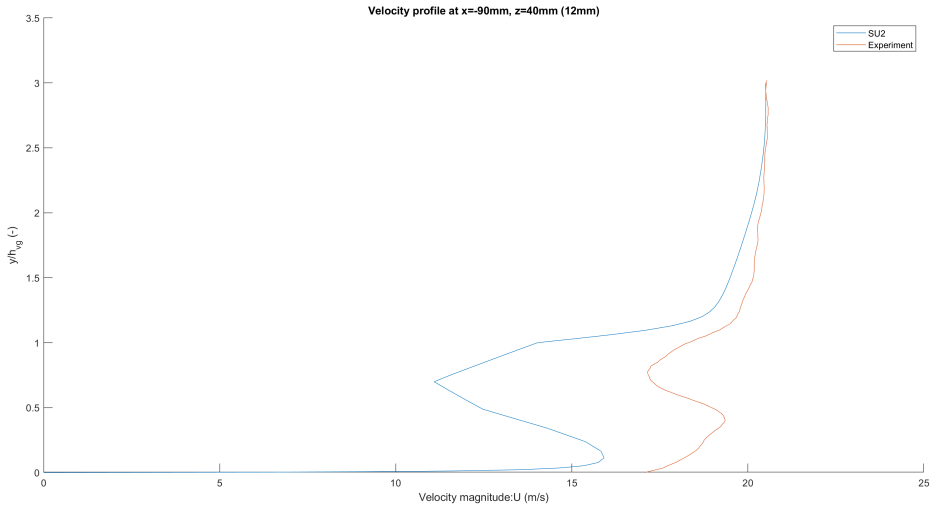

Figure 263: Velocity profiles VG vs Experiment z=40mm, x=-90mm (12mm)

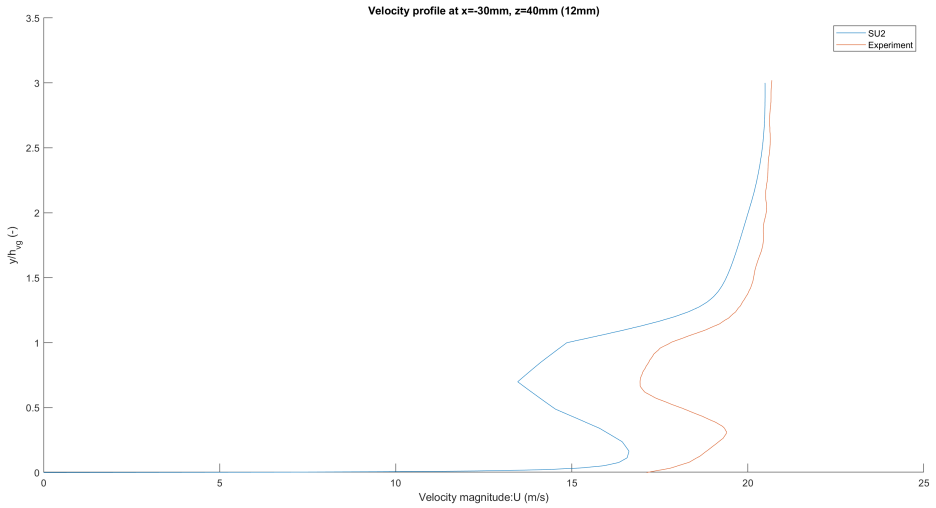

Figure 264: Velocity profiles VG vs Experiment z=40mm, x=-30mm (12mm)

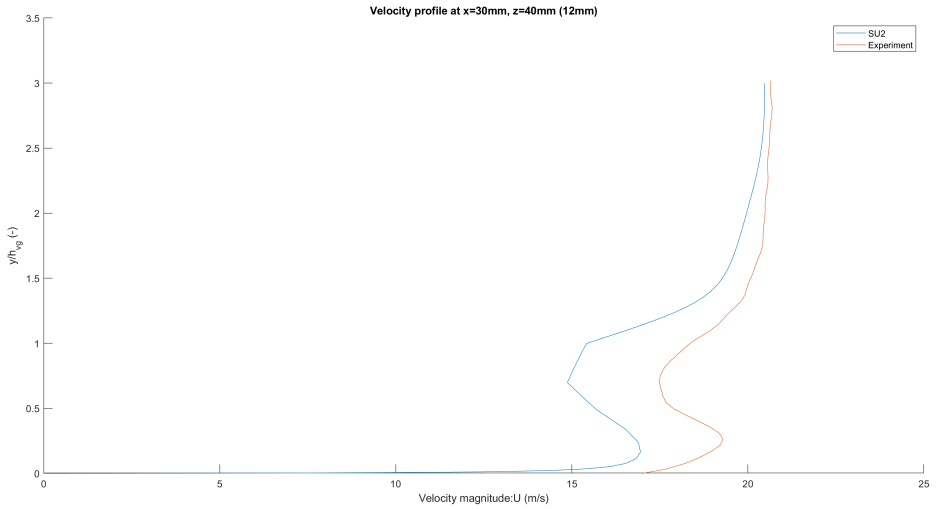

Figure 265: Velocity profiles VG vs Experiment z=40mm, x=30mm (12mm)

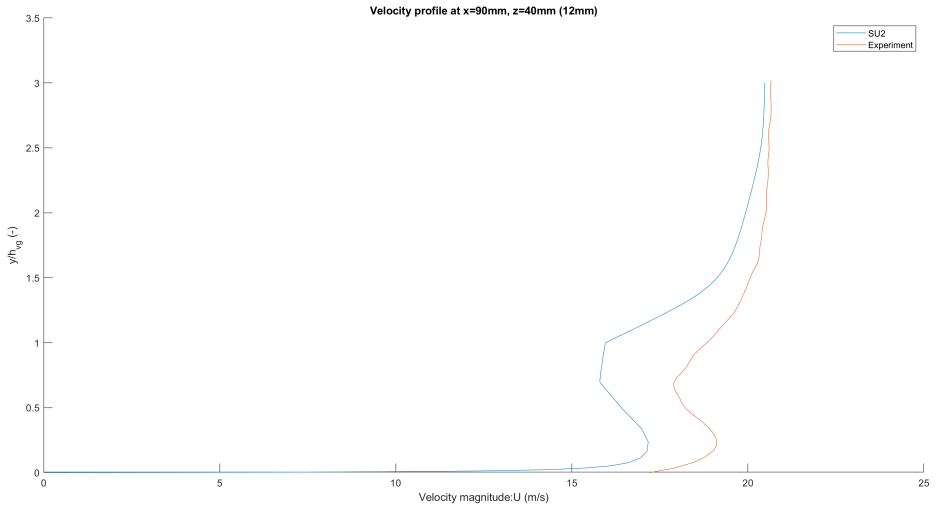

Figure 266: Velocity profiles VG vs Experiment z=40mm, x=90mm (12mm)

7.4 Appendix D

7.4.1 Turbulent shear profiles VG vs Experiment z=-40mm (free)

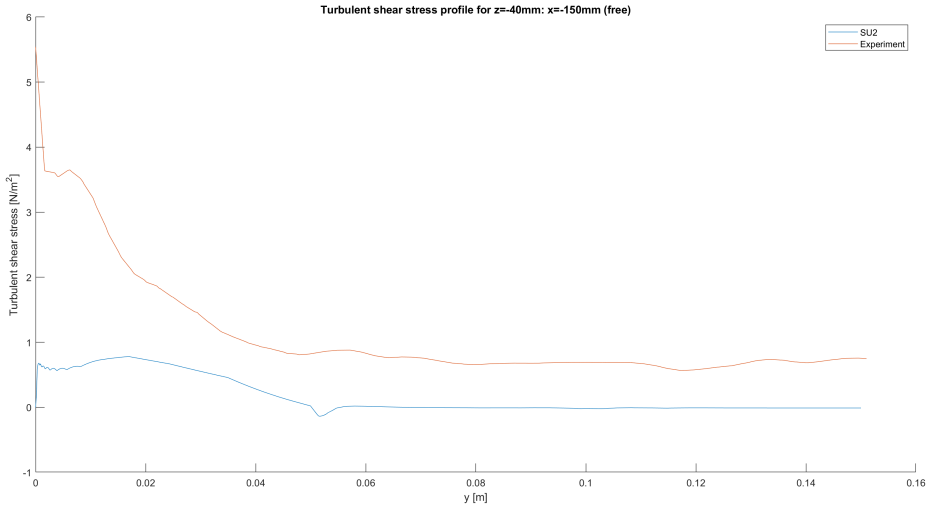

Figure 267: Turbulent shear profiles VG vs Experiment z=-40mm, x=-150mm (free)

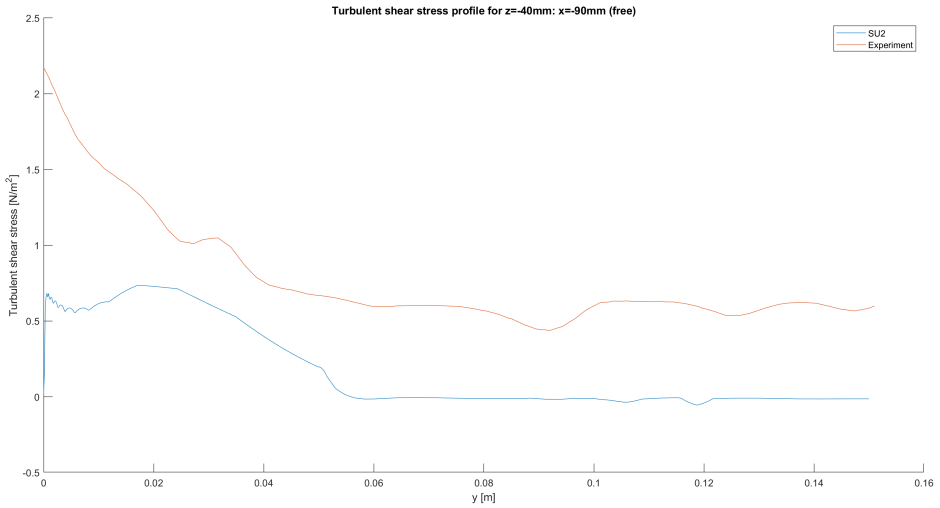

Figure 268: Turbulent shear profiles VG vs Experiment z=-40mm, x=-90mm (free)

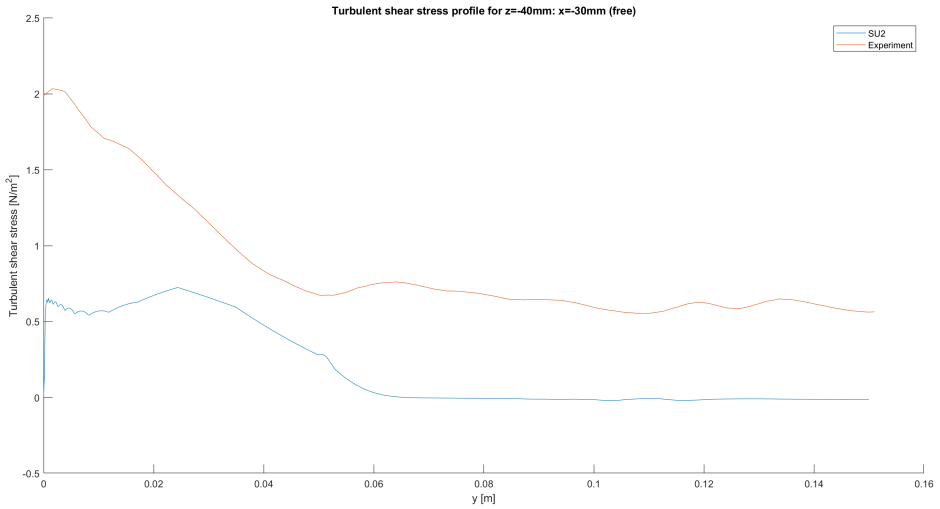

Figure 269: Turbulent shear profiles VG vs Experiment z=-40mm, x=-30mm (free)

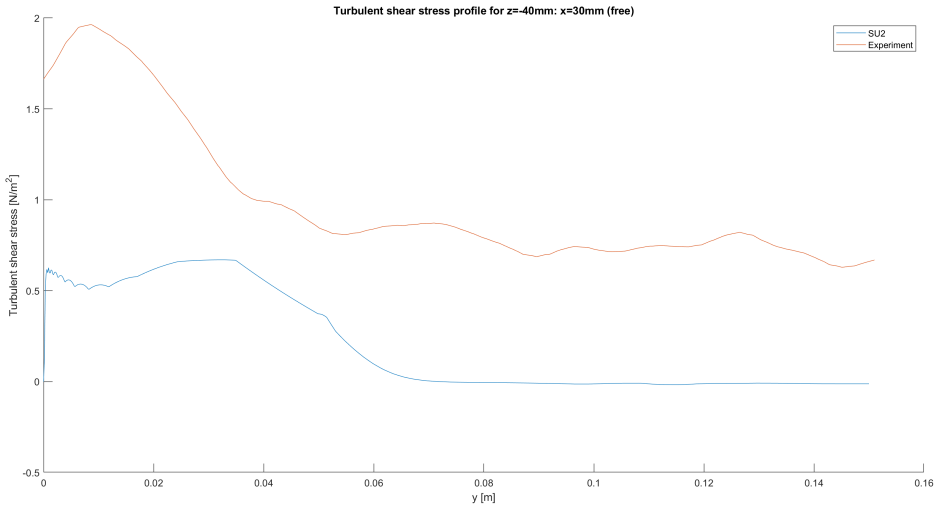

Figure 270: Turbulent shear profiles VG vs Experiment z=-40mm, x=30mm (free)

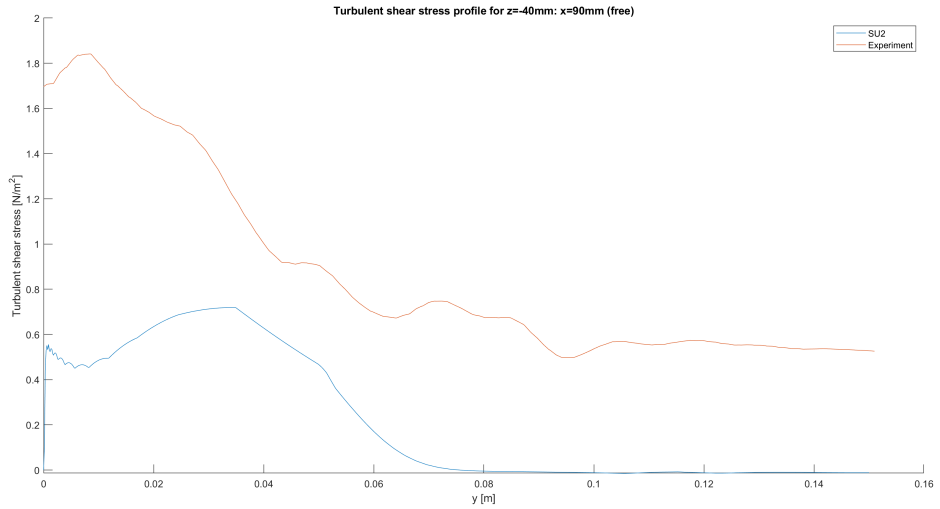

Figure 271: Turbulent shear profiles VG vs Experiment z=-40mm, x=90mm (free)

7.4.2 Turbulent shear profiles VG vs Experiment z=-40mm (8mm)

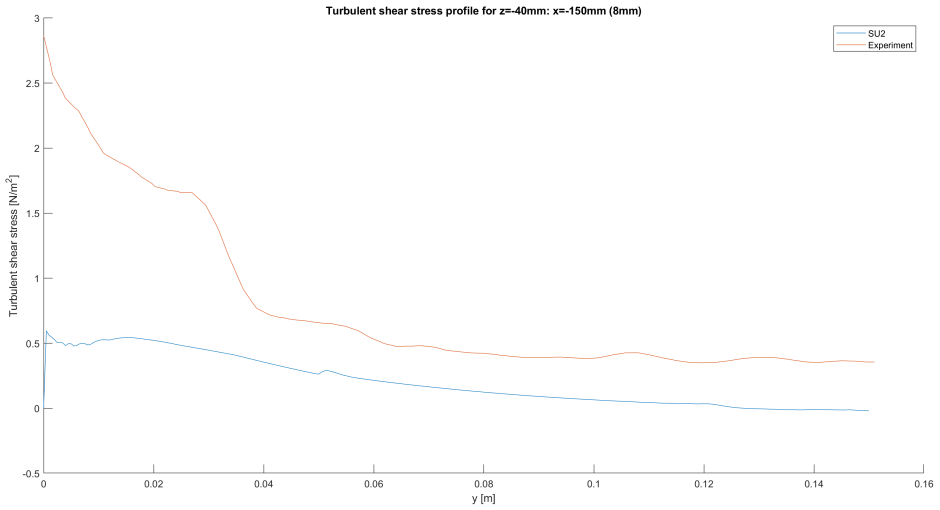

Figure 272: Turbulent shear profiles VG vs Experiment z=-40mm, x=-150mm (8mm)

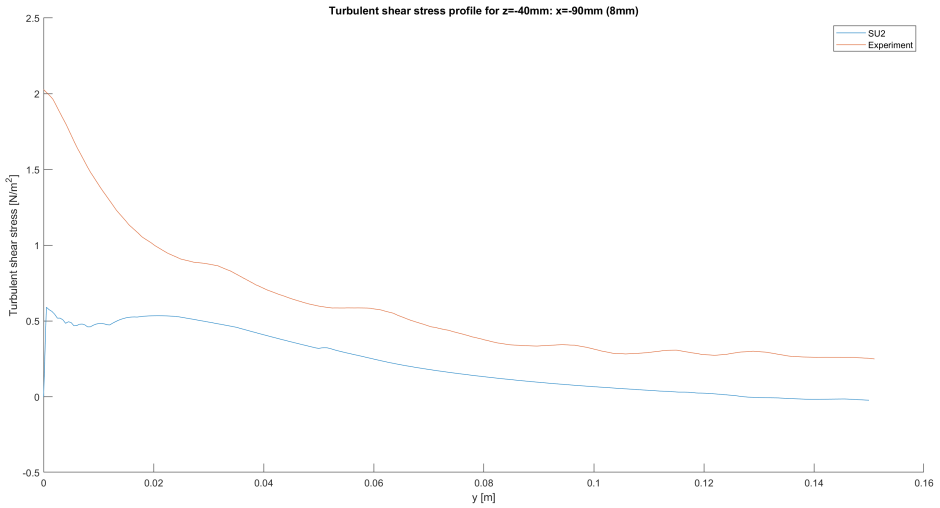

Figure 273: Turbulent shear profiles VG vs Experiment z=-40mm, x=-90mm (8mm)

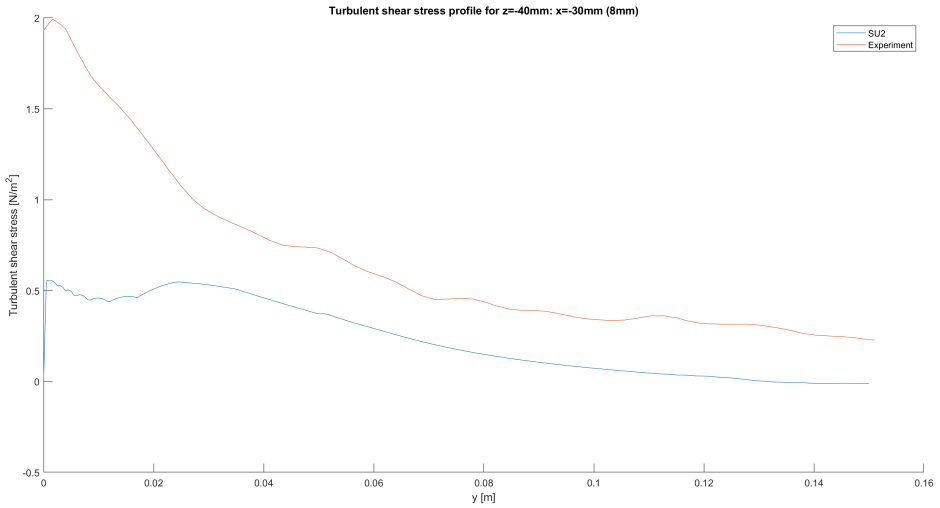

Figure 274: Turbulent shear profiles VG vs Experiment z=-40mm, x=-30mm (8mm)

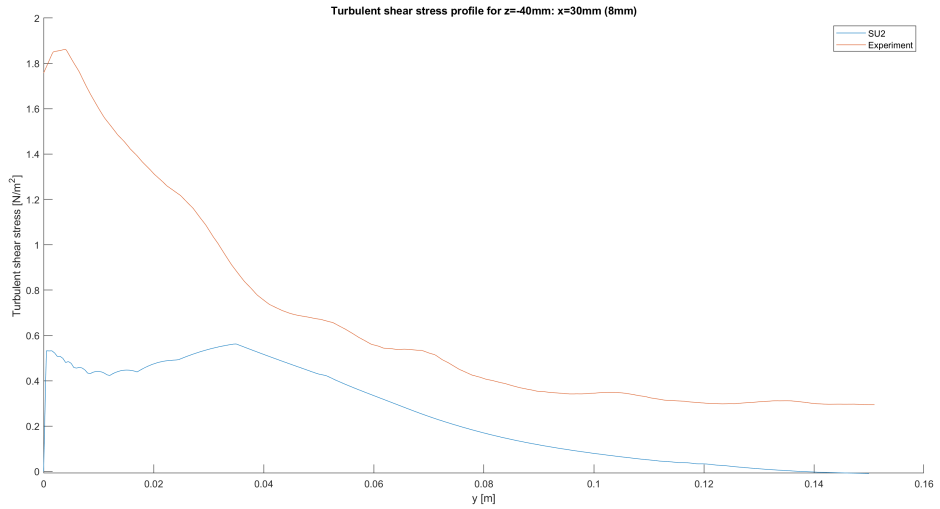

Figure 275: Turbulent shear profiles VG vs Experiment z=-40mm, x=30mm (8mm)

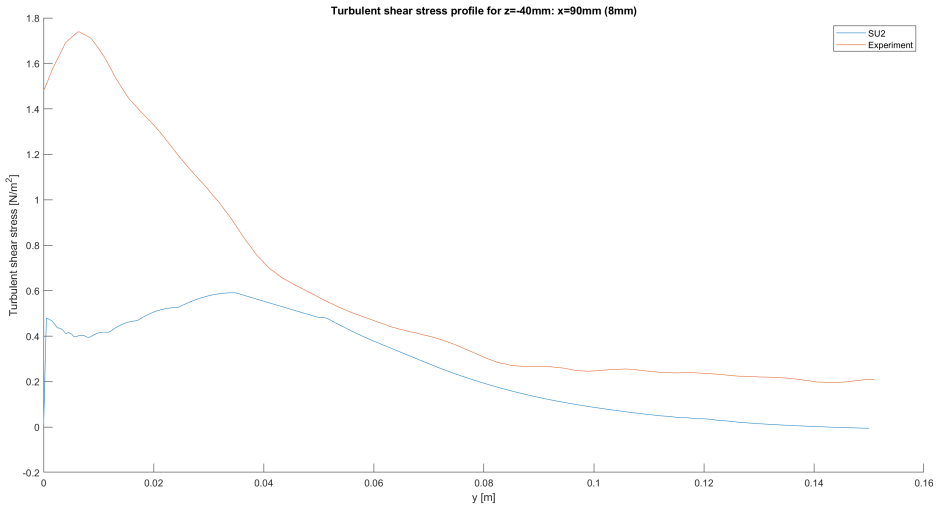

Figure 276: Turbulent shear profiles VG vs Experiment z=-40mm, x=90mm (8mm)

7.4.3 Turbulent shear profiles VG vs Experiment z=-40mm (12mm)

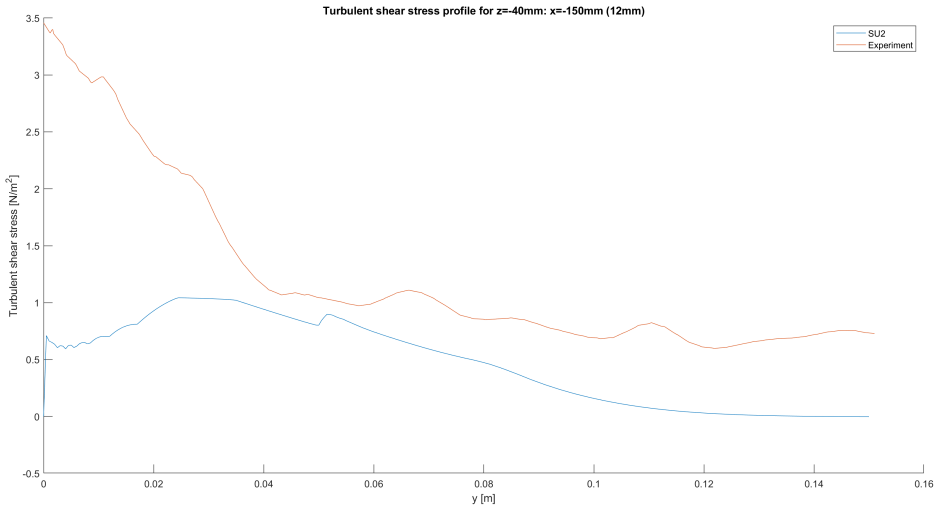

Figure 277: Turbulent shear profiles VG vs Experiment z=-40mm, x=-150mm (12mm)

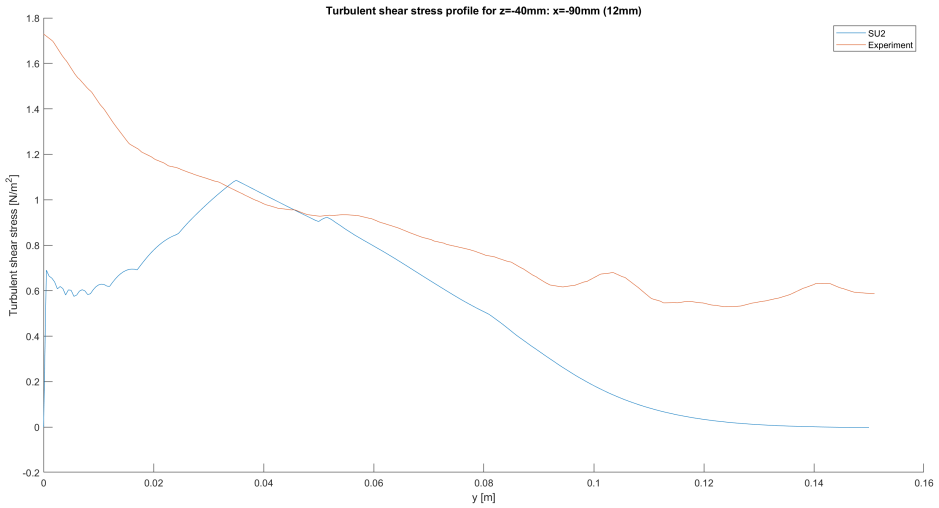

Figure 278: Turbulent shear profiles VG vs Experiment z=-40mm, x=-90mm (12mm)

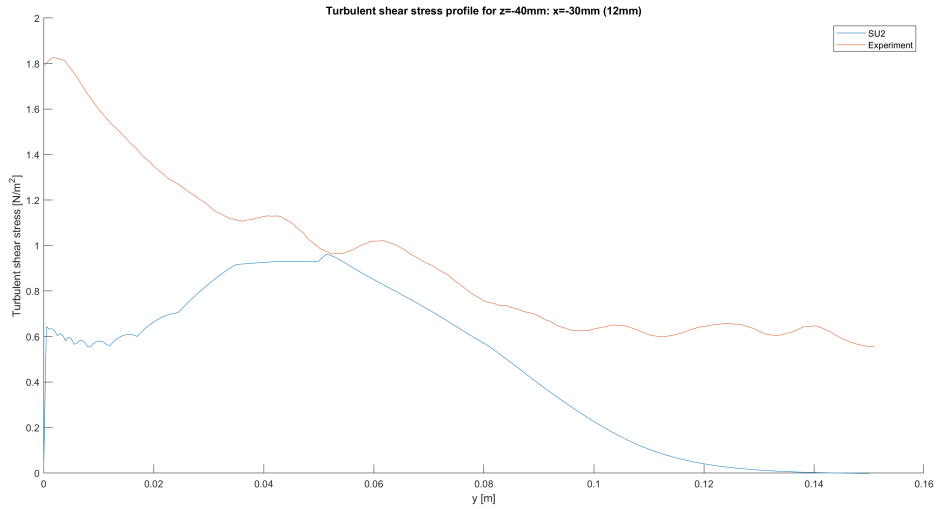

Figure 279: Turbulent shear profiles VG vs Experiment z=-40mm, x=-30mm (12mm)

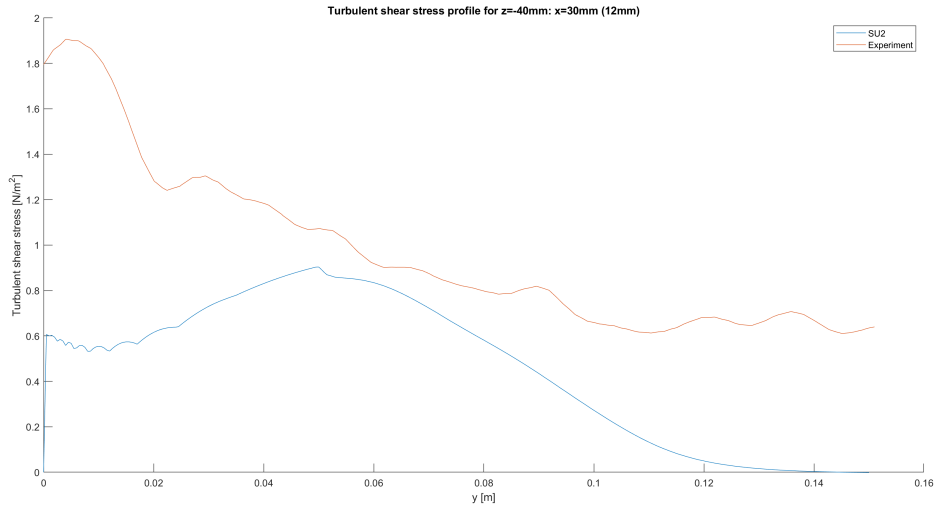

Figure 280: Turbulent shear profiles VG vs Experiment z=-40mm, x=30mm (12mm)

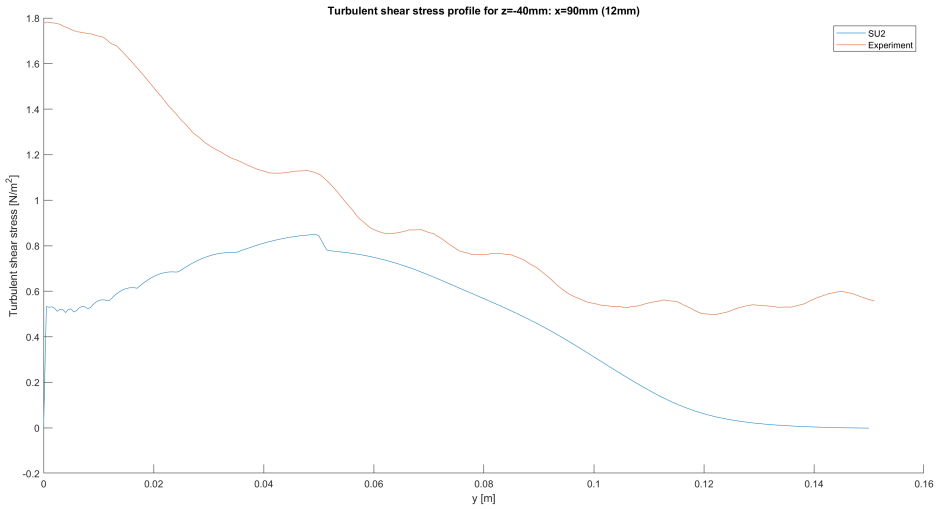

Figure 281: Turbulent shear profiles VG vs Experiment z=-40mm, x=90mm (12mm)

7.4.4 Turbulent shear profiles VG vs Experiment z=0mm (free)

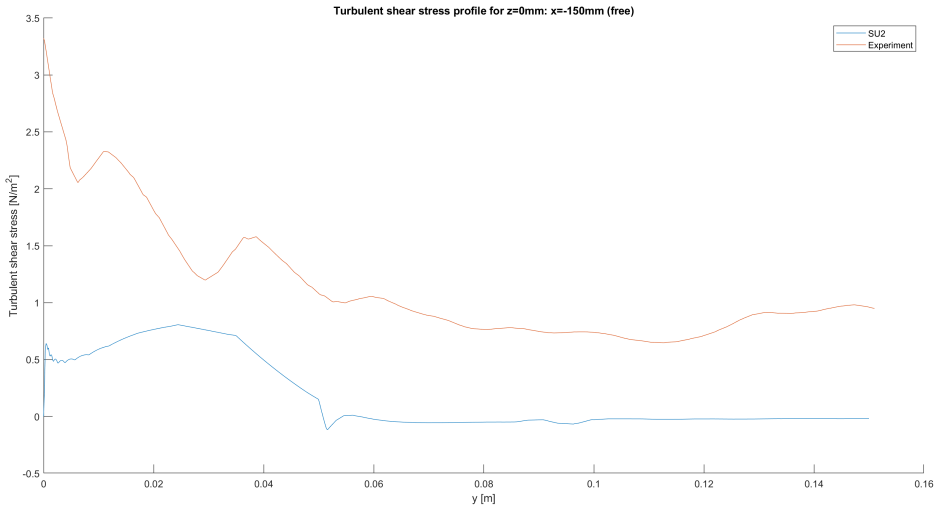

Figure 282: Turbulent shear profiles VG vs Experiment z=0mm, x=-150mm (free)

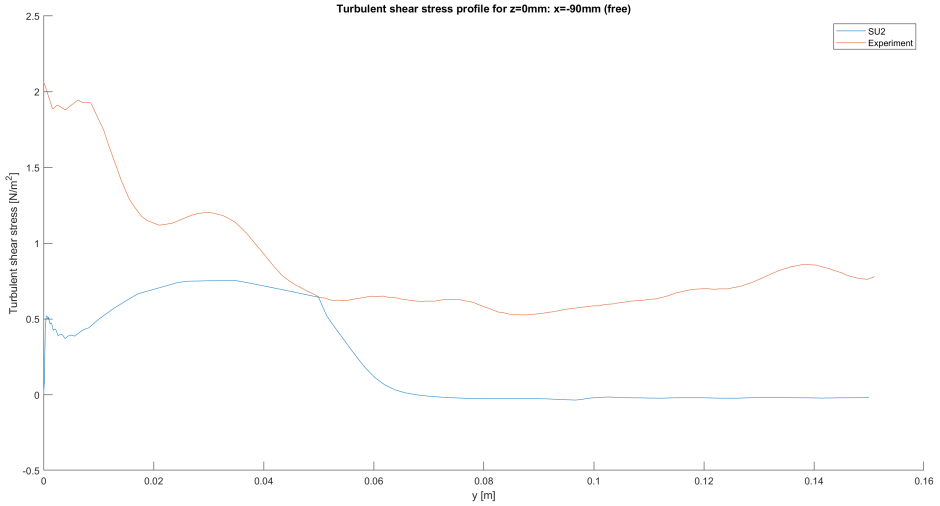

Figure 283: Turbulent shear profiles VG vs Experiment z=0mm, x=-90mm (free)

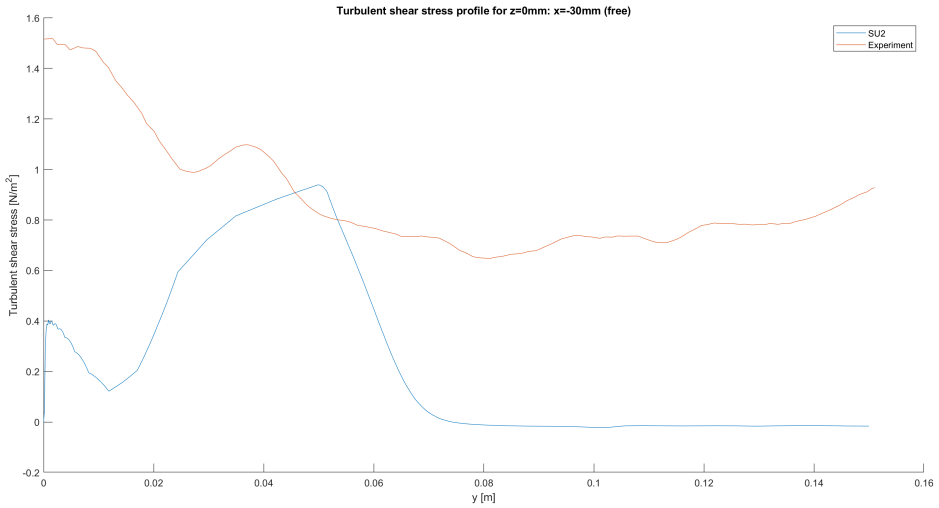

Figure 284: Turbulent shear profiles VG vs Experiment z=0mm, x=-30mm (free)

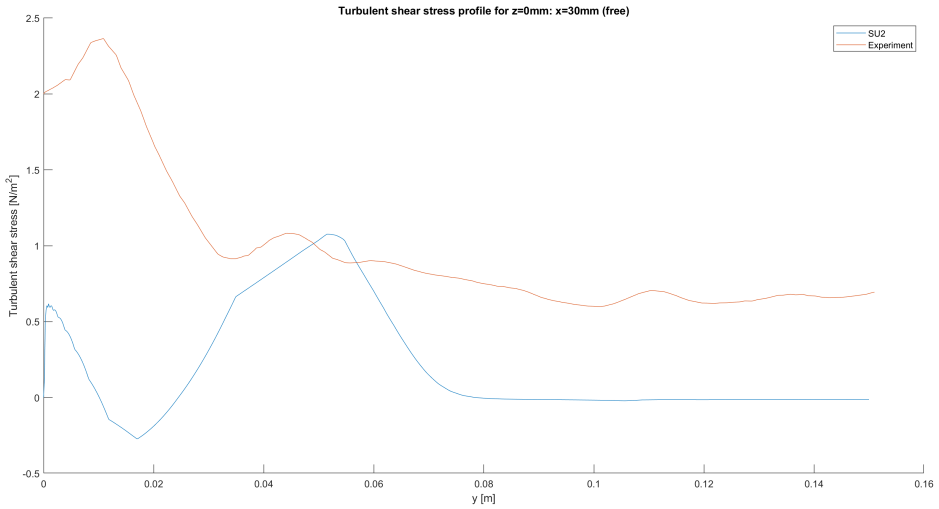

Figure 285: Turbulent shear profiles VG vs Experiment z=0mm, x=30mm (free)

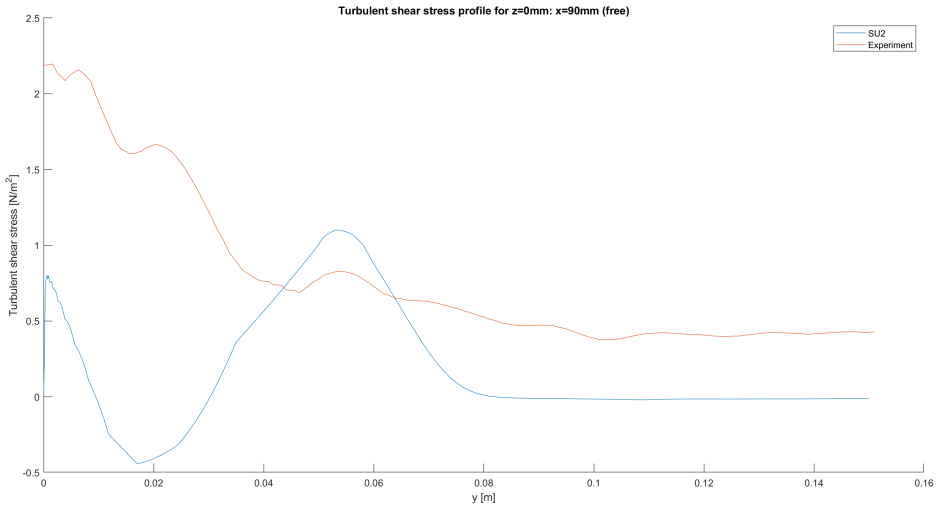

Figure 286: Turbulent shear profiles VG vs Experiment z=0mm, x=90mm (free)

7.4.5 Turbulent shear profiles VG vs Experiment z=0mm (8mm)

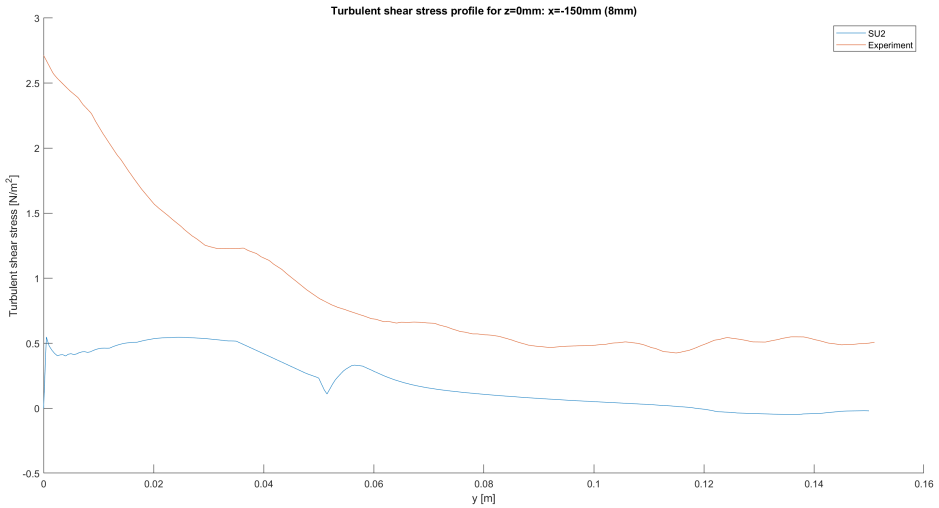

Figure 287: Turbulent shear profiles VG vs Experiment z=0mm, x=-150mm (8mm)

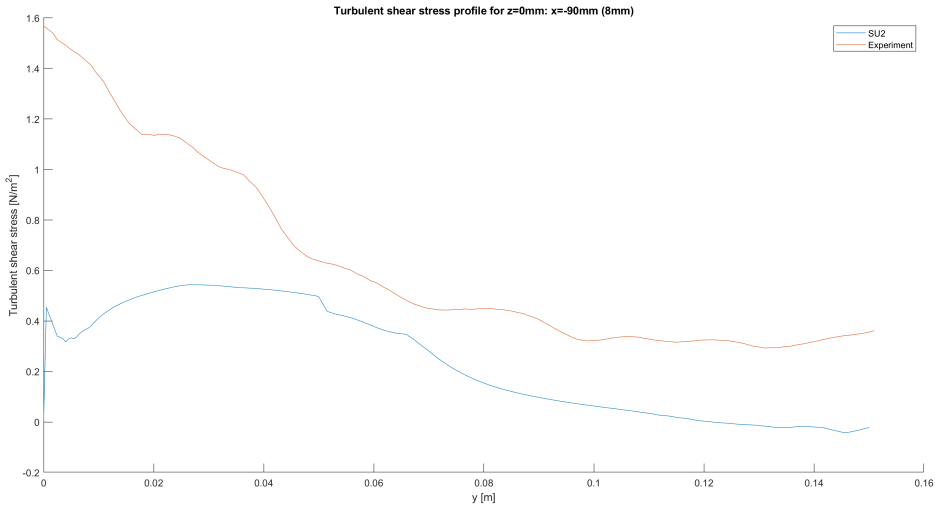

Figure 288: Turbulent shear profiles VG vs Experiment z=0mm, x=-90mm (8mm)

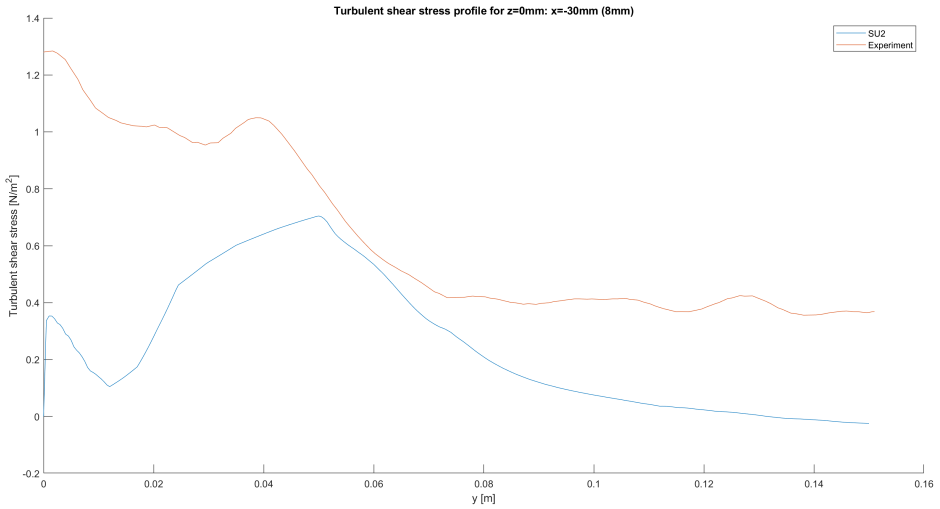

Figure 289: Turbulent shear profiles VG vs Experiment z=0mm, x=-30mm (8mm)

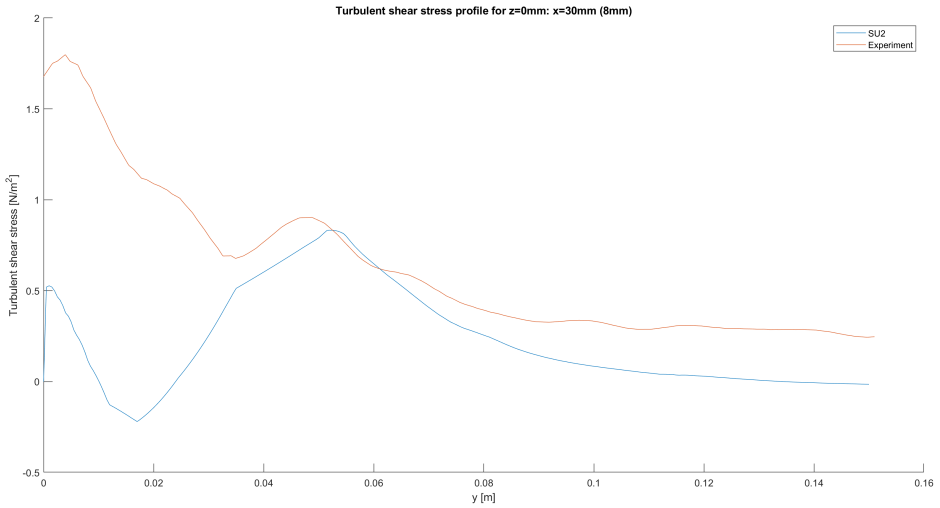

Figure 290: Turbulent shear profiles VG vs Experiment z=0mm, x=30mm (8mm)

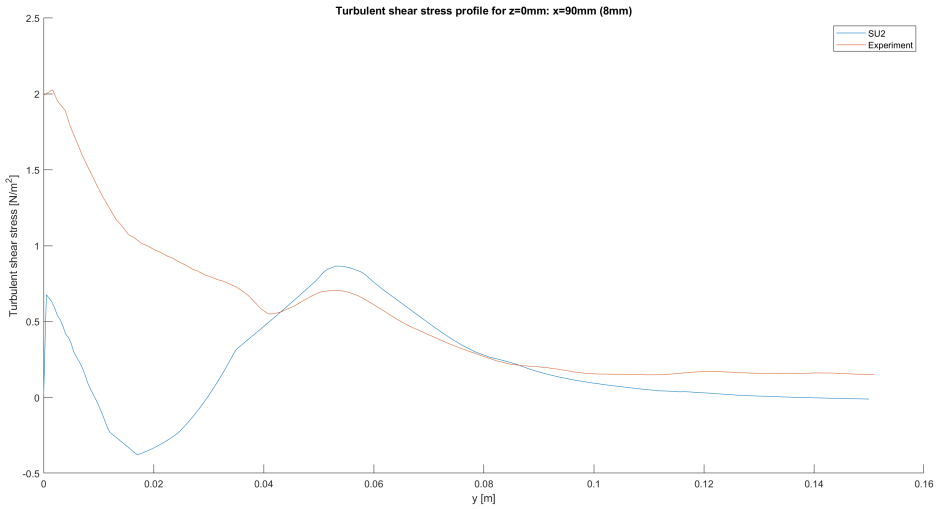

Figure 291: Turbulent shear profiles VG vs Experiment z=0mm, x=90mm (8mm)

7.4.6 Turbulent shear profiles VG vs Experiment z=0mm (12mm)

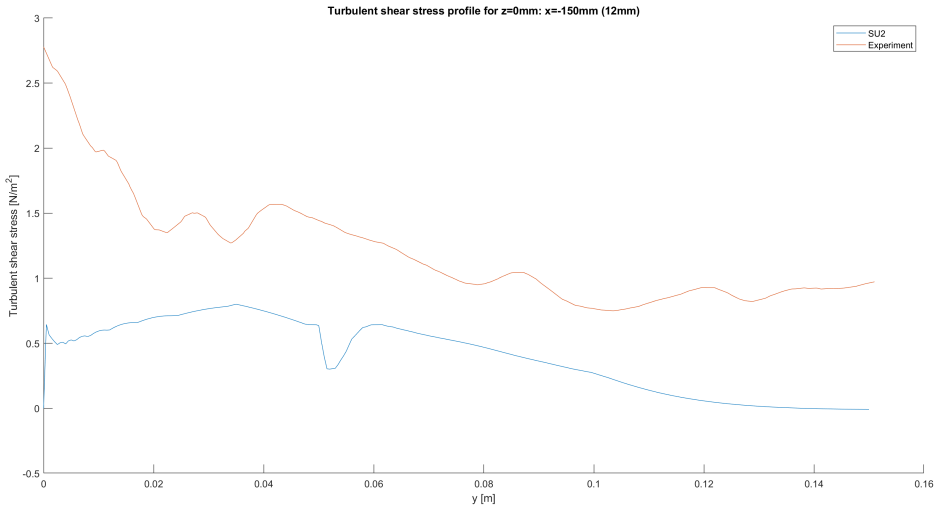

Figure 292: Turbulent shear profiles VG vs Experiment z=0mm, x=-150mm (12mm)

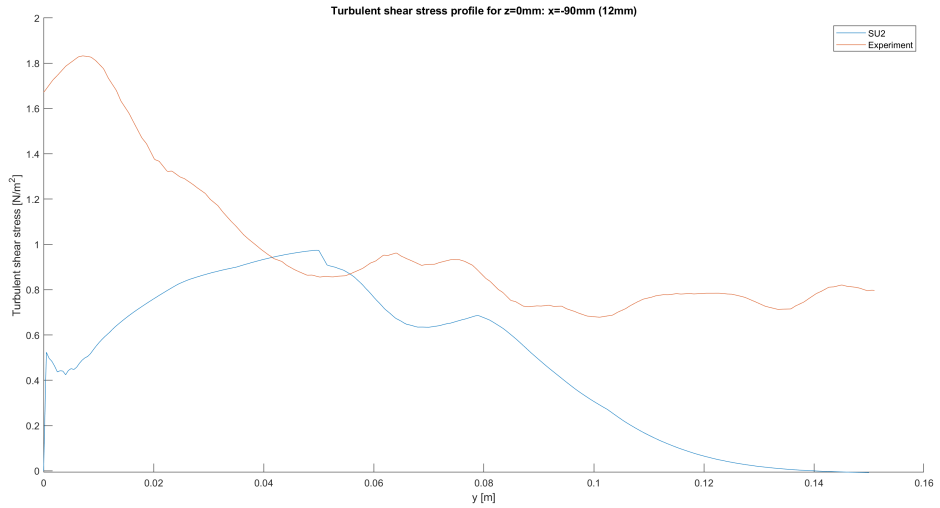

Figure 293: Turbulent shear profiles VG vs Experiment z=0mm, x=-90mm (12mm)

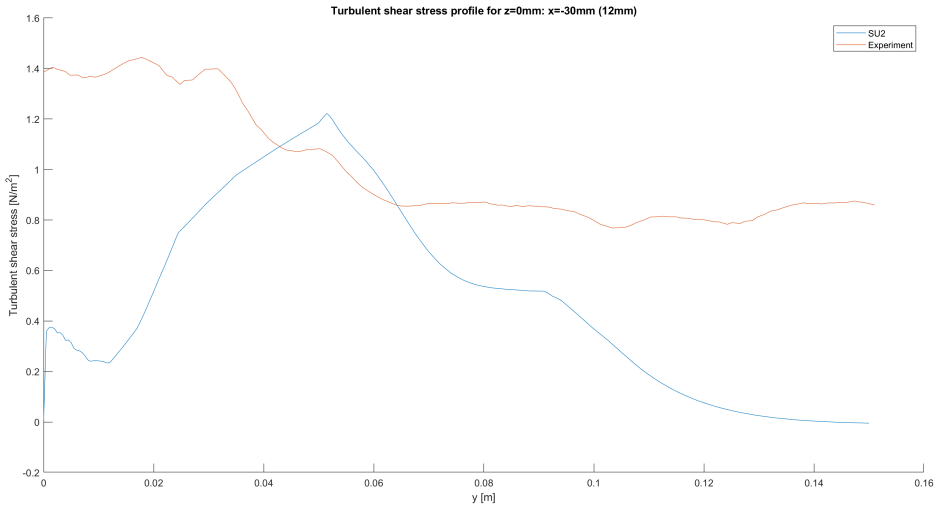

Figure 294: Turbulent shear profiles VG vs Experiment z=0mm, x=-30mm (12mm)

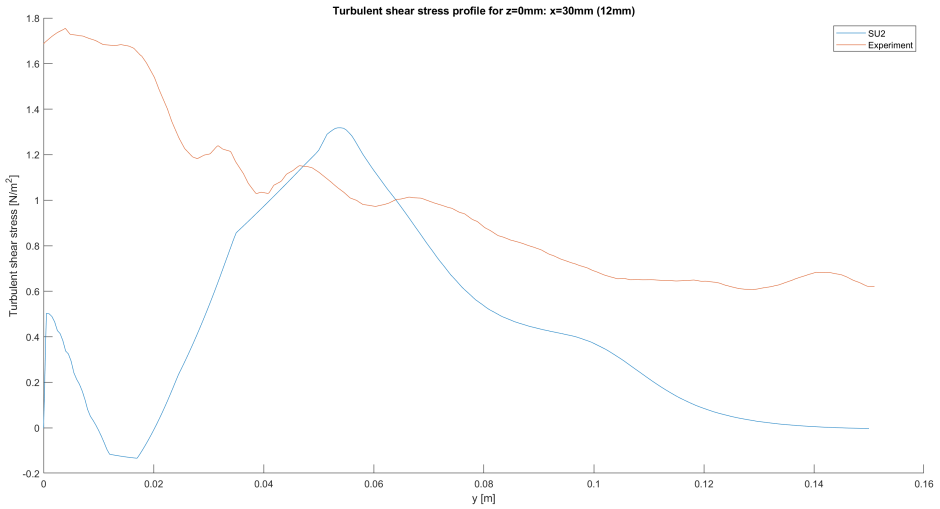

Figure 295: Turbulent shear profiles VG vs Experiment z=0mm, x=30mm (12mm)

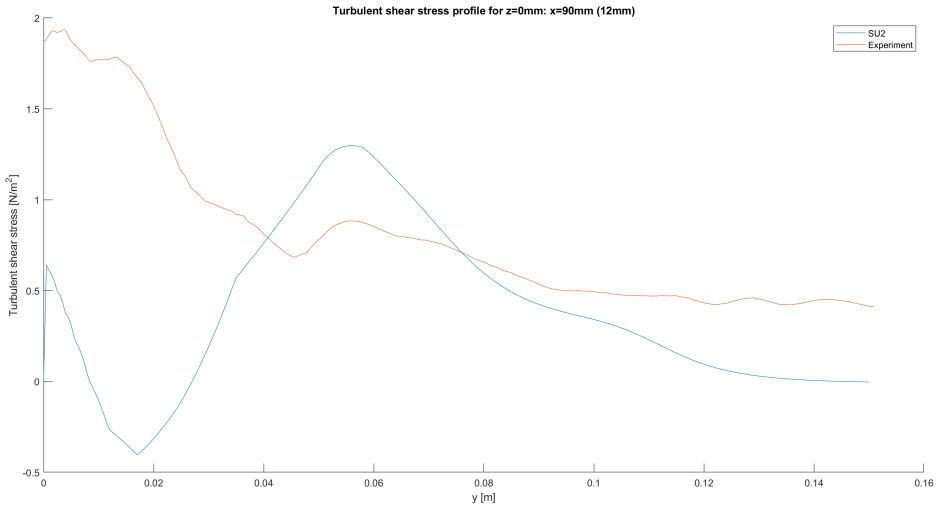

Figure 296: Turbulent shear profiles VG vs Experiment z=0mm, x=90mm (12mm)

7.4.7 Turbulent shear profiles VG vs Experiment z=40mm (free)

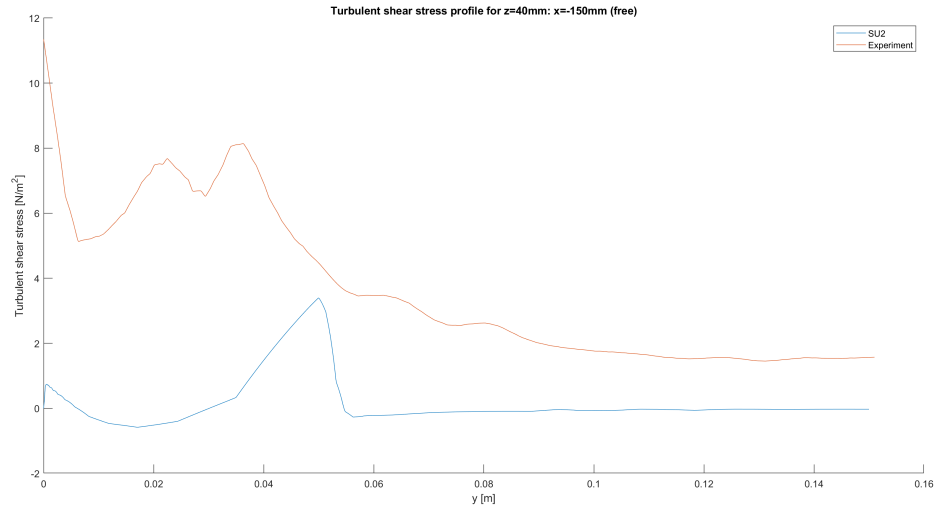

Figure 297: Turbulent shear profiles VG vs Experiment z=40mm, x=-150mm (free)

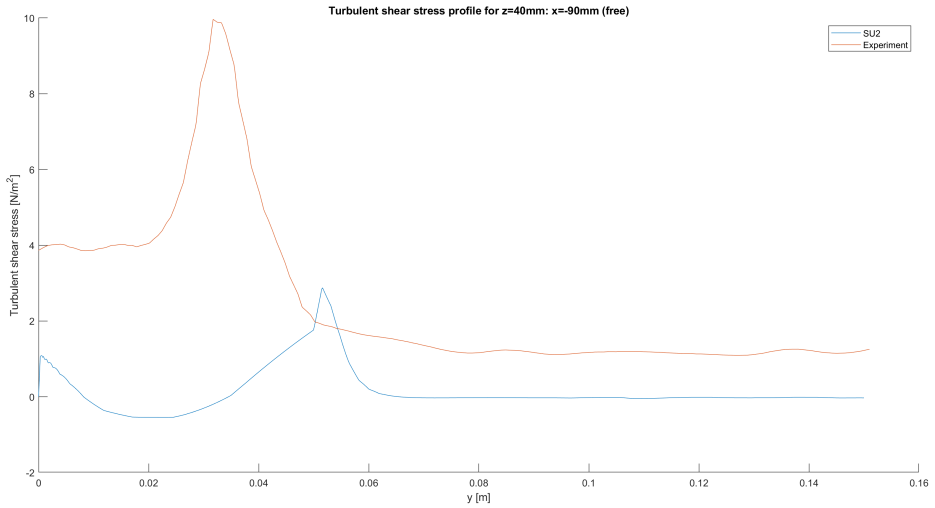

Figure 298: Turbulent shear profiles VG vs Experiment z=40mm, x=-90mm (free)

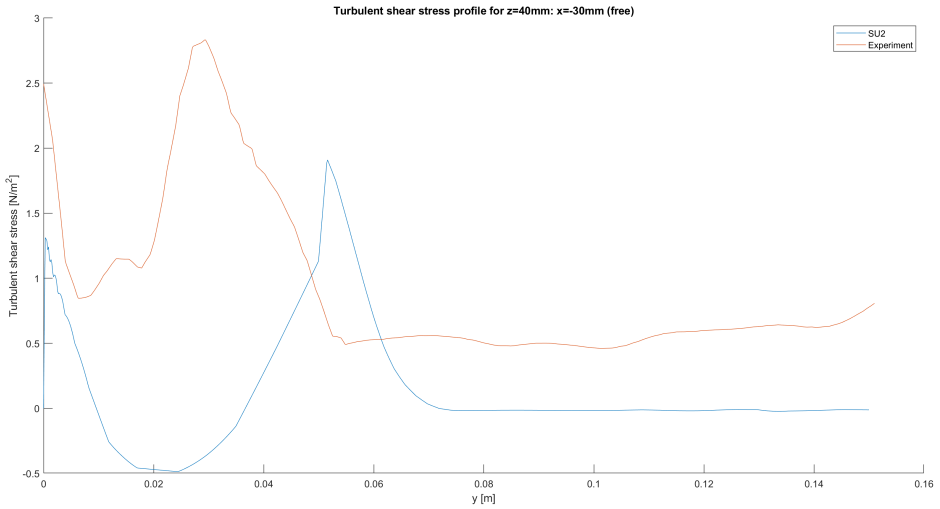

Figure 299: Turbulent shear profiles VG vs Experiment z=40mm, x=-30mm (free)

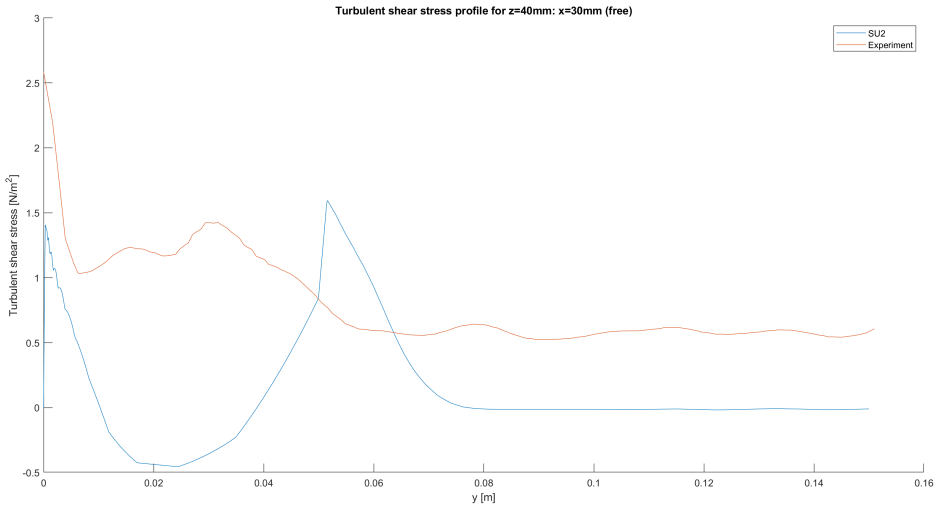

Figure 300: Turbulent shear profiles VG vs Experiment z=40mm, x=30mm (free)

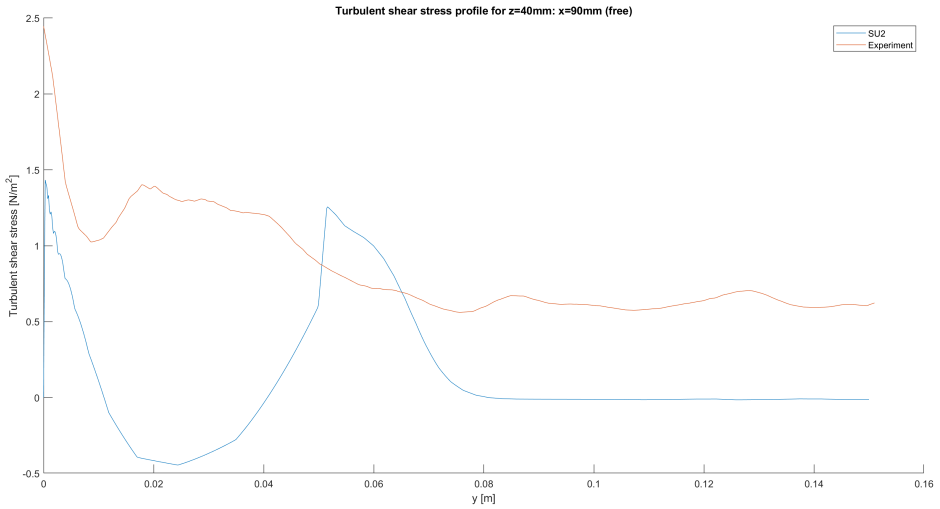

Figure 301: Turbulent shear profiles VG vs Experiment z=40mm, x=90mm (free)

7.4.8 Turbulent shear profiles VG vs Experiment z=40mm (8mm)

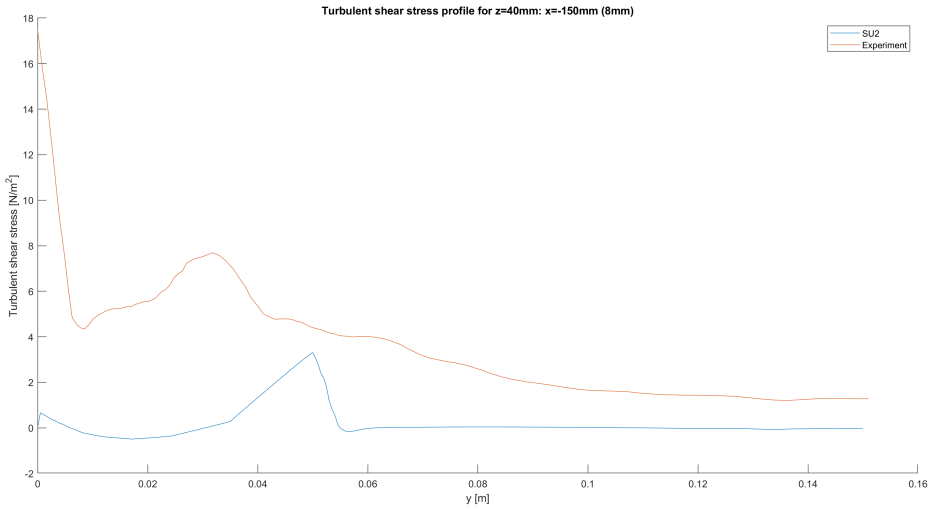

Figure 302: Turbulent shear profiles VG vs Experiment z=40mm, x=-150mm (8mm)

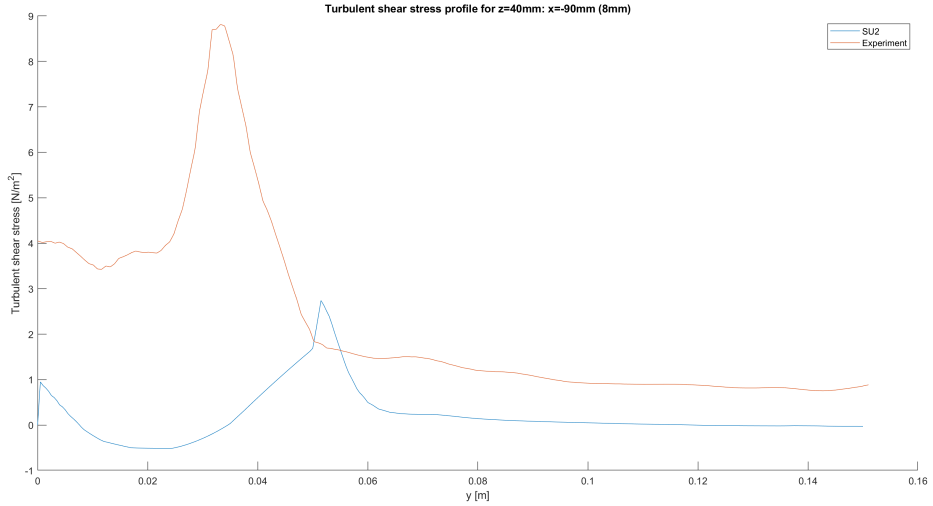

Figure 303: Turbulent shear profiles VG vs Experiment z=40mm, x=-90mm (8mm)

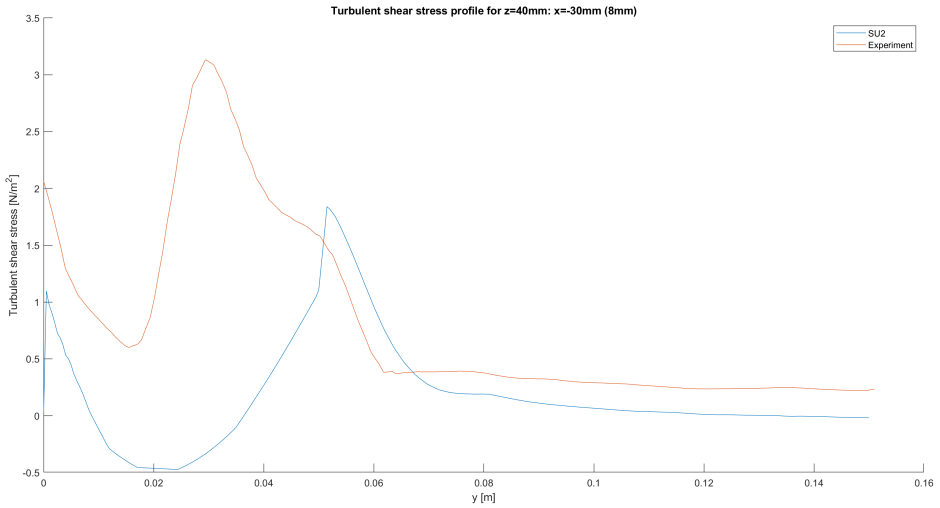

Figure 304: Turbulent shear profiles VG vs Experiment z=40mm, x=-30mm (8mm)

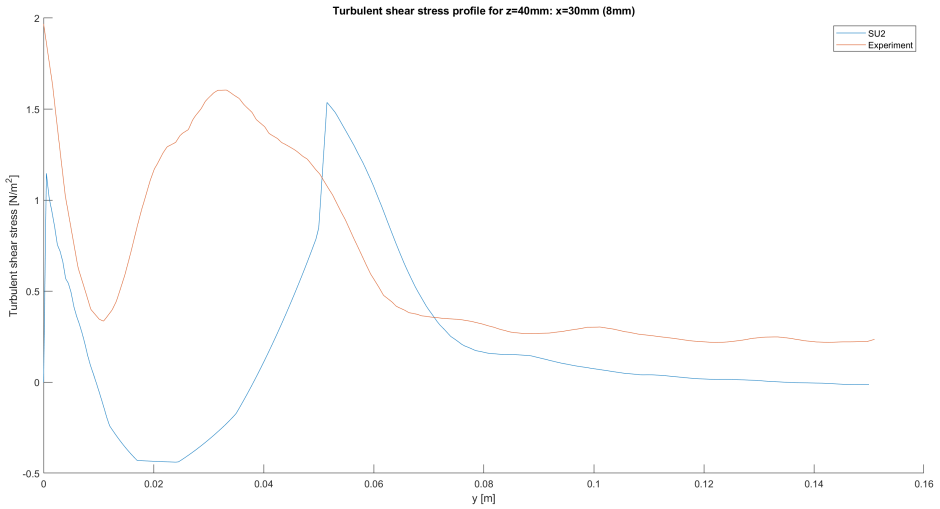

Figure 305: Turbulent shear profiles VG vs Experiment z=40mm, x=30mm (8mm)

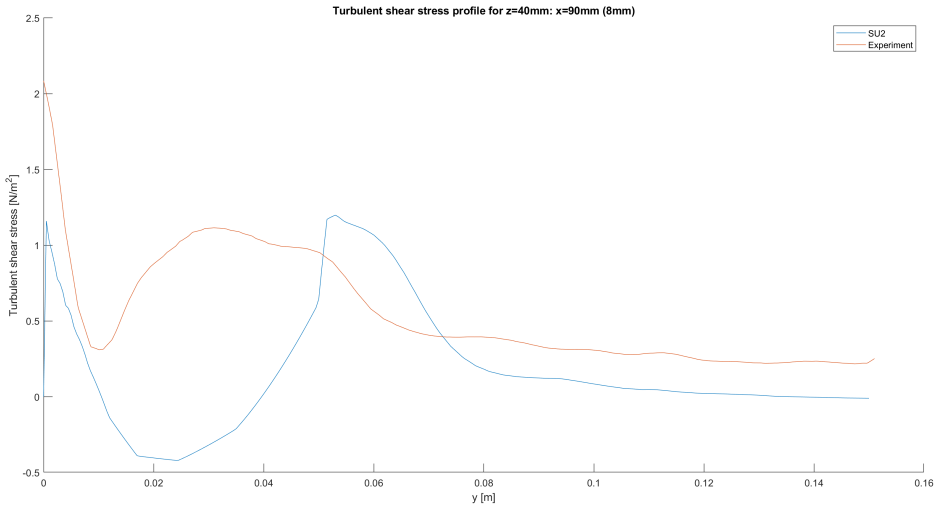

Figure 306: Turbulent shear profiles VG vs Experiment z=40mm, x=90mm (8mm)

7.4.9 Turbulent shear profiles VG vs Experiment z=40mm (12mm)

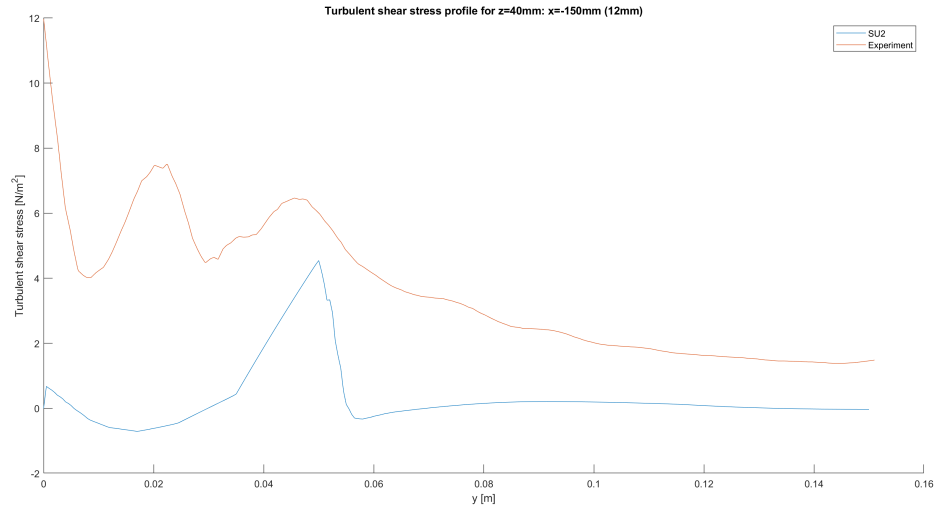

Figure 307: Turbulent shear profiles VG vs Experiment z=40mm, x=-150mm (12mm)

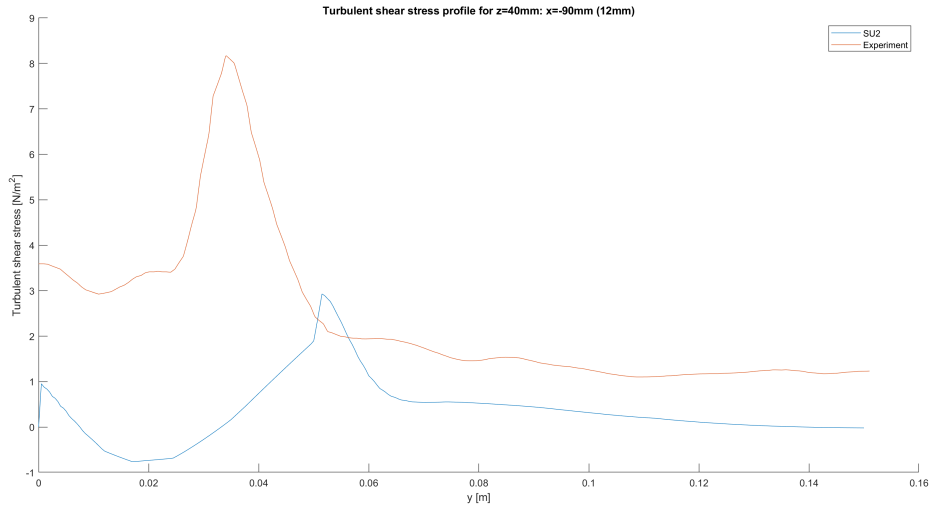

Figure 308: Turbulent shear profiles VG vs Experiment z=40mm, x=-90mm (12mm)

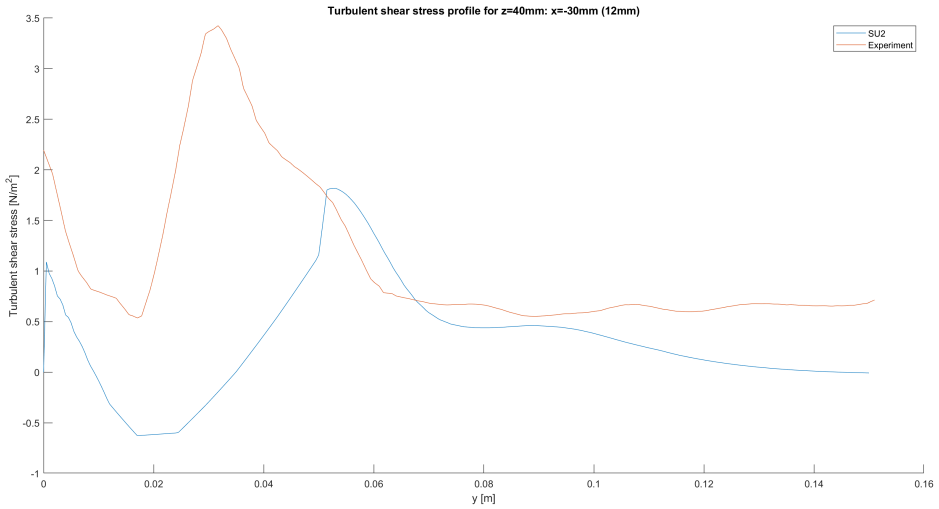

Figure 309: Turbulent shear profiles VG vs Experiment z=40mm, x=-30mm (12mm)

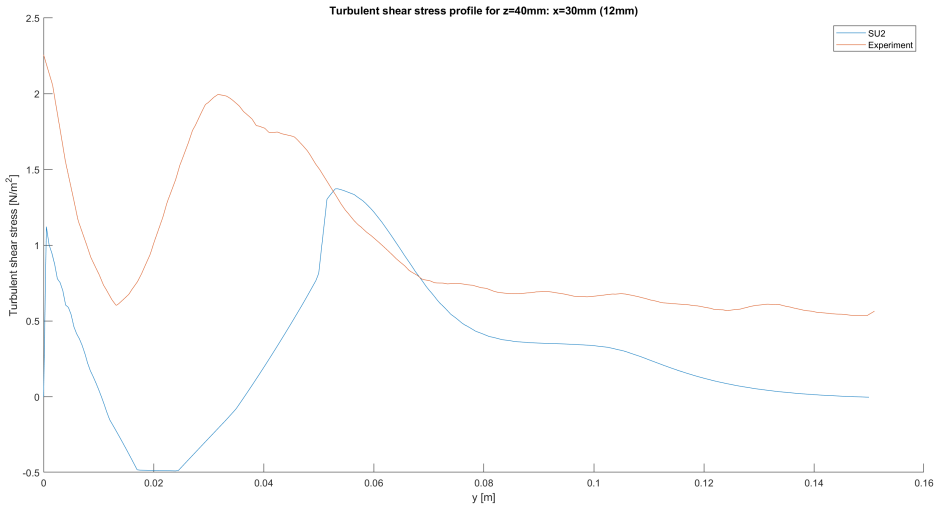

Figure 310: Turbulent shear profiles VG vs Experiment z=40mm, x=30mm (12mm)

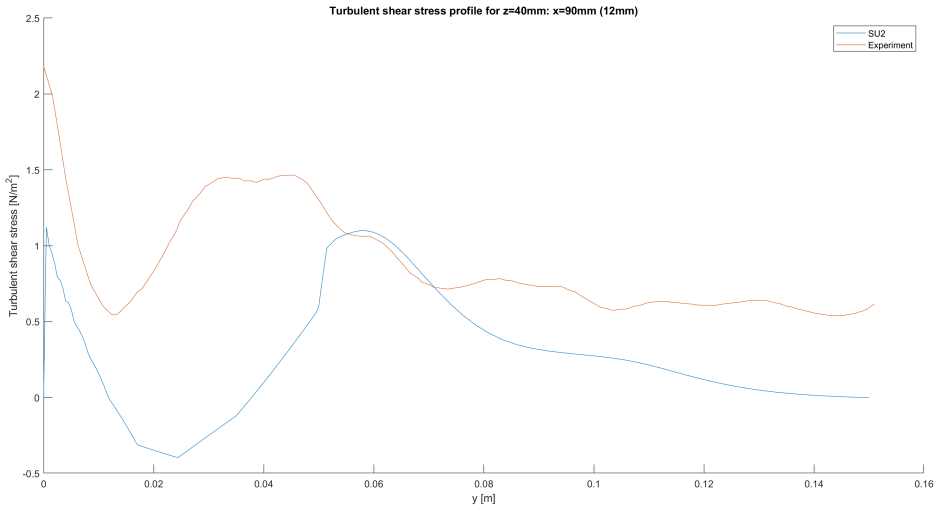

Figure 311: Turbulent shear profiles VG vs Experiment z=40mm, x=90mm (12mm)